Linac Design for Intense Hadron Beams

DISSERTATION

zur Erlangung des Doktorgrades

der Naturwissenschaften

vorgelegt beim Fachbereich Physik

der Johann Wolfgang Goethe-Universität

Frankfurt am Main

von

CHUAN ZHANG

aus Zhejiang

Frankfurt am Main 2009

D 30

vom Fachbereich Physik der

Johann Wolfgang Goethe-Universität als Dissertation angenommen.

Aller Anfang ist schwer, auch beim Beschleuniger.

Contents

Zusammenfassung

(Deutsche Version von „Summary")

Energie und Umwelt sind zwei Hauptthemen im 21. Jahrhundert. Zurzeit wird der für das tägliche Leben benötigte Energiebedarf hauptsächlich aus fossilen Quellen abgedeckt, doch die dadurch verursachte Luftverschmutzung und der Treibhauseffekt bedrohen ernsthaft die Weiterentwicklung der Menschheit. Eine weitere Energiequelle, welche einen Großteil der Elektrizität für den Weltverbrauch liefert, ist die Kernspaltung. Jedoch stellen die ständig anwachsenden Mengen von radioaktivem Müll mit Halbwertszeiten von über eine Million Jahre ein wachsendes Problem dar.

Die Beschleunigerphysik und –technologie eröffnet eine Lösungsmöglichkeit dieses Problems, weil beschleunigergestützte intensive Neutronenquellen eine wichtige Rolle für eine saubere nukleare Energieerzeugung übernehmen können:

- Beschleunigergetriebene unterkritische Reaktorsysteme (englisch: „Accelerator Driven Systems", ADS) ermöglichen eine leichte Kontrolle des Reaktorbetriebes, so dass die Kernbrennstoffe vollständiger und sicherer verbraucht werden.

- Das von der Europäischen Union geförderte Forschungsprogramm für die Transmutation von hoch radioaktiven Abfällen EUROTRANS wendet die ADS-Technologie an mit dem Ziel, die Radiotoxizität und Menge des radioaktiven Abfalls stark zu mindern.

- Die „International Fusion Material Irradiation Facility" (IFMIF) wird geeignete Materialien für Fusionsreaktoren wie ITER durch Beschuss mit Neutronen untersuchen und so einen langfristigen Beitrag für eine sauberere und effizientere Erzeugung von Kernenergie durch Fusionsreaktionen leisten.

Deshalb ist die Forschung und Entwicklung von Hochleistungs-Treiber-Linearbeschleuniger (Linacs) von weltweiter Bedeutung. Wie das Sprichwort (auch in China) sagt: „Aller Anfang ist schwer", so ist der Nieder- und Mittelenergiebereich gewöhnlich der anspruchsvollste Teil eines Beschleunigers. In der vorliegenden Dissertation wurden Strahldynamikuntersuchungen bei starkem Einfluss der Raumladungseffekte durchgeführt, wobei intensive Hadronenstrahlen im niedrigen und mittleren Energiebereich durch Hochfrequenz-Quadrupol- (englisch: „RFQ") und H-Mode Driftröhrenstrukturen (DTL) beschleunigt werden. Neben dem 5 bzw. 30mA, 17MeV Protoneninjektor (RFQ und DTL) für EUROTRANS und dem 125mA, 40MeV Deuteronen – DTL für IFMIF, wurde auch die strahldynamische Auslegung eines 200mA, 700keV Protonen-

RFQs für die intensive Neutronenquelle FRANZ an der Goethe-Universität Frankfurt untersucht.

Die markantesten Eigenschaften des FRANZ-RFQs sowie des IFMIF-DTLs sind die Strahlintensitäten von 200mA respektive 125mA, welche jeweils Rekordwerte für Protonen- und Deuteronen-Linacs darstellen. Obgleich die geplanten Intensitäten der beiden Entwicklungsstufen XT-ADS (5mA) und EFIT (30mA) des EUROTRANS-Projektes sich im Rahmen der technologischen Möglichkeiten moderner Beschleuniger befinden, stellte in diesem Fall die Option einer leichten Ausbaumöglichkeit des XT-ADS Entwurfes für EFIT wegen der unterschiedlichen Teilchenströme eine besondere Herausforderung dar.

Die am Los Alamos National Laboratory (LANL) unter Vernachlässigung der Raumladungskräfte entwickelte Vier-Sektionen-Prozedur für den RFQ-Entwurf war im Falle des 200mA FRANZ-RFQs sowie des EUROTRANS-RFQs nicht geeignet. Unter Aufgabe des von LANL entwickelten konstantes B-Kriteriums (konstante transversale Fokussierstärke), welches in den vorliegenden Fällen zu ineffizienten Parametersätzen geführt hätte, wurde ein neues Designkonzept für intensive Teilchenstrahlen mit der Bezeichnung „Balanced and Accelerated Beam Bunching at Low Energy" (BABBLE, siehe Seiten 55–58) ausgearbeitet.

Dieses ist im Einklang mit dem Prozess der Strahlformierung unter Berücksichtigung der Raumladungseffekte und hat folgende Hauptmerkmale: 1) Die Synchronphase wird am Eingang konstant bei φ_s=-90° gehalten, während die Modulation der Elektroden langsam erhöht wird. Dadurch erfährt der Strahl eine symmetrische und gemäßigte Fokussierung innerhalb der gesamten 360° Phasenakzeptanz. 2) In der nachfolgenden Hauptfokussierungs-Sektion wird B erhöht um die immer größer werdende transversale Defokussierung zu kompensieren, wodurch auch die Geschwindigkeit und Stabilität des Fokussierungsprozesses erhöht wird. 3) Zu Beginn der Hauptbeschleunigung kommt es durch die schnell anwachsende Teilchengeschwindigkeit zu einer natürlichen Reduktion der transversalen Defokussierung, so dass auch B entsprechend reduziert wird, um das longitudinale Emittanzwachstum zu vermeiden und um größere Aperturen zu ermöglichen.

Unter Ausnutzung der Vorteile der mäßigen anfänglichen Fokussierung sowie der daran anschließenden schnellen Fokussierung im Kräftegleichgewicht gemäß der „BABBLE"-Strategie, konnten ein 2m langer RFQ für FRANZ mit 98% Transmission und geringem Emittanzwachstum sowie ein 4.3m langer RFQ für EUROTRANS mit sehr geringen Teilchenverlusten und flachem Emittanzverlauf sowohl für 5mA wie auch für 30mA entworfen werden. Diese Ergebnisse bestätigen die „BABBLE"-Strategie als allgemeinen Design-Ansatz, welcher effi-

ziente RFQs mit guter Strahlqualität in einem weiten Bereich der Strahlintensitäten (0mA bis 200mA und höher) ermöglicht.

Beim Entwurf des IFMIF DTLs sowie des Injektor DTLs für EUROTRANS, welche als erste Anwendungen der neuartigen, supraleitenden CH-Driftröhrenstruktur dienen könnten, wurden mit großer Sorgfalt versucht, die Designkriterien bei neuen Randbedingungen wie längere Driftstrecken, supraleitende transversale Fokussierelemente und hohe Beschleunigungsgradienten möglichst gut zu erfüllen. Im Falle des IFMIF-DTL wurde das ursprüngliche IAP-Design wesentlich verbessert, sowohl im Hinblick auf den Aufbau des Beschleunigers wie auch strahldynamisch. Es wurden ausreichend Driftstrecken für die Kryoelemente, Diagnosekomponenten, Tuner und Steeringmagnete vorgesehen, ferner wurden supraleitende Solenoidlinsen eingesetzt und die Beschleunigungsgradienten angepasst (siehe Seiten 78–80). Daraus resultierte ein realistischerer, zuverlässiger und effizienter Entwurf. Darüber hinaus wurden die Spezifikationen und Lagen der transversal fokussierenden Elemente (siehe Seiten 81–82), sowie die Phasen- und Energieablagen zwischen Schwerpunkt der Teilchenverteilung und Sollteilchen am Eingang der φ_s=0° Sektionen neu bestimmt (siehe Seiten 83–84), wodurch verbesserte Ergebnisse in allen Raumebenen erzielt wurden. Im Falle des EUROTRANS Injektor-DTLs, wurden zusätzlich zu den obengenannten Maßnahmen Konzepte zur Anpassung der Strahldynamik für zwei verschiedene Strahlintensitäten entwickelt, wie zum Beispiel der Einsatz kurzer, abstimmbarer Rebunching-Kavitäten mit φ_s = -90° (siehe Seite 116).

In den Simulationsrechnungen für beide DTL-Entwürfe wurden keine Strahlverluste bei mäßigen Emittanzwachstumsraten festgestellt. Somit waren beide Designstudien sehr nützlich für die Realisierung zuverlässiger und ausbaufähiger supraleitender H-Mode Driftröhrenbeschleuniger für Teilchenstrahlen bis 125mA.

Um das wohlbekannte Problem beim Übergang zwischen zwei verschiedenen Typen von Beschleunigerstrukturen zu lösen, wurden Anpassungsmethoden zwischen dem RFQ und dem auf der KONUS-Strahldynamik basierenden H-Mode DTL entwickelt. Dabei ist die Grundidee, die Anpassung innerhalb des RFQ und nicht in der RFQ-DTL-Übergangssektion zu bewerkstelligen, weil im RFQ bei niedrigen Teilchengeschwindigkeiten eine sehr effiziente, geschwindigkeitsunabhängige Fokussierung bereitgestellt wird.

Beim FRANZ-Projekt wurde die longitudinale Ausgangsverteilung nach dem sogenannten longitudinalen Rotationsverfahren (siehe Seiten 62–63) manipuliert, um die Phasenbreite des Strahls zu minimieren und den Strahl in die Akzeptanz der KONUS-Struktur anzupassen. Beim EUROTRANS-Injektor wurde die Strahlanpassung transversal gemacht (siehe Seiten 107–110): Durch zwei zusätzliche Übergangszellen am Ausgang des RFQ wurden die transversalen Aus-

gangsellipsen in achsensymmetrische Lage (mit ähnlichen Halbachsen) gedreht, was von Vorteil für den weiteren Strahltransport durch den Driftröhrenbeschleuniger ist. Die Designerfahrung mit beiden Beschleunigerentwürfen zeigt, dass sich die verwendeten Methoden für die longitudinale und transversale RFQ-DTL-Anpassung sehr effizient auf das Gesamtergebnis ausgewirkt haben.

Ein weiteres wichtiges Thema der vorliegenden Dissertation sind Maschinenfehler-Studien. Üblicherweise geht man bei Strahldynamiksimulationen von idealen Betriebsbedingungen und fehlerfreien Beschleunigerkomponenten aus. Jedoch sind verschiedene mechanische, Strahl- und Feldfehler bei der Herstellung und im Betrieb nicht zu vermeiden. Deshalb waren strahldynamische Untersuchungen der Auswirkungen dieser Fehler im Falle der drei untersuchten Hochstrombeschleuniger essenziell notwendig, um das Risiko der Aktivierung von Komponenten zu minimieren und eine hohe Zuverlässigkeit zu garantieren.

Entsprechend der Möglichkeiten der verwendeten Simulationsprogramme, wurden sieben verschiedene RFQ und vier verschiedene DTL-Fehlerarten beim FRANZ-RFQ sowie beim IFMIF-DTL eingesetzt. Im Falle des EUROTRANS-Injektors wurden kombinierte RFQ und DTL-Fehler untersucht. Für eine bessere Überprüfung der Fehlerauswirkungen wurden neue Analysefunktionen ausgearbeitet, welche nicht von den bisher verwendeten Simulationsprogrammen angeboten wurden, so zum Beispiel gemeinsame 99% Strahlenveloppen (siehe Seiten 128–129) aus mehreren Simulationsläufen (anstelle von nur gemeinsamen 100% Enveloppen), zusätzliches Emittanzwachstum für 99% der Strahlteilchen (siehe Seite 131) usw. Dadurch konnten die wenigen Teilchen mit „schlechten" Koordinaten am Rande der Verteilungen eliminiert werden, so dass die Analyse der verbliebenen Teilchen klarere Ergebnisse in Bezug auf die Auswirkungen der Maschinenfehler liefert. Selbst bei Berücksichtigung von Fehlern zeigten alle Designentwürfe hohe Toleranzgrenzen.

Aufgrund der guten Ergebnisse in den Simulationen, sowohl mit als auch ohne Maschinenfehler, wird der Entwurf für den FRANZ-RFQ als Grundlage für die endgültige Auslegung verwendet. Der Entwurf für IFMIF stellte sich als der konkurrenzfähigste unter den drei bisherigen Vorschlägen heraus, und der Entwurf des EUROTRANS-Injektors wurde als offizielles Referenzdesign für das Projekt angenommen.

1. Introduction

Recently, high-power (typically ~MW) driver linacs (HPDL) have been widely proposed in Asia, Europe and North America with the motivation to generate various secondary particles by bombarding a target with energetic light ions (e.g. H^+, H^-, D^+, but the proton is in the majority). Such installations have numerous important applications in many fields, for example:

- Neutron sources for structure and dynamics studies of condensed matter, control of fission-based energy production, transmutation of radioactive waste, materials test for fusion reactors and tritium production.
- RIB (Radioactive Ion Beam) facilities for nuclear physics research.
- Muon and neutrino factories for particle physics research.

Table 1-1: Worldwide HPDL projects (≥0.8MW average beam power).

Parameter \ Project	P_{beam} [MW]	W [GeV]	I_{peak} [mA]	ζ [%]	L [m]	Primary particle	Secondary particle	Status
LAMPF (LANSCE)	0.8	0.8	17	~10	~800	H^+	pion, neutron	operating since 1972
SNS	1.6	1	26	6	335	H^+	neutron	operating since 2006
FNAL 8GeV PD	2	8	25	1	678	H^-	neutrino	proposed
EUROTRANS	1.5-2.4	0.6	2.5-4	100	>200	H^+	neutron	proposed
	16	0.8	20					
CERN HP-SPL	≥4	5	40	2-6	534	H^-	neutrino, RIB	proposed
EURISOL	5	1	5	100	240	H^+, H^-, D^+, $^3He^{2+}$	RIB	proposed
IFMIF	5	0.04	125	100	≤43	D^+	neutron	proposed
ESS	5.0-7.3	1.3	114	3.3-4.8	648	H^+, H^-	neutron	proposed

Two operating and six proposed MW driver linacs are listed in Table 1-1. The average beam power is defined by $P_{beam} = W \cdot I_{peak} \cdot \zeta$, where W is the beam energy, I_{peak} the peak current and ζ the duty factor. The LAMPF linac is a full room-temperature (RT) machine, and all the others mainly depend on the RF superconducting (SC) technology. The rapid development of this technology in the past decades has enabled a new generation of HPDLs with new-type accelerating cavities, which are compact and very effective, having high accelerating fields, allowing large duty factors up to CW operation, and can be built and operated at reasonable costs. This opens the possibility for the realization of several accelerator-based facilities with very high beam power.

Generally speaking, an HPDL needs to meet the following three common requirements, which are determined by the high-power operation and the dedicated applications:

- Beam losses must be low, because lost particles can induce the negative effects such as: 1) Activation of accelerators. 2) Damage to accelerator components. 3) Increase of vacuum pressure. 4) Quenching of SC cavities. If hands-on maintenance is required, the activation concern will put the lowest limit to beam losses, typically a few W/m at high energy. For example, 1W/m for 1GeV protons is corresponding to a residual dose of below 1mSv/hr after 30 days irradiation and 4 hours cool-down [CHO99].

- High reliability. It is important for long-term applications, because beam trips can for example damage the sub-critical core by sharp temperature variations.

- Minimum capital and operating costs, a natural demand for such powerful facilities.

Table 1-2: Advantages and disadvantages of SC cavities.

Advantage	Disadvantage
- Negligible RF power dissipation - No cooling problems (even CW operation is easy) - High accelerating gradients - Large bore apertures (low beam losses) - High transverse focusing fields from SC magnets	- Usually no internal magnetic lens is allowed, as the maximum tolerable RF magnetic field for the superconductor Niobium is ~0.2T - Relatively complicated and expensive construction - The cryo-system is necessary

To meet the stringent requirements for modern high-power driver linacs, solutions and optimizations should be found from the following three aspects:

- Operating modes: due to the unique features listed in Table 1-2, the main part of a modern HPDL shall be operated at SC; and together with SC, the high-duty-factor (even continuous wave, CW) operation is favourable for realizing an intense HPDL with high reliability.

- Accelerating structures: to obtain the maximum efficiency for the whole machine, different accelerators suitable for different beam-velocity ranges should be used. A typical configuration of the accelerating structures for a modern HPDL is shown in Fig. 1-1. The RFQ (Radio-Frequency Quadrupole) accelerator characterized by velocity-independent electric focusing is the standard injector to capture, bunch and pre-accelerate low-energy, high-intensity beams (in a high-current RFQ, unfortunately particle losses are usually not fully avoidable, therefore it can be used only in the RT mode; otherwise the losses will increase the heat load to the helium by an inacceptable factor). For the medium-β section, the RT cavities (H-type, Alvarez-type and coupled-cavity drift-tube linacs), the SC cavities (Cross-bar H-type, $\lambda/4$, $\lambda/2$ and spoke structures), and mostly a mixture of all these RT and SC structures can be used. For $\beta > 0.5$, SC elliptical (reentrant) resonators are the dominant candidates (recently, multi-spoke cavities are also possible).
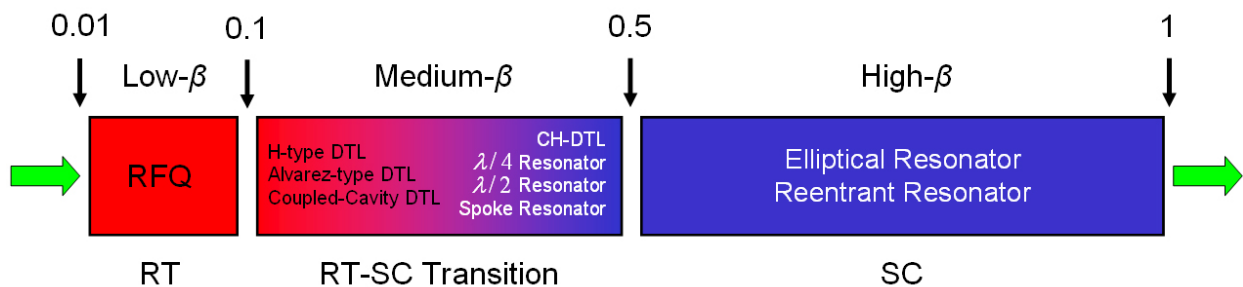
Fig. 1-1: The typical layout for modern HPDL machines.

- Beam dynamics: the space-charge fields of intense hadron beams can be as strong as the external fields. This weakens the focusing strength and can dramatically lead to emittance growths, halo formation and beam losses, etc. Therefore, unconventional design procedures have to be developed and applied to reach good beam qualities while keeping a compact layout.

As well known, the low-energy end is the most difficult part for designing a large hadron linac, because the space-charge effects are particularly serious for slow beams and furthermore the initial performance has a direct influence to the whole facility. To address the problems of low- and medium-β beam acceleration for high-power driver linacs especially at high beam in-

tensities, this dissertation is focusing on the physics design studies of the RFQ accelerator and the RT and SC H-type DTL structures. Totally, three HPDL projects have been involved:

- EUROTRANS: a European research programme, which is joined by 31 partners (research agencies and nuclear industries) with the contributions from 16 universities. It is aiming to demonstrate the transmutation of high-level nuclear waste in an ADS way.

- IFMIF: an international cooperation to simulate the intense neutron flux in a nuclear fusion environment for testing and qualifying the fusion-reactor materials which can allow the realization of commercial fusion power production.

- FRANZ: the first "Lighthouse Project" at the new Riedberg Campus of Frankfurt University with the motivation to develop a small-scale, multi-purpose neutron experiment platform for both in-house education and scientific research.

For EUROTRANS, IFMIF and FRANZ, the common goal is to develop a powerful neutron source based on an intense driver linac with a peak intensity of 2–4mA (20mA), 125mA and 200mA, respectively. Comparing with the other two facilities, FRANZ is a mini one, but its ultra-high intensity, which is close to the space-charge limit of the today's linac technology, makes it as a suitable test bed for EUROTRANS, IFMIF and other high-power linac projects.

The whole dissertation will be organized in the following way: 1) First, a brief introduction to the EUROTRANS, IFMIF and FRANZ projects for illustrating the backgrounds and challenges to the design studies of their high-power driver linacs. 2) Second, the basic principles of operation and main RF geometries of the adopted RFQ and H-type DTL structures for the low- and medium-β parts of these three facilities are briefly presented in order to provide a basis for the further discussions. 3) Finally, the detailed linac design studies for EUROTRANS, IFMIF and FRANZ will be presented in three independent chapters (the order of the three projects has been arranged to avoid repetitive contents for a same kind of accelerating structure):

- RFQ design for FRANZ (120keV – 700keV).
- DTL design for IFMIF (5MeV – 40MeV).
- Front-end (RFQ + DTL) design for EUROTRANS (50keV – 17MeV).

Generally speaking, the study procedure used for each job is as follows: 1) To show the constraints and problems which are challenging to the conventional design methods. 2) To develop and apply the optimization strategies for meeting the design goals. 3) To carefully investigate the behaviour of the obtained design in case of mechanical and field errors. The last one is a very important topic of this dissertation, because as mentioned the operation of HPDL machines should be reliable and safe.

2. An Overview of the Involved Projects

Particle accelerators were originally invented and are still being mainly developed as the exploring tools of the subatomic world. Along with the progress in accelerator physics and technology, however, various non-research applications have been also widely found and quickly expanded. Among them, the utilization of accelerators for the energy development is now of an increasing common interest.

Due to the rapid economic growth and expanding population, the energy crisis is more and more serious for the whole world. Though the fossil energy resources are currently contributing ~80% of the required energy for our life, they are limited by the weaknesses of shrinking deposits and environmental disruptions. Recently, new prospects have been opened by using clean and renewable energy generated from natural resources such as sun, wind, water and geothermal heat. Subjected to the weather or geographical conditions and the conversion efficiency, however, they are not sufficient to be taken as the major sources of energy in the near future. Despite some existing problems and difficulties, nuclear energy is one promising potential substitute for the traditional fossil energy.

Having been put into industrial operation for several decades, the conventional nuclear electricity generation is based on the fission reactions. But, for this method, the safety of operation and the treatment of radioactive waste are two major worries from the public. Proposed by C. Rubbia in 1993 [CAR93], applying a particle accelerator as a spallation neutron source to operate a sub-critical fission reactor seems to be a solution: on one hand, the accelerator can serve as a "one-button switch" to the reactor; on the other hand, this technology is able to not only burn the fuel more completely (compared with a normal reactor), but also open the possibility to reduce the radiotoxicity and volume of the existing waste greatly. Started by EU, EUROTRANS is a pioneering research programme aiming to investigate and demonstrate such kind of accelerator-based transmuters.

Actually, another way of nuclear power production using fusion reactions has more advantages:

- The resulted energy density from fusion reactions can be many times greater than that from fission reactions.
- Fusion fuels are cheap and abundant.
- Almost zero risk of an accident and no direct radioactive waste (only some short-lived ones from the reactor walls struck by energetic neutrons).

To realize a commercial fusion power plant, however, suitable construction materials are still under development for the fusion reactor, in which the neutron flux will be ~100 times that in a fission one. Based also on a particle accelerator, an international project called IFMIF has been proposed to simulate the intense neutron flux in a fusion environment for testing and qualifying the radiation properties of candidate materials.

Obviously, a common characteristic for EUROTRANS and IFMIF is to produce intense neutrons as the secondary particles of the high-power light ions from a linac. As a test bed of such large facilities, an ultra-intense keV-range neutron source called FRANZ has been planned to be driven by a 200mA, ~2MeV proton linac, which beam specs are particularly suitable to investigate some challenging R&D problems for modern driver linacs e.g. the limits by the space-charge effects.

2.1 EUROTRANS: EUROpean Research Programme for the TRANSmutation of High Level Nuclear Waste in an Accelerator Driven System

The Accelerator-Driven System has been firstly proposed as an energy amplifier to breed a sub-critical fission reactor for cleaner and inexhaustible nuclear power production [CAR93]. Recently, its another application for transmuting high-level nuclear waste is of great interests.

A statistics in 2001 showed that the 145 European nuclear power plants were producing 850TWh of electricity (~35% of all generated energy) as well as ~2500 tons of spent fuels including 1% of Pu annually [ADS01]. As shown in Fig. 2.1-1, the red curve indicates that it will take >1 million years for the radiotoxicity of the nuclear waste to be naturally decreased to the level of the raw uranium ore if the spent fuel is directly buried in the deep geological repositories as the tradition. However, the blue curve implies that a two-step process – firstly a chemical separation and then an irradiation treatment in a fast and intense neutron flux by an ADS system – can not only remarkably shorten the decay time for reaching the reference radiotoxicity level to below 700 years but also greatly reduce the volume and heat load of the radioactive waste.

Launched by European Union in 2005, the EUROTRANS project [BIA05] is dedicated to perform R&D studies towards a European Transmutation Demonstration (ETD) in two phases:

- To construct a 50–100MW$_{th}$ eXperimental facility demonstrating the technical feasibility of Transmutation in an Accelerator Driven System (XT-ADS).
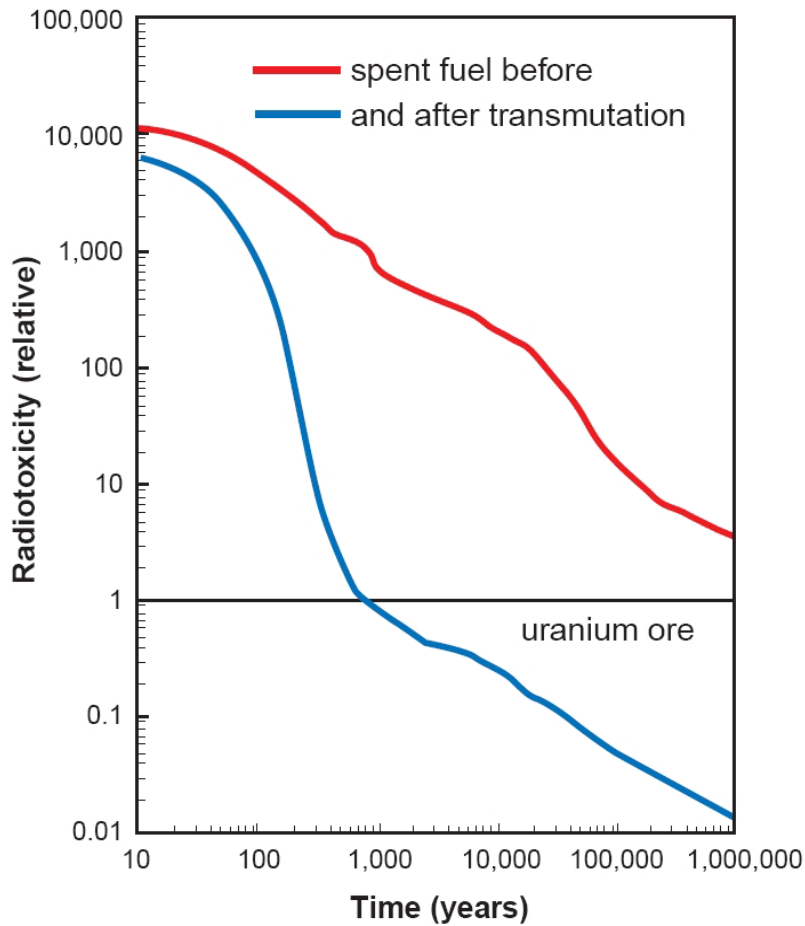- To realize a several hundred MW$_{th}$ modular European Facility for Industrial Transmutation (EFIT).

Fig. 2.1-1: Comparison of the decay time of the radiotoxicity of nuclear waste to the reference level of the original uranium ore before and after transmutation [ADS01].
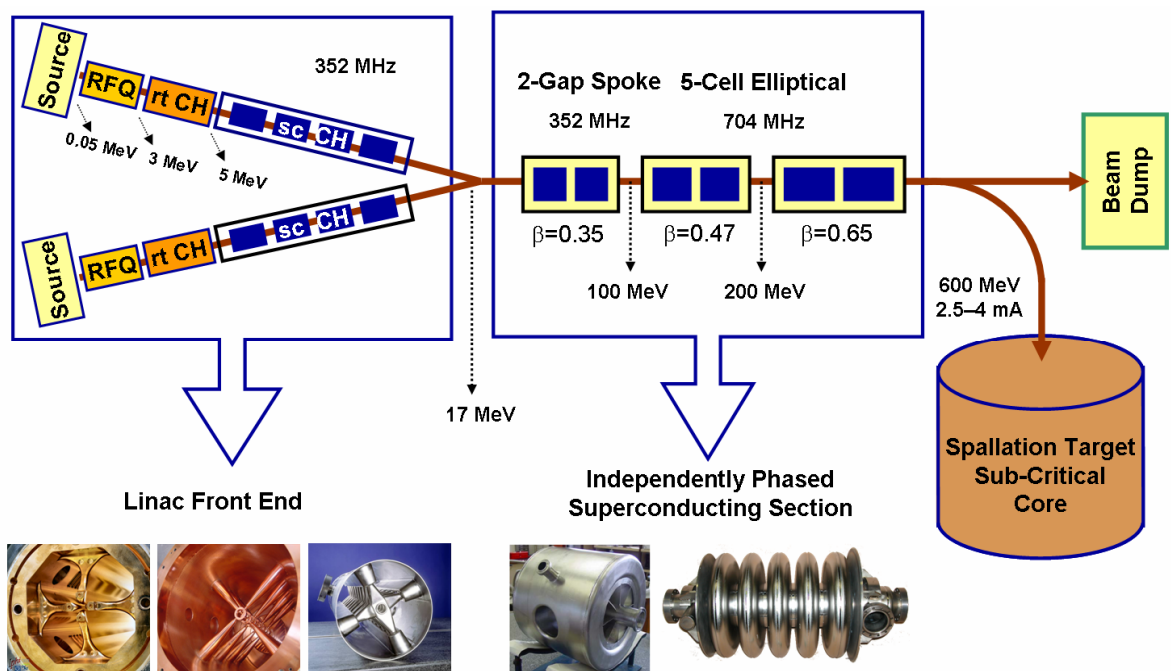

Fig. 2.1-2: The reference layout of the planned EUROTRANS facility [POD08a].

The reference layout of the planned EUROTRANS facility is schematically shown in Fig. 2.1-2, where the CW driver accelerator consists of a linac front end responsible for accelerating the protons to 17MeV and an independently phased superconducting section for covering the rest energy gain. As listed in Table 2.1-1, the intensity and energy of the required proton beam on the spallation target in the XT-ADS phase are specified as 2.5–4mA and 600MeV, which will be upgraded to 20mA and 800MeV, respectively, in the EFIT phase.

Table 2.1-1: Specifications of the required proton beams for XT-ADS and EFIT [BIA07].

Phase / Parameter	XT-ADS	EFIT
Peak beam intensity [mA]	2.5 – 4	20
Output beam energy [MeV]	600	800
Beam trip number (>1s)	< 5 per 3-month operation cycle	< 3 per year
Beam stability	Energy: ± 1 %, Intensity: ± 2 %, Size: ± 10 %	
Beam time structure	CW, with 200μs zero-current holes	

Determined by the ADS application, the leading constraint for the EUROTRANS driver linac is that only very few beam trips will be allowed in order to avoid the fatal damages caused by sharp temperature variations to the sub-critical core. The prescribed limit of the unwanted beam trips exceeding one second is <20 per year for XT-ADS or <3 per year for EFIT, which is two or three orders of magnitude less than the operation performance of existing accelerators [PIC00]. With such ambitious goals, the EUROTRANS accelerator design is facing unusual challenges to ensure the extremely high reliabilty.

Meanwhile, for an easy upgrade from XT-ADS to EFIT without additional R&D efforts, a very special idea is to design a robust and flexible linac layout which can work well with both beam intensities required by the XT-ADS and EFIT phases. Leaving safety margins, 5mA and 30mA have been chosen as the design beam intensities for the two phases, respectively. Though these intensities are well within the capability of today's linac techonology, the space-charge effects are quite different in both cases. Therefore, how to realize a current-adaptable accelerator design is another stringent task.

2.2 IFMIF: International Fusion Materials Irradiation Facility

Fusion is one known technology possible to produce a large fraction of electricity for the world in a cleaner and safer way than the traditional methods, e.g. thermal and fission-driven energy productions. However, one bottleneck of the realization of an industrial fusion power plant is to develop suitable reactor materials, which can sustain such as >30dpa/year (displacement per atom per year) of damages from the intense neutron flux with high energies up to 14MeV in a typical D-T fusion environment [IFM04].
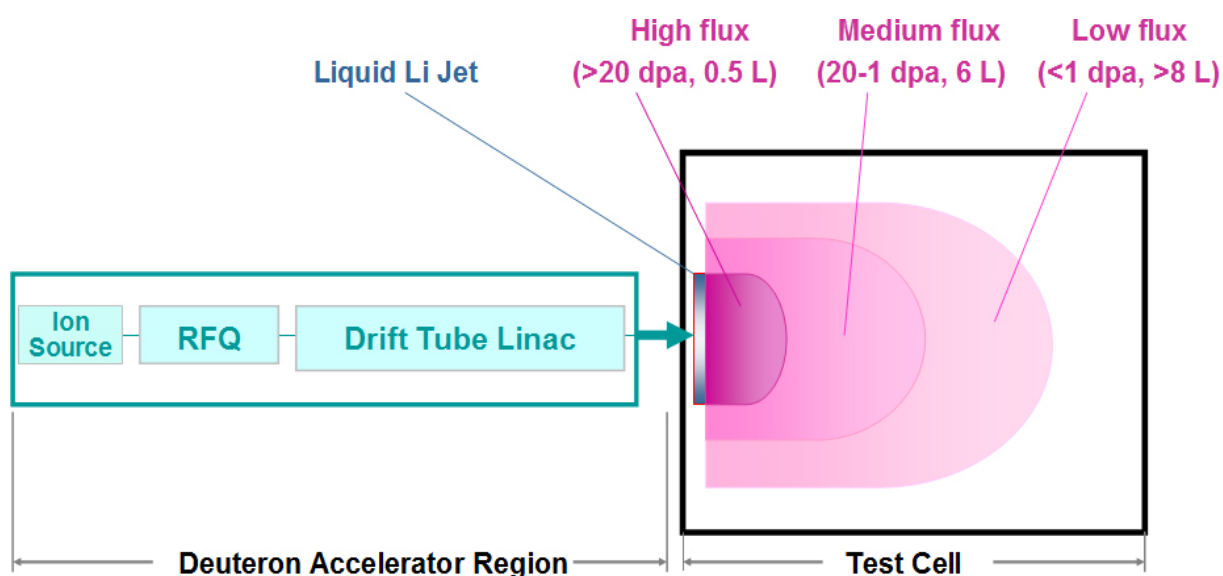

Fig. 2.2-1: Principle of the accelerator-based neutron source for IFMIF [IFM04].

As shown in Fig. 2.2-1, the proposed IFMIF facility will be able to produce comparable neutrons to those in a fusion reactor and provide an irradiation and testing volume of a reasonable size for candidate materials. With a broad spectrum peaked at 14MeV, the expected total neutron flux of $>10^{17}$n/s will be yielded via the D-Li stripping reaction by striking a liquid Li target with 250mA, 40MeV deuterons from linacs. In the test cell, there will be three regions of different-level (from high to low) neutron fluxes to allow irradiating a broad test matrix of samples and materials at the same time.

A concrete demonstration of the IFMIF plant, which is mainly composed of an accelerator system, a Li target and a test cell, is given in Fig. 2.2-2. The accelerator system consists of two identical 175MHz, CW linacs working in parallel, and each of them includes: 1) An ion source, which generates a 150mA, 100keV deuteron beam. 2) An LEBT (low energy beam transport)

section to transfer and match the beam to the accelerating structures. 3) An RFQ accelerator to provide a 125mA, 5MeV bunched beam at output. 4) A DTL accelerator to continue bringing the beam to 40MeV (in the reference design, this part was relied upon the conventional room-temperature Alvarez-type linac structure with post couplers [IFM04]; however, recently two new proposals mainly based on the state-of-the-art superconducting technology are becoming more competitive). 5) Finally an HEBT (high energy beam transport) section, which comprises a chain of non-linear multipole lenses, to tailor the beam for resulting in a flat rectangular beam footprint on the Li target.

This two-linac scheme has been adopted in order to:

- Reduce the required extremely high peak current of 250mA by a factor of two according to the capability of modern RF linacs.
- Provide operational redundancy in case of the failure of one linac.
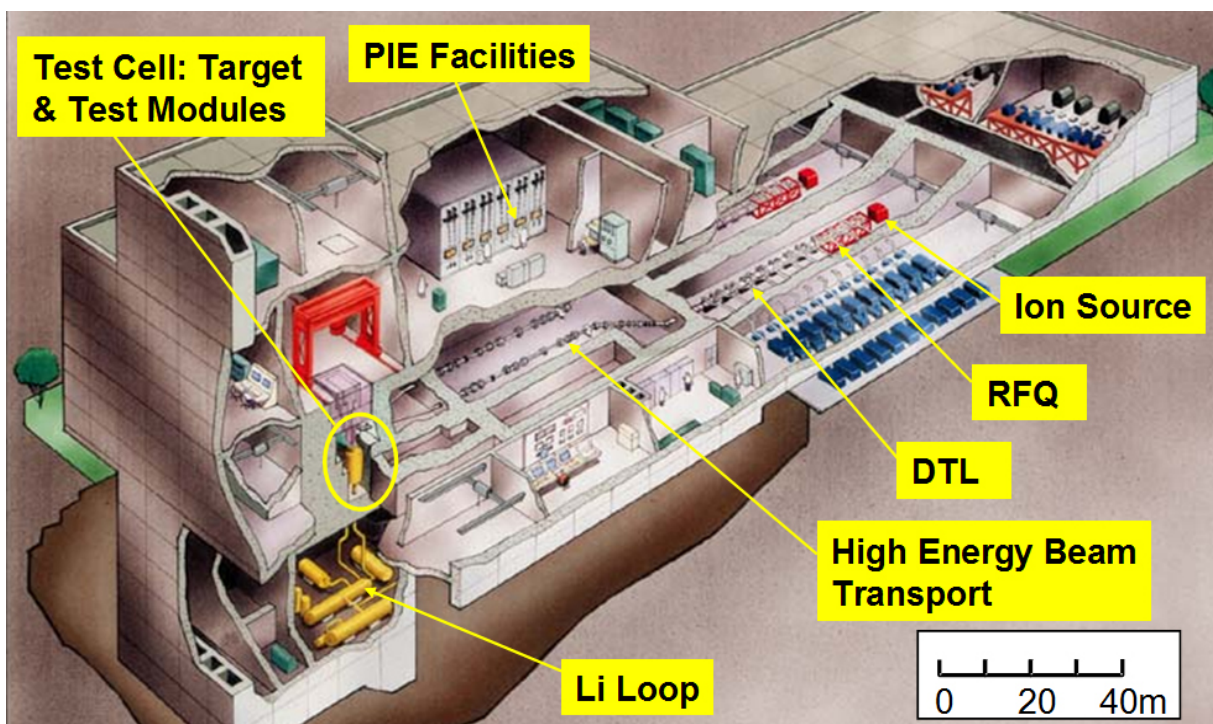

Fig. 2.2-2: An overview of the IFMIF plant [IFM04].

Figure 2.2-3 shows the number of neutrons generated by each lost deuteron as a function of the deuteron energy E_{D^+} for the D-D or D-Cu reactions which could happen in the copper accelerators [IFM96]. Clearly, the neutron yield will increase dramatically with increasing deuteron energy from 5MeV to 40MeV [IFM96].
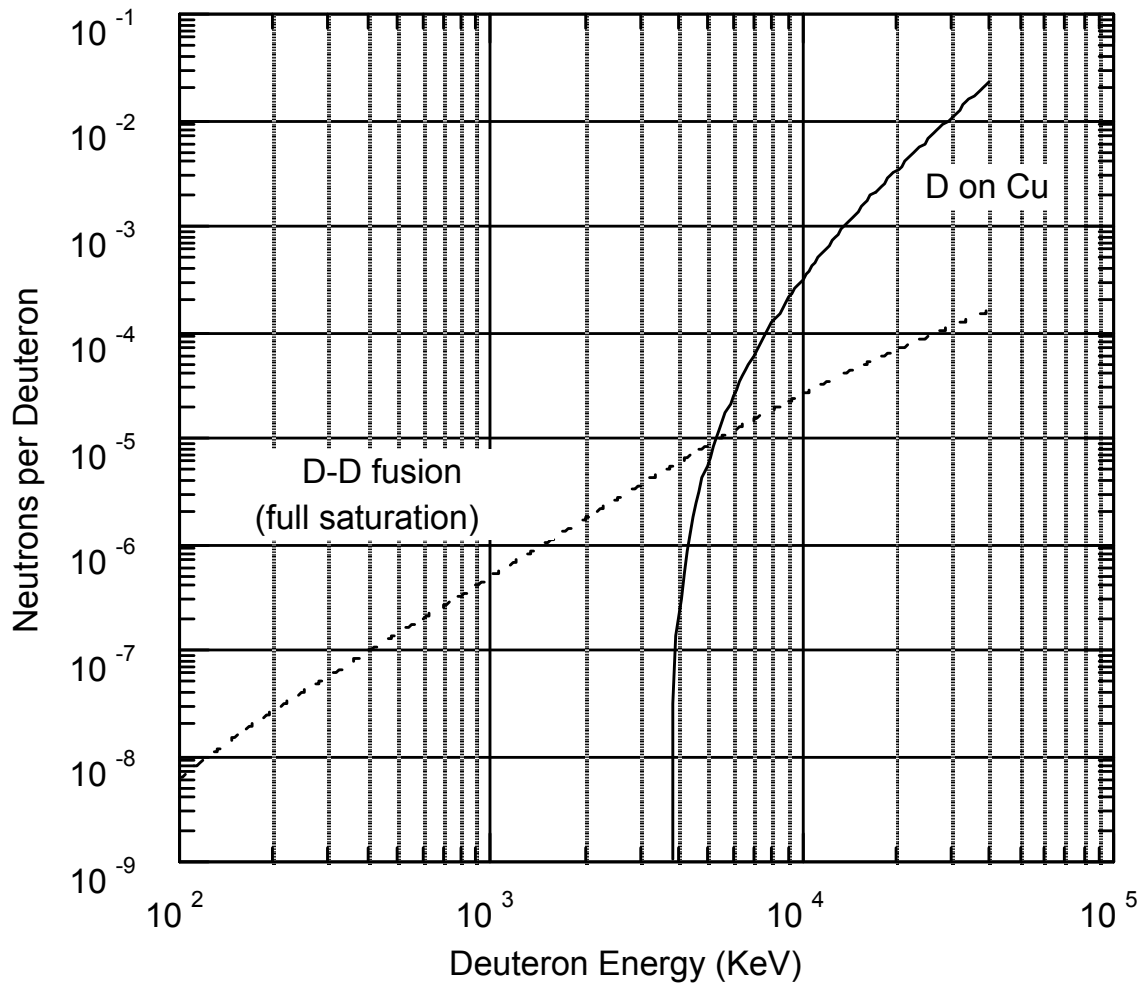
Fig. 2.2-3: Neutrons yield per lost deuteron via the D-D fusion reaction and the direct interaction of the deuterium with copper [IFM96].

For SC accelerating structures, the experiments have shown that neutron yield is lower in niobium than in copper by a factor of about two at $E_{D^+} = 10 - 15\text{MeV}$, and one could use that assumption up through 40MeV [DEL93].

Nevertheless, for the sake of hands-on maintenance, the primary concern for the design work of this intense deuteron accelerator is that almost no lost particle should appear in the DTL part.

On the other hand, in order to fulfill achieving a $20\text{cm} \times 5\text{cm}$ rectangle, uniform-distributed beam spot on the neutron-production target, it is also very important to keep the beam quality as good as possible during acceleration.

2.3 FRANZ: Frankfurt Neutron Source at the Stern-Gerlach-Zentrum

As a successor of the retired neutron source, which was based on a 3.7MV Van-de-Graaff accelerator at Forschungszentrum Karlsruhe (FZK), the FRANZ facility planned at the Stern-Gerlach-Zentrum will be able to increase the neutron intensity by three orders of magnitude, because a more advanced driver linac is possible by taking advantage of the accumulated experience in the long-term development of linear RF accelerators for low- and medium-energy beams at Institute for Applied Physics (IAP), Frankfurt University.

Table 2.3-1: Comparison of FRANZ with existing intense pulsed neutron sources [RAT07a].

Facility	Neutron flux at sample positions[*] $[cm^{-2}s^{-1}]$	Repetition rate [Hz]	Flight path [m]	Pulse width [ns]	Neutron energy range [keV]
FZ Karlsruhe	$1 \cdot 10^4$	250000	0.8	0.7	1-200
DANCE Los Alamos	$5 \cdot 10^5$	20	20	250	th-10^5
n_TOF CERN	$5 \cdot 10^4$	0.4	185	6	th-10^6
GELINA Geel	$5 \cdot 10^4$	800	30	1	th-10^5
ORELA Oak Ridge	$2 \cdot 10^4$	525	40	8	th-10^4
Elbe Dresden	$1 \cdot 10^5$	500000	3.7	0.4	50-10^4
FRANZ Frankfurt	$1 \cdot 10^7$	250000	0.8	1	1-200 (500)

* The given fluxes in Column 1 are valid only at neutron energies around 100keV.

Table 2.3-1 compares the expected performance of the FRANZ facility with the corresponding parameters of the existing intense pulsed neutron sources in the world. Obviously, FRANZ is ambitious to become the most powerful keV-range neutron source, which can provide extremely short (ΔT=1ns) neutron pulses with a pulse repeat rate up to 250kHz and a flux in the order of $10^7/$ (cm²s). The specs of such neutrons have been found very attractive for various experiments in nuclear astrophysics, transmutation physics, biophysics, materials research, detector development, and so on [RAT07a], so the FRANZ facility can not only provide in-house education in different experimental physics fields but also open a wide future of scientific research programs in cooperation with other institutes e.g. FZK and GSI.

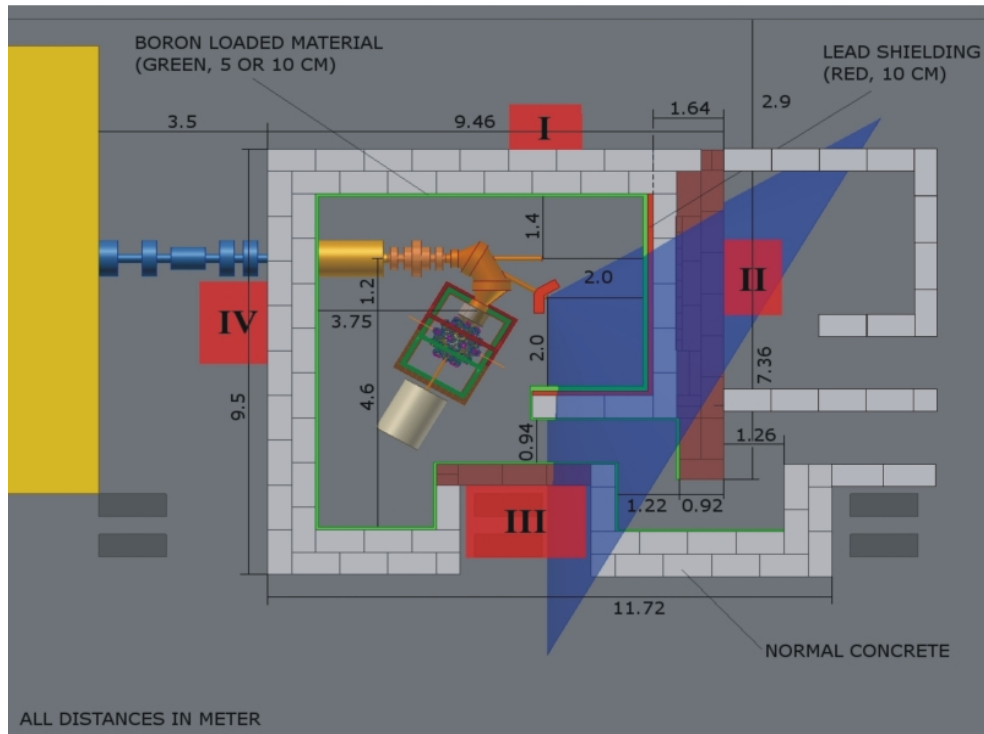Fig. 2.3-1: An overview of the FRANZ experiment hall [MEU08].

To be installed and operated at a campus, FRANZ should be first safe and compact. The maximum energy of the produced neutrons has been limited to below 500keV, according to the capability of the designed shielding system for the FRANZ experiment hall (see Fig. 2.3-1).
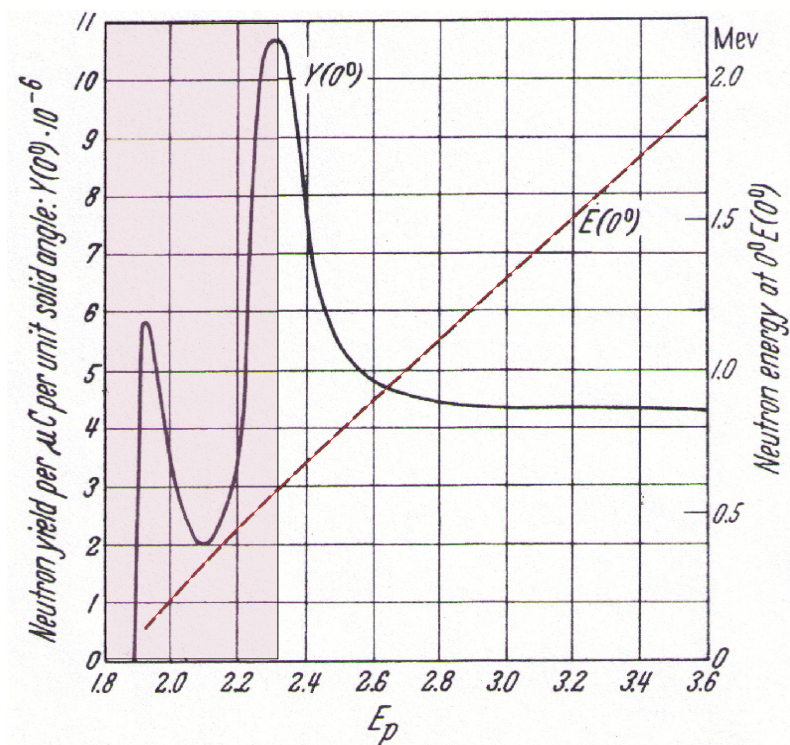

Fig. 2.3-2: Neutron yield and maximum neutron energy in forward direction (0°) [FLÜ59].

The neutron production will use the following reaction:

$$p + {}^{7}Li \rightarrow {}^{7}Be + n - 1.646\,MeV \tag{2.3-1}$$

Determined by the relationship between the neutron yield and the proton energy (see Fig. 2.3-2), the energy of the proton beam output from the 175MHz FRANZ driver linac has been chosen variable within 1.87–2.1MeV to tune the neutron energy in the range of 0–500keV. The required peak current $\sim 10^{10}$ protons/ns for the production of the demanded neutron flux will be achieved by following the Mobley's concept [MOB51] to compress 9–10 intense micro beam-bunches from the linac into one common 1ns time slot on the Li target (see Fig. 2.3-3).
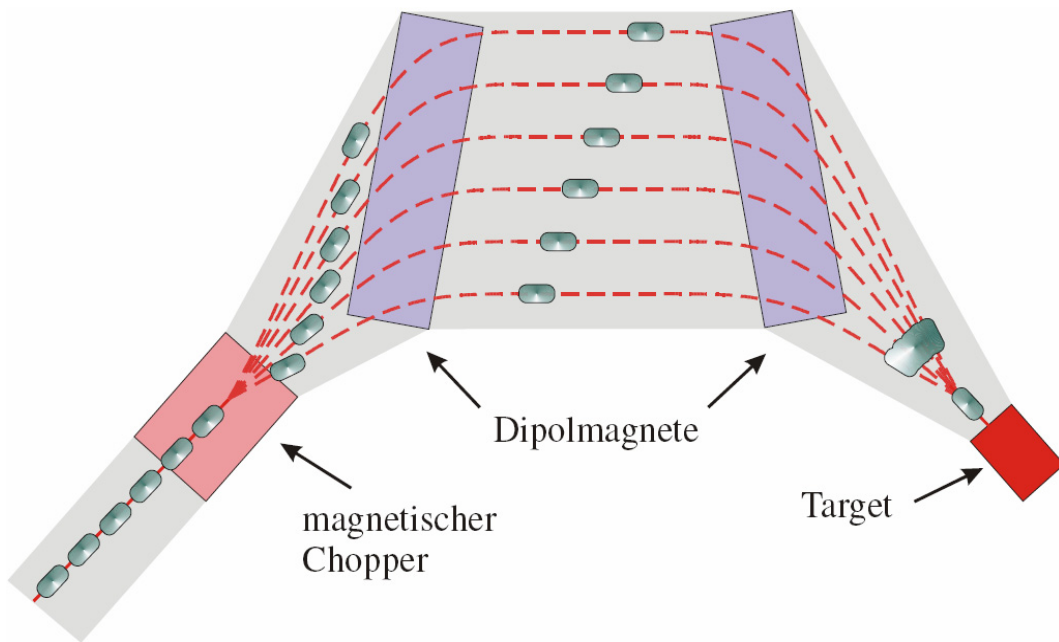
Fig. 2.3-3: Principle of the Mobley-type bunch compressor [RAT07a].

The definition of the peak beam current is given as below [PAR05]:

$$I_{beam} = qNf_{bunch} \tag{2.3-2}$$

where q is the charge per particle, N is the number of particles per bunch, and f_{bunch} is the bunch frequency. At 175MHz, if nine 150–200mA of micro-bunches from the linac are compressed, the total peak proton current on target will be 8–10A, which corresponds to ~ 4–6×10^{10} protons/ns. For the FRANZ RFQ, the design intensity has been chosen as 200mA.

200mA is a record intensity for the reported RF hadron linacs. Obviously, the greatest challenge to the FRANZ RFQ is to overcome the significantly strong space-charge effects which are close to the limit during beam bunching and acceleration. Meanwhile, how to achieve an efficient linac design with a compact structure and minimum costs is also necessary for FRANZ such a university-based facility.

3. Efficient Low- and Medium-β Linac Structures

For an RF linac, the choice of the synchronous phase φ_s, which is the phase between the RF wave and the synchronous particle, is critical. In an accelerating gap, if $\varphi_s < 0°$, the RF field is increasing with time, so a particle will see a smaller field or a larger field if it comes earlier or later than the synchronous phase, respectively, which means that all particles in the beam bunch can get a restoring force longitudinally; at the same time, however, caused by the radial components of the RF field, the defocusing effects in the second half gap will be larger than the focusing effects in the first half gap, so on the whole the beam will be defocused transversely. On the contrary, if $\varphi_s > 0°$, unstable longitudinal but stable transverse particle motions will take place. Obviously, if only the RF field is applied on the beam, there is always a contradiction between the longitudinal and radial directions in a single accelerating gap, no matter φ_s is positive or negative.

But, there are many ways to realize overall stabilities simultaneously in both longitudinal and radial planes for an accelerating channel. According to the difference in choosing φ_s, all low- and medium-β linacs can be generally reduced to four categories as follows:

- **Conventional DTL (Drift-Tube Linac, $\varphi_s < 0°$)**

  In this kind of accelerating structure, a sequence of magnetic quadrupole lenses are housed in the drift tubes for overcome the transverse instability problem. According to the Lorentz force equation $\boldsymbol{F} = q(\boldsymbol{E} + \boldsymbol{v} \times \boldsymbol{B})$, the magnetic force is proportional to the particle velocity, so there will be a technical difficulty to produce tiny but powerful magnets for a slow beam at injection, especially when the beam intensity is high.

- **RFQ (Radio-Frequency Quadrupole, $\varphi_s < 0°$)**

  Characterized by the velocity-independent electric focusing, which are provided by the RF field and realized by four electrodes (with modulations for producing the accelerating fields, see Fig. 3.1-1), the RFQ accelerator is an ideal pre-DTL injector structure.

- **APF (Alternating-Phase Focusing, $\varphi_s > 0°$ and $\varphi_s < 0°$)**

  Another idea also only using the RF field is called APF, which provides longitudinal and radial focusing forces in turn along the accelerating channel by means of a special

configuration of φ_s (e.g. the synchronous phases are of opposite signs and appropriate magnitudes in adjacent accelerating gaps) to achieve net stabilities in all planes. However, because of the shortcomings such as low acceleration rate, low current limit, design difficulty and construction complexity, APF has been only adopted by a few linacs for low pulsed currents in practice.

- **KONUS (Combined $0°$ Structure, mainly $\varphi_s = 0°$) [RAT98]**

  It applies the $0°$ synchronous phase to most accelerating cells, which can reach maximum acceleration efficiency and significantly reduce the transverse RF defocusing effects. Consequently, it is feasible to adopt lens-free slim drift tubes, which are favorable not only to achieve high shunt-impedance but also to realize multi-cell superconducting low- and medium-β accelerating structures. The accumulated defocusing effects and phase instabilities can be compensated by introducing independent magnetic lenses and short negative-synchronous-phase rebunching sections, respectively.

As one of the most efficient solutions to accelerate the low- and medium-β intense beams, the combination of the RFQ and the KONUS-based H-type DTL has many attractive features e.g. compact structures, high-intensity capacity and good beam qualities. Therefore, it has become an ideal injector candidate for large accelerators including high-power driver linacs. The first practical example of such a combination is the GSI high-charge-state injector (Hochladungsinjektor, HLI) [RAT91], which was built in 1991 and is still in routine operation now. The FRANZ, IFMIF and EUROTRANS projects will be three new important applications of this combination.

3.1 Radio-Frequency Quadrupole Accelerator

The history of the RFQ accelerator was started with an idea so-called "spatially homogeneous quadrupole focusing" proposed by Kapchinskiy and Teplyakov (K-T) in 1968 and formally published in 1970 [KAP70, VLA70]. Shown in Fig. 3.1-1, the basic idea of the RFQ accelerator is: the accelerating-field components are produced by introducing a periodic perturbation to the fundament RF quadrupole structure longitudinally while retaining the electric quadrupole focusing fields. However, the significance of this invention was not recognized until LANL (Los Alamos National Laboratory) performed a series of intensive studies to check if it could be applicable in several future accelerator programs interested in high-current, low-emittance ion

beams. In 1980, a 425MHz four-vane RFQ was built for a proof-of-principle experiment and it successfully accelerated a 26mA proton beam from 100keV to 640keV with a transmission efficiency of 87% [HAM80]. Since then, the RFQ has been quickly developed as a standard accelerating structure for low-energy (up to several MeV/u) beams.
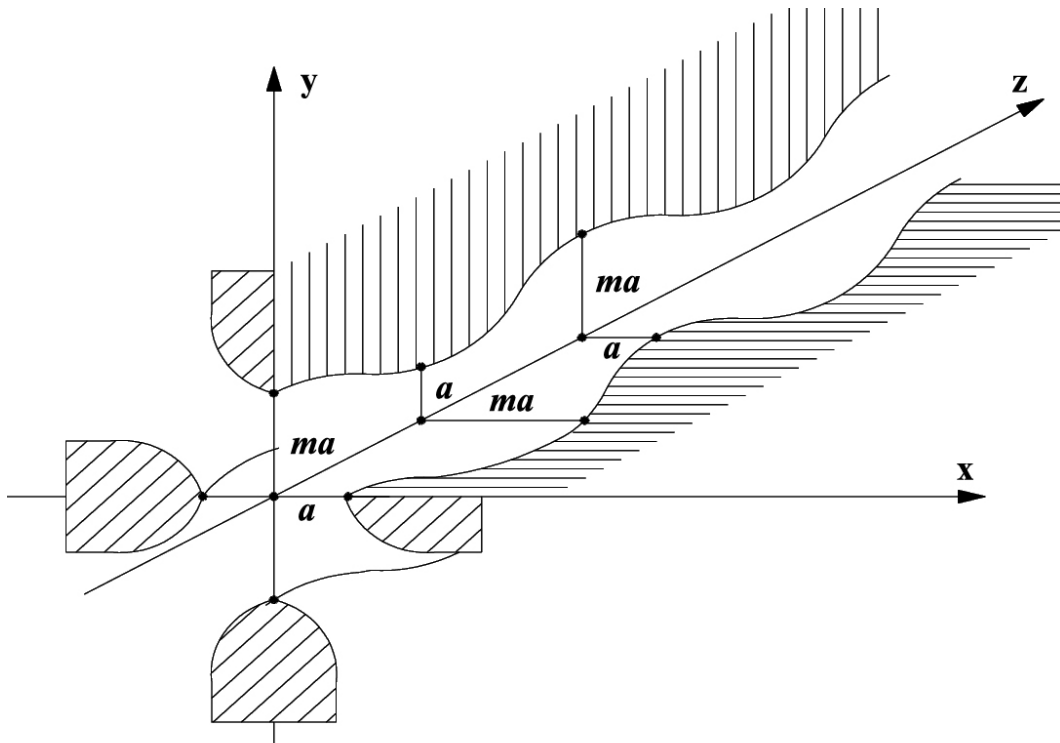

Fig. 3.1-1: RFQ electrode modulations for accelerating-field components, where *a*: minimum electrode aperture, *m*: modulation parameter, *ma*: maximum electrode aperture [LOM05].

In the last three decades, various RF geometries were developed to drive the four electrodes resonantly, but finally only a few of them have survived. Demonstrated schematically in Fig. 3.1-2, the most representative RFQ accelerating structures [KLE83] are: 1) The double-H resonator [TEP68], which has been adopted by the first experimentally tested 148.5MHz RFQ machine to accelerate an 189mA proton beam from 100 to 620keV with a transmission efficiency of 53% [GOL75]. 2) The four-vane resonator [STO79], the LANL version of the four-chamber resonator as well as the first RFQ structure developed outside of the USSR. 3) The split-coaxial resonator (SCR) [MÜL81] and the four-rod resonator [SCH83], which were invented in Germany originally for heavy-ion acceleration. Generally speaking, all RFQ resonators fall into two categories: the resonant-cavity type (e.g. double-H, 4-vane and split-coaxial) and the resonant-transmission-line (or simply as resonant-line) type (e.g. 4-rod). An overview of the main characteristics of these four kinds of RFQ structures is given in Table 3.1-1.

(a) Four-vane [STO79]

(b) Four-rod

(c) Double-H

(d) Split-coaxial
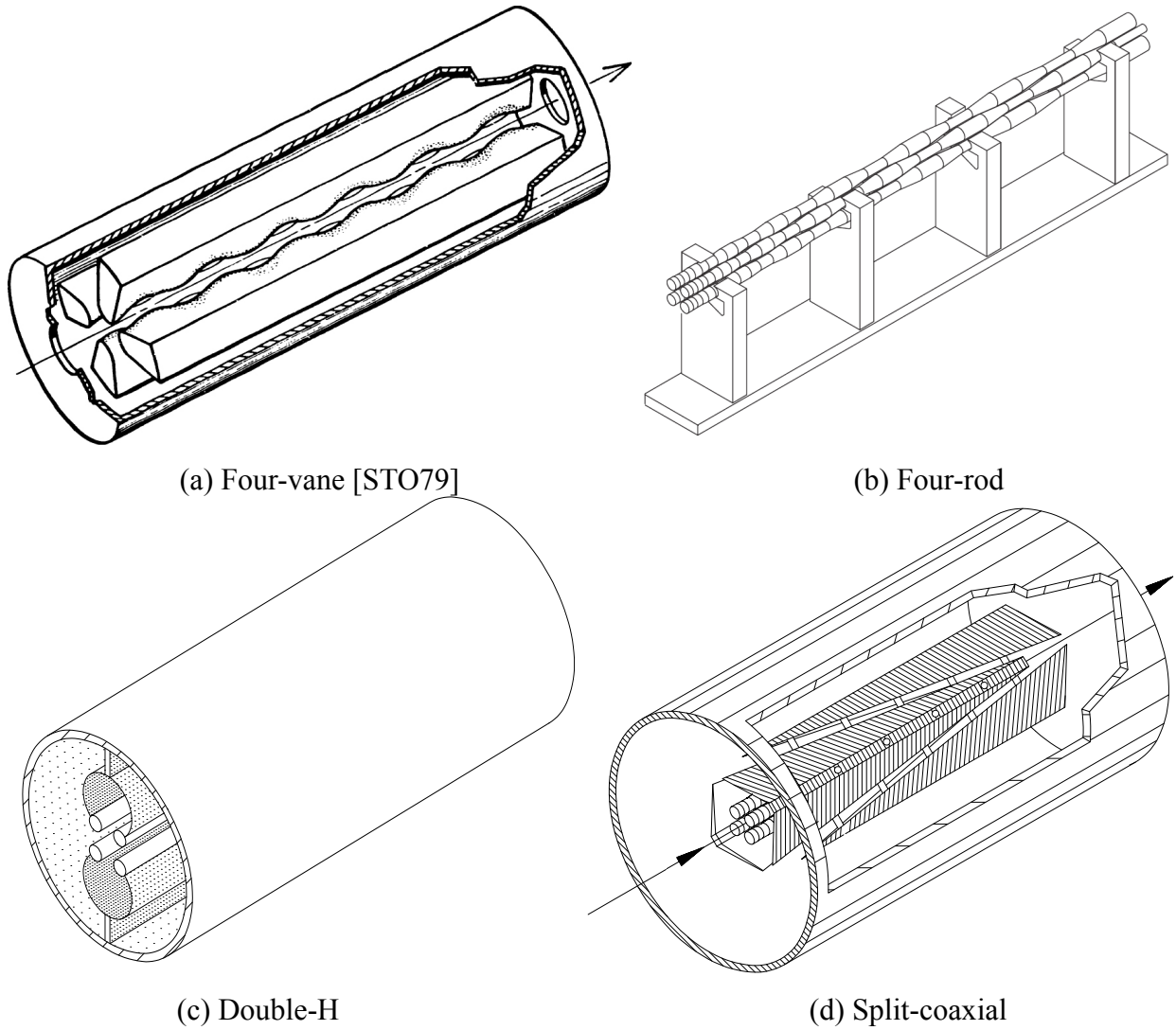
Fig. 3.1-2: Different RFQ resonators (Courtesy of A. Schempp).

Table 3.1-1: A glance at representative RFQ structures.

Feature Type	Field mode	Ion species	Typical frequency f [MHz]	Cavity dimension dependence of f
4-Vane	TE_{210}-like	mainly light ions	100 – 400	mainly on radial dimensions
4-Rod	π-0-$\lambda/2$	hydrogen to uranium	5 – 200	almost independent to the cavity dimensions
Double-H (IH)	TE_{110}-like	mainly light ions	100 – 400 ($\leq$100)	mainly on radial dimensions
SCR	TEM-like	mainly heavy ions	several to ~100	on both longitudinal and radial dimensions

In the following text, the fundamental working principle of the RFQ accelerator will be briefly introduced in one subsection, while the other two subsections will present the 4-rod and 4-vane RFQ geometries, which have been chosen as the initial accelerating structures by the FRANZ, IFMIF and EUROTRANS facilities, respectively.

3.1.1 Principle of Operation

The essential parts of an RFQ accelerator are the four electrodes, which are symmetrically surrounding the beam axis and in alternating polarities. Fig. 3.1.1-1 shows a profile plot of a pair of adjacent RFQ electrodes and their surface electric-field components. In the picture, it is clear that: 1) The cell length L_{cell} of an RFQ accelerator is $\beta_s \lambda / 2$. 2) At the two ends of a cell, one opposed pair of electrodes has the minimum distance a from the axis, while another pair of electrodes has the maximum distance ma from the axis. 3) At the middle of a cell where the RFQ accelerator has quadrupole symmetry, all electrodes are equidistant to the axis and the distance r_0 is called the mid-cell aperture or the effective aperture.
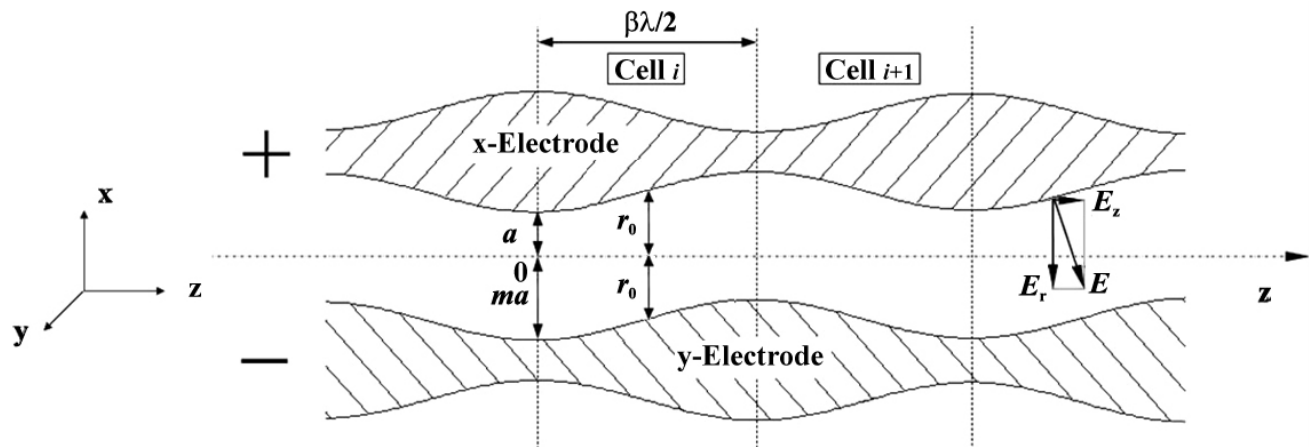
Fig. 3.1.1-1: RFQ electrodes and the electric-field components [SCH96].

Using the cylindrical coordinates, the electric-field potential with the time variation included can be written as:

$$U(r,\theta,z,t) = V(r,\theta,z)\sin(\omega t + \phi) \qquad (3.1.1\text{-}1)$$

where ω is the angular frequency of the RF field and ϕ is the initial phase. Because in an RFQ accelerator the electric fields are concentrated between the four electrode tips, which form a volume with much smaller dimensions than the RF wavelength, the quasi-static approximation

[WAN08] can be used to describe the electric-field potential. Therefore, $V(r,\theta,z)$ satisfies the following Laplace's equation:

$$\nabla^2 V(r,\theta,z) = \frac{\partial^2 V}{\partial r^2} + \frac{1}{r}\frac{\partial V}{\partial r} + \frac{1}{r^2}\frac{\partial^2 V}{\partial \theta^2} + \frac{\partial^2 V}{\partial z^2} = 0 \qquad (3.1.1\text{-}2)$$

Demonstrated in Fig. 3.1.1-1, it is clear that Eq. (3.1.1-2) should satisfy the following conditions determined by the geometry characteristics of the RFQ (e.g. quadrupole symmetry and longitudinal modulations):

$$\begin{cases} V(r,\theta,z) = V(r,\theta,-z) \\ V(r,\theta,z) = V(r,\theta,z+\beta\lambda) \\ V(r,\theta,z) = V(r,-\theta,z) \\ V(r,\theta,z) = V(r,\pi\pm\theta,z) \\ V(r,\theta,z) = -V(r,\theta\pm\frac{\pi}{2},\frac{\beta\lambda}{2}-z) \end{cases} \qquad (3.1.1\text{-}3)$$

Based on the above five conditions and the method of separation of variables, one can obtain a general solution for Eq. (3.1.1-2) as below:

$$V(r,\theta,z) = \frac{V_0}{2}\left\{\sum_{s=0}^{\infty} A_{0,(2s+1)} r^{2(2s+1)} \cos[2(2s+1)\theta] + \sum_{n=1}^{\infty}\sum_{s=0}^{\infty} A_{ns} I_{2s}(nkr)\cos(2s\theta)\cos(nkz)\right\} \qquad (3.1.1\text{-}4)$$

where $s+n=2p+1$ (p=0, 1, 2, …), $V_0/2$ is the electrode potential, I_{2s} is the modified Bessel function of order $2s$, and $k = \frac{2\pi}{\beta_s \lambda}$ with β_s being the ratio of the velocity of the synchronous particle to the speed of light in vacuum and λ being the RF wavelength.

Owning an infinite number of terms, however, this solution is impractical for use. Therefore, K-T proposed to choose a proper geometry of the electrode to make the lowest-order terms most important to the beam so that the other terms can be ignored. When s=0 and n=1, Eq. (3.1.1-4) has the form of:

$$V(r,\theta,z) = \frac{V_0}{2}[A_{01}r^2\cos(2\theta) + A_{10}I_0(kr)\cos(kz)] \qquad (3.1.1\text{-}5)$$

where A_{01} and A_{10} are two constants determined by the electrode geometry. In Eq. (3.1.1-5), the first term describes the potential of an electric quadrupole for focusing, and the second one provides a longitudinal field for acceleration. It is, therefore, called as the two-term potential function, an important basis of the RFQ beam dynamics.

Because $V(r,\theta,z)$ is constant along an electrode, one gets the following relationships from Fig. 3.1.1-1:

$$V(a,0,0) = V\left(r_0,0,\frac{\beta_s\lambda}{4}\right) = V\left(ma,0,\frac{\beta_s\lambda}{2}\right) = \frac{V_0}{2} \tag{3.1.1-6}$$

Consequently, A_{01} and A_{10} can be solved from Eq. (3.1.1-5) as:

$$\begin{cases} A_{10} = \dfrac{m^2-1}{m^2 I_0(ka)+I_0(kma)} \\[2ex] A_{01} = \dfrac{1}{a^2}\dfrac{I_0(ka)+I_0(kma)}{m^2 I_0(ka)+I_0(kma)} = \dfrac{1}{r_0^2} \end{cases} \tag{3.1.1-7}$$

For the sake of convenience, another two dimensionless coefficients are defined as:

$$\begin{cases} A \equiv A_{10} \\ X \equiv A_{01}a^2 = 1 - AI_0(ka) \end{cases} \tag{3.1.1-8}$$

where A and X are known as the acceleration efficiency factor and the focusing efficiency factor, respectively. In case of no electrode modulation (i.e. m=1), one gets A=0 and $X=1$, so the RFQ of the moment is only a pure electric quadrupole focusing channel. When m increases, A also increases, which implies that the longitudinal electric field is produced; but at the same time X decreases, which imposes an upper limit on m because a sufficient focusing efficiency should be ensured to confine the beam. The typical beam-energy range covered by the RFQ accelerator is from several keV/u to several MeV/u.

Substituting $A_{01} = X/a^2$ and $A_{10} = A$ into Eq. (3.1.1-5), one gets:

$$V(r,\theta,z) = \frac{V_0}{2}\left[X\left(\frac{r}{a}\right)^2\cos(2\theta) + AI_0(kr)\cos(kz)\right] \tag{3.1.1-9}$$

In Cartesian coordinates (x=$r\cos\theta$, y=$r\sin\theta$), the above equation can be rewritten as:

$$V(x,y,z) = \frac{V_0}{2}\left[\frac{X}{a^2}(x^2-y^2) + AI_0(kr)\cos(kz)\right] \tag{3.1.1-10}$$

As the gradients of the above potential function, the electric-field components for the three dimensions – each should be multiplied by $\sin(\omega t+\phi)$ – can be obtained as below:

$$\begin{cases} E_x = -\dfrac{XV_0}{a^2}x - \dfrac{kAV_0}{2}I_1(kr)\dfrac{x}{r}\cos(kz) \\[2ex] E_y = \dfrac{XV_0}{a^2}y - \dfrac{kAV_0}{2}I_1(kr)\dfrac{y}{r}\cos(kz) \\[2ex] E_z = \dfrac{kAV_0}{2}I_0(kr)\sin(kz) \end{cases} \tag{3.1.1-11}$$

Considering the paraxial particle motion in one of the transverse planes (e.g. the xoz plane), one gets:

$$\frac{d^2x}{dt^2} = \frac{q}{M}E_x \tag{3.1.1-12}$$

where q is the charge and M is the mass.

Linearizing for small arguments, $I_1(kr) \approx kr/2$, one obtains:

$$\frac{d^2x}{dt^2} + \left[\frac{qXV_0}{Ma^2} + \frac{qk^2AV_0}{4M}\cos(kz)\right]x\sin(\omega t + \phi) = 0 \tag{3.1.1-13}$$

In the square brackets of the above equation, the left term is the quadrupole focusing term, and the right one is the RF defocusing term due to the electrode modulation. Because $kz = \dfrac{2\pi z}{\beta\lambda} = \omega t$, Eq. (3.1.1-13) can be transformed to:

$$\frac{d^2x}{dt^2} + \left\{\frac{qXV_0}{Ma^2}\sin(\omega t + \phi) + \frac{qk^2AV_0}{8M}\left[\sin(2\omega t + \phi) + \sin\phi\right]\right\}x = 0 \tag{3.1.1-14}$$

As $\overline{\sin(2\omega t + \phi)}$ equals to 0 for one unit cell, the term containing this factor can be ignored if x is assumed constant throughout the cell. By this, Eq. (3.1.1-14) can be simplified to:

$$\frac{d^2x}{dt^2} + \left[\frac{qXV_0}{Ma^2}\sin(\omega t + \phi) + \frac{qk^2AV_0}{8M}\sin\phi\right]x = 0 \tag{3.1.1-15}$$

Replacing the independent variable t by $\tau = \dfrac{\omega t + \phi}{2\pi}$, one obtains the following equations in the form of the well-known Mathieu equation as:

$$\begin{cases} \dfrac{d^2x}{d\tau^2} + [\Delta_{rf} + B\sin(2\pi\tau)]x = 0 \\[2mm] \dfrac{d^2y}{d\tau^2} + [\Delta_{rf} - B\sin(2\pi\tau)]y = 0 \\[2mm] \dfrac{d^2z}{d\tau^2} + (-2\Delta_{rf})z = 0 \end{cases} \tag{3.1.1-16}$$

with:

$$\begin{cases} \Delta_{rf} \equiv \dfrac{\pi^2 qAV_0\sin\phi}{2Mc^2\beta^2} \\[3mm] B \equiv \dfrac{qXV_0\lambda^2}{Mc^2a^2} \end{cases} \tag{3.1.1-17}$$

where Δ_{rf} is the RF defocusing factor, and B is the transverse focusing strength (a more frequently used physical quantity than the focusing efficiency factor X in the beam dynamics design studies).

Using the smooth approximation, the external-field phase advance of the transverse oscillations per focusing period can be evaluated from Eqs. (3.1.1-16) as:

$$\sigma_{0t}{}^2 = \frac{B^2}{8\pi^2} + \Delta_{rf} \tag{3.1.1-18}$$

Similarly, the longitudinal zero-current phase advance per focusing period can be expressed in the form of:

$$\sigma_{0l}{}^2 = -2\Delta_{rf} \tag{3.1.1-19}$$

Including the space-charge effects, Eqs. (3.1.1-16) should be modified by adding the corresponding defocusing factors $\Delta_{sc,l}$ and $\Delta_{sc,t}$ as:

$$\begin{cases} \dfrac{d^2x}{d\tau^2} + [\Delta_{rf} + \Delta_{sc,t} + B\sin(2\pi\tau)]x = 0 \\[2mm] \dfrac{d^2y}{d\tau^2} + [\Delta_{rf} + \Delta_{sc,t} - B\sin(2\pi\tau)]y = 0 \\[2mm] \dfrac{d^2z}{d\tau^2} + (-2\Delta_{rf} + \Delta_{sc,l})z = 0 \end{cases} \tag{3.1.1-20}$$

with:

$$\begin{cases} \Delta_{sc,t} = -\dfrac{3Z_0 qI\lambda[1-f(p)]}{8\pi M_0 c^2 R_t^2 R_l \beta_s^2 \gamma^3} \\[3mm] \Delta_{sc,l} = -\dfrac{3Z_0 qI\lambda f(p)}{4\pi M_0 c^2 R_t^2 R_l \beta_s^2 \gamma^3} \end{cases} \tag{3.1.1-21}$$

where $\Delta_{sc,l}$ and $\Delta_{sc,t}$ are obtained using a three-dimensional ellipsoid model for a beam bunch with the following related parameters [GLU70, WAN80]:

R_t:　　the mean transverse radius of the bunch

R_l:　　the longitudinal radius of the bunch

I:　　　the average beam current

$f(p)$:　　the ellipsoid form factor

$$f(p \equiv R_l / R_t) = \begin{cases} \dfrac{1}{1-p^2} - \dfrac{p\cos^{-1}p}{(1-p)^{3/2}} & (p<1) \\[3mm] \dfrac{p\cosh^{-1}p}{(p^2-1)^{3/2}} - \dfrac{1}{p^2-1} & (p>1) \\[3mm] \dfrac{1}{3} & (p=1) \end{cases} \tag{3.1.1-22}$$

For $0.8 < p < 5$, $f(p) \approx \dfrac{1}{3p}$

Z_0:　　the free-space impedance ($Z_0 = \dfrac{1}{\varepsilon_0 c} = 376.73\Omega$).

Accordingly, the phase advances with space charge per focusing period can be given as:

$$\begin{cases} \sigma_t^{\,2} = \dfrac{B^2}{8\pi^2} + \Delta_{rf} + \Delta_{sc,t} \\[2mm] \sigma_l^{\,2} = -2\Delta_{rf} + \Delta_{sc,l} \end{cases} \tag{3.1.1-23}$$
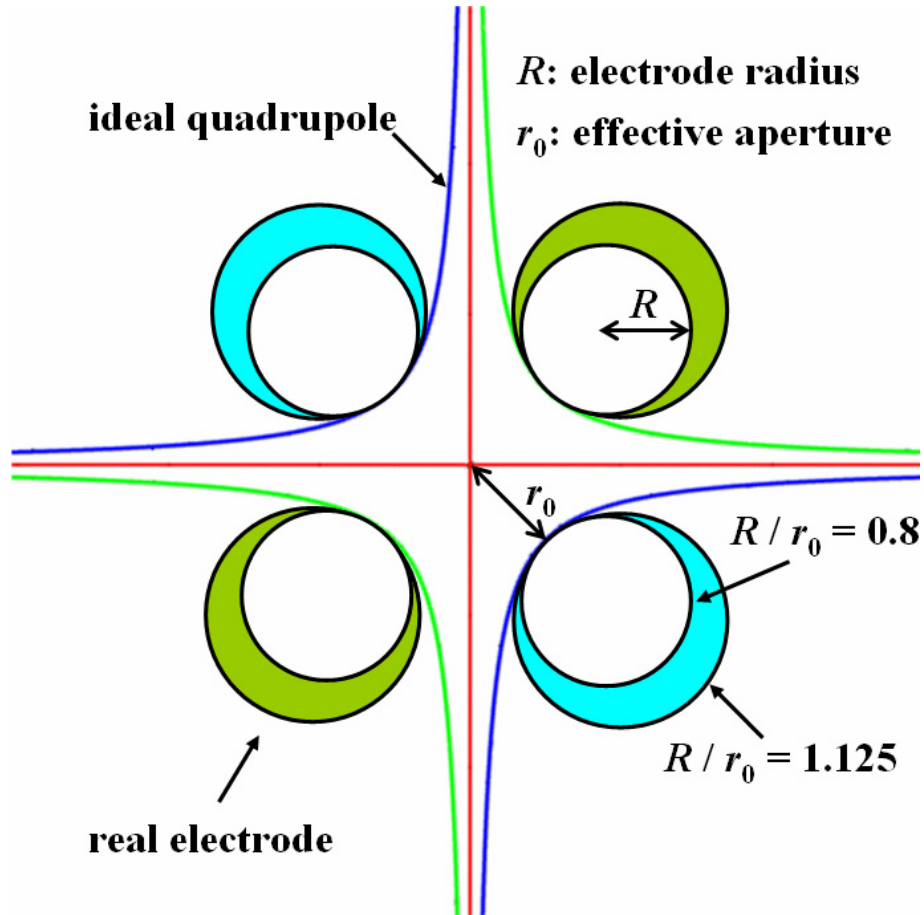

Fig. 3.1.1-2: Ideal and real RFQ electrode tips.

The electrode-tip surfaces specified by the two-term potential should have the forms of hyperbolae as shown in Fig. 3.1.1-2. In practice, however, they are not feasible because of two reasons: 1) The inconvenience for machining. 2) A high sparking risk induced by the too narrow minimum gap distance between the adjacent electrodes. Demonstrated also in the picture, the electrodes used in reality usually have circular cross-sections, so the two-term potential description should be improved to represent the quadrupole symmetry and longitudinal periodicity modulation of the real electrodes more exactly. In early 1991, the first eight terms of Eq. (3.1.1-4) were introduced into the PARMTEQ (Phase And Radial Motion in Transverse Electric Quadrupoles) simulation code and the code was consequently renamed as PARMTEQM, whereas "M" means "Multipoles" [PAR05]. The eight terms are the non-periodic quadrupolar and do-

decapolar terms (A_{01}, A_{03}), the first periodic monopolar, octopolar, dodecapolar and quadrupolar terms (A_{10}, A_{12}, A_{23}, A_{21}), and the second periodic monopolar and octopolar terms (A_{30}, A_{23}). The potential function used by the PARMTEQM code is:

$$V(r,\theta,z) = \frac{V_0}{2}\left\{\begin{array}{l} A_{01}\left(\dfrac{r}{r_0}\right)^2\cos(2\theta) + A_{03}\left(\dfrac{r}{r_0}\right)^6\cos(6\theta) \\ + A_{10}I_0(kr)\cos(kz) + A_{12}I_4(kr)\cos(4\theta)\cos(kz) \\ + A_{23}I_6(2kr)\cos(6\theta)\cos(2kz) + A_{21}I_2(2kr)\cos(2\theta)\cos(2kz) \\ + A_{30}I_0(3kr)\cos(3kz) + A_{32}I_4(3kr)\cos(4\theta)\cos(3kz) \end{array}\right\} \quad (3.1.1\text{-}24)$$

where the non-periodic coefficients are normalized by r_0.

3.1.2 Four-Rod Structure

Essentially, the 4-rod RFQ structure is a multi-cell Quarter-Wave Resonator (QWR or $\lambda/4$ resonator). In a $\lambda/4$ resonator cell as illustrated in Fig. 3.1.2-1, the supporting parts i.e. the stems are shortcut at one end to use the nodes of the voltage, and they are conducted by the capacitive electrodes at the another end to achieve a certain voltage.
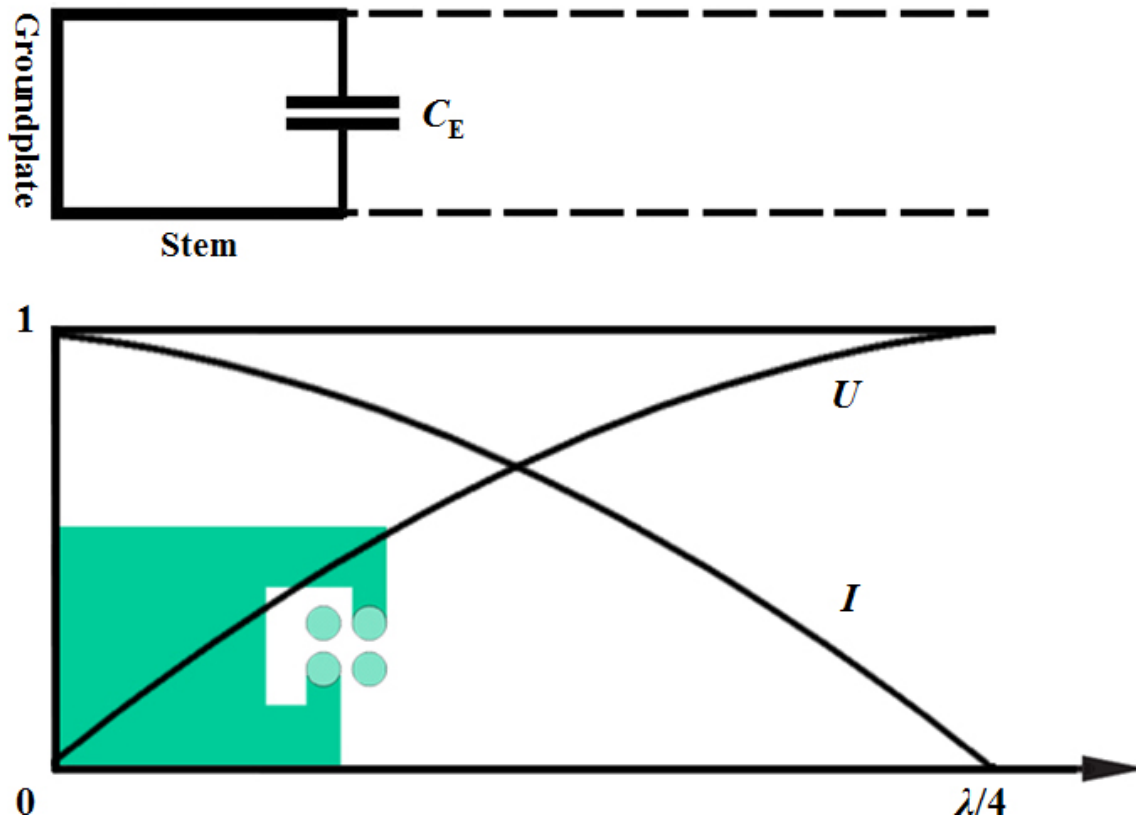

Fig. 3.1.2-1: Principle of a $\lambda/4$ resonant-line structure.

Schematically, Fig. 3.1.2-2 gives a part of the side view of a 4-rod RFQ. Clearly, the 4-rod RFQ is a chain of λ/4 resonator cells coupled together by the magnetic field lines surrounding the stems. The voltages on any two neighboring electrodes are of equal amplitudes but reverse signs. The opposite electrodes which have a same voltage sign form a pair, and an array of stems, whose bottoms are grounded on a common ground-plate, are alternately carrying the different pairs of electrodes. Traditionally, the electrodes have the rod shape; however, a kind of mini-vane like electrodes with very similar RF properties are more popular due to the convenient water-cooling and the better mechanical stability at high beam currents and high duty factors.
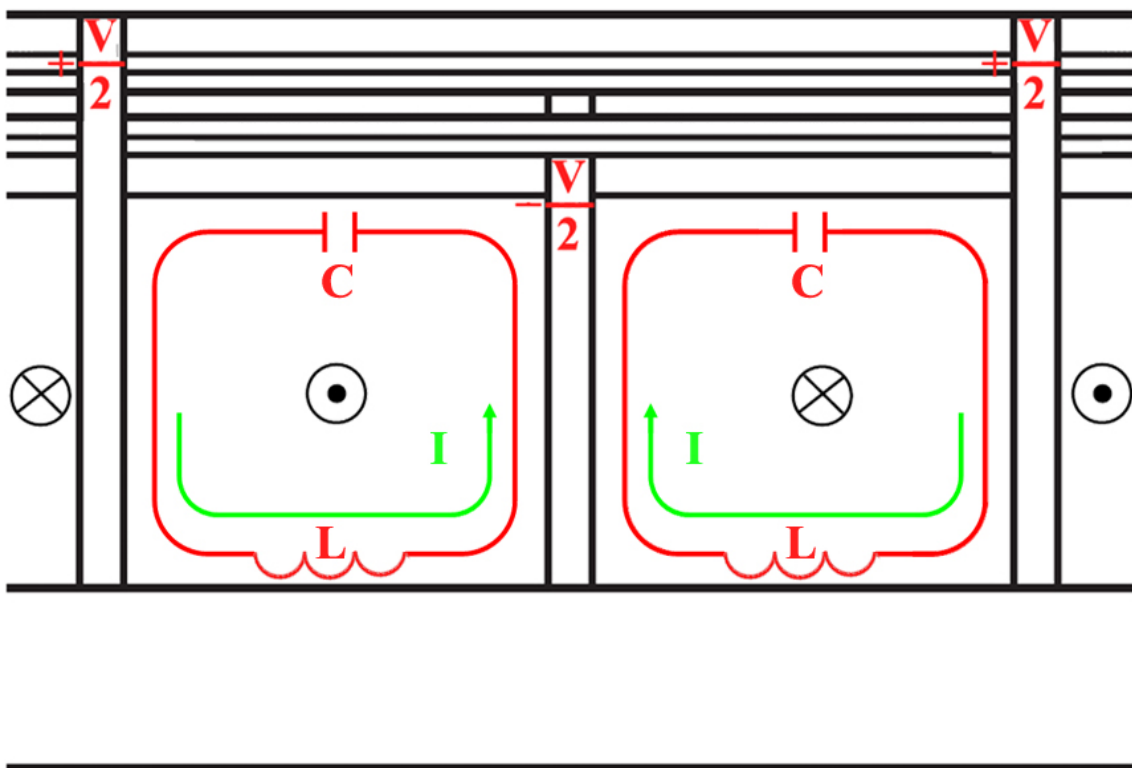

Fig. 3.1.2-2: Side view of a part of the 4-rod RFQ.

The 4-rod RFQ belongs to the family of resonant-line structures, so its resonant frequency f is mainly decided by the height of the stems, the distance between neighboring stems and the ratio of the electrode radius to the electrode aperture. In this case, therefore, the cavity wall has very little influence on the inner structure and is mainly used for RF radiation shielding and vacuum keeping. Consequently, it gives the advantages as follows:

- Because the transverse dimensions of the cavity have no direct relationship with f, the 4-rod RFQ can be always compact even at low frequencies (typically, a 4-rod RFQ has only about a half of the radial dimension of a resonant-cavity one at a low frequency).

- The auxiliaries such as tuner and RF couplers can be easily added on the cavity wall without worries to compensate the influences.

- It is also permitted opening a long groove on the cavity wall to make the installation, alignment and tuning processes more simply.

Compared with the 4-vane RFQ, the 4-rod RFQ usually has a relatively lower quality factor Q, because the concentrated RF field on the inner structure causes an about 2–4 times higher RF power density. Generally speaking, it is a challenge for a 4-rod RFQ to work at very high frequencies, say over 350MHz, especially in case of CW operation. Nevertheless, the specific shunt impedance:

$$R_\mathrm{p} = \frac{U_\mathrm{inter\text{-}vane}^2 \times L_\mathrm{tank}}{P}$$

(3.1.2-1)

and the required RF power are usually still comparable for both structures.

Another highlighted advantage of the 4-rod RFQ is the excellent flexibility. The inner structure of a 4-rod RFQ can be easily adjusted to meet different practical demands: 1) First, keeping the cavity compact, the 4-rod RFQ can either use straight stems for light-ion acceleration at a high resonant frequency e.g. 200MHz or use spiral stems for heavy-ion acceleration at a low frequency even several MHz. 2) Second, if the stem spacing permits, cylindrical stems can be applied to reduce the high power density on the sharp edges of the straight stems. 3) Last but not least, by means of a moveable tuning plate, the 4-rod RFQ provides the possibility to vary the resonant frequency or the output energy without changing the structure itself [ENG96].

Because of the mentioned features, the 4-rod structure will be adopted for the 175MHz FRANZ RFQ.

3.1.3 Four-Vane Structure

At high frequencies, the skin effect becomes significant, so the cooling of a room-temperature resonant-line structure is usually difficult. In this case, the 4-vane RFQ, a kind resonant-cavity structure which is of a relatively even RF power density, is more favorable. As shown in Fig. 3.1.3-1, the 4-vane RFQ consists of a conducting cavity loaded with four vane-like electrodes, which equally divide the cavity into four quadrants. Because of the vane geometry, it can be easily cooled and operated at CW. Working in a TE_{210}-like mode, the 4-vane RFQ cavity excites the electric field near the vane tips transversely and the magnetic field parallel to the beam axis in the quadrants longitudinally. Obviously, the RF properties of a 4-vane RFQ are determined by not only the electrodes but also the cavity wall.

Fig. 3.1.3-1: An equivalent circuit model for the 4-vane RFQ.

Meanwhile, the coupling between the four quadrants is weak, as the magnetic field lines have to travel long paths. Therefore, the 4-vane RFQ structure is relatively sensitive to mechanical machining errors. A quadrupole asymmetry will result in unequal RF excitation in each quadrant, and consequently unwanted dipole modes, which can influence the beam acceleration harmfully and can cause emittance growth even particle losses, will appear. On the other hand, mechanical errors and the cavity auxiliaries e.g. coupler loops, tuner and vacuum ports also interfere with the field tilts of the 4-vane RFQ structure. The longitudinal field tilt sensitivity is proportional to $(L_{\text{tank}} / \lambda)^2$, where L_{tank} is the structure length and λ is the wave length, so a suggested length threshold of a 4-vane cavity is $L_{\text{tank}} \leq 2\lambda$ [JAM84]. To some extent, it also decides that this kind of RFQ is more suitable to work at high frequencies.

For the 350MHz, CW LEDA (Low-Energy-Demonstration Accelerator) RFQ [YOU94] such an 8-meter-long 4-vane machine (see Fig. 3.1.3-2), LANL has successfully developed a new construction method to separate the whole RFQ into several individually driven structures and then to couple them together. Now, this coupled-cavity technique has become a standard

method followed by all subsequent large 4-vane RFQ accelerators, also including the newly-planned IFMIF-RFQ and EUROTRANS-RFQ. Certainly, more manufacture difficulties and costs have to be faced.

Fig. 3.1.3-2: The 8m-long LEDA-RFQ accelerator [YOU94].

3.2 H-Type Drift-Tube Linac

Owning a dominant longitudinal electric-field component, the TM (Transverse Magnetic) modes are the natural choices for the conventional linacs, e.g. the Alvarez-type accelerator. Since J.P. Blewett pointed out that the Interdigital H-type (IH) drift-tube linac structure could be an attractive solution for proton beam acceleration up to 30MeV at the 1956 CERN symposium [BLE56], the H-type structure has been intensively studied. Because of the excellent behavior in many aspects, such as the RF efficiency, the beam quality and the operation reliability, the H-type DTL has been developed as an important branch of the linear hadron accelerators during the last several decades.

Table 3.2-1: A comparison between the Alvarez-type DTL and the H-type DTL.

Structure / Feature	Alvarez-type	H-type
Field mode	TM_{010}	IH: $TE_{11(0)}$ CH: $TE_{21(0)}$
Structure mode	2π	π
Period length	$\beta_s \lambda$	$\beta_s \lambda / 2$
β range	$0.04 - 0.5$	$0.016 - 0.5$
Frequency range [MHz]	$100 - 400$	$30 - 800$
Max. achievable accelerating gradient [MV/m]	2	IH: 10.7 CH: 7
Operation mode	RT	RT & SC

Compared with the Alvarez-type linac, the H-type structure mainly has the following advantages (see Table 3.2-1):

- Low RF losses on the cavity wall because of the cross-sectional current flow paths.
- Low capacity load per length due to the slim drift-tube geometry.
- Wider applicable energy and frequency ranges.
- Significantly higher achievable accelerating gradients.
- Possible superconducting operation.

Though applicable also for conventional beam dynamics strategies, the H-type DTL accelerators together with the special KONUS concept are particularly efficient for accelerating low- and medium-β beams. In Fig. 3.2-1, the realized room-temperature and superconducting KONUS-based H-type DTL structures at Frankfurt University are presented.
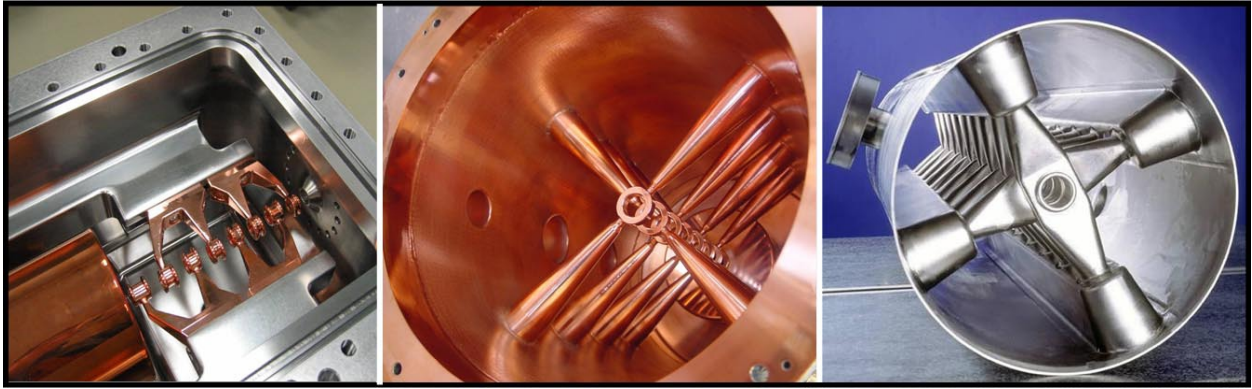
Fig. 3.2-1: H-type DTL family [POD07]

(left: the 216.816MHz RT IH-DTL for HICAT; middle: the 340MHz RT CH-DTL Prototype for FAIR; right: the 360MHz SC CH-DTL Prototype).

3.2.1 Combined 0° Structure

The structure of a multi-cell RF linear accelerator is usually designed for a fixed β-profile of the synchronous particle. Using the paraxial approximation i.e. the displacement of a particle from the axis r is assumed constant through a cell, the energy gain of this particle is [WAN08]:

$$\Delta W = qV_0 T(r,k)\cos\varphi_s \qquad (3.2.1-1)$$

with:

$$\begin{cases} V_0 \equiv \int_{-L/2}^{L/2} E(0,z)dz \\ T(r,k) \approx \int_{-L/2}^{L/2} E(r,z)\cos(kz)dz / V_0 \end{cases} \qquad (3.2.1-2)$$

where q is the charge, φ_s is the synchronous phase, V_0 is the axial RF voltage, L is the cell length, and T is the so-called transit time factor which is always <1 as a reduction factor of the energy gain due to the time-varying RF field.

Around the "ideal" synchronous particle, the "real" particles of the accelerated beam bunch, which have more or less different positions, divergence angles, phases and energies, will perform the so-called synchrotron oscillations. Such oscillations can be described by the energy difference ($\Delta W_{i,s} = W_i - W_s$) and the phase difference ($\Delta \varphi_{i,s} = \varphi_i - \varphi_s$) between a test particle in the bunch and the synchronous particle. The variations of $\Delta \varphi_{i,s}$ and $\Delta W_{i,s}$ with position satisfy the following "synchronous equations" [LAP00]:

$$\begin{cases} \dfrac{d\Delta\varphi_{i,s}}{dz} = \omega(\dfrac{dt_i}{dz} - \dfrac{dt_s}{dz}) = \dfrac{\omega}{c}(\dfrac{1}{\beta_i} - \dfrac{1}{\beta_s}) \approx -\dfrac{\omega}{\beta_s c}\dfrac{\Delta\beta_{i,s}}{\beta_s} = -\dfrac{\omega\Delta W_{i,s}}{M_0 c^3 \beta_s^3 \gamma_s^3} \\[3mm] \dfrac{d\Delta W_{i,s}}{dz} = qE_0 T(\cos\varphi_i - \cos\varphi_s) \end{cases} \qquad (3.2.1\text{-}3)$$

where $E_0 \equiv V_0 / L$ is the average electric field.

Accordingly, a second-order differential equation can be given as below:

$$\frac{d}{dz}\left(\beta_s^3 \gamma_s^3 \frac{d\Delta\varphi_{i,s}}{dz} \right) + \frac{\omega qE_0 T}{M_0 c^3}(\cos\varphi_i - \cos\varphi_s) = 0 \qquad (3.2.1\text{-}4)$$

Compared with the particle velocity itself, the particle-velocity change in a gap is usually so small that β_s and γ_s can be assumed constant in a cell. By this, one simplifies Eq. (3.2.1-4) to:

$$\frac{d^2\Delta\varphi_{i,s}}{dz^2} + \frac{\omega qE_0 T}{M_0 c^3 \beta_s^3 \gamma_s^3}[\cos(\varphi_s + \Delta\varphi_{i,s}) - \cos\varphi_s] = 0 \qquad (3.2.1\text{-}5)$$

Multiplying the above equation by $\dfrac{d\Delta\varphi_{i,s}}{dz}$, one gets:

$$\frac{d}{dz}\left[\underbrace{\frac{1}{2}\left(\frac{d\Delta\varphi_{i,s}}{dz}\right)^2 + U(\Delta\varphi_{i,s})}_{\equiv \mathrm{H}} \right] = 0 \qquad (3.2.1\text{-}6)$$

with the following definition:

$$\frac{dU(\Delta\varphi_{i,s})}{d\Delta\varphi_{i,s}} \equiv \frac{\omega qE_0 T}{M_0 c^3 \beta_s^3 \gamma_s^3}[\cos(\varphi_s + \Delta\varphi_{i,s}) - \cos\varphi_s] \qquad (3.2.1\text{-}7)$$

The expression H inside the square brackets of Eq. (3.2.1-6) represents a constant total energy of oscillation: the first part is the kinetic energy term, and the second part is the potential energy term.

In Eq. (3.2.1-7), one gets $\dfrac{dU(\Delta\varphi_{i,s})}{d\Delta\varphi_{i,s}} = 0$ when $\Delta\varphi_{i,s} = 0$ or $-2\varphi_s$, which are correspond-

ing to the minimum and the maximum of the potential trough $U(\Delta\varphi_{i,s})$, respectively. Using the

condition $U(0) = 0$ and integrating Eq. (3.2.1-7), one obtains $U(\Delta\varphi_{i,s})$ as:

$$U(\Delta\varphi_{i,s}) = \frac{\omega q E_0 T}{M_0 c^3 \beta_s^3 \gamma_s^3}[\sin(\varphi_s + \Delta\varphi_{i,s}) - \Delta\varphi_{i,s}\cos\varphi_s - \sin\varphi_s] \qquad (3.2.1\text{-}8)$$

Substituting the above equation and the first equation of Eq. (3.2.1-3) into Eq. (3.2.1-6), one

gets:

$$\frac{1}{2}\left(\frac{\omega\Delta W_{i,s}}{M_0 c^3 \beta_s^3 \gamma_s^3}\right)^2 + \frac{\omega q E_0 T}{M_0 c^3 \beta_s^3 \gamma_s^3}[\sin(\varphi_s + \Delta\varphi_{i,s}) - \Delta\varphi_{i,s}\cos\varphi_s - \sin\varphi_s]$$
$$= Const. \qquad (3.2.1\text{-}9)$$

Considering the cases of the minimum and the maximum for $U(\Delta\varphi_{i,s})$, the following equa-

tion can be given:

$$\frac{\omega(\Delta W_{i,s})^2}{2M_0 c^3 \beta_s^3 \gamma_s^3} + q E_0 T[\sin(\varphi_s + \Delta\varphi_{i,s}) - (2\varphi_s + \Delta\varphi_{i,s})\cos\varphi_s + \sin\varphi_s] = 0 \quad (3.2.1\text{-}10)$$

Based on Eq. (3.2.1-10), the trajectory of any particle in the longitudinal phase space can be

plotted. When $\Delta\varphi_{i,s} = -2\varphi_s$, one gets the separatrix, the boundary of the stable region (called

bucket) for the particle trajectories. With a "fish"-like separatrix, the top picture of Fig. 3.2.1-1

demonstrates the classic case $(-90° < \varphi_s < 0°)$ for hadron linacs. As shown in the middle pic-

ture, a maximum phase acceptance of $360°$ can be realized if $\varphi_s = -90°$, but the energy gain of

the synchronous particle is zero. On the contrary, at $\varphi_s = 0°$, the separatrix and the bucket don't

exist any more, as the full field has been used for acceleration (see the bottom picture).

In a conventional DTL accelerator, the synchronous phase of an accelerating gap is typically

chosen as $-30°$ to achieve the phase-stability longitudinally, and meanwhile additional mag-

netic focusing elements have to be housed in the drift tubes to focus the beam transversely.

Different than the traditional negative-synchronous-phase structure, the "Combined $0°$

Structure" (KONUS: Kombinierte Null Grad Struktur) [RAT98] applies the $0°$ synchronous

phase to most accelerating cells. The fundamental motivation of this special KONUS beam dy-

namics concept is to minimize the transverse RF defocusing effects by maximizing the accelera-
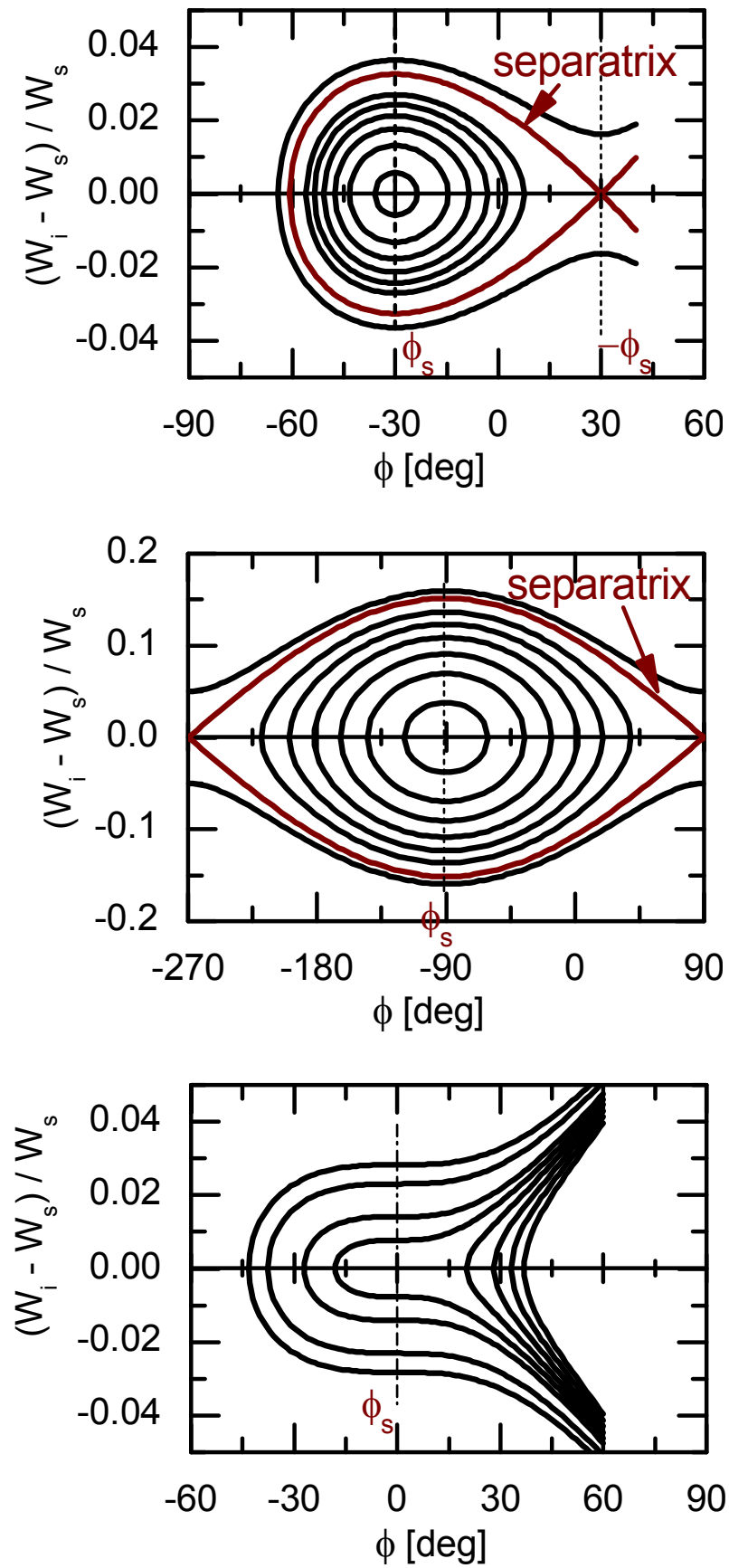
tion efficiency.

Fig. 3.2.1-1: Particle trajectories in the longitudinal phase space for

$\varphi_s = -30°$ (top), $\varphi_s = -90°$ (middle) and $\varphi_s = 0°$ (bottom) (Courtesy of R. Tiede).

In Fig. 3.2.1-2, the situations of the longitudinal particle motions at both a negative synchronous phase and the 0° synchronous phase are compared. Obviously, if φ_s is changed from the conventional negative value to 0°, the separatrix which provides the stable area for longitudinal particle trajectories will shrink to zero.
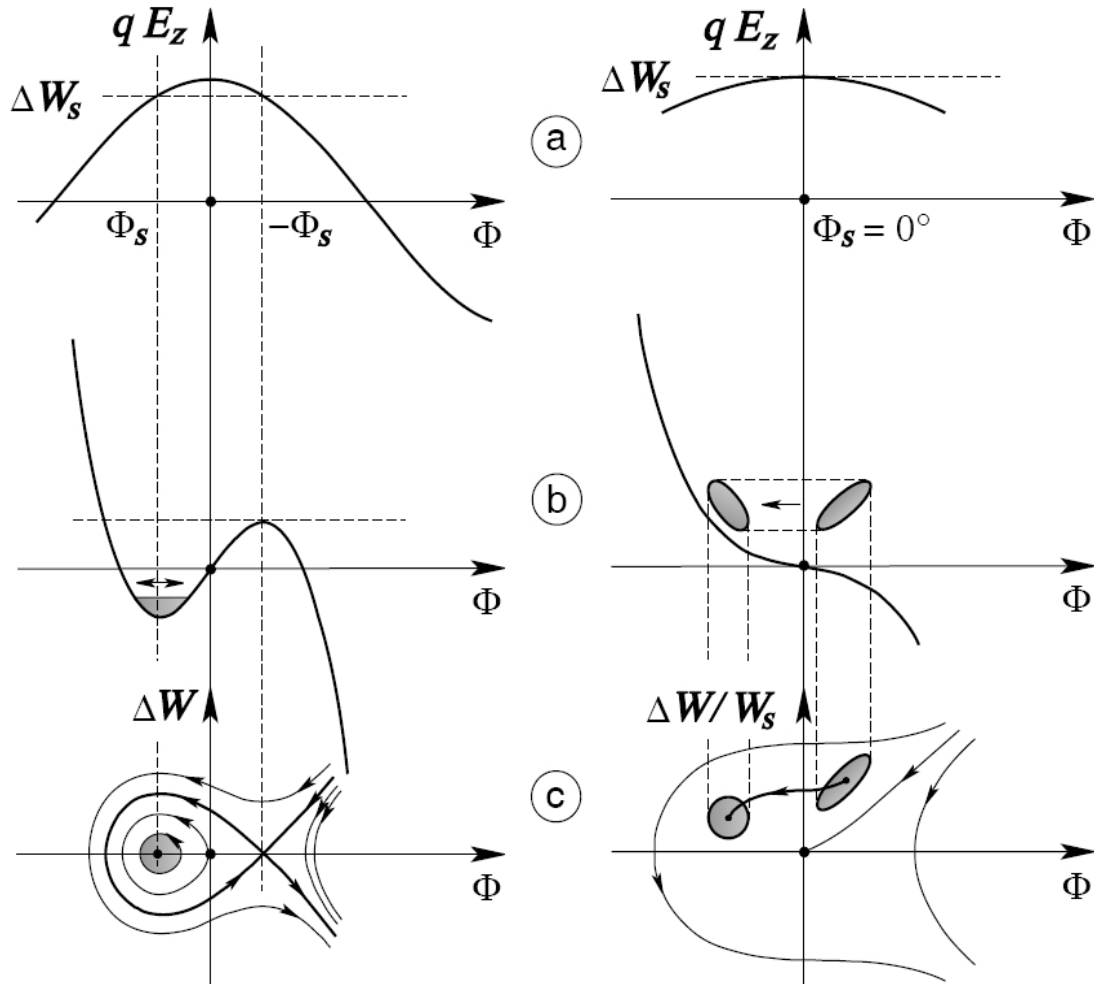
Fig. 3.2.1-2: Longitudinal particle motions (left: $\varphi_s<0°$, right: $\varphi_s=0°$)

ⓐ: The accelerating field as a cosine function of the phase; ⓑ: The longitudinal potential well;

ⓒ: Particle trajectories in longitudinal phase spaces [RAT98].

In the longitudinal phase space, therefore, only the area marked with dark arrows is used by KONUS (see Fig. 3.2.1-3) to control the instability of the longitudinal particle motion. Obviously, for a 0°-synchronous-phase section, the beam injection should be unconventionally asynchronous with the energy of the synchronous particle lower (typically 3%) than the energy of the beam-bunch-center particle. On the other hand, the 0° section has to be ended before $\Delta W_{i,s}$ decreases to 0 and a new synchronous particle should be redefined as above again. In fact, the phases seen by the particles in the beam bunch are not fixed at 0° but slip from ~0° to the nega-

tive direction of the $\Delta\Phi$ axis, so the radial RF defocusing effect as well as the longitudinal focusing effect are almost nothing at the beginning of a 0º-synchronous-phase section and then both of them will be gradually increased. If the 0º section can be properly stopped, the beam can get relatively stable motions in both transverse and longitudinal directions without external transverse focusing, so using slim drift tubes is feasible.
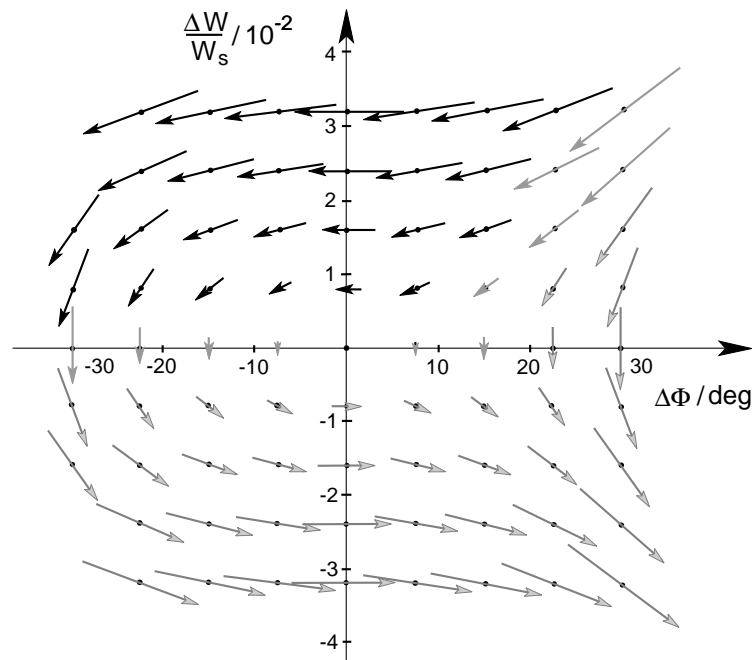

Fig. 3.2.1-3: The particle trajectories in the longitudinal phase space at $\varphi_s=0°$

and the usable area (marked with black arrows) for KONUS [RAT98].

For long and intense linacs, however, such a preliminary lattice which consists only 0º-synchronous-phase sections is not adequate any more. To compensate the accumulated longitudinal instability and transverse defocusing effects, it is necessary to use a so-called "Combined 0° Structure" which introduces additional longitudinal and transverse focusing elements at the two ends of each 0º-synchronous-phase section.

The first realized "Combined 0° Structure", the IH cavity of the GSI HLI injector, is a typical example to study the KONUS dynamics. The longitudinal and transverse beam envelope evolutions along this cavity are demonstrated in the top and bottom pictures of Fig. 3.2.1-4, respectively. Clearly, one can see that a KONUS period consists of the following three elements: 1) A multi-cell 0º-synchronous-phase section for main acceleration. 2) An independent transverse focusing element e.g. a quadrupole lens (usually a triplet) in case of an RT operation or a solenoid in case of an SC operation. 3) A short rebunching section using conventional negative synchronous phases for longitudinal focusing and matching.
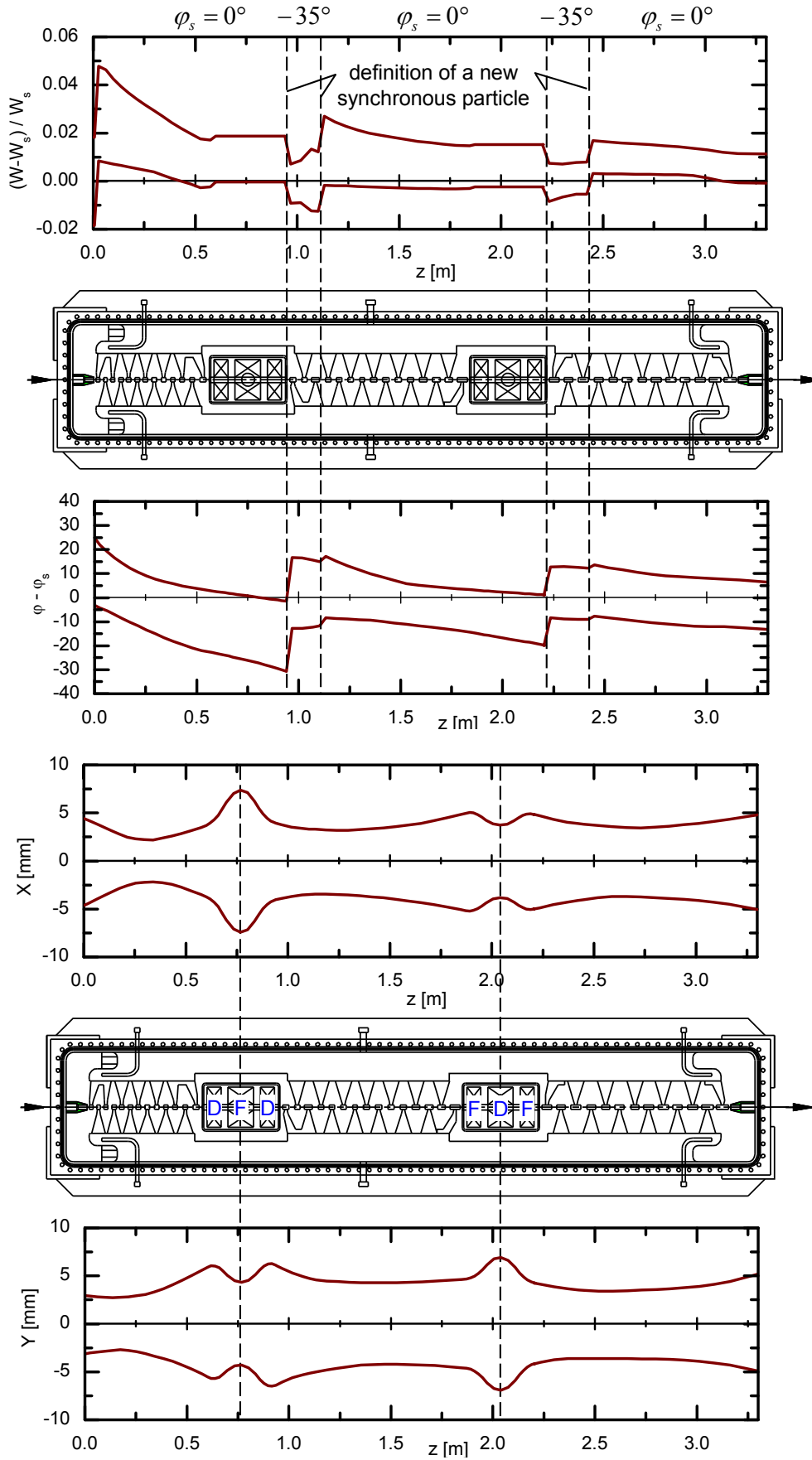
Fig. 3.2.1-4: Beam envelope evolutions (top: longitudinal; bottom: transverse) along an example KONUS structure – the HLI IH cavity (Courtesy of R. Tiede).

As seen above, KONUS does not use the traditional FODO lattice, but a special DFD O FDF lattice. Accordingly, instead of a constant multiple of the unit cell (e.g. $2\beta_s\lambda$ for an Alvarez-type structure and $\beta_s\lambda$ for an RFQ structure), the part between the exits of two consecutive focusing elements is used as a period to define the phase advances for a KONUS structure, with the advantage of using the same geometrical positions for the transverse and longitudinal phase advance calculations [TIE08].

Obviously, the phase advances are resulted by the overall effects of all elements in a KONUS period with different impacts on the particle motion, so they are not easy to be calculated analytically. But fortunately, nowadays powerful multi-particle numerical simulation tools are available, so it is not a problem to get the phase advance values for the KONUS structures.

The phase advances of a KONUS design are still comparable to those applied in conventional linac designs [TIE08]: 1) For low-current applications, $\sigma_t > 90°$ (typically around 120°) is sometimes necessary, especially at low energies, because of the relatively small focusing-element density; and with increasing beam energy, σ_t will be gradually decreased to below 90°. 2) For high-current designs, $\sigma_t < 90°$ is usually kept throughout.

3.2.2 Room-Temperature IH and CH Structures

Operating in the TE modes, the H-type cavities are characterized by the directions of the RF magnetic field lines, which are parallel and anti-parallel with respect to the beam axis and turning around at the cavity ends to form closed loops [RAT00]. For hadron acceleration, the two low TE modes, TE_{111} and TE_{211}, whose field distributions in the corresponding pillbox cavities are shown in Fig. 3.2.2-1, are often used.

The resonant frequency for an H-type pillbox cavity can be calculated by the following formula [POD08a]:

$$f_{H_{mnp}} = c \cdot \sqrt{\left(\frac{x'_{mn}}{2\pi R}\right)^2 + \left(\frac{p}{2L}\right)^2} \qquad (3.2.2-1)$$

where: c: the speed of the light in vacuum

       x'_{mn}:   the zeros of the derivatives of the Bessel functions J'_m

            (for IH: $x'_{11} = 1.841$, and for CH: $x'_{21} = 3.054$ [WAN08])

       R: the cavity radius
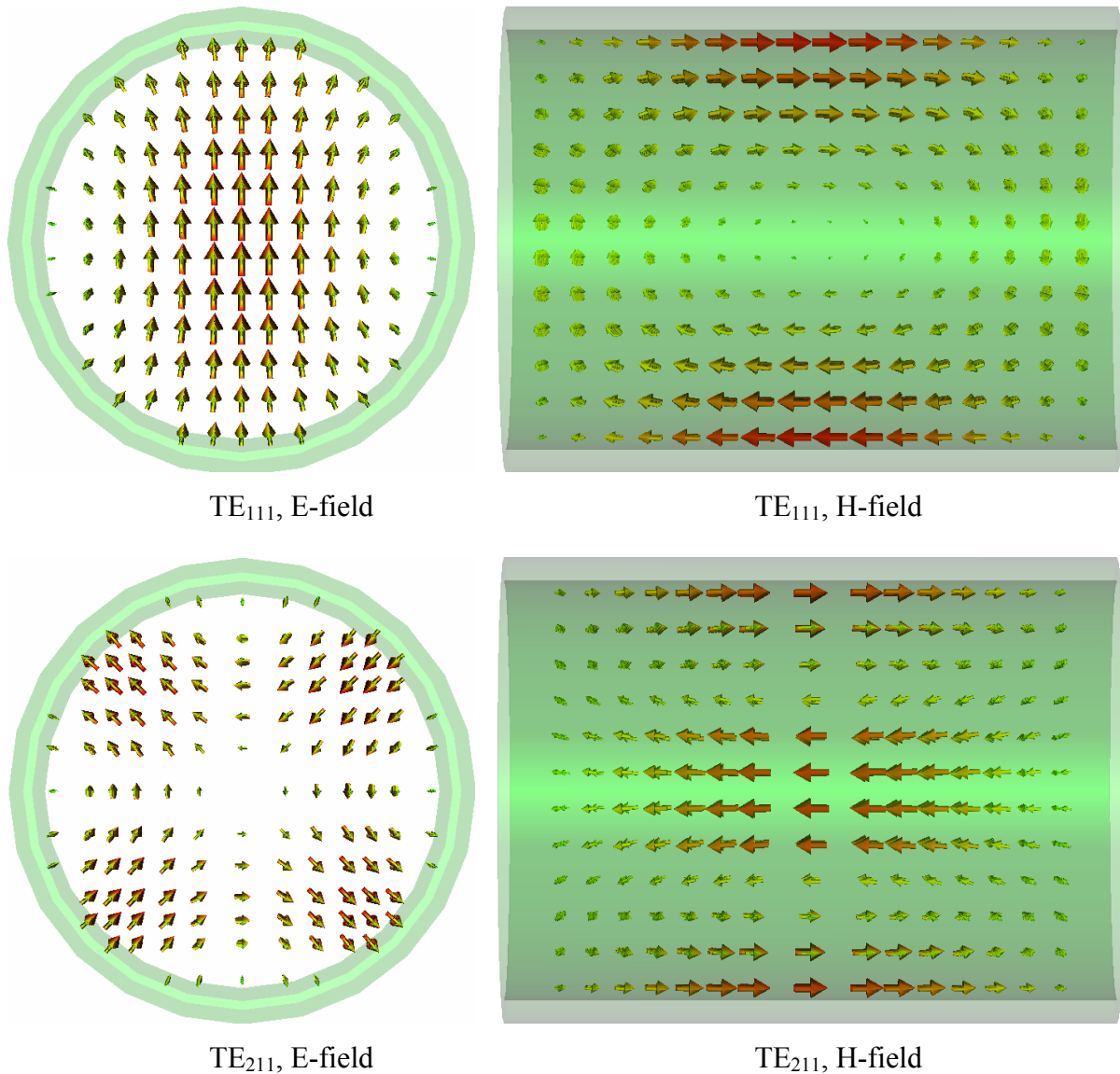
       L: the cavity length

TE₁₁₁, E-field

TE₁₁₁, H-field

TE₂₁₁, E-field

TE₂₁₁, H-field

Fig. 3.2.2-1: Field patterns for the TE_{111} and TE_{211} modes (Courtesy of M. Busch).

In a TE-mode pillbox cavity, however, only the transverse electric-field components exist. As shown in Fig. 3.2.2-2, the longitudinal electric-field component required for beam acceleration will be produced by introducing a sequence of drift tubes, which are connected to the cavity wall by interdigital or cross-bar stems, along the beam axis. Correspondingly, an H-type drift-tube linear accelerator can be categorized as either an IH structure or a CH (Cross-bar H-type) structure.
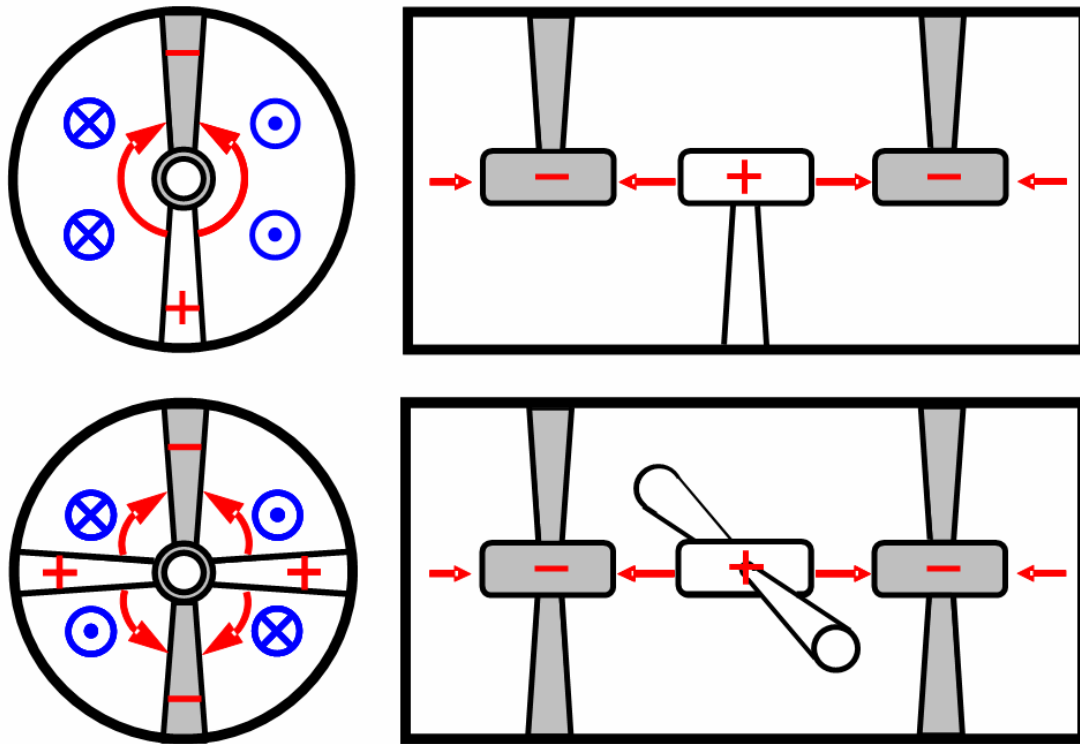
Fig. 3.2.2-2: Schematic diagrams for a comparison of the electromagnetic fields in the IH (top) and CH (bottom) cavities (Courtesy of R. Tiede).
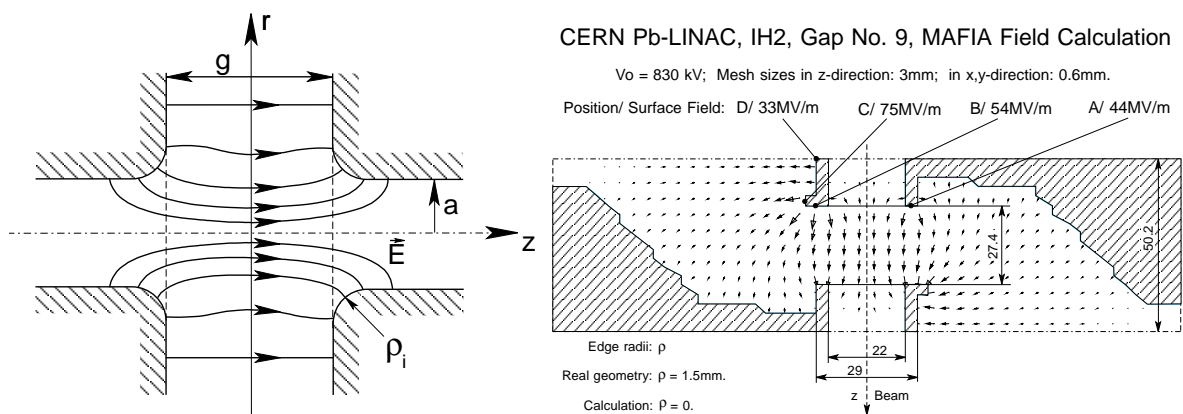

Fig. 3.2.2-3: Field patterns between the Alvarez-type thick-walled tubes [RAT98] (left) and between the KONUS-based slim tubes [BRO98] (right).

Taking advantage of the KONUS beam dynamics concept, the H-type DTL can adopt slim drift tubes (ratio of the tube outer radius to inner radius $r_o/r_i = 1.4$ typically) without any integrated focusing elements. Compared with the conventional thick-walled tubes carrying lenses

(see the left picture of Fig. 3.2.2-3), this kind of slim-tube geometry results in many attractive features as follows: 1) Significantly high accelerating gradients. 2) A very high sparking limit. 3) Low capacitance contributions to the cavity. 4) Easy and cheap construction.

A good example is the IH2 cavity of the CERN lead linac. As shown in the right picture of Fig. 3.2.2-3, electric fields of about 54MV/m, ~3.5 times as great as the Kilpatrick sparking limit, have been reached on the faces of the new-type slim drift tubes [BRO98]. Correspondingly, the overall voltage gain for the IH2 cavity is ~10.7MV/m (in pulsed operation), which is about 3–4 times higher than the typical value for a conventional Alvarez-type cavity. All these advantages lead the IH-DTL to become a kind of efficient accelerating structure in the energy range from 100keV/u to 30MeV/u.

Comparing with the calculated frequency of the corresponding pillbox cavity by Eq. (3.2.2-1), the measured resonant frequency of a built H-type DTL cavity is significantly lower for both H-modes because of the loaded accelerating electrodes. For example: 1) The loaded resonance frequency for the HICAT IH cavity ($\overline{R} = 0.151$ m and $L = 3.76$ m) f_{load}=216.816MHz, which is ~37% of the corresponding H_{111}-mode pillbox cavity f_0=583.085MHz. 2) In case of the SC CH-DTL prototype (R=0.136m and L=1.048m), f_{load}=360MHz, f_0=1080.94MHz, and $f_{\text{load}}/f_0 \approx 33\%$.

If the required resonant frequency is higher than 300MHz, the transverse dimensions of an IH structure will be too small to make a realistic mechanical design. Fortunately, at a high frequency up to 800MHz, the CH structure still owns reasonable transverse dimensions, so it can extend the applicable energy range of the H-type structures up to 150MeV/u. Furthermore, because high mechanical rigidity and easy cooling are available from the crossed-stem geometry, the CH structure opens the options for high-duty-factor even CW applications.

A comparison of the RF power efficiencies between different RT multi-cell accelerating structures is given in Fig. 3.2.2-4, where $Z_{\textit{eff}}$ is the so-called effective shunt impedance and it is defined by [RAT00]:

$$Z_{\textit{eff}} \cdot \cos^2 \varphi_s \equiv \frac{V_{\text{gain}}^2}{P_{\text{loss}} \cdot L_{\text{tank}}} \qquad (3.2.2-2)$$

where:

V_{gain} :   the cavity voltage gain including the transit time factor T and the synchronous

   phase φ_s

P_{loss} :   RF power losses

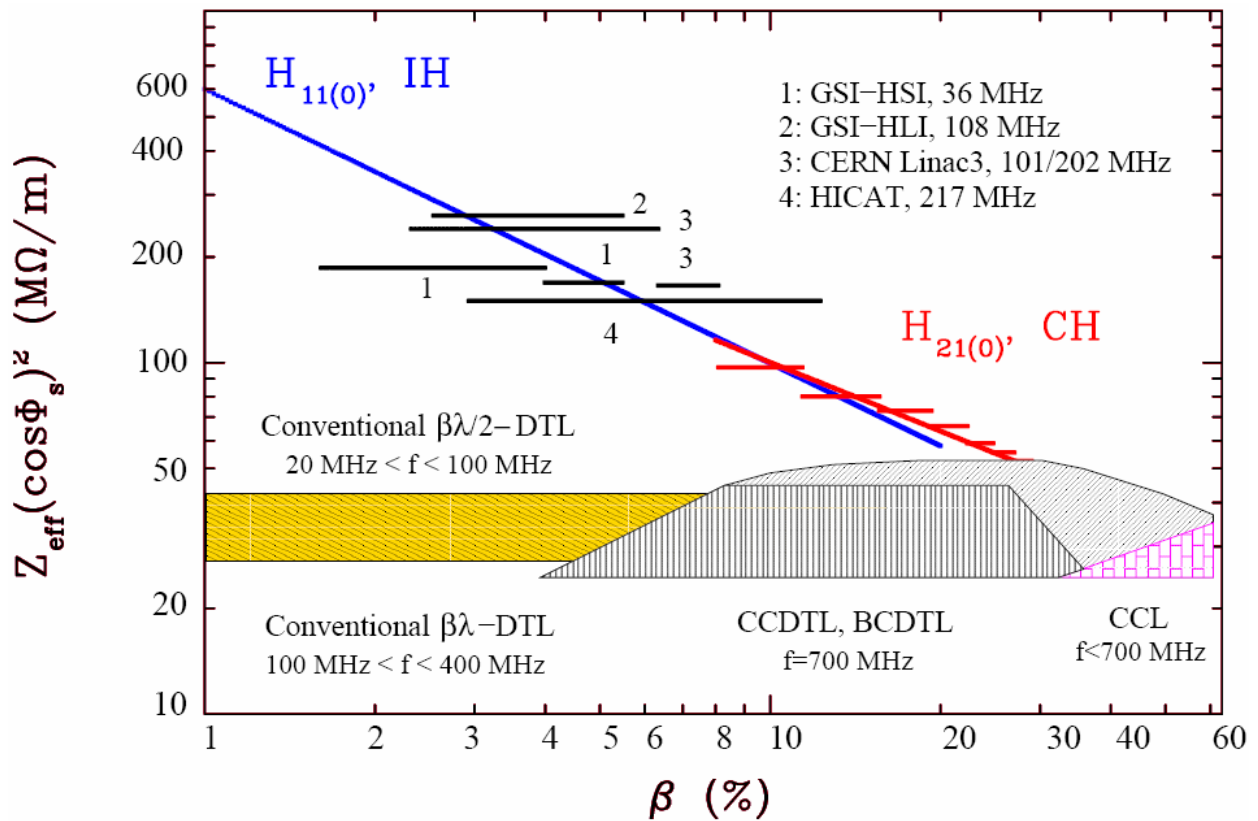L_{tank} :   the cavity length

Fig. 3.2.2-4: Effective shunt impedance including the synchronous phase φ_s of different RT multi-cell accelerating structures as a function of the particle velocity β. The blue bars represent some existing IH-DTLs and the red one for the designed GSI proton CH-DTL [POD08a].

Obviously, behind the RFQ accelerator, the KONUS-based H-type DTL is the most efficient RT low- and medium-β linear accelerating structure up to β=0.3.

3.2.3 Superconducting CH Structure

At present, the R&D of efficient RF superconducting cavities is a hotspot for the accelerator physics community. Among the salient characteristics e.g. high accelerating gradients and large bore apertures, the most attractive one of an SC accelerating structure is that the RF power dissipation can be dramatically minimized, which is significantly important for modern high power machines especially when they are operated at high duty factors.

In case of room temperature, the skin depth, i.e. the distance an RF electromagnetic wave can penetrate beneath the surface of the conductive cavity wall, can be calculated by the following equation:

$$\delta = \sqrt{\frac{2}{\omega\mu\sigma}} \qquad (3.2.3\text{-}1)$$

where ω is the angular frequency of the wave, μ is the permeability of the material, and σ is the electrical conductivity of the material.

Accordingly, the RF surface resistance of the cavity wall (typically in the order of mΩ) is:

$$R_s = \frac{1}{\sigma\delta} = \sqrt{\frac{\omega\mu}{2\sigma}} \qquad (3.2.3\text{-}2)$$

For an SC cavity, R_s can be expressed as [PAD08]:

$$R_s = \underbrace{A\left(\frac{1}{T}\right)f^2 \exp\left(-\frac{\Delta(T)}{kT}\right)}_{\equiv R_{BCS}} + R_0 \qquad (3.2.3\text{-}3)$$

where A is a constant depending on the material properties of the superconductor, T is the temperature, $\exp\left(-\dfrac{\Delta(T)}{kT}\right)$ is the Boltzmann factor with 2Δ as the energy gap of the superconductor, R_{BCS} calculated by the BCS (Bardeen-Cooper-Schrieffer) theory [PAD08] is the main contribution to R_s, and R_0 is referred to the residual resistance which is determined by several factors, e.g. the frozen magnetic fields, the defect and impurity of the materials. Therefore, in the superconducting state, R_s can be significantly decreased to the order of nΩ, and consequently the RF power consumption can be ignored.

Because of the relatively robust geometry, the CH structure is also a promising candidate for the state-of-the-art superconducting accelerators. As a result of the KONUS dynamics approach, a long lens-free CH cavity is feasible, and the independent magnetic focusing elements can be easily shielded to get rid of frozen current contributions. Therefore, the development of SC CH-DTL has overcome the lack of efficient superconducting low- and intermediate-energy cavities, whereas "efficient" means a large energy gain per cavity.

As shown in Fig. 3.2.3-1, a 360MHz superconducting CH-prototype cavity has been built and many cryogenic tests have been performed at Frankfurt University since 2005. After a new surface preparation including an additional Buffered Chemical Polishing (BCP) and High Pressure Rinsing (HPR) at ACCEL in 2007, the present record of the measured effective accelerating gradient (shown in Fig. 3.2.3-2) is 7MV/m, which corresponds to an effective voltage of 5.6MV and to a peak electric field of 36MV/m, and the RF surface resistance $R_s = 88\,\text{n}\Omega$ [POD07].
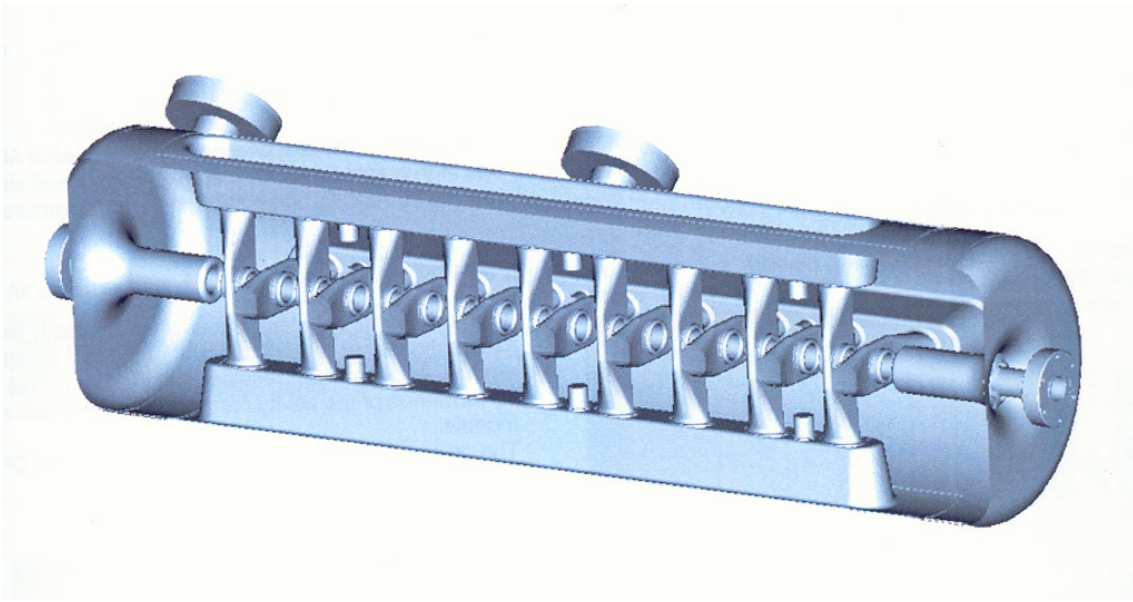
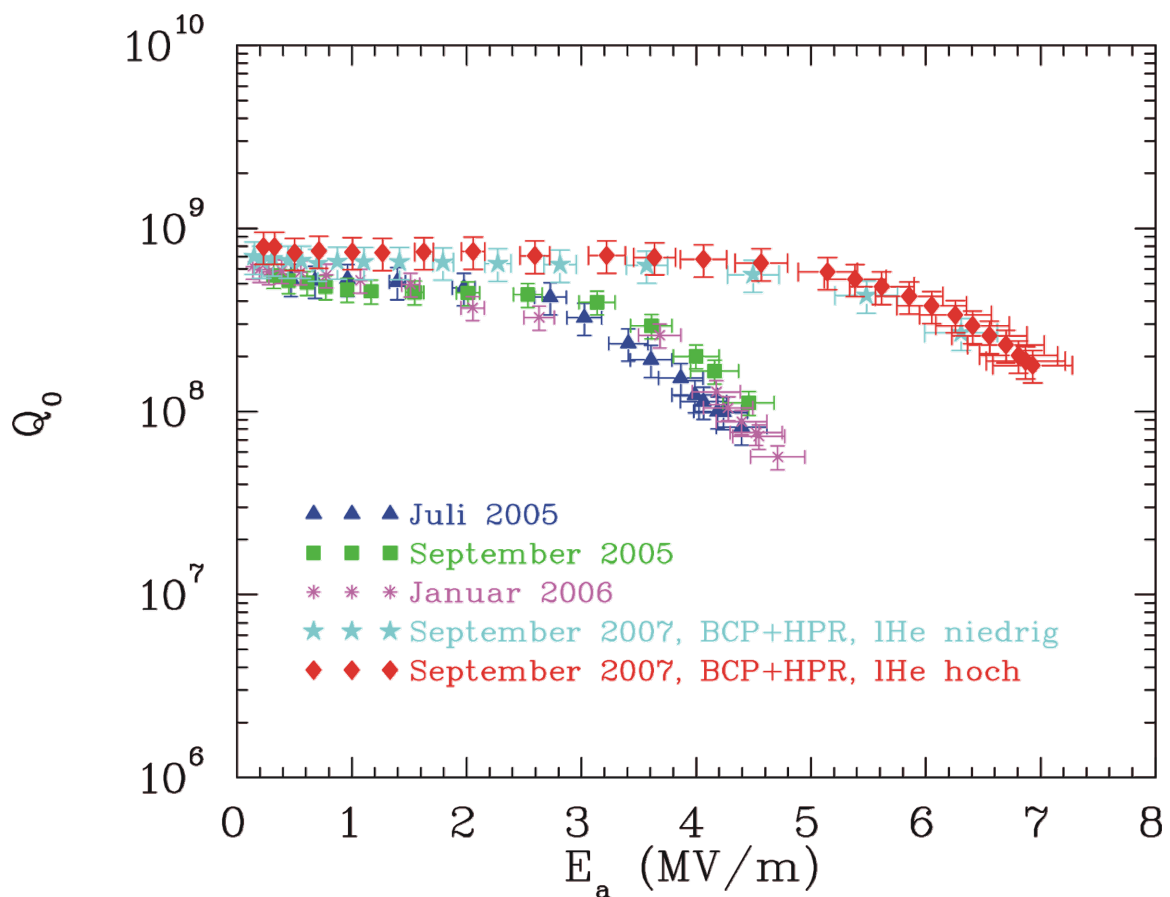Fig. 3.2.3-1: Superconducting CH-prototype cavity (Courtesy of H. Podlech).

Fig. 3.2.3-2: Measured Q_0-values as functions of the accelerating gradient E_a. In former tests the cavity was limited to the gradients of about 4.7MV. After a surface preparation at ACCEL, the performance has been improved significantly [POD07].
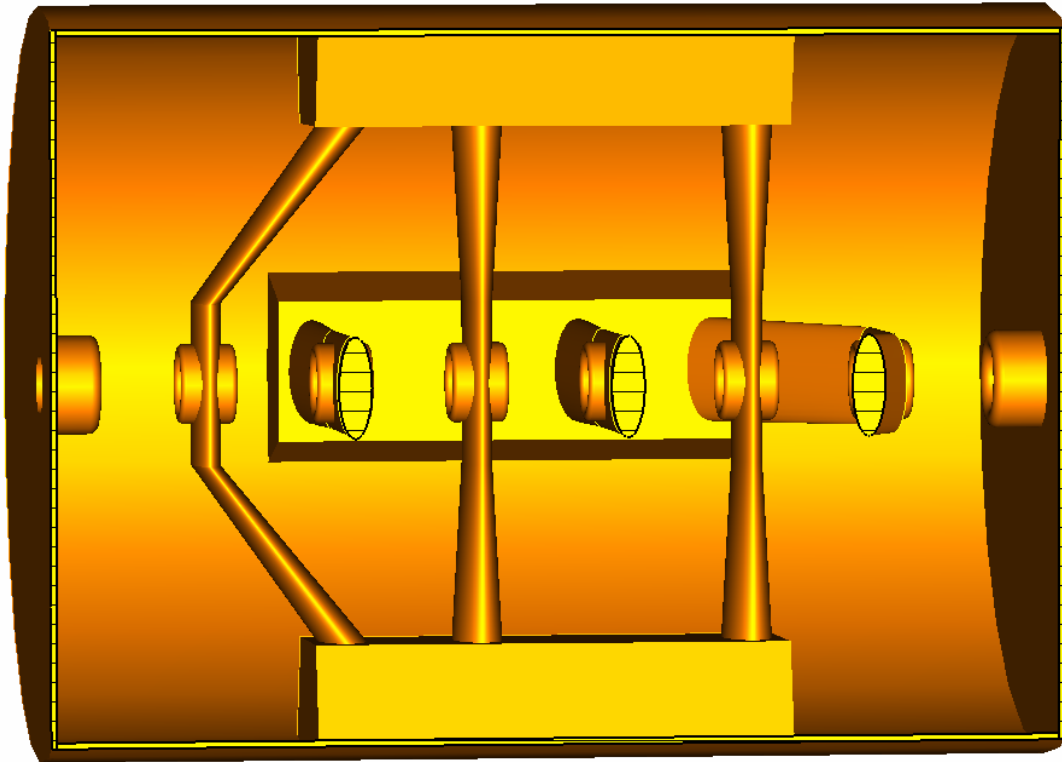
Fig. 3.2.3-3: Optimizations of the superconducting CH structure for high-power applications

(Courtesy of H. Podlech).

To work with high-power beams interesting to modern HPDL projects e.g. IFMIF and EU-ROTRANS, the geometry of the SC prototype cavity has to be further optimized. Therefore, recently a new superconducting CH cavity is under intensive studies. As schematically shown in Fig. 3.2.3-3, the following improvements have been done:

- Firstly, the stems, whose elliptical bases have the long axes originally parallel to the beam axis, have been rotated by 90° in order to provide more space to contain larger RF power couplers.

- The original major tuner system, which tunes the cavity by pushing on the end cells, has been replaced by two membrane tuners (for fast and slow tuning, respectively) located between the stems. The advantage is that the drift spaces for the end-cells can be considerably reduced, which is of particular importance to improve the beam dynamics design.

- Shorter girders and inclined end-stems have been adopted. They can not only further shorten ~20% of drift space for the end-cells but also make the electric-field distribution along the cavity flatter (see Fig. 3.2.3-4).
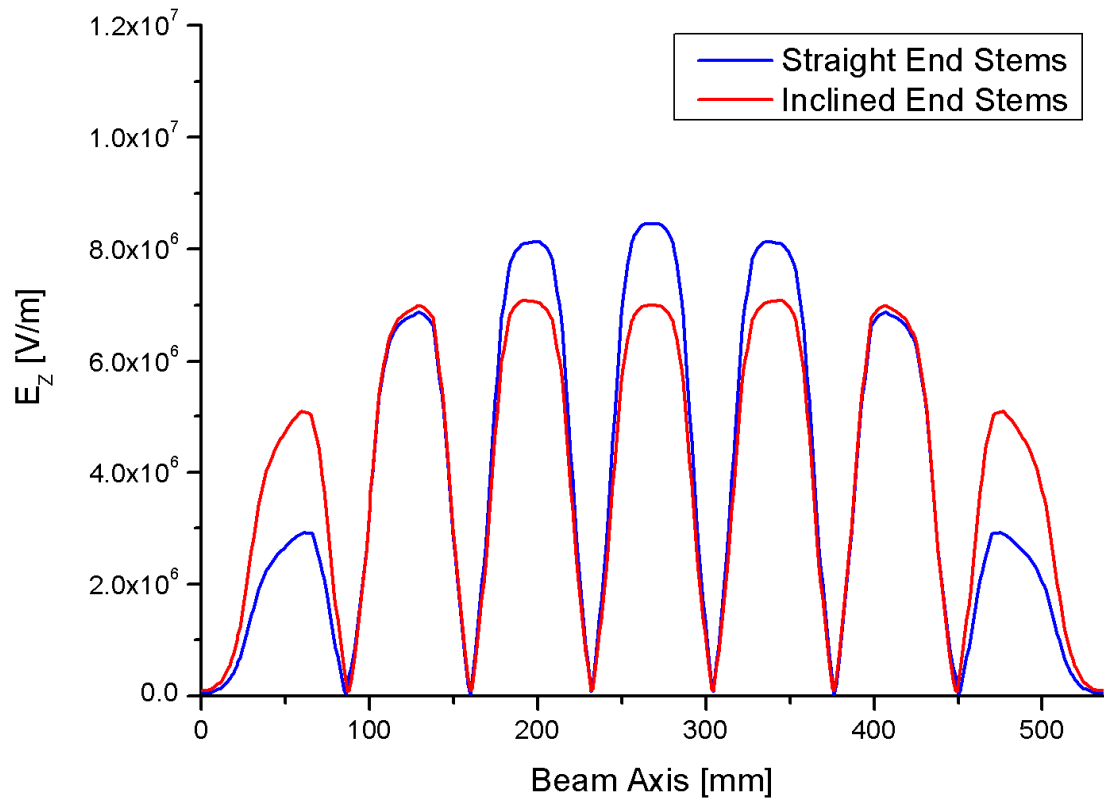
Fig. 3.2.3-4: Electric field profiles with straight and inclined end-stems (Courtesy of M. Busch).
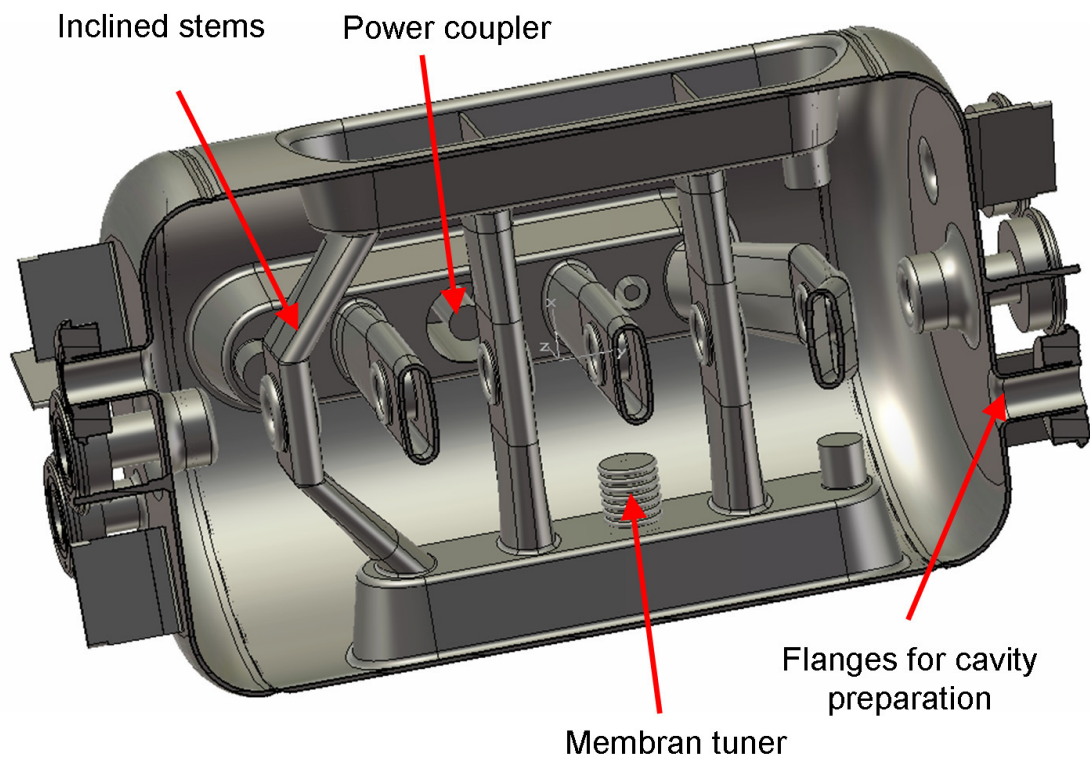

Fig. 3.2.3-5: The new 325MHz SC CH cavity [POD08b].

Based on the above efforts, finally a new SC CH cavity, which geometry is demonstrated in Fig. 3.2.3-5 and parameters are given in Table 3.2.3-1, has been developed.

Table 3.2.3-1: Main parameters of the new 325MHz SC CH cavity [POD08b].

β	0.1585
f [MHz]	325.224
$L_{\beta\lambda}$ [mm]	505
Accelerating cells	7
Aperture diameter [mm]	30
E_a [MV/m]	5
E_p / E_a	6
B_p / E_a [mT/(MV/m)]	13
G [Ω]	64
R_a / Q_0 [Ω]	1265
$R_a R_s$ [Ω^2]	80000

As the first SC CH-structure to be applied on a beam, the new cavity has been designed to work at 325.224MHz, because it will be put in the β=0.1585 part of the high-charge-state injector at GSI for a proof-of-principle experiment.

The beam test will accumulate important experience for the EUROTRANS project and the IFMIF project, because they have been foreseen as the first real applications of this kind of novel superconducting accelerating structure.

4. RFQ Design for FRANZ

The FRANZ facility, a unique pulsed neutron source planned at Frankfurt University, will use a 175MHz, up to 200mA proton radio-frequency quadrupole accelerator as the first accelerating structure. The design of such an ultra-intense RFQ is subjected to not only the challenging space-charge effects but also the stringent constraints for a university-based facility, e.g. compact dimensions and minimum costs. To meet the design goals, two unconventional optimization strategies – the so-called "BABBLE" design procedure and Longitudinal-Rotation Technique – have been developed and applied. For the acquired optimum design scheme, various off-design conditions have been used to check its robustness and potential capability.

Proposed as a multi-purpose experimental physics platform as well as a test bed for the R&D of modern high-power driver linacs, the FRANZ facility has been conceived as a small-scale but ultra-intense neutron source, which can provide a $\sim 10^7/ (cm^2 s)$ neutron flux in the range $0 - 500keV$.
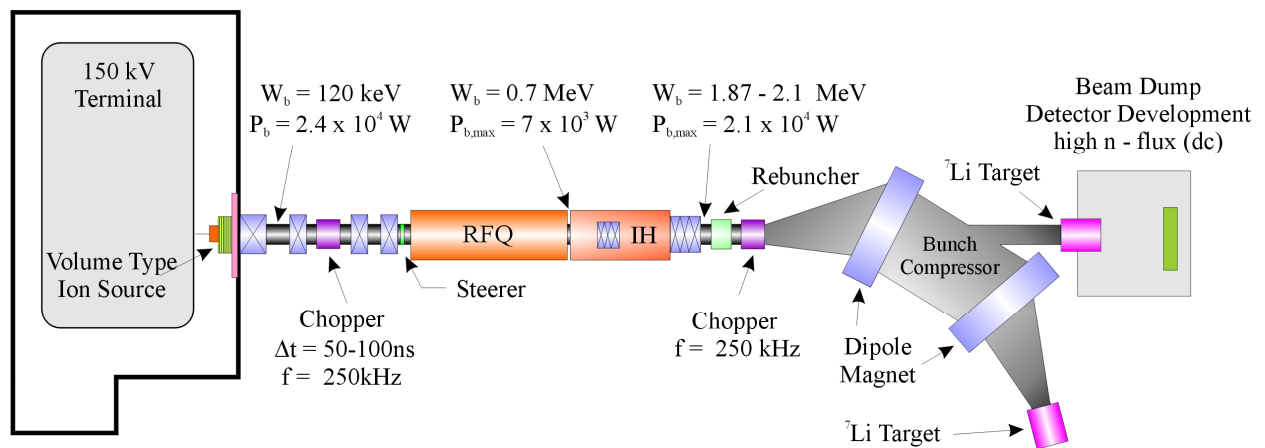

Fig. 4-1: FRANZ schematic layout (Courtesy of O. Meusel)

As shown in Fig. 4-1, this unique neutron source will mainly consist of the following components: 1) A volume plasma ion source based on a 150kV platform to provide a 120keV, up to 200mA proton beam. 2) A 250kHz chopper to shape the beam time structure as required. 3) A 175MHz linac complex to accelerate the proton beam to 2.0MeV. 4) A short rebuncher cavity to allow the adjustment of the final energy in the range of 2.0±0.2MeV. 5) A Mobley-type com-

pressor to push up to 10 micro beam bunches from the linac into a 1ns time slot. 6) Finally a solid or liquid ^{7}Li target to recieve up to ~10A protons for the neutron generation via the ^{7}Li (p, n) Be^7 reaction.

One highlight of the FRANZ driver linac is 200mA such an ultra-high design beam intensity. Because the induced strong space-charge effects will be most significant at the low-energy end, a relatively high input energy of 120keV has been chosen for the proton beam. The particle acceleration will be completed in two steps:

- A four-rod RFQ accelerator to capture, shape, bunch and pre-accelerate the input beam until 0.7MeV.

- An IH-DTL accelerator to continue boosting the protons to 2.0MeV.

The transition energy between the RFQ and the IH-DTL has been decided as 0.7MeV to make use of the relatively higher acceleration efficiency of the H-type DTL so that the overall length of the driver linac can be as short as possible.

Table 4-1 gives a worldwide survey of the RFQ machines which peak currents are 100mA or higher, and for comparison the corresponding performances demanded by the planned FRANZ RFQ are also listed together.

Table 4-1: ≥100mA RFQ projects in the world [ZHA08].

Parameter / Project	I_{peak} [mA]	ion	f [MHz]	W_{in} / W_{out} [MeV]	U [kV]	$\varepsilon_{in}^{trans.,norm.,rms}$ [π mm mrad]	L [m]	Status
ATS RFQ III*	100	H$^-$	425	0.100/2.070	111	0.13 (x) 0.22 (y)	2.9	Tested
IPHI$^\#$	100	H$^+$	352.2	0.095/5.000	87-123	0.25	8.0	Under construction
JAERI BTA*	100	H$^+$	201.25	0.100/2.000	113	0.65	3.4	Tested
LEDA$^\#$	105	H$^+$	350	0.075/6.700	67-117	0.20	8.0	Tested
IFMIF$^\#$	140	D$^+$	175	0.100/5.000	111-151	0.20	12.3	Under design
CERN RFQ2*	200	H$^+$	202.56	0.090/0.750	178	0.40	1.8	Operating
FRANZ$^\#$	200	H$^+$	175	0.120/0.700	85	0.40	~2.0	Under design

*: pulsed operation; #: CW operation.

The arguments of this configuration for the FRANZ RFQ are:

- The size of the FRANZ experiment hall is $\sim 9.5 \times 9.5 \text{m}^2$, so the length of the RFQ accelerator has been limited to within ~2m to make sure enough space for other components.

- The input normalized rms transverse emittance, 0.4 π mm mrad, has been adopted referring to the corresponding value of another 200mA RFQ i.e. the CERN RFQ2 [BIS84, HIL98, JAM97].

- An inter-electrode voltage of 85kV has been chosen for reliable CW operation.

Obviously, it is challenging for the FRANZ RFQ to reach the performances similar to those of the CERN RFQ2 machine, but using only about a half of the inter-electrode voltage.

4.1 Classic Design Approach

For the FRANZ RFQ, which covers the energy range only from 120keV to 700keV, it is more important to bunch the proton beam well than to accelerate it. However, the chosen input energy of 120keV is relatively too high to fulfill the bunching task easily, because:

- To bunch a fast beam is more difficult than to bunch a slow one. According to Eq. (3.2.1-3), the variation of $\Delta \varphi$ with position z is inversely proportional to $\beta_s^3 \gamma_s^3$ for a same ΔW.

- The length of a bunching cell is longer at a higher injection energy, which goes directly against the goal to realize a compact RFQ structure.

Furthermore, the phase and energy spreads of the output beam from the FRANZ RFQ have to fit into the longitudinal acceptance of the following IH-DTL which will be designed by the special KONUS dynamics concept.

In short, there are two major jobs for the FRANZ RFQ design: 1) To complete a fast but stable beam bunching within a ~2m-long structure and in the presence of significantly strong space-charge effects. 2) To achieve a good matching between the RFQ and the IH-DTL.

4.1.1 LANL Four-Section Procedure

For the RFQ beam dynamics design, the LANL (Los Alamos National Laboratory) Four-Section Procedure (FSP) [CRA79] is a classic technique, which divides an RFQ into four sequential sections: firstly, an Radial-Matcher (RM) section serves to adapt the input beam to a time-dependent focusing system; then a Shaper (SH) section and a Gentle-Buncher (GB) section help to longitudinally change the input beam (typically continuous) to proper, small bunches one

after another; and finally a fast energy gain will be achieved by a so-called Accelerator (ACC) section.

Holding the longitudinal small oscillation frequency ω_l and the geometric length Z_ψ of the separatrix constant, the GB section originally proposed by K-T [KAP70] is the essence of the LANL design method. The ω_l and Z_ψ are determined by the formulae as follows:

$$\begin{cases} \omega_l^2 = \dfrac{\pi^2 qAV_0 \sin(-\varphi_s)}{M\beta^2\lambda^2} \\ Z_\psi = \dfrac{\psi\beta\lambda}{2\pi} \end{cases} \qquad (4.1.1\text{-}1)$$

where ψ is the angular width only related to the synchronous phase φ_s by $\tan\varphi_s = \dfrac{\sin\psi - \psi}{1 - \cos\psi}$.

Theoretically, the conditions in Eq. (4.1.1-1) can lead to an adiabatic beam bunching: the beam bunch length and the longitudinal charge density distribution can be maintained constant throughout the whole beam compressing process. Though this approach was developed in the zero-current case, numerical simulation studies have shown that in the presence of space-charge effects within certain premises, it is still effective to reach a nearly constant bunch density and keep the emittance growths well under control [WAN08]. However, there is also a remarkable disadvantage that the resulted acceleration efficiency A is very low at the entrance to the RFQ where φ_s must be close to -90° to accept a DC input beam.

A good solution to reach high capture efficiency as well as to achieve a reasonable RFQ length simultaneously is to introduce a short pre-buncher called "shaper" before the GB section. At the expense of some emittance growths from a fast compression, the shaper pushes φ_s and the electrode modulation m from their initial values -90° and 1 up to certain values, which can shorten the bunching to an acceptable level, respectively. At the end of this two-stage buncher, the beam phase width and the electrode aperture a are smallest, so this position, which can be a bottleneck for the whole RFQ design, is one of the most critical places for space-charge effects.

Besides the longitudinal bunching problem, how to properly match the input beam into the RFQ is also crucial. The characteristics of the input beam are independent of time, but the acceptance ellipse at the beginning of an RFQ is changing due to the time-varying field. To overcome this difficulty, a radial-matching section, bell-mouth like and normally several focusing periods long, is used as the initial part of the RFQ. Here, the electrodes have quadrupole symmetry with a quickly shrinking aperture so that the transverse focusing strength B can be increased from almost 0 to its full value.

Finally, at the end of the GB section, an accelerator section, where a, m and φ_s, are all kept constant, is usually added to bring the beam to the required final energy quickly.

In addition, a distinctive characteristic of the Four-Section Procedure is that the transverse focusing strength B is kept invariant after the RM section in order to result in a constant mid-cell aperture r_0, i.e. a position-independent capacitance, along the main RFQ channel for easy RF tuning.

4.1.2 Test Design Studies

Variations of the LANL design procedure have been made at IAP to get shorter RFQs, which will reduce the required RF power and the system costs, and they have been successfully applied in various RFQ projects. Based on this design concept for compact RFQs [SCH96], further optimizations with respect e.g. to energy spread and emittance growth have been made.

The design work of the FRANZ RFQ has been started with some test studies based on the LANL method. To use the Four-Section Procedure, firstly some basic parameters have to be decided.

The one of the first priority is the synchronous energy at the end of the GB section, W_{GB}, which has been properly set as 550keV, a value slightly smaller than the output energy W_{out}=700keV. This is because the FRANZ RFQ, for which the total increase in energy is quite small, has a more important task to fulfill an efficient bunching process for a 200mA beam.

The next step is to choose the maximum values of the synchronous phase $\varphi_{s,\,max}$ and the electrode modulation $m_{\,max}$. Typically, $\varphi_{s,\,max}$=-30° and $m_{\,max}$=1.8–2. However, to well bunch such a 200mA beam over a limited distance, $\varphi_{s,\,max}$=~-40° and $m_{\,max}$=~1.6 have been conservatively adopted to avoid steep jumps in parameter variations.

Another key parameter, which has direct influences not only on the total length of the machine but also on the overall beam performance, is the synchronous energy at the end of the Shaper, W_{SH}. Normally, a higher W_{SH}, which permits a slow bunching, can lead to a good beam quality, but a long structure as well. In case of the FRANZ RFQ, which has been restricted to be ~2m long, the highest W_{SH} to be used is 125keV.

On the basis of the above-made choices, a sweep of the FSP-style designs for the FRANZ RFQ has been carried out with respect to the mid-cell aperture r_0 from 0.48–0.66cm in twelve steps. Based on the simulations using the well-known PARMTEQM computer code [PAR05] and 10^5 input macro-particles in a 4D-Waterbag distribution (*Note: if no special statement, this simulation configuration will be used for all RFQ designs mentioned in this dissertation*), the

main structure and RF parameters of the obtained LANL-type design schemes are compared in Table 4.1.2-1, where E_k is the Kilpatrick factor representing the ratio of the maximum surface electric field to the Kilpatrick limit, a_{min} is the minimum electrode aperture of the RFQ and L is the total length of the RFQ. Clearly, with an increasing r_0, E_k is decreasing from 1.66 to 1.20 and meanwhile a_{min} is increasing from 0.36cm to 0.49cm, respectively. The maximum electrode modulation and the RFQ length, within 1.63–1.65 and 207–216cm, respectively, are both a little larger than the expected values.

Table 4.1.2-1: FSP-style designs for the FRANZ RFQ.

r_0 [cm]	E_k	$\varphi_{s, max}$ [°]	a_{min} [cm]	m_{max}	L [cm]
0.481	1.66	-40	0.358	1.628	206.91
0.497	1.60	-40	0.370	1.629	209.60
0.513	1.55	-40	0.382	1.631	209.01
0.530	1.50	-40	0.394	1.632	208.46
0.546	1.45	-40	0.407	1.633	211.14
0.562	1.40	-40	0.419	1.634	210.47
0.579	1.36	-40	0.431	1.636	213.10
0.595	1.32	-40	0.443	1.639	212.47
0.611	1.29	-40	0.455	1.639	215.11
0.627	1.26	-40	0.467	1.641	214.27
0.643	1.23	-40	0.479	1.643	216.90
0.659	1.20	-40	0.491	1.645	216.07

Corresponding to the FSP-style designs, the beam transmission efficiencies for transported and accelerated particles as well as the transverse focusing strengths B are plotted as the functions of r_0 in Fig. 4.1.2-1. Obviously, along with an increasing r_0, there are marginal improvements in both T_{total} and $T_{accelerated}$ at the beginning, but gradual declines happen after $r_0=0.627$.

However, as the transverse focusing strength B is going down linearly, both of the output rms normalized transverse emittances grow dramatically especially when $r_0 \geq 0.546$ (see Fig. 4.1.2-2). From these two figures, it is easy to see that: 1) A mid-cell aperture smaller than 0.546 can not provide a large enough transport area for the particles. 2) But when $r_0 > 0.546$, the available transverse focusing forces are not sufficient any more. Based on an overall consideration of the behaviors in both transmission efficiency and emittance growths, the design with $r_0=0.546$ has been regarded as the best one among all these designs. Here, this scheme is named as "Design-0" to provide the basis for further analyses.
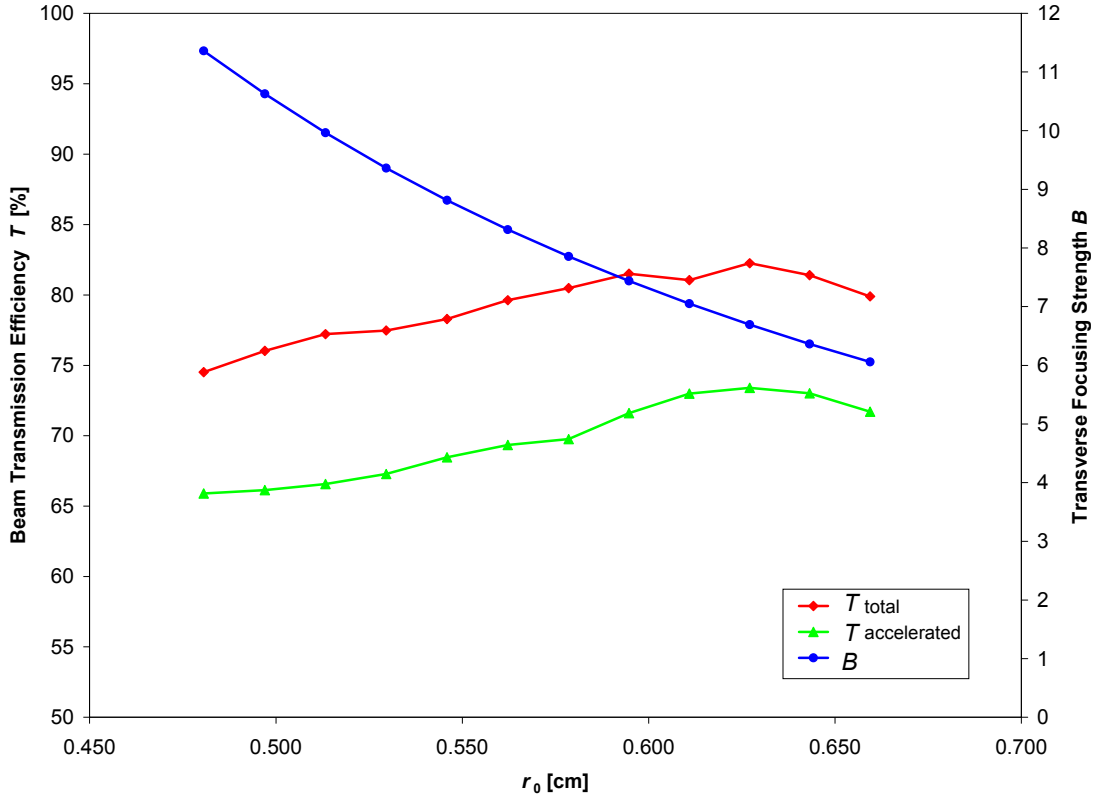
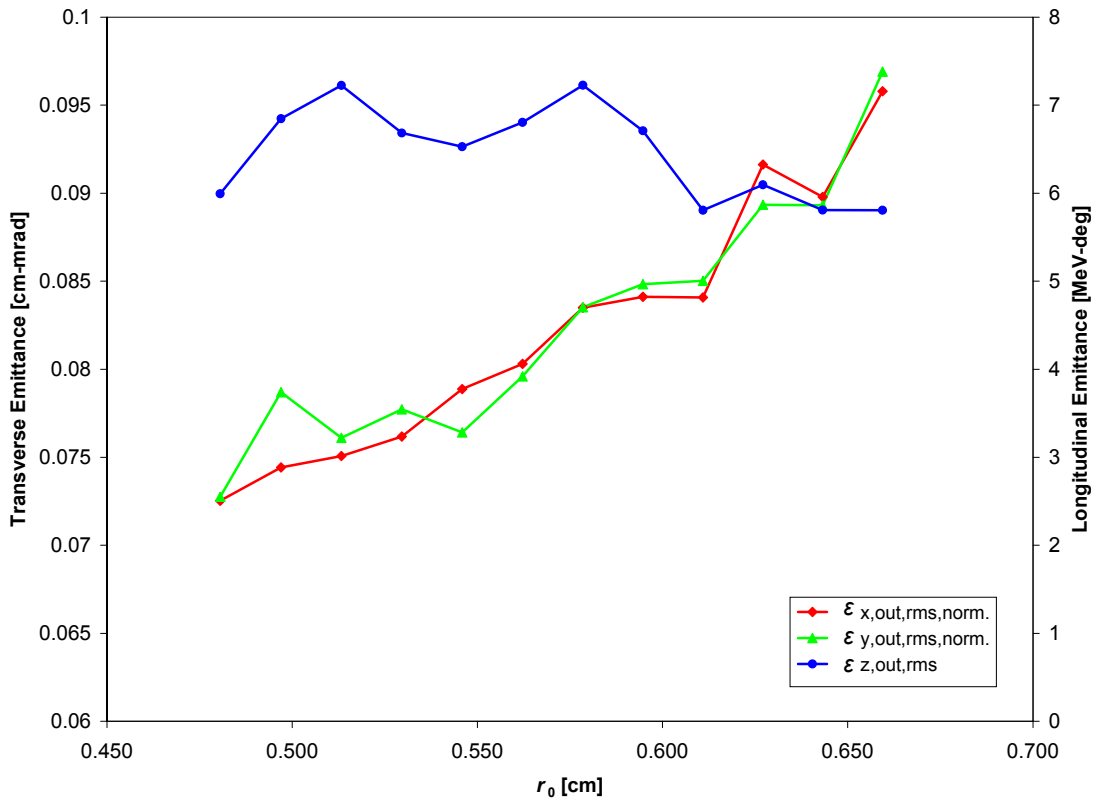Fig. 4.1.2-1: Beam transmission efficiencies and transverse focusing strengths vs. r_0.

Fig. 4.1.2-2: Output transverse and longitudinal emittances vs. r_0.

Table 4.1.2-2: Four-section partitioning of the Design-0 scheme.

Section	Cell Range	Length [cm]	B
RM	1 – 4	5.5	0.010 – 8.920
SH	5 – 20	22.8	8.920
GB	21 – 104	158.5	8.920
ACC	105 – 112 (Cell113 is the exit fringe field cell)	24.3	8.920

The four sections of the Design-0 scheme are distinguished as shown in Table 4.1.2-2, while the evolutions of the main dynamics parameters, a, m, φ_s, the synchronous energy W_s and the inter-electrode voltage V, along the accelerating channel are demonstrated in Fig. 4.1.2-3.
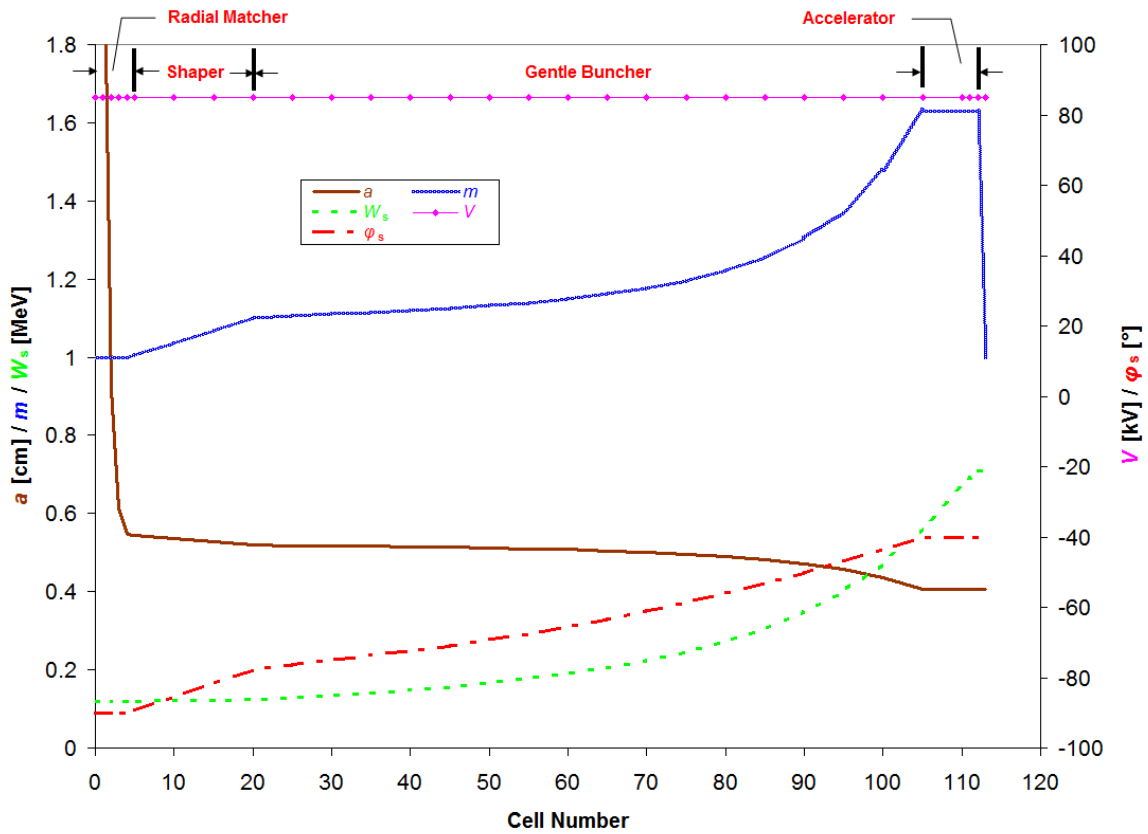
Fig. 4.1.2-3: Main RFQ parameters versus cell number for Design-0.

4.2 Optimization Strategies

From the test design studies, in which the highest total transmission efficiency for all these FSP-style designs is <85%, one can conclude that the traditional LANL strategy is not sufficient

to realize a satisfying design for the 200mA FRANZ RFQ such an ultra-intense machine. Therefore, some unconventional optimization concepts have to be developed.

4.2.1 New Design Procedure for Intense Beams: "BABBLE"

To improve the LANL Four-Section Procedure, one must firstly get at the root of the problem. In the main RFQ, the forces seen by the accelerated beam will experience the following changes: when the beam is gradually bunched longitudinally with slight acceleration, the space-charge force is increasing with the decreasing bunch size and behaves most significantly at the end of the bunching stage; and when the real acceleration begins, the transverse defocusing force will be weakened as the beam velocity rises rapidly. Apparently, the Four-Section Procedure is inconsistent with the natural beam developing process in the RFQ, because it arbitrarily holds the transverse focusing strength B constant after the RM section, which can let the travelling particles feel unbalanced forces between the transverse and longitudinal planes and turn unstable. The more intense the accelerated beam is, the more serious the problems will be.

To realize an efficient bunching for the FRANZ RFQ, a new design strategy so-called "BABBLE" (Balanced and Accelerated Beam Bunching at Low Energy) has been developed based on the following basic idea: to vary the transverse focusing strength B along the RFQ according to the corresponding space-charge conditions at different positions – namely during the bunching B should be increasing with the space-charge force until the transverse defocusing force is weakened, and afterwards it should go down accordingly – to keep the whole beam development under a transverse-longitudinal force balance.

If the above-mentioned important condition is satisfied, the evolution speeds of the synchronous phase and the modulation parameter can be retuned to improve the bunching process:

- Firstly in the original SH section, the relatively steep "jumps" of φ_s and m can be replaced by a gentle increase, respectively. Especially at the beginning, a certain distance where φ_s is kept at -90° is very important to provide the beam a maximum-separatrix-bunching period, while m is slowly climbing up to produce the longitudinal field gradually.

- "Protected" by the ascending B, both of the rising speeds of φ_s and m are allowed to complete a turning from slow to fast, where in the last half part of this turning period, φ_s and m can rise much more rapidly than in the original GB section so that the length growth caused by the foregoing slowed bunching can be compensated.

- When B starts to fall down, φ_s and m can continue increasing linearly at the achieved high increment speeds or at slightly lower speeds than the current ones (it depends on the in-

tensity of the accelerated beam and the requirements on the transverse emittance growths, etc.); this is a stage with a mixture of bunching and accelerating.

- After the beam is well bunched, B, φ_s and m can be held constant – same as in the original ACC section – for a stable acceleration until the required output energy is reached.

In accordance with the new "BABBLE" strategy, the evolutions of B, φ_s and m along the RFQ in the Design-0 scheme have been improved in the ways shown in Fig. 4.2.1-1 and Fig. 4. 2.1-2, respectively. From the pictures, the following differences can be seen:

- As in the original RM section, the new B is firstly taped from almost 0 to 5.4 over 4 cells but with a 40% lower magnitude; then it is steadily increased to the maximum between Cell5 – Cell60; finally, it is smoothly decreasing in the rest part.
- Until Cell20, the new φ_s still equals to -90°; the turning periods for the new φ_s and m end at Cell65 (but actually also at Cell60, the additional 5 cells are for a smooth transition to the next stage); then they are almost linearly increased to the RFQ exit at somewhat depressed speeds due to 200mA such an ultra-high intensity.
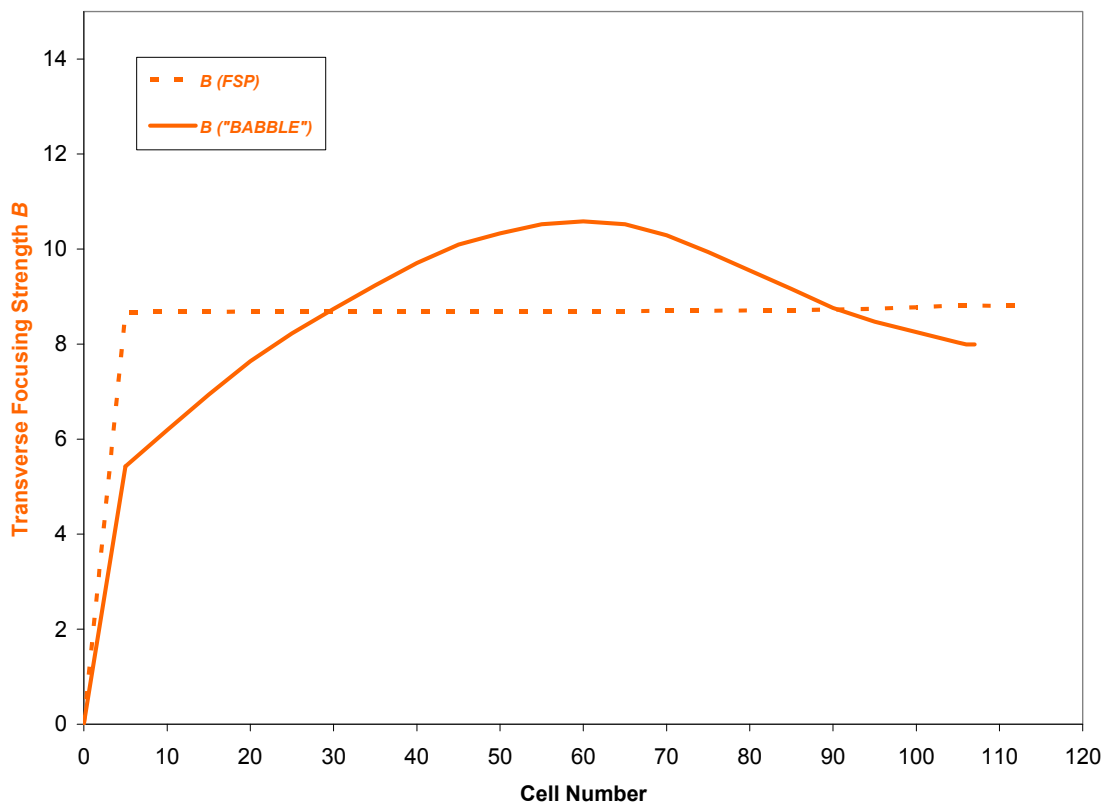

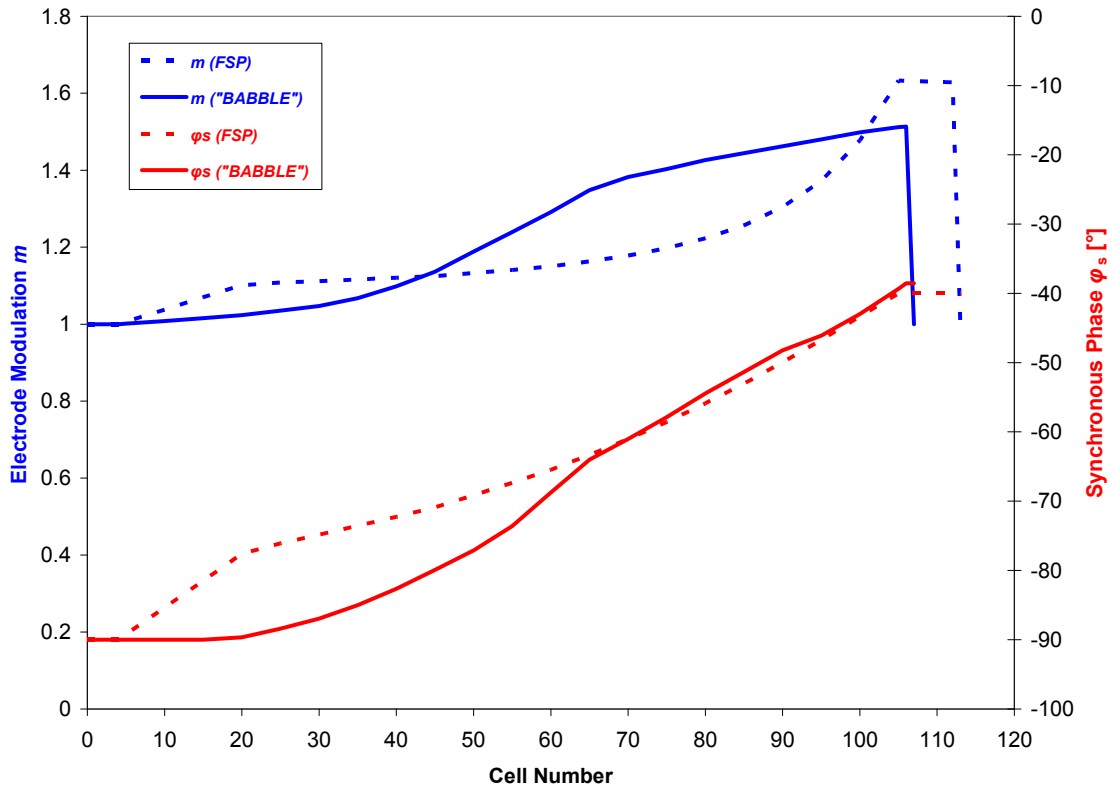Fig. 4.2.1-1: B vs. cell number before (FSP) and after ("BABBLE") optimization.

Fig. 4.2.1-2: φ_s and m vs. cell number before (FSP) and after ("BABBLE") optimization.
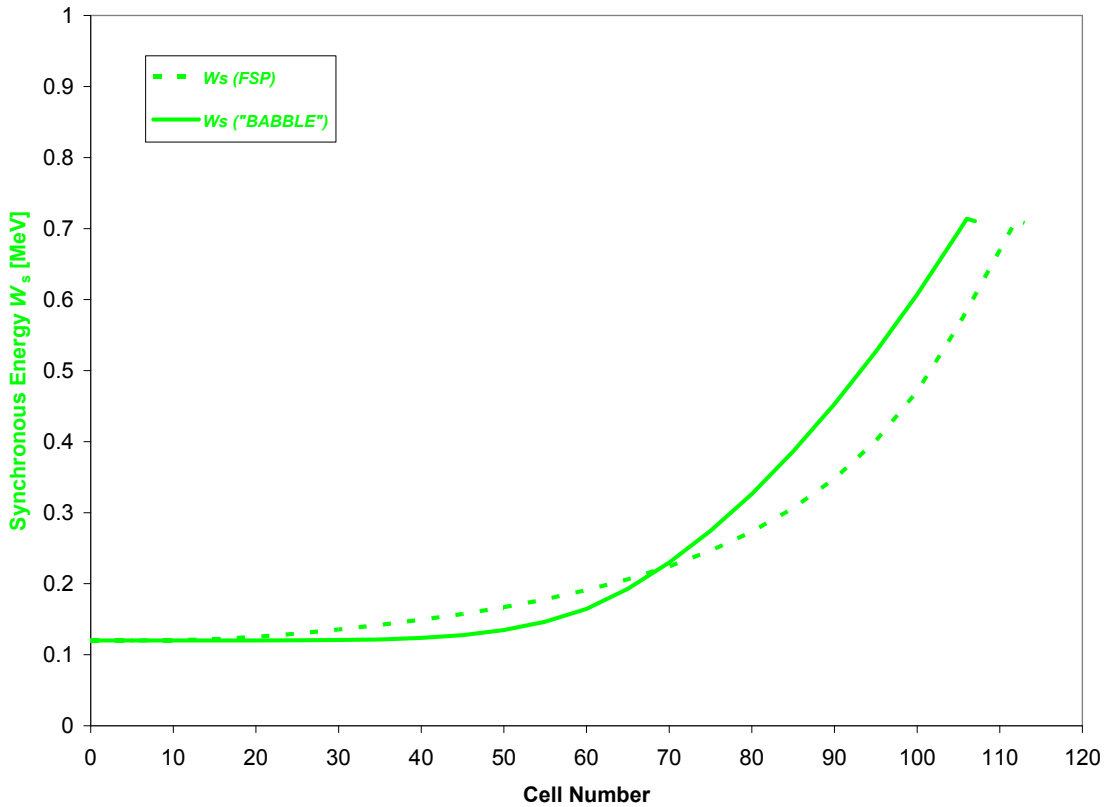

Fig. 4.2.1-3: W_s vs. cell number before (FSP) and after ("BABBLE") optimization.

In Fig. 4.2.1-3, the synchronous energies as the functions of cell number before and after optimization are compared. Clearly, in the "BABBLE" case, there is nearly no acceleration until

Cell60, but afterwards the beam gets a much faster energy gain so that it approaches already the final energy using 6 less cells than the FSP case.

As a result of the "BABBLE" optimization, a new design scheme called "Design-1", with the improved variations of the main parameters shown in Fig. 4.2.1-4, has been obtained for the FRANZ RFQ. Actually, the "BABBLE" method also divides an RFQ into four sections, but using different partitioning rules and making relatively smooth transitions between sections (so each section might extend to its neighboring section for one to several cells). For the Design-1 scheme, the sections are distinguished as below:

- **Maximum-Separatrix (MS) Section:** characterized by φ_s = -90°; besides the functions of the original RM, it performs a symmetrical (See Chap. VI) and soft bunching with a maximum phase acceptance (full 360°); being 27.4cm long, it covers Cell1–Cell20.

- **Main Bunching (MB) Section:** it starts from the end of the MS section and stops at Cell60 (extends to Cell65), where B reaches the maximum over a length of 56.8cm.

- **Mixed Bunching-Accelerating (MBA) Section:** 110.7cm long (Cell61/66–Cell106) with a decreasing B.

- **Main Accelerating (MA) Section:** same to the original ACC section; because the total energy increase of the FRANZ RFQ is low, this section is not used (nevertheless, the Design-1 RFQ has only totally 107 cells and is ~15cm shorter than the Design-0 one).
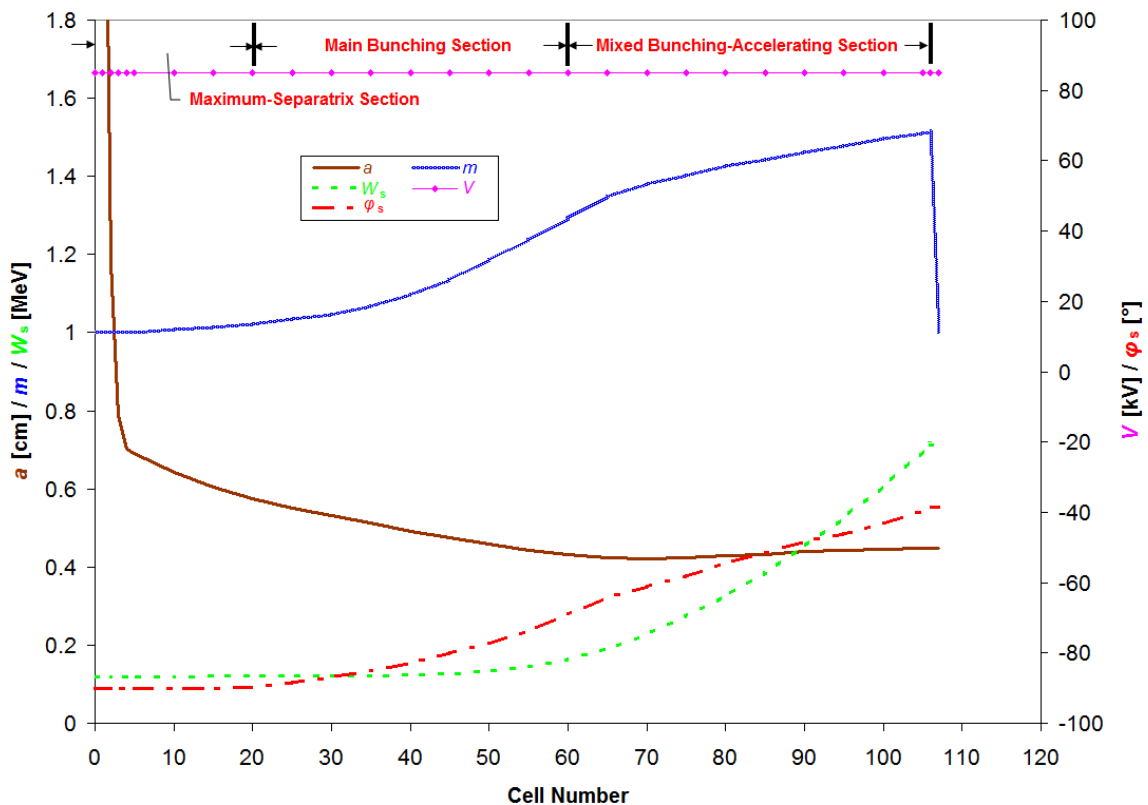

Fig. 4.2.1-4: Main RFQ parameters versus cell number for Design-1.

The beam transport simulation results of the Design-1 scheme have confirmed the efficiency of the "BABBLE" optimization applied to the Design-0 one.

First of all, the total beam transmission efficiency has risen from 78.3% to 98.3%, while the transmission efficiency for the accelerated particles has a significant growth from 68.5% to 96.0% as well. Fig. 4.2.1-5 gives a comparison of the lost particle distributions between the two designs, where the three dimensions are representing the cell number, the particle energy and the ratio of the lost particles, respectively.
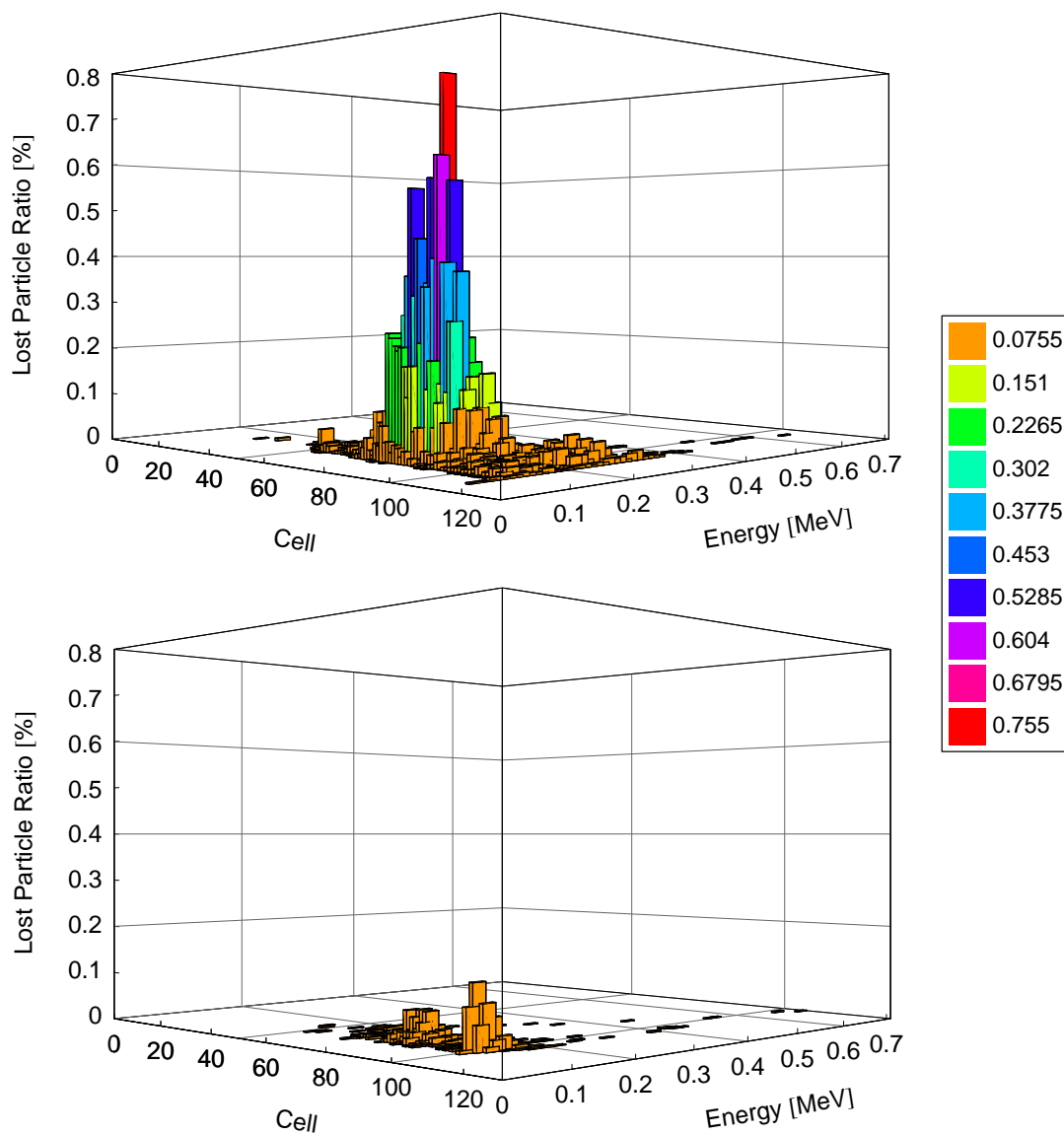

Fig. 4.2.1-5: Lost particle distributions for Design-0 (top) and Design-1 (bottom).

It's clear that the "peak" of beam losses, corresponding to ~20% of the input macro-particles, has been almost removed after the "BABBLE" optimization. One can further notice that in case of Design-0, though most lost particles appear at the positions already close to the RFQ exit, their energies are less than 200keV. This means during the bunching process, more

and more particles slipped out the shrinking separatrix, the boundary of the stable region (called bucket) for particle trajectories, and when the fast acceleration started, they were lost quickly. In short, the FSP method has not successfully focused the 200mA proton beam longitudinally.

Second, in order to have a better observation on the bunching process, the variations in transverse and longitudinal emittances along the beam axis for both cases are plotted in Fig. 4.2.1-6, where the dashed lines are responsible to Design-0 and the solid lines for Design-1. In case of Design-0, because the space-charge forces were increasing with a reduced bunch size but without an effective control, the transverse emittances were keeping moving up until Cell84, where both of them had a growth rate by about a factor of two (if the large beam losses did not start to happen there, one can expect that the transverse emittances would reach the top at Cell104, the end of the gentle buncher); on the other hand, the remarkable increase in the longitudinal emittance shows again that the beam bunch was getting looser and looser about the synchronous particle. Different than the Design-0 case, the developments of the emittances in all planes, especially the transverse ones, were well under control along the Design-1 RFQ (though the longitudinal emittance curve for 100% of transported particles had an obvious increase at the downstream of the RFQ, it is easy to see from the "99%" curve that the "noise" came from less than 1% of "bad" particles). The fairly flat emittance evolutions after the "BABBLE" optimization show that the new strategy has held the beam under a balance of forces between the transverse and longitudinal planes almost throughout the FRANZ RFQ.
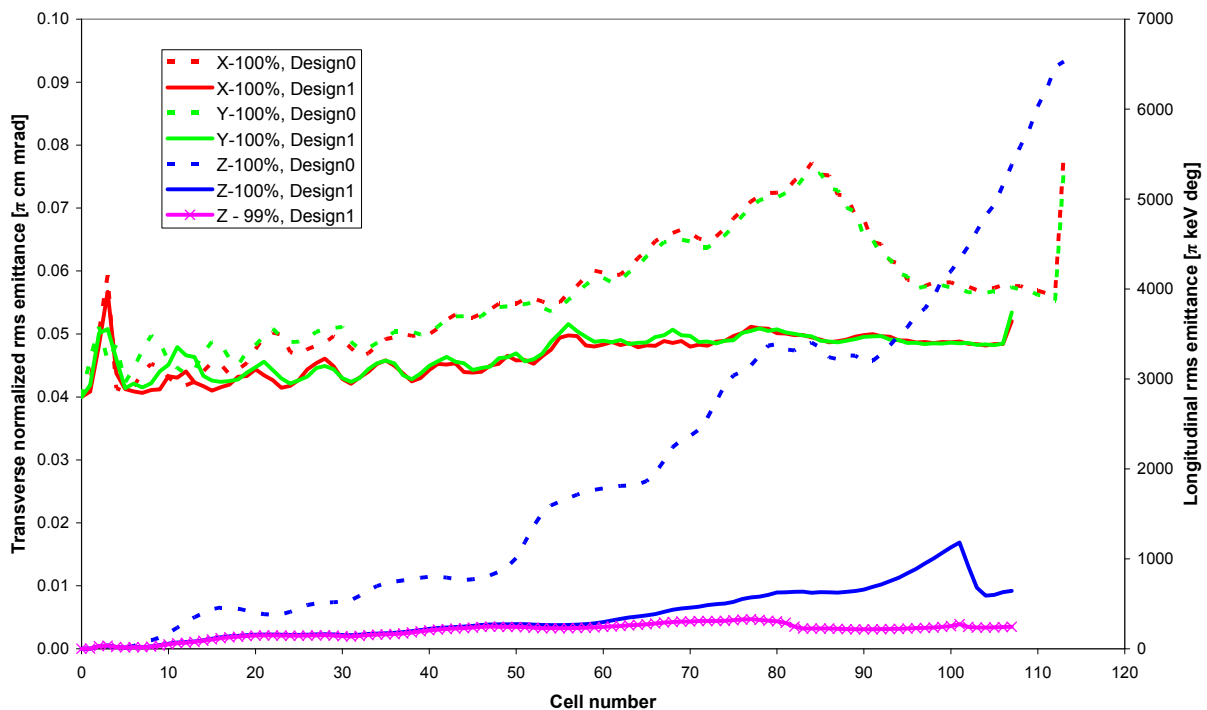

Fig. 4.2.1-6: Emittance growths along the RFQ for Design-0 (top) and Design-1 (bottom).
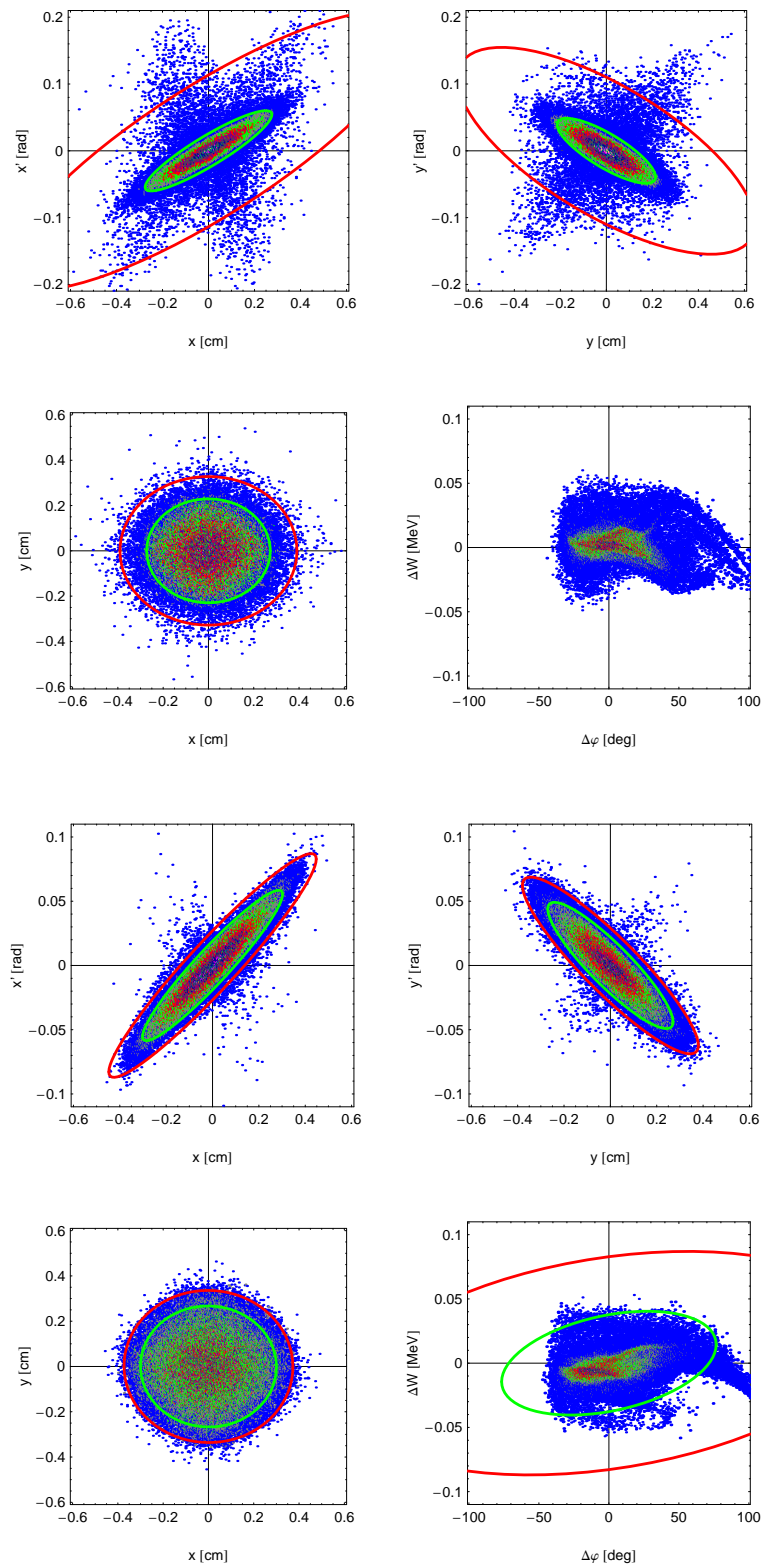
Fig. 4.2.1-7: Output particle distributions for Design-0 (top) and Design-1 (bottom).

Finally, the output particle cluster plots of the transverse and longitudinal phase spaces for the two designs are demonstrated in Fig. 4.2.1-7, where: 1) The scaling of the divergence for the

Design-0 scheme is two times that for the Design-1 one. 2) For both cases, the red and green ellipses, which shapes and orientations are referenced to the corresponding rms ellipse, are containing 99% and 90% of transported particles, respectively. 3) The particle densities are distinguished by 10 colors, and the blue color used for the outermost regions corresponds to the densities between 0 and 10% of the peak one.

Clearly, among the limited transported particles from the Design-0 RFQ, there are still lots of halo particles in the transverse planes, and meanwhile there should be a long beam "tail" in the longitudinal direction, as the ellipses are too large to be shown in the plot range. Therefore, the total quantity of the particles really usable for the following IH-DTL will be not too much. However, the plots for Design-1 RFQ indicate that the beam is concentrated in all spaces.

The detailed simulation results of both Design-0 and Design-1 will be presented in the next section together with the optimum design.

4.2.2 Longitudinal-Rotation Technique

Because of the strict length restriction and the modest inter-electrode voltage, the Design-1 RFQ has been able to maximally bunch the main beam into the range of ~ ±40°. However, it is still not sufficient to provide a satisfying matching to the successive IH-DTL machine. As mentioned, to achieve the best efficiency, the most suitable design approach for the H-type DTL accelerating structure is the KONUS beam dynamics concept, which is characterized by special configurations of the synchronous phases and energies for the accelerating gaps. Therefore, KONUS has relatively strict requirements to the longitudinal acceptance especially the phase spread $\Delta\varphi$ of the input beam. The typical input phase spread for an H-type DTL is between ±20° and ±30°. According to the actual situation of the FRANZ RFQ, this range is too difficult to be reached if a good beam bunching is required. Therefore, the goal of the phase spread of the RFQ output beam has been slightly relaxed to ±35°, which is reasonable because the following IH-DTL is a short machine with only very limited 0° gaps.

Based on the Design-1 scheme, another optimization strategy so-called the Longitudinal-Rotation Technique, which can rotate the output beam to a more vertical position in longitudinal phase space, has been proposed. As shown in Fig. 4.2.2-1, the rotation was realized by giving the evolution of the synchronous phase an unconventional "kick" – φ_s had gone back to more negative, ~60°, for a short time – at the end of the RFQ in order to provide the beam a harder compression longitudinally again. Of course, it could be at some expenses such as a longer structure and a larger energy spread. For facilitating the discussions, after the longitudinal-

rotation the modified Design-1 scheme is renamed as Design-2, which is almost identical to the former one except the short part behind Cell97.
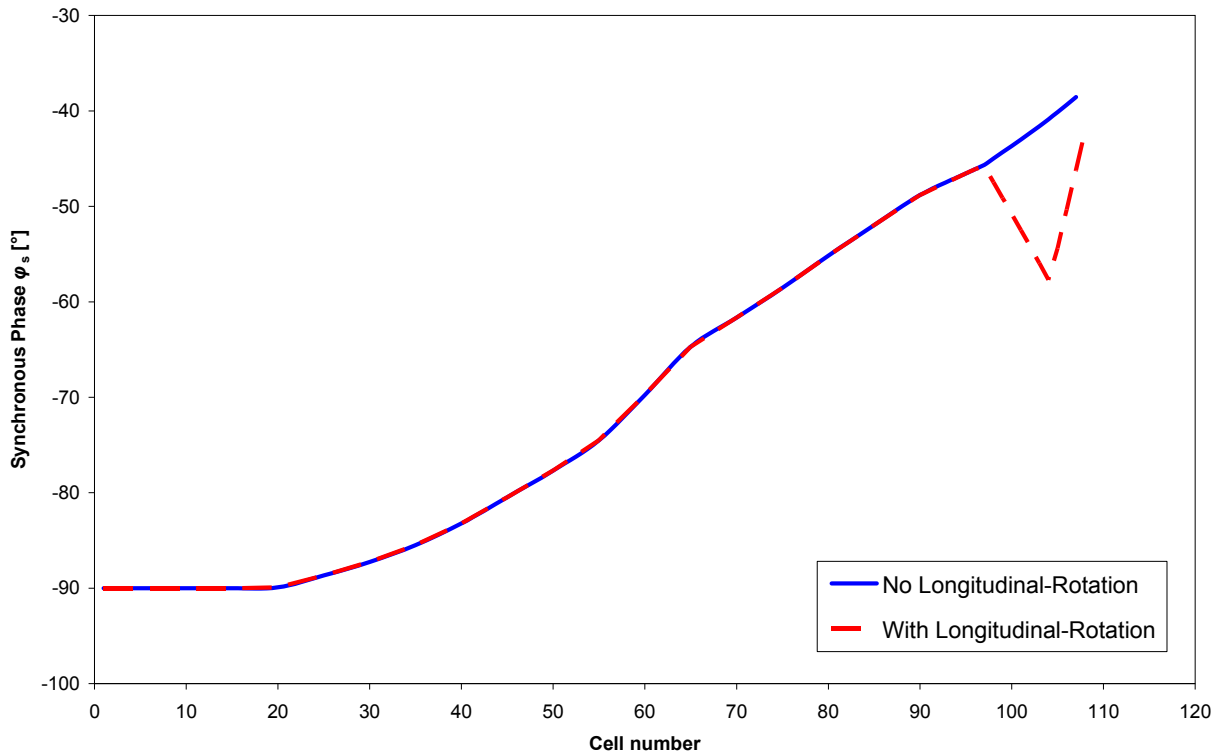

Fig. 4.2.2-1: φ_s vs. cell number before and after the longitudinal rotation.
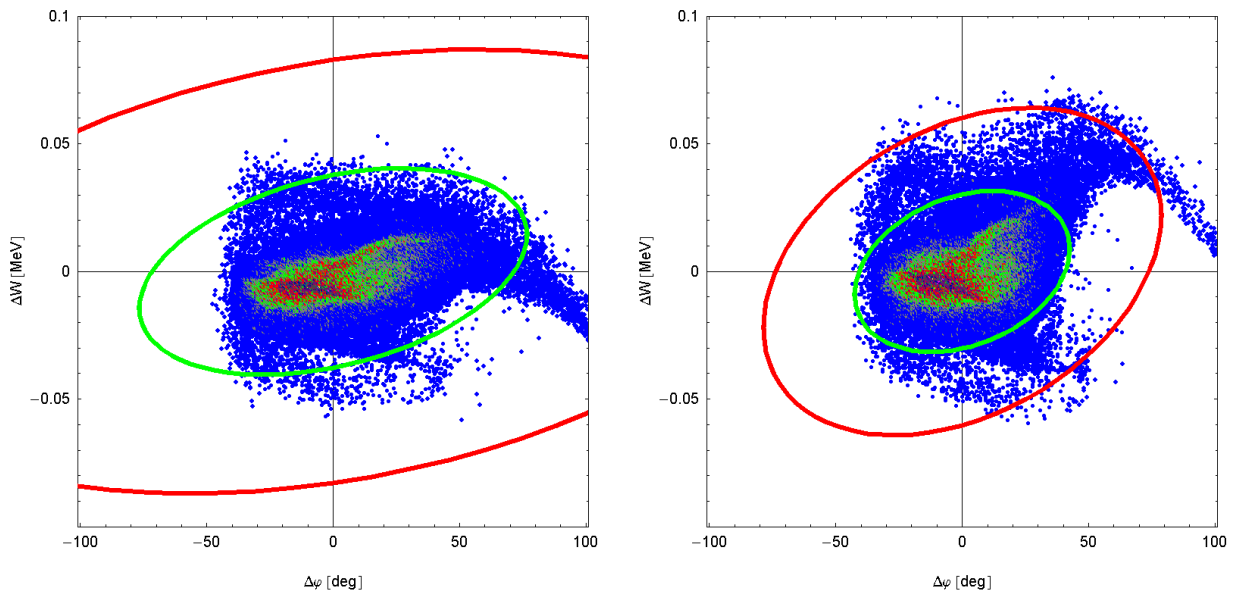

Fig. 4.2.2-2: Output longitudinal phase-space projections (left: Design-1, right: Design-2).

In Fig. 4.2.2-2, the output longitudinal phase spaces without and with the longitudinal rotation are compared, where the left picture demonstrates the situation for Design-1, and the right

one is for Design-2. As the last time, the two ellipses are including 99% and 90% of transported particles, respectively. It's clear that the output particle distribution has been rotated as expected in the longitudinal phase space with an obviously narrowed phase spread but a slightly larger energy spread. Meanwhile, the ellipses show that the particles are more concentrated after the rotation.

For the Design-2 scheme, the effective beam transmission efficiency has been checked as a function of the phase-spread limit. In Fig. 4.2.2-3, the two curves represent the cases of energy spread limits $\Delta W = \pm 30\text{keV}$ and $\pm 40\text{keV}$, respectively. For the required phase spread of $\pm 35°$, both effective beam transmission efficiencies are over 90%. Therefore, the main output beam from the RFQ could be safely matched into the downstream IH-DTL.
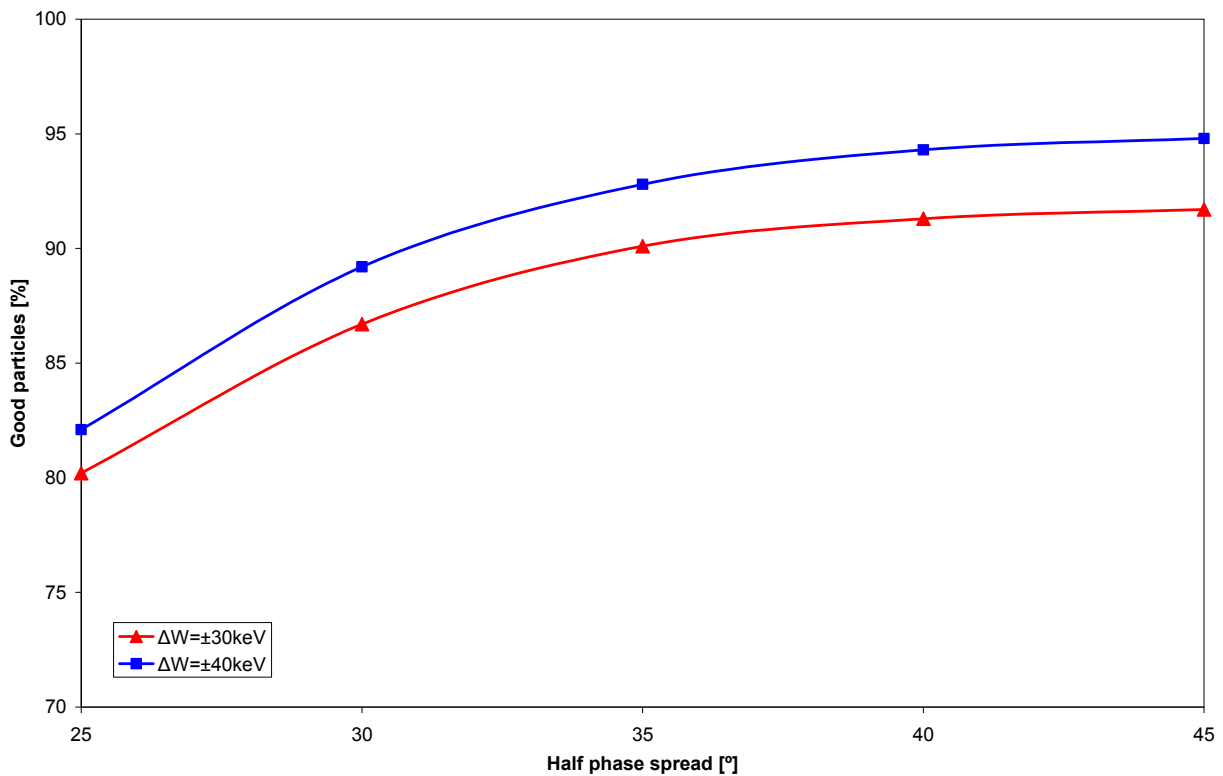

Fig. 4.2.2-3: Effective beam transmission efficiency as a function of phase-spread limit.

The detailed design parameters and simulation results for Design-0, -1 and -2 listed in Table 4.2.2-1 show that the Longitudinal-Rotation Technique is very efficient: all parameter values of Design-2 e.g. the beam transmission efficiency and the output transverse emittances are almost same as those of Design-1, except that the total length is only ~3cm longer (which means just one more cell is needed), but the output longitudinal emittance has been improved by ~20%.

Table 4.2.2-1: Three beam dynamics designs for the FRANZ RFQ.

Design / Parameter	Design-0	Design-1	Design-2
Design approach	LANL-FSP	"BABBLE"	"BABBLE"
Longitudinal-Rotation	No	No	Yes
Frequency [MHz]	175		
Input / output energy [MeV]	0.120 / 0.700		
Beam current [mA]	200		
Inter-electrode voltage [kV]	85		
$\varepsilon_{in}^{trans., norm., rms}$ **[π mm mrad]**	0.40		
Kilpatrick factor	1.45	1.59	1.59
Minimum aperture [cm]	0.41	0.42	0.42
Maximum modulation	1.63	1.51	1.51
$\varepsilon_{out}^{x, norm., rms}$ **[π mm mrad]**	0.79	0.52	0.53
$\varepsilon_{out}^{y, norm., rms}$ **[π mm mrad]**	0.76	0.53	0.52
$\varepsilon_{out}^{z, rms}$ **[π MeV deg]**	6.53	0.64	0.51
Cavity length [cm]	211.14	196.05	199.01
Total number of cells	113	107	108
Beam transmission [%]	78.3	98.3	98.3

In conclusion, the performance of the Design-2 scheme has well met the project requirements:

- The high transmission efficiency is not only favorable to reach an as high as possible proton intensity on the n-production target, but also comfortable for the future routine maintenance.
- The whole RFQ is 1.99m in length, so it is as compact as demanded.
- The Kilpatrick factor is 1.59, which is slightly higher than the Design-0 one but still safe enough for the planned CW operation.

4.3 Design-Stability Investigations

Using simulated off-design conditions to test the safety margins and the potential capabilities of a designed RFQ accelerator is of practical importance for the future construction and operation.

According to the capability of the PARMTEQM simulation code, seven kinds of non-ideal cases have been investigated without changing the designed RFQ structure:

- Input beam current (I_{in}).

- Input transverse emittance (ε_{in}).

- Twiss parameter α_{in} of the input emittance ellipse.

- Twiss parameter β_{in} of the input emittance ellipse.

- Vibration of the inter-electrode voltage (V_{fac}).

- Energy spread of the input beam (δW).

- Transverse beam displacement from the beam axis at injection (δx).

Table 4.3-1: Stability-investigation settings for the FRANZ RFQ.

Setting / Parameter	Design value	Variation steps	Step length
I_{in} [mA]	200	Smaller I_{in}: 6 Larger I_{in}: 4	25
$\varepsilon_{in}^{trans.,unnorm.,real}$ [π mm mrad]	150.06	Smaller ε_{in}: 3 Larger ε_{in}: 7	20
α_{in}	1.75	Smaller α_{in}: 5 Larger α_{in}: 5	0.1
β_{in} [cm/rad]	14.74	Smaller β_{in}: 5 Larger β_{in}: 5	1.0
V_{fac}	1.0	Smaller V_{fac}: 5 Larger V_{fac}: 5	0.01
δW [%]	0	Smaller δW: 0 Larger δW: 10	± 1
δx [mm]	0	Smaller δx: 0 Larger δx: 10	0.1

Including the design values, the variation step numbers and the step lengths, the settings shown in Table 4.3-1 were defined for the tolerance-investigation studies on the Design-2 scheme of the FRANZ RFQ. For each case, 10 steps of variations with a same interval were generated with respect to the design value (*Note: the variations are not necessary to be symmetric about the design value*). In addition, I_{in} and ε_{in} were mainly used to check the operation flexibility or the upgradability, so relatively larger step lengths of variations have been particularly chosen for them. The intervals for other quantities were referenced to the operation and measurement experiences.

For the convenience of comparison, the studies have been started with the premise of varying only one parameter per time. Therefore, in most cases only the nominal design has a matched input beam. The following results of the other designs for the tolerance investigations could be somewhat better if the input beam parameters are adjusted to be matched.

Firstly, with a changing input beam current from 50mA to 300mA, the evolutions of the beam transmission efficiency and the output beam current are shown in Fig. 4.3-1. Clearly, between 50mA and 200mA, the transmission curve is quite flat, and afterwards it slowly goes down; however, even at 300mA which is 1.5 times as high as the design intensity, the beam transmission efficiency is still over 92%. Another curve shows that the relationship between the output beam current and the input one is quasi-linear, which means the current limit is still far away to be reached.
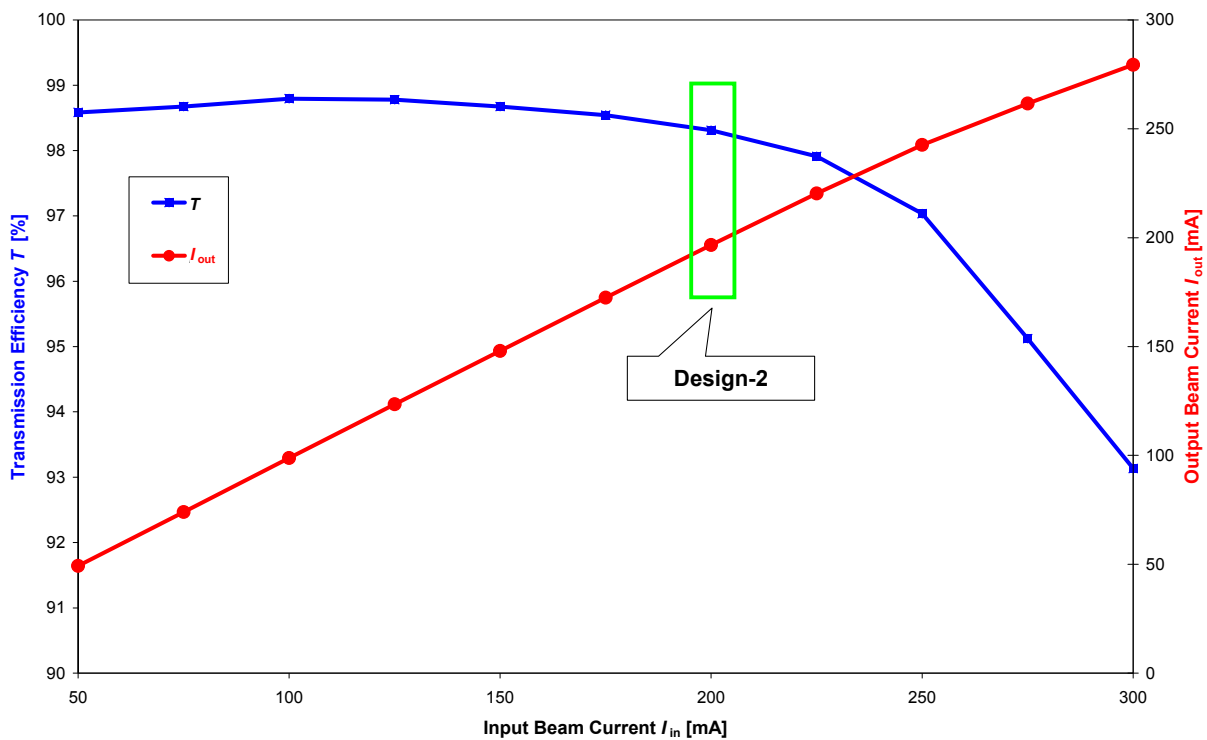

Fig. 4.3-1: T and I_{out} vs. I_{in}.

Secondly, the unnormalized total transverse input emittance has been investigated as the independent variable. For 200mA such an ultra-high intensity, it makes sense to check more "larger input emittances" than smaller values. Corresponding to the given $\varepsilon_{in}^{trans.,unnorm.,total}$ values, different-sizes of transverse input emittance ellipses are plotted in Fig. 4.3-2, where the one with an area of 0.015006 π cm rad ($\Leftrightarrow$ 0.40 π mm mrad as a normalized rms value) is representing the nominal case.
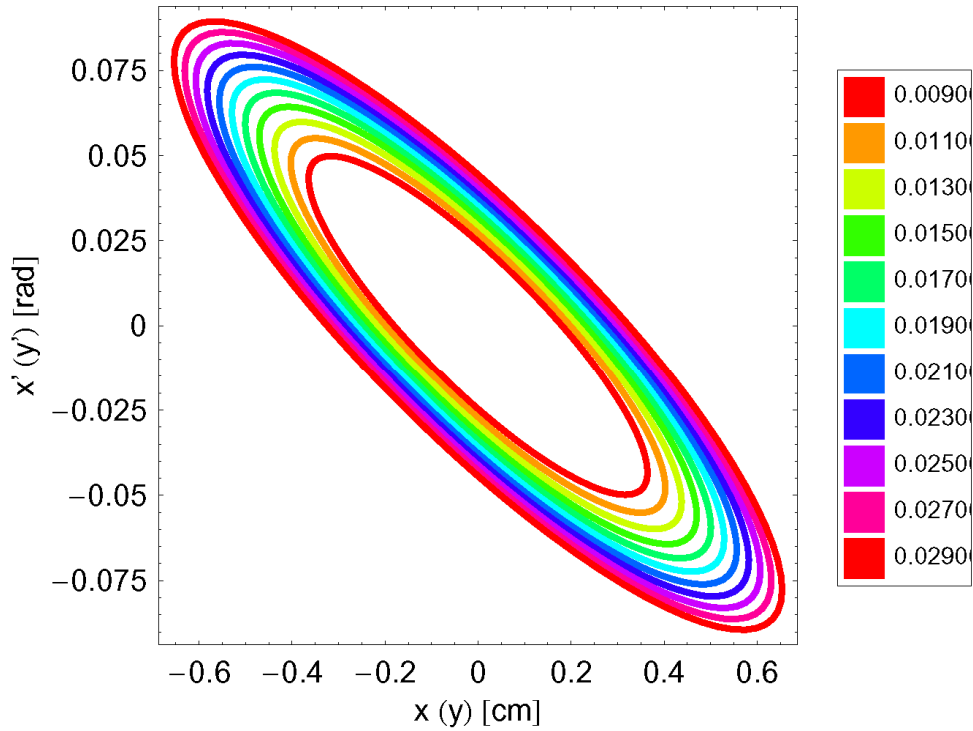
Fig. 4.3-2: Different transverse input emittance ellipses for different ε_{in}.

Obviously, the output emittances and especially the beam transmission T are insensitive to the changes, even when the transverse input emittance is 0.029 π cm rad, almost 2 times of the design value (see Fig.4.3-3). It leaves a large operational margin for the ion source.

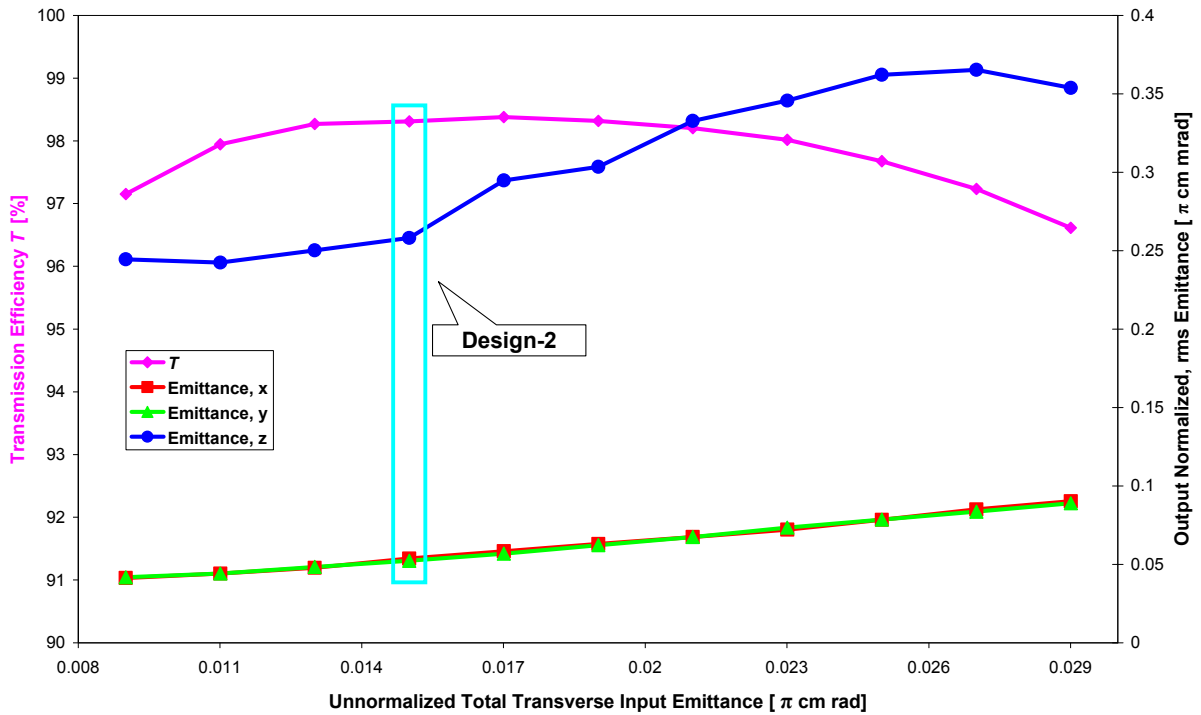Fig. 4.3-3: T and ε_{out} vs. ε_{in}.

Then the mismatching cases were explored with the Twiss parameters, α and β, of the input emittance ellipse. The relationship between the Twiss parameters and the emittance is shown in Fig. 4.3-4 and described by the formula Eq. (4.3-1).
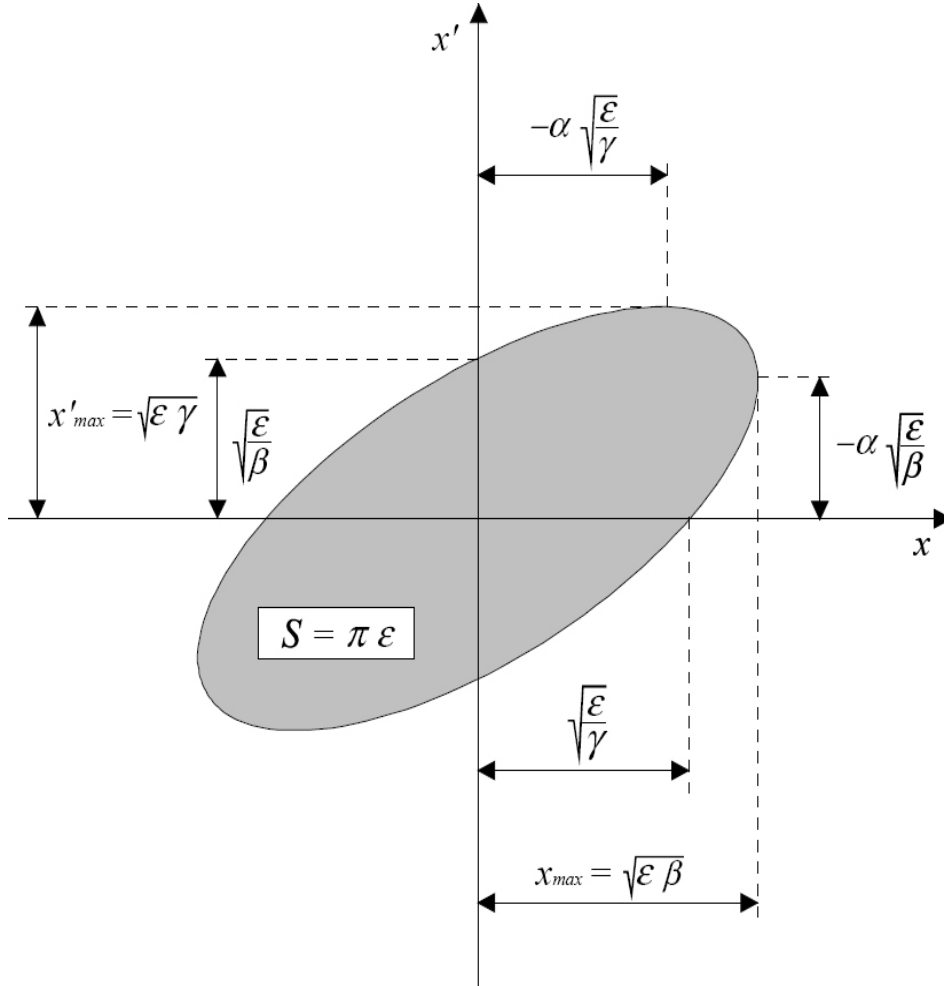

Fig. 4.3-4: The emittance ellipse.

$$\varepsilon = \gamma x^2 + 2\alpha xx' + \beta x'^2 \qquad (4.3\text{-}1)$$

with:

$$\gamma \equiv \frac{1+\alpha^2}{\beta} \qquad (4.3\text{-}2)$$

where $\pi\varepsilon$ is the area of the ellipse containing the particles.

With a varying α or β, the shape and orientation of the transverse input emittance ellipse are changing as shown in Fig. 4.3-5, where the light-blue ones, i.e. the middle ones, are representing the Design-2 case. Obviously, α is influencing on not only the shape but also the orientation of the ellipse, while β is simply rotating the ellipse, so the effects from the β variation could be faster and more harmful.
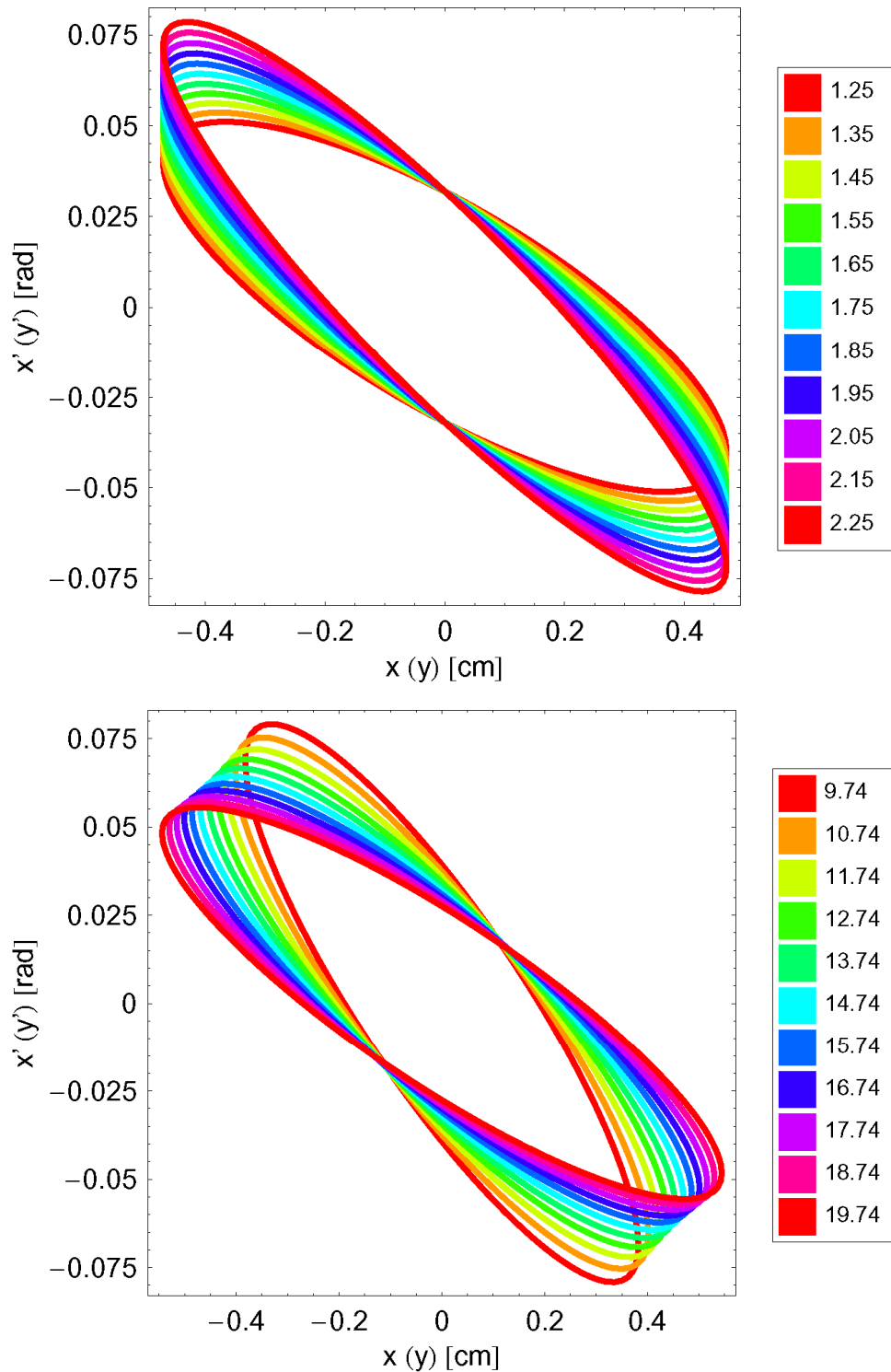
Fig. 4.3-5: Transverse input emittance ellipses changing with α (top) or β (bottom).

To keep the chapter compact, the results of another study on the inter-electrode voltage factor (the ratio of the imposed inter-electrode voltage to the design one) have been plotted together with the results for α and β in Fig. 4.3-6. Because for all these three cases the design value is in the same order in the test list, the abscissa can use the test step (the tests have been started from small values to large ones) as the independent variable. Because of the same reason, the results

for both the input energy spread δW and the displacement of beam injection δx are presented together in Fig. 4.3-7.
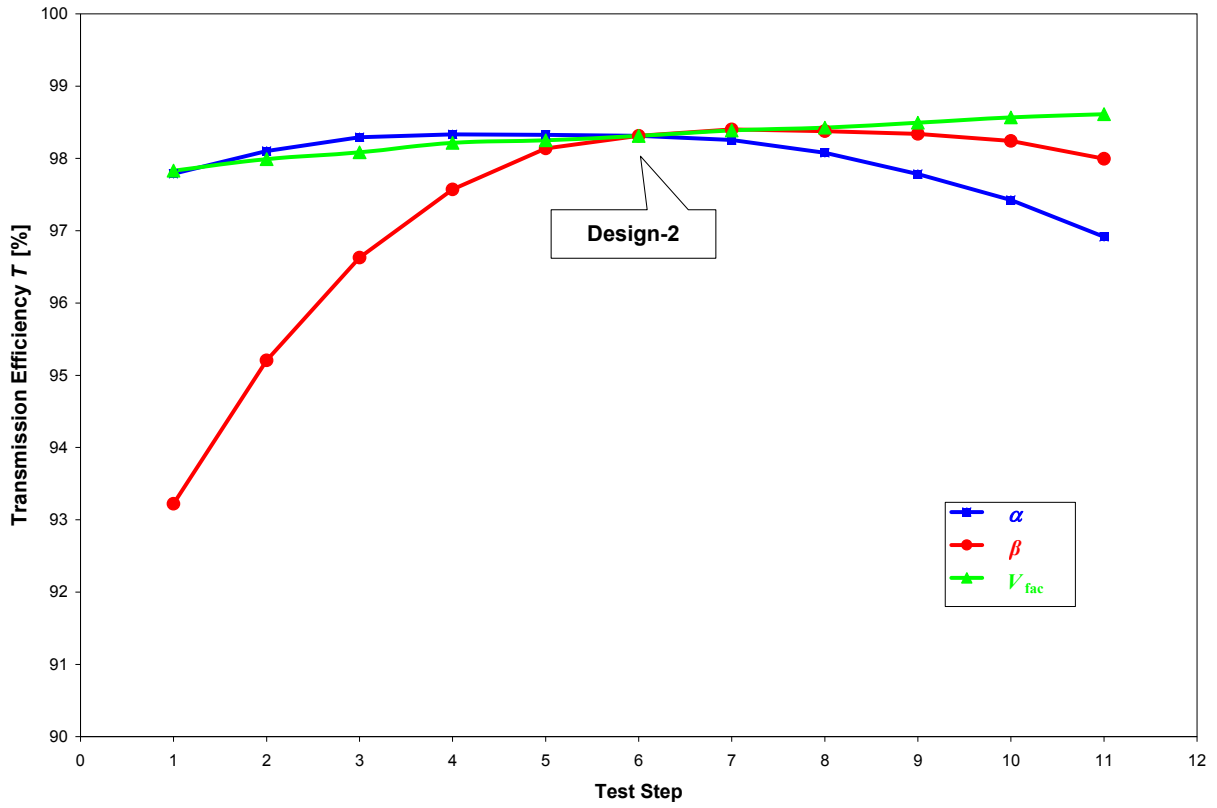

Fig. 4.3-6: T vs. α, β or V_{fac}.

Fig. 4.3-7: T vs. δW or δx.
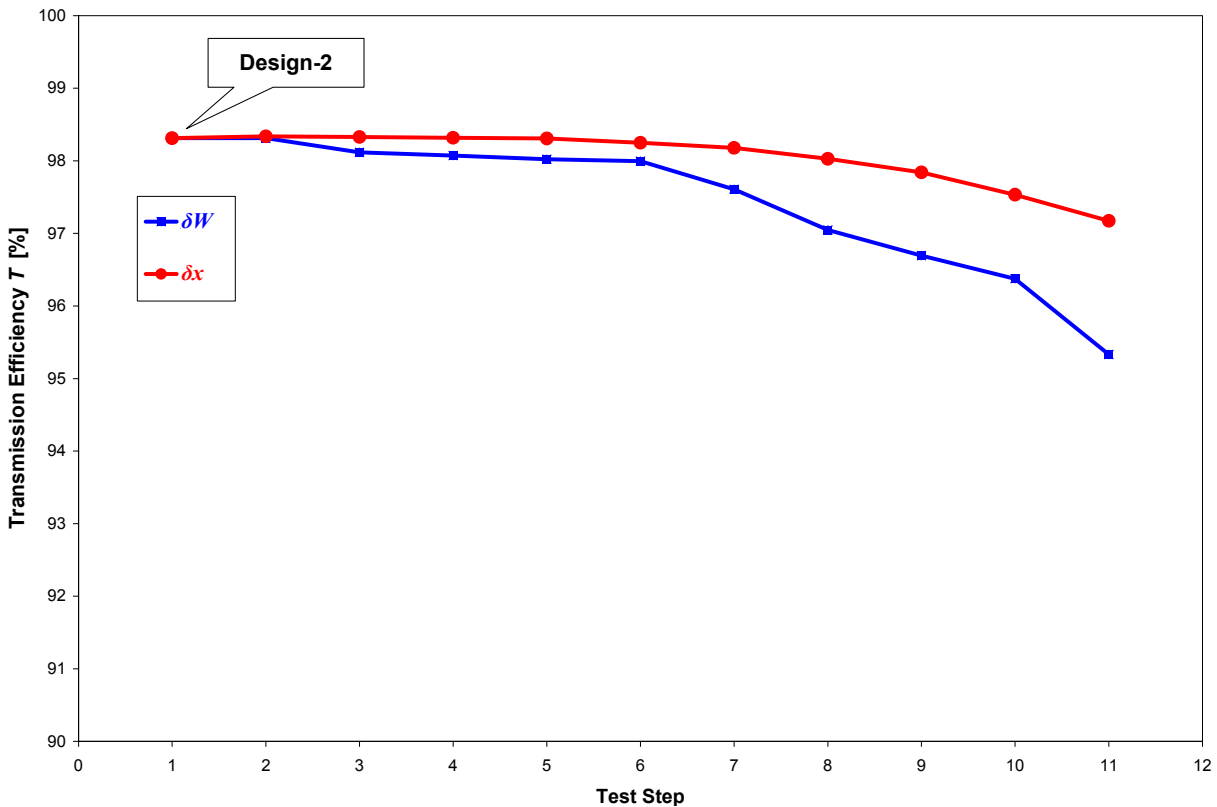
For all above-performed parameter-scanning checks, the minimum beam transmission is still >93%, which indicates that Design-2 scheme is robust enough to allow future upgrade and flexible operation.

4.4 Conclusions

The test design studies show that the classic RFQ design approach, the LANL Four-Section Procedure, which was developed at the end of 1970s by neglecting the space-charge forces, is not sufficient to provide a satisfying design for the 200mA FRANZ RFQ. The shortcomings of the LANL method are as below:

- The strongly "pushed" bunching in the SH section is the source of unstable particles (as well known, the upstream of an RFQ has a crucial influence to the performance of the whole machine; if the beginning is bad, the situation can not be easily improved by the rest part).
- The parameter variations in the GB section are too slow to make the RFQ short.
- The constant-B law makes the design work not flexible.

To realize a balanced and accelerated beam bunching at low energy for modern high-intensity RFQ accelerators, a new design procedure called "BABBLE" has been proposed. By adapting the transverse focusing strength B to the changing space-charge effects and properly retuning the variation speeds of the synchronous phase and the electrode modulation along the RFQ, the beam can be longitudinally focused under balance of forces in a reasonable, smooth and efficient way.

The optimization design practice of the FRANZ RFQ has shown that at a moderate inter-electrode voltage, the "BABBLE" strategy is feasible to achieve a design for a high-intensity up to 200mA RFQ with the following features simultaneously:

- Low particle losses.
- High beam quality.
- A compact structure.
- Robustness to various errors in wide ranges.

In addition, the Longitudinal-Rotation technique has also opened an option to solve the longitudinal matching problem between an RFQ accelerator and a KONUS-based H-type DTL accelerator.

5. DTL Design for IFMIF

Based on an accelerator-driven neutron source using the D-Li stripping reaction, the International Fusion Materials Irradiation Facility (IFMIF) is aiming to build an appropriate test environment for the development of fusion reactor materials. The required 250mA, 40MeV deuterons on the Li target will be provided by two 125mA CW driver linacs working in parallel. Though the RFQ accelerator has been decided as the initial accelerating structure up to several MeV at the very beginning, until now IFMIF is still looking for an efficient drift-tube linac to continue the acceleration to 40MeV with high beam qualities and to permit hands-on maintenance. The original as well as reference DTL candidate is the conventional normal-conducting (NC) Alvarez-type structure, but a later proposal based on the H-type structure and the superconducting technology has become an attractive alternative. The focal point of this chapter is the optimization on the preliminary H-type DTL design for IFMIF with respect to the linac system and the beam dynamics. Besides a more realistic linac-layout configuration and considerably smaller transverse beam sizes and emittance growths, the greatly improved robustness against various non-ideal construction and operation conditions, which has been confirmed by more thorough error studies, is another advantage of the new design. Finally, a brief comparison between the reference Alvarez-DTL design, the new version of the H-type DTL design and another competitive SC DTL option using the HWR (Half-Wave Resonator) structure is presented.

To simulate the high-flux neutrons in a fusion enviorment, the accelerator system of the IFMIF facility has to deliver 250mA, 40MeV deuterons on a liquid Li target with a rectangular (20cm×5cm) and uniform beam footprint in a CW mode [IFM04]. For 250mA which is beyond the intensity record of the present RF hadron linac technology, a two-linac scheme is more favorable because it can not only divid the peak current in half but also provide operational redundancy. In each driver linac, the beam acceleration will be done in two steps:

- An RFQ accelerator: 95keV – 5MeV.
- An DTL accelerator: 5MeV – 40MeV.

The reference linac layout was discribed in the IFMIF Comprehensive Design Report (CDR) published in 2004:

- For the RFQ accelerator, a design based on the Equipartitioning Procedure (EP) (see [JAM07] for details) has been adopted (therefore, the output beam of the reference EP-RFQ will be used as the basis of our DTL design studies).

- Concerning the DTL part, an NC Alvarez-type structure based on the CEA (Commissariat à l'Energie Atomique – French Atomic Energy Commission) design has been nominated.

Table 5-1: Top-level performance requirements and characteristics
for the IFMIF DTL [IFM04].

Requirement	Specification	Detail / Comment
Particle type	D^+	H^{2+} for testing (avoids activation)
DTL type	Alvarez	With post couplers
Number of DTL tanks	10	
Total length	30.3 m	Based upon the CEA design
RF operating frequency	175 MHz	
Beam input energy	5 MeV	
Beam output energy	40.2 MeV	Based upon the CEA design
Beam input current	125 mA	
Beam output current	125 mA	Current loss < 0.3 µA/m (3 nA/m goal)
Total RF power (beam + cavity)	6.45 MW	10 RF tubes, 20 RF couplers
Beam power	4.40 MW	
Beam efficiency	68 %	Based upon the CEA design
Beam aperture	2.5 cm	Diameter
Synchronous phase	-45 to –30 deg	Based upon the CEA design
Norm. rms transverse emittance	$\leq 0.4\ \pi$ mm mrad	Based upon the CEA design
Norm. rms longitudinal emittance	$\leq 0.8\ \pi$ mm mrad	Based upon the CEA design
Duty factor	CW	Pulsed tune-up and start-up
Maintainability	Hands-on	Design not to preclude remote maintenance

According to the CEA design, the top-level specifications for the IFMIF DTL are summarized and given in Table 5-1, while a schematic layout of the whole IFMIF driver linac is shown in Fig. 5-1, where the DTL part consisting of a short MEBT (Medium Energy Beam Transport) section and ten Alvarez-type tanks is ~30m long.
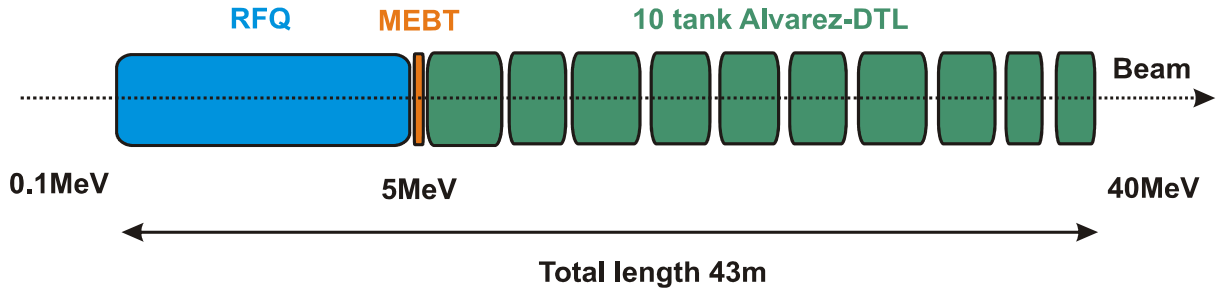

Fig. 5-1: Layout of the reference RFQ + Alvarez-DTL linac for IFMIF [SAU07].

In the required total RF power for the normal-conducting reference Alvarez-DTL, ~2MW will be dissipated on the RF structures. It will not only result in remarkable operation costs but also bring unusual challenges to the cooling issues for such a CW machine. Up to now, these problems are still remaining unsolved for the NC accelerator technology.

5.1 H-Type DTL Designs

Enabled by the advance in RF superconductivity, a promising solution mainly based on SC H-type structures has been proposed by IAP [SAU07]. As demonstrated in Fig. 5.1-1, this alternative IFMIF driver linac replaced the 10-tank Alvarez-DTL by a 11.5m-long, 8-tank (1 NC and 7 SC) CH-DTL (for the convenience of discussion, this design is named as "CH-Design-1"). Taking advantage of the high RF efficiency of the SC CH modules, the project budget could be greatly cut down due to a significant length reduction of ~20m and an SC operation for the main part of the DTL.
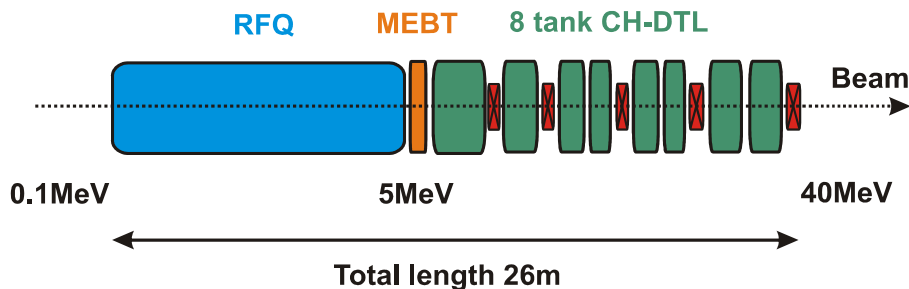

Fig. 5.1-1: Alternative layout of the IFMIF driver linac with 8 CH-tanks [SAU07].

Using the output particle distribution of the reference EP-RFQ (generated by the PARMTEQM code with 10^6 of input macro-particles) as the input distribution, the beam transport simulation of the 8-tank CH-DTL with drift-tube apertures ranging from 30mm to 100mm showed the beam transmission efficiency was 100%. However, as shown in Fig. 5.1-2, the transverse emittance growths of CH-Design-1 are 226% and 145%, respectively, which are much larger than the corresponding values of the reference design: 54% and 117%.
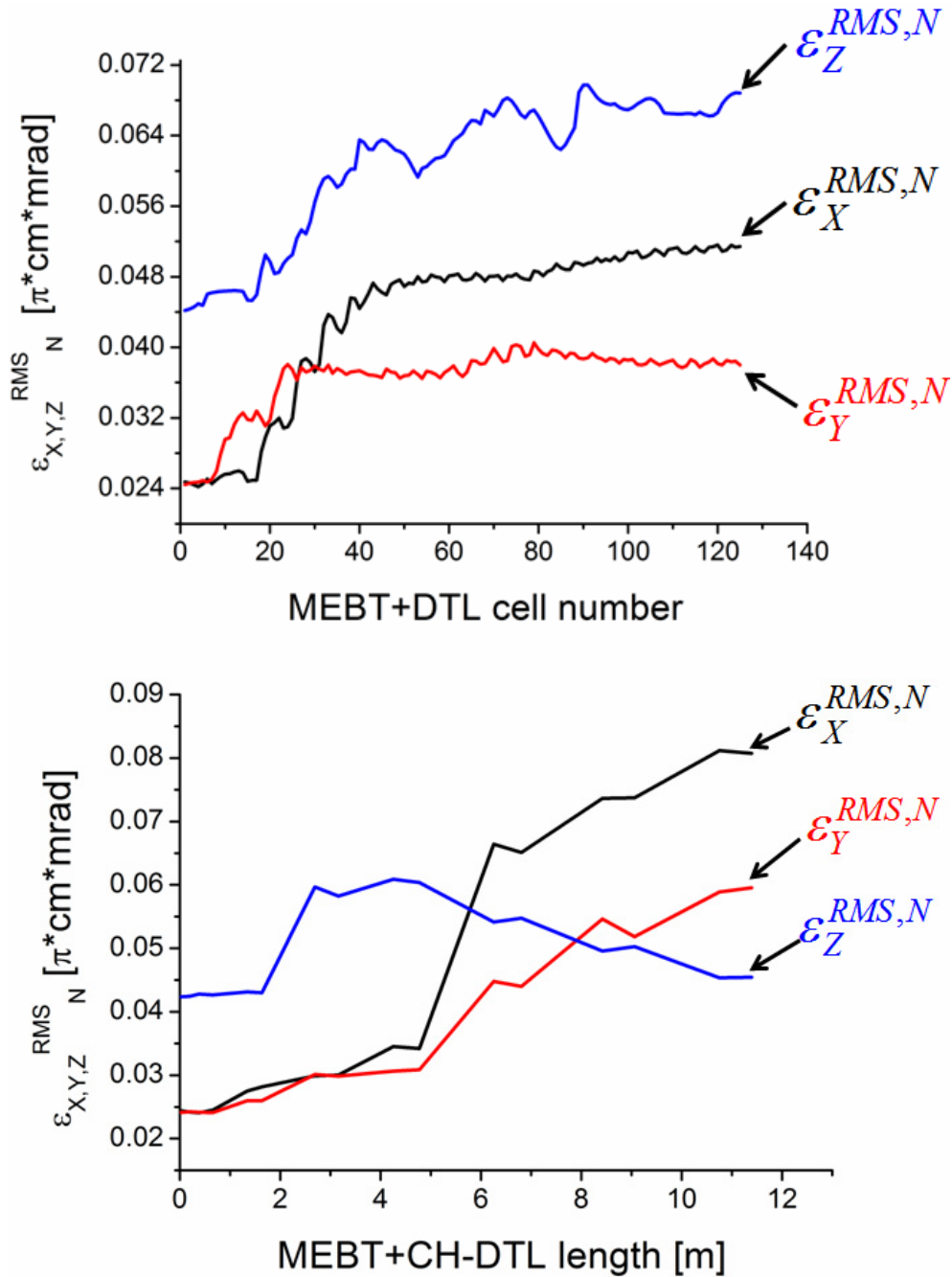

Fig. 5.1-2: Comparison of transverse and longitudinal emittance growths between the reference Alvarez-DTL design (top) and the 8-tank CH-DTL design (bottom) [SAU07].

Other two drawbacks of the exploratory CH-Design-1 [RAT07b] are:

- Involving iron yokes, the quadrupole focusing method has been used for both NC and SC cavities, which gives a risk in increased RF losses caused by non-zero static magnetic fields.

- The drift spaces between cavities are somewhat too short for a reasonable technical design.

To overcome all these shortcomings, further design studies were recommended by the two expert meetings at the end of 2006 and early in 2007 within the EU IFMIF initiative for checking the superconducting CH approach for IFMIF.
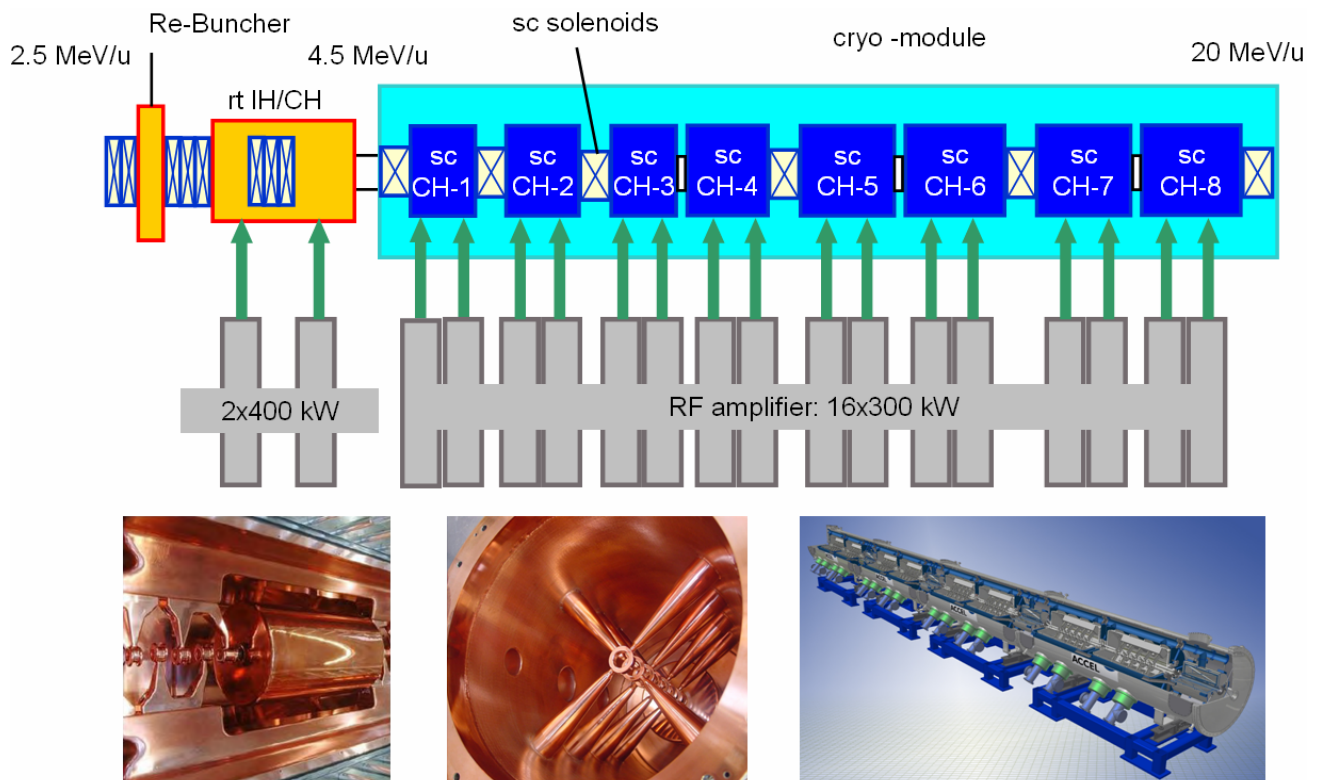
5.1.1 Linac Layout Improvements

Fig. 5.1.1-1: A new proposal of the H-type DTL layout for IFMIF

(Courtesy of H. Podlech and ACCEL).

Introducing one more SC CH-cavity, a new IFMIF-DTL layout proposed by IAP is demonstrated in Fig. 5.1.1-1, where the "Re-Buncher" is namely the MEBT and the NC DTL cavitiy of the CH-Design-1 has been added an IH option – without changing the beam dynmaics issues –

because of the higher shunt impedance of the IH structure. For comparison, the new design will be hereinafter called as "CH-Design-2".

The new DTL layout is a result of a series of changes and improvements with respect to the following requirements: 1) To further decrease the project costs. 2) To be more reasonable for the technical design. 3) To leave larger safety margins. 4) To improve the beam quality.

First of all, the originally planned 1MW RF amplifiers have been decided to be replaced by the more standard 300kW ones, which can reduce the capital costs. However, as the CH-Design-1 layout is already compact enough, the amount of cavities in the new design should be kept similar. To meet this requirement, the following decisions were made:

- To use two 300kW RF power couplers to feed every new SC CH-cavity.
- To drop the accelerating gradient, which is defined in Eq. (5.1.1-1), of each SC CH-cavity from the original 5.5–6MV/m to ~5MV/m (see Fig. 5.1.1-2).

$$E_a \equiv \frac{\text{summation of effective gap voltages}}{\text{summation of period lengths}} \qquad (5.1.1\text{-}1)$$

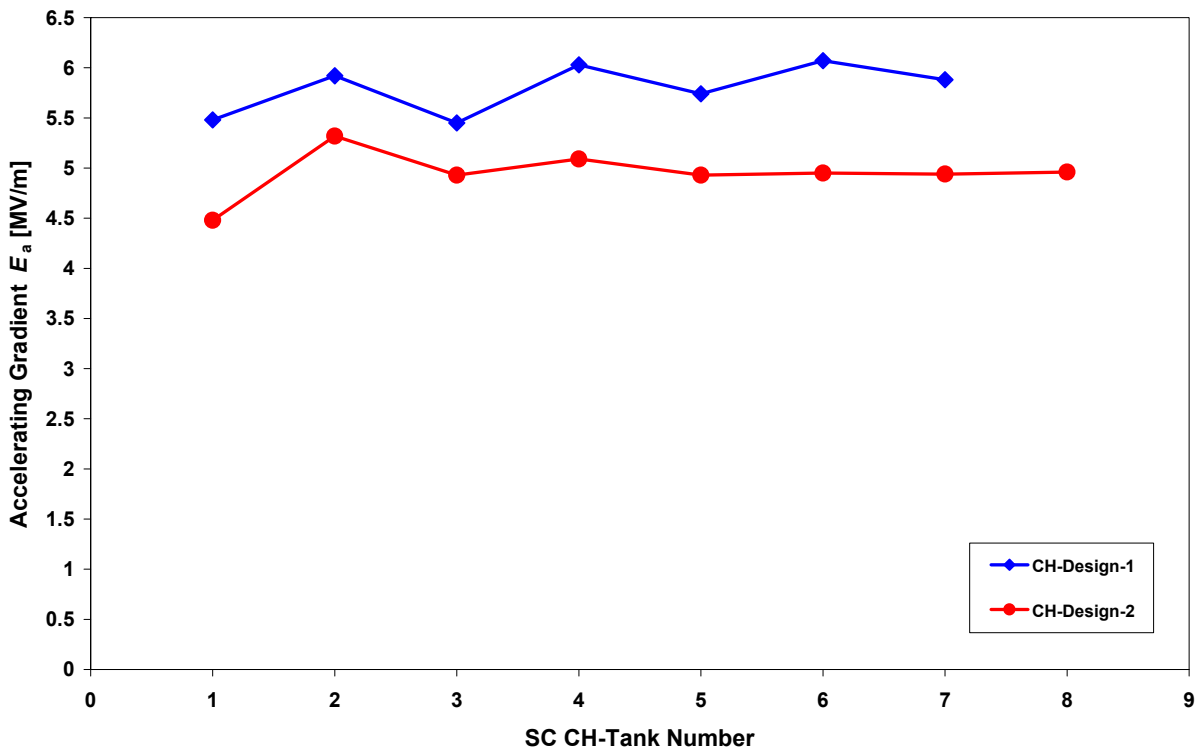Thus, finally only one more SC CH-cavity is needed.

Fig. 5.1.1-2: Preliminary and new accelerating-gradient settings of the SC CH-cavities.

Taking over a part of the beam-acceleration task from the original RT-CH cavity, this addtional SC CH-cavity can not only keep the whole structure compact but also save more RF power by shortening the RT-CH cavity.

Consequently, the number and effective voltages of the gaps in every cavity have been adjusted as shown in Fig. 5.1.1-3. Compared with the old design, the new layout has even one less gap. Meanwhile, the decreased gap voltages are also favorable to leave more saftey margins for reliable operation.
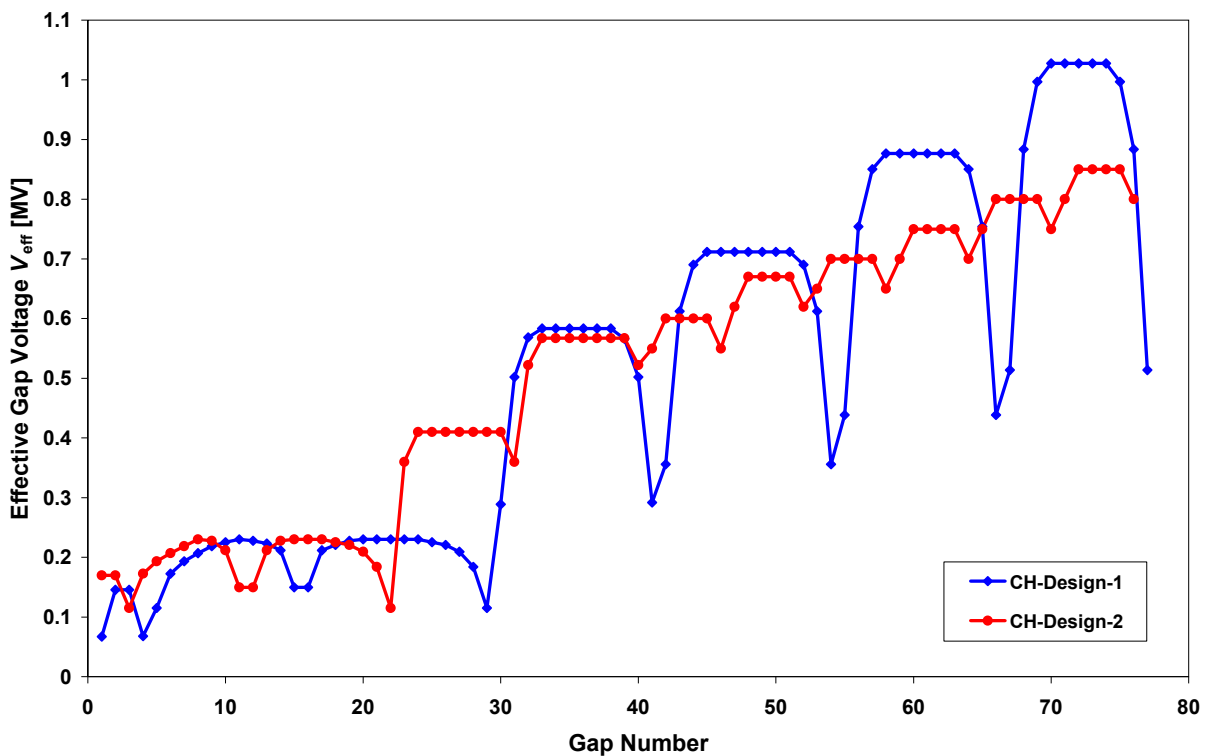

Fig. 5.1.1-3: Effective gap voltages of the H-type DTL layout before and after adjustment.

Secondly, the quadrupole lenses in the cold part have been all replaced by SC solenoidal lenses, which have the following attractive features:

- SC solenoid magnets can reach much stronger field strengths, ~ 4–10 times higher than the upper limit of the quadrupole ones.
- To provide the same transverse focusing, the SC solenoids are considerably shorter than the quadrupole lenses (in the IFMIF case, 12–15cm against 25–40cm).
- SC solenoids are safer to the superconducting state because no iron yokes are involved.
- Different than the quadrupole lens, which always focus the beam in one transverse plane but meanwhile defocus it in another transverse plane, the solenoids can focus the beam in

both transverse planes simultaneously. The resulted similar beam developments in the radial directions are very helpful to achieve good beam qualities.

Thirdly, the free drift space – excluding the space occupied by the transverse focusing element – between each two neighboring cavities has been considerably lengthened to reserve enough room not only for the cavity end-cell design and mechanical cavity coupling but also for housing other important non-accelerating components, for example: 1) The cryo-module and helium vessel for SC operation. 2) Tuner for cavity tuning. 3) Beam diagnostic devices. 4) Steerer for orbit corrections.

The important adjustments of the separations between the cavities are as follows:

- RFQ to MEBT: 17 => 25cm.

- MEBT to RT-CH: 25 => 38cm.

- RT-CH to SC-CH-1: this distance has been held almost same, but the free drift space has an increase of ~13cm in length because of the compact solenoid.

- The solenoid-free cold regions (i.e. SC-CH-3 to -4, SC-CH-5 to -6 and SC-CH-7 to -8): from 7, 9 and 10 => 16, 16 and 21cm, respectively.

The first two changes have been partly realized by shortening the MEBT re-buncher from 4 gaps to 2 gaps, which is also useful to decouple the beam from the cavity and ease the RF control under operation [RAT07b].

A brief comparison of the linac-system parameters between CH-Design-1 and -2 is made in Table 5.1.1-1.

Table 5.1.1-1: Preliminary and new H-type DTL layout designs.

Design Parameter	CH-Design-1	CH-Design-2
Number of RT tanks	2 (1 MEBT and 1 RT-CH)	2 (1 MEBT and 1 RT-CH)
Number of SC tanks	7	8
Total number of gaps	77	76
Number of RT lenses	8 (1 doublet and 7 triplets)	3 (1 doublet and 2 triplets)
Number of SC lenses	0	6
Total DTL length [m]	11.4	12.2

The preliminary and new H-type DTL layouts are demonstrated in Fig. 5.1.1-4, where the energy values are corresponding to the energies of the bunch-center particles at the end of all cavities, and the SC solenoids are marked in green.
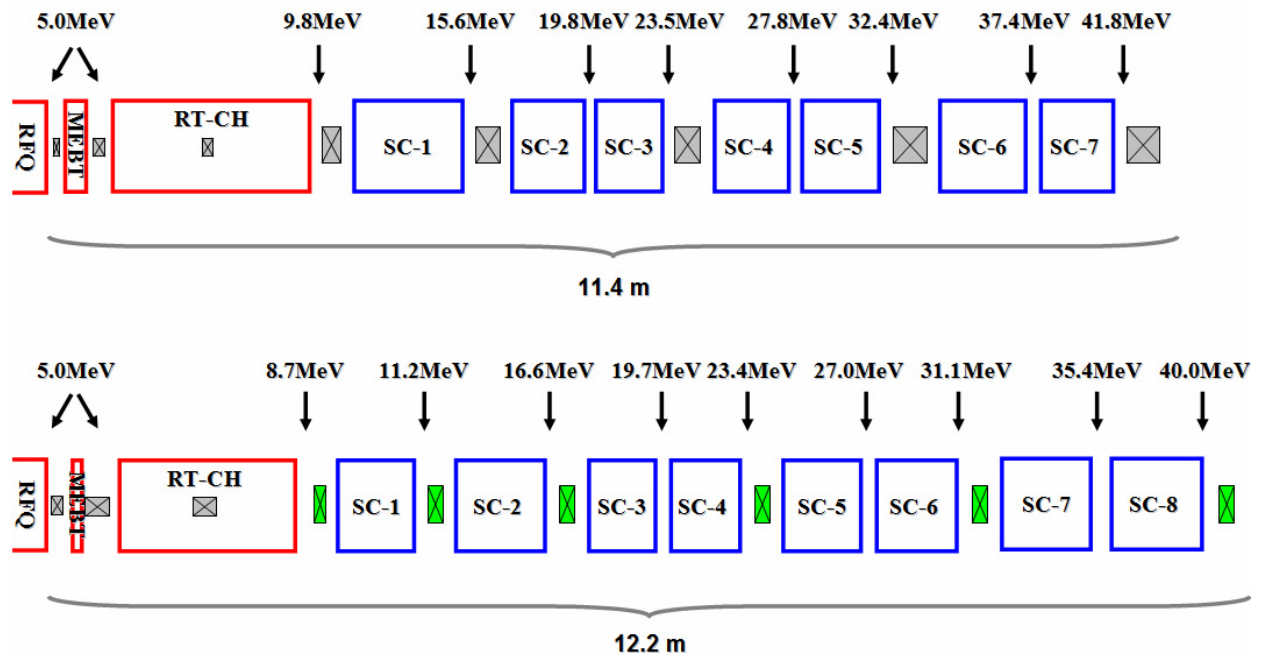

Fig. 5.1.1-4: Comparison of the DTL layouts between CH-Design-1 (top) and -2 (bottom).

5.1.2 Beam Dynamics Optimizations

Besides the above-mentioned improvements which were mainly done for the linac system, there were also some other important optimizations dedicated to the beam dynamics.

First efforts have been made for the radial beam dynamics. In Fig. 5.1.2-1, the transverse beam envelopes along the DTL are plotted for the CH-Design-1 case. Though the whole beam has successfully travelled through the accelerating channel, the following potential problems have to be overcome against various inevitable errors in construction and operation:

- At $z=\sim 1.6$m where the third lens locates, the envelopes are relatively too close to the bore aperture in the transverse planes, so this position could be a "bottleneck" of the whole machine.
- The beam envelopes become diverging at $z=\sim 4$m, and this situation continues until the exit of the DTL accelerator for both planes (actually shown in Fig. 5.1-2, the sudden and steep growths of transverse emittances have started from the same position), so the end of the SC-CH-1 cavity should be the most critical point for optimization.
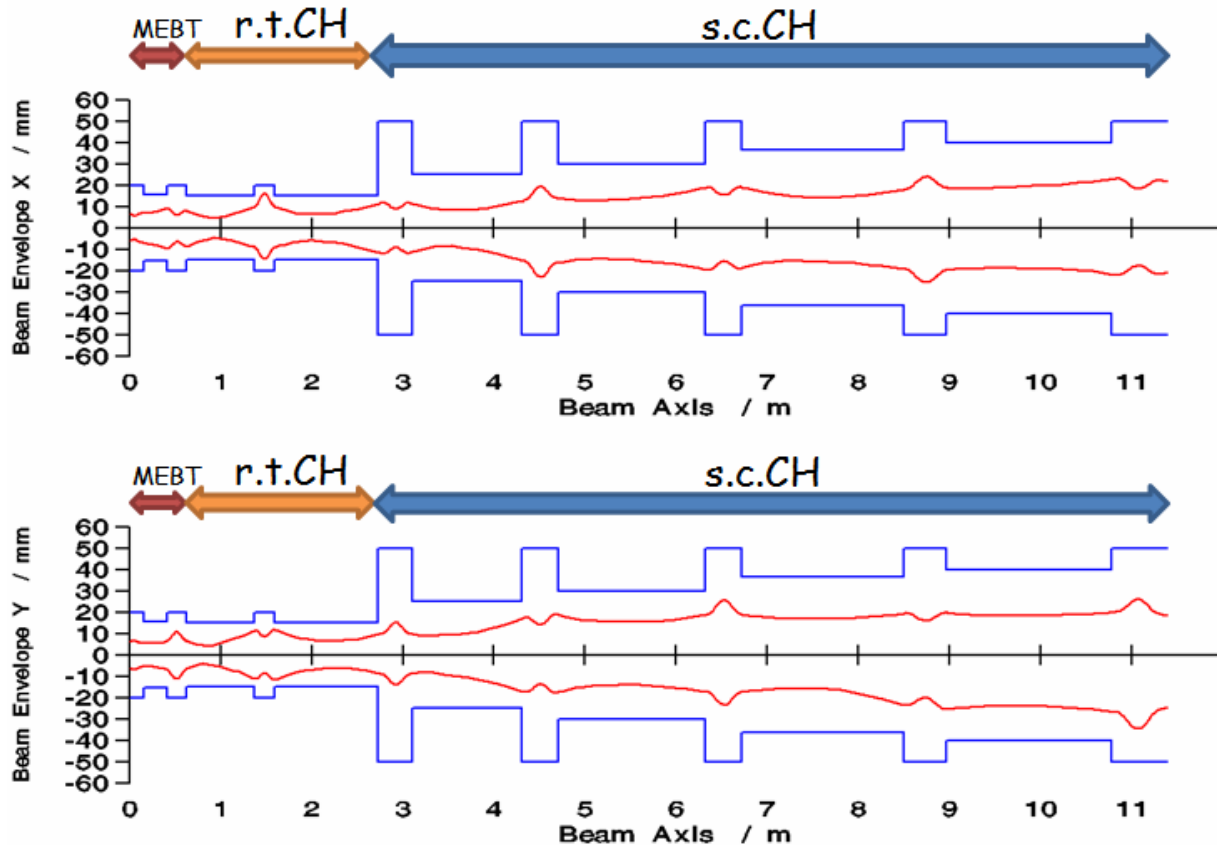
Fig. 5.1.2-1: Transverse beam envelopes along the DTL of CH-Design-1 [SAU07].

To address the first problem, the lenses in the warm part have been properly lengthened by 2–9cm, respectively, to make larger apertures possible. Finally, the lens aperture has been raised from 4cm to 5cm and the magnetic field strengths have been accordingly decreased by ~30%. This procedure is favourable to achieve a relatively longer and gentler transverse focusing at the beginning of the DTL part as well as is important to enlarge the safety margins.

The improvement of the situation in the cold part was realized not only by taking advantage of the much higher focusing strengths available from the SC solenoids but also by shifting every lens standing behind the SC-CH-2 cavity forward by one cavity, for example, the lens originally between the SC-CH-3 and -4 cavities has been moved to the location between the SC-CH-2 and -3 cavities. Performed in terms of the focal lengthes of the solenoids, the lens shifting helped keeping the beam divergences under control.

Using the same input distribution, the LORASR [TIE06] simulation of CH-Design-2 gave satisfying results. As shown in Fig. 5.1.2-2, in the RT part, the outermost particle has an enlarged minimum distance, ~10mm, to the bore aperture; while in the SC part, the new beam envelopes experience relatively stable oscillations and have obviously smaller sizes at the output. Consequently, the bore aperture in the cold part could be shrunk from 10cm to 9cm.
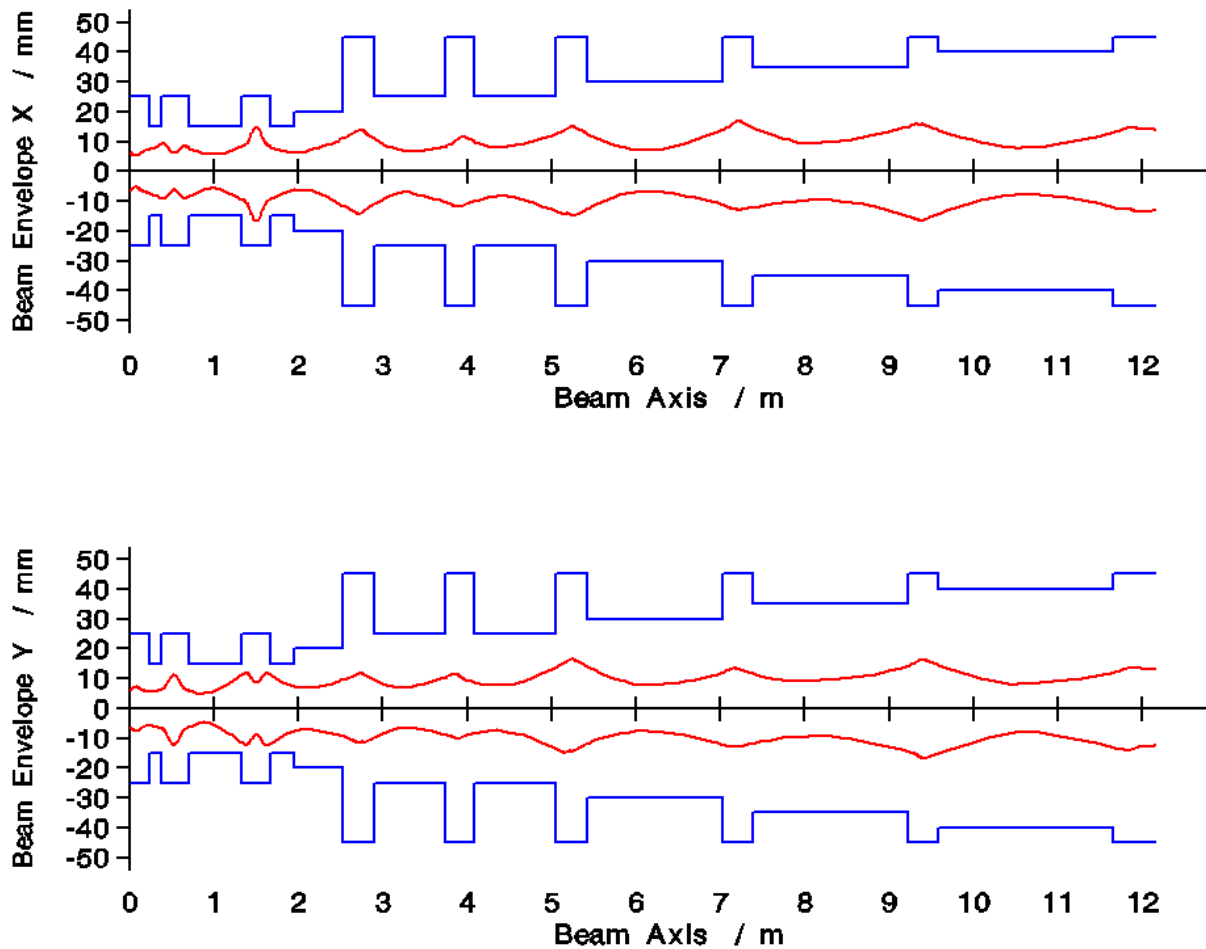
Fig. 5.1.2-2: Transverse beam envelopes along the DTL of CH-Design-2.

On the other hand, the longitudinal beam dynamics should be improved as well. After the optimizations of the radial beam dynamics, the transverse beam-bunch dimensions are considerably smaller, so the space-charge effects of the beam, especially for such a 125mA intense beam, become dramatically stronger. As a natural result, the beam should feel a much larger defocusing force in the longitudinal direction, so how to balance the increased defocusing effects is a critical point to avoid a fast longitudinal emittance growth. The optimization has been done by adjusting the phase- and energy-differences between the bunch-center particle and the synchronous particle at the beginning of every $\varphi_s=0°$ section as following:

- The phase difference, $\Delta\varphi$, in the first gap of each 0° section has been modified from the original value 0° − -5° to ~-5°.

- Meanwhile, the relative energy difference, $\Delta W/W$, at the beginning of each 0° section has been increased by 1% or even more.
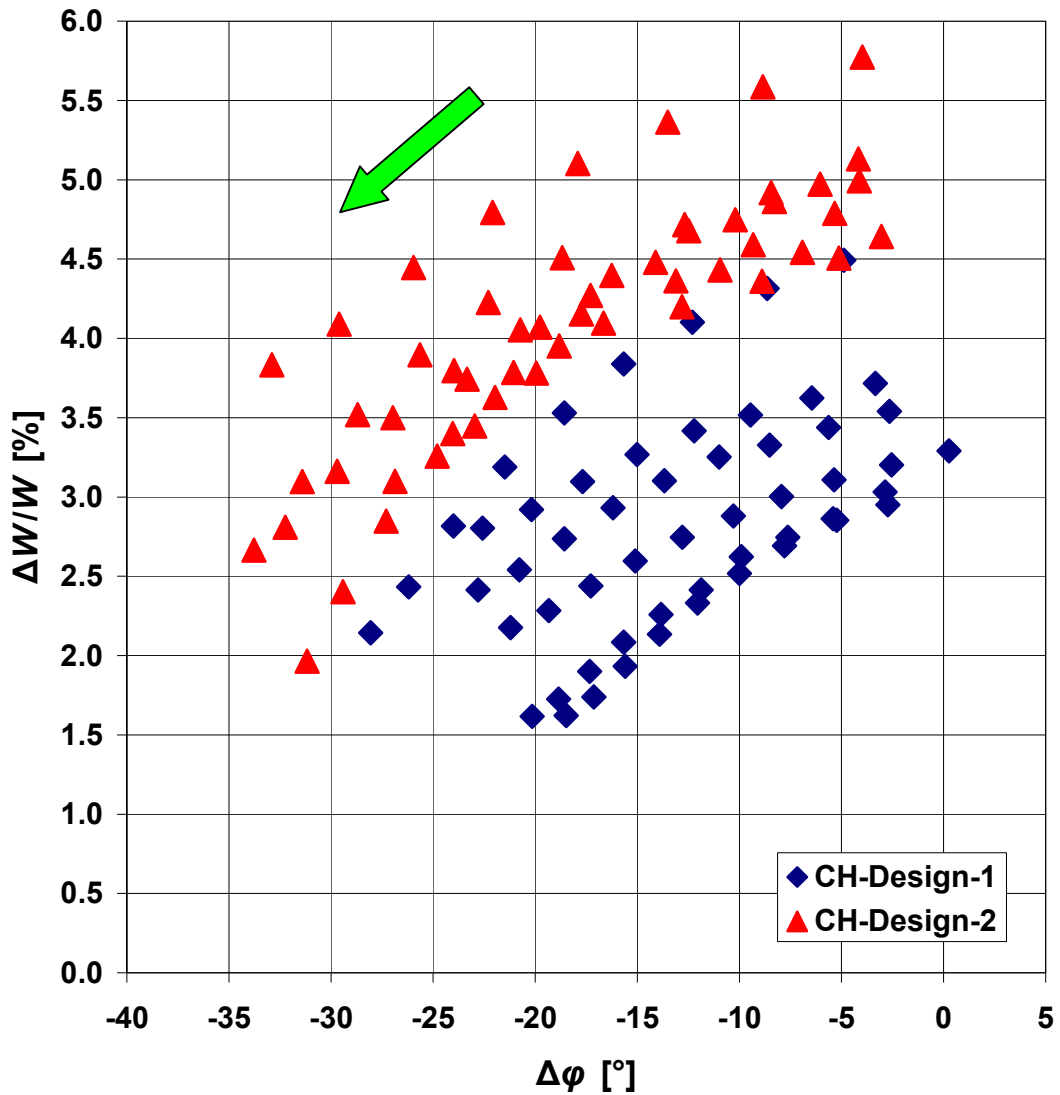
Fig. 5.1.2-3: Comparison of bunch-center motions in 0° sections between CH-Design-1 and -2.

Marked with blue diamonds and red triangles, respectively, the old and new bunch-center motions in the 0° sections are shown in Fig. 5.1.2-3, where the green arrow shows that in every 0° section the beam bunch slips down from up-right to low-left because of the phase- and energy-differences. However, caused by a more-negative starting $\Delta\varphi$ and a larger starting $\Delta W/W$, the beam bunch can move to the negative direction of the $\Delta\varphi$ axis faster and experience also more-negative phases. As discussed before, a more-negative phase leads to a stronger longitudinal bunching to the beam bunch. In this way, therefore, the longitudinal beam dynamics of the new design has been improved. The evolutions of the longitudinal beam envelopes are compared in Fig. 5.1.2-4. Clearly, in each plot of the new design, the two boundary lines of the beam are still developing in parallel; and at the DTL exit, the final energy and phase-spreads are comparable to those of the original case.
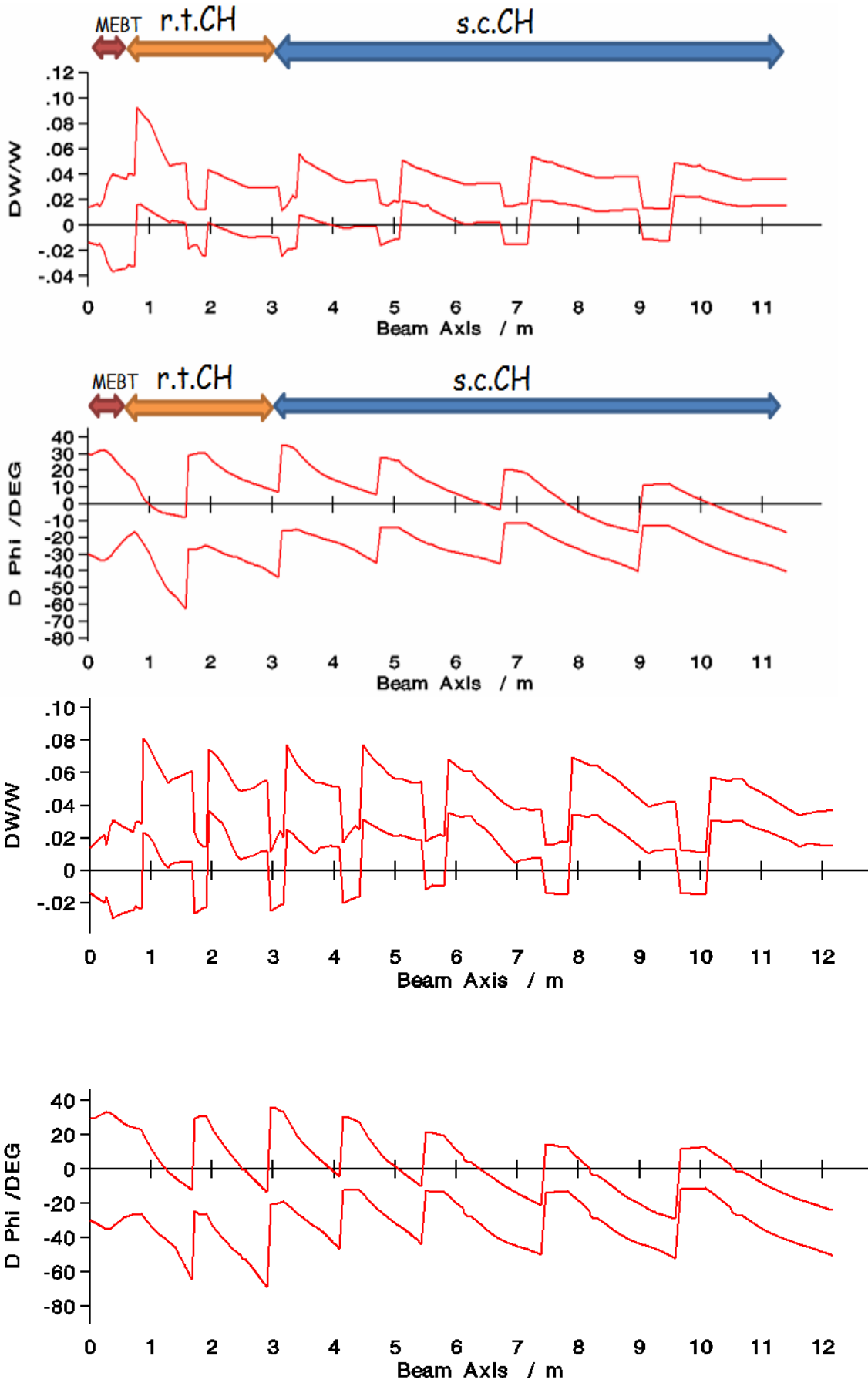
Fig. 5.1.2-4: Longitudinal beam envelopes along the DTL of

CH-Design-1 (top) [SAU07] and CH-Design-2 (bottom).

For a better evaluation of the beam quality, the output particle distributions in all planes for the two designs are firstly checked in Fig. 5.1.2-5 (*Note: the scalings are different*), where each black ellipse is including 95% of all particles, and the value given on the top of each plot is the corresponding normalized, real emittance. Obviously, the beam quality has been improved in both transverse planes, while the output longitudinal particle distribution has been kept still similar to the original one.
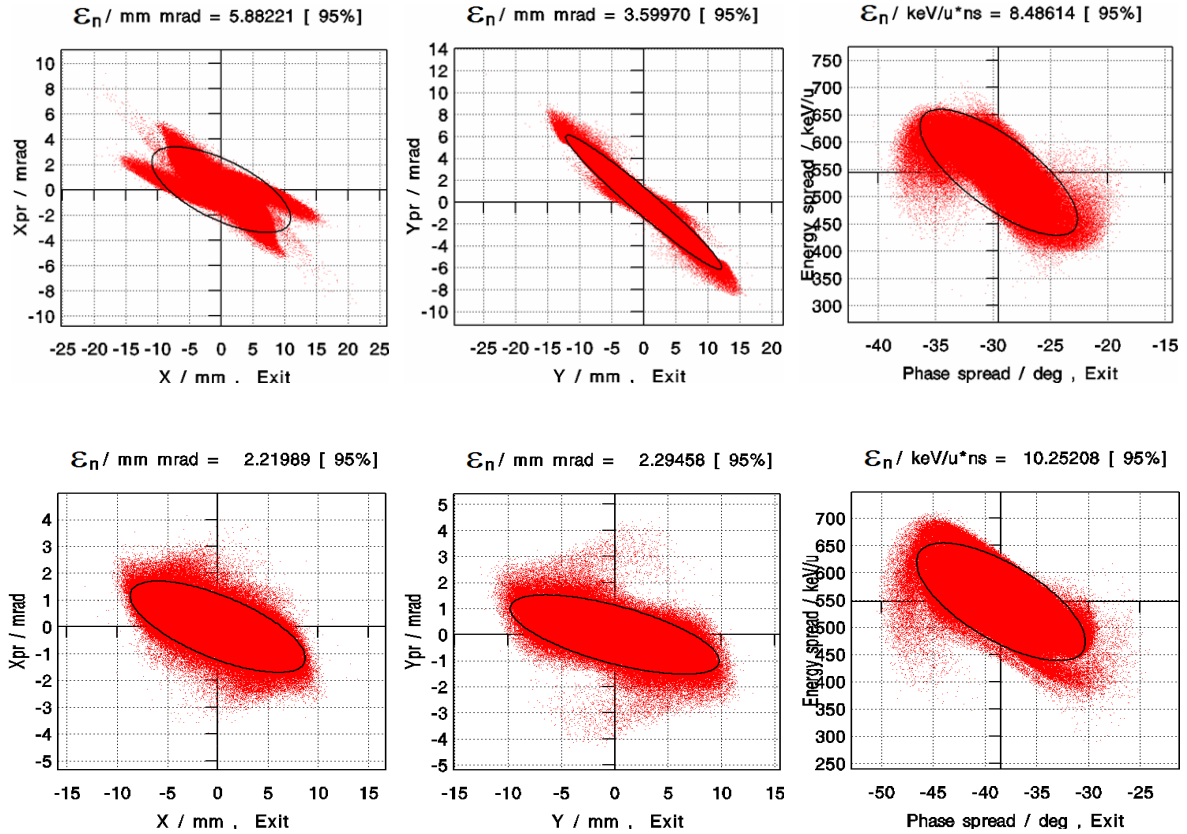
Fig. 5.1.2-5: Longitudinal beam envelopes along the DTL of

CH-Design-1 (top) [SAU07] and CH-Design-2 (bottom).

Second, the transverse beam envelopes for 100%, 99% and 95% of all particles, respectively, are plotted in Fig. 5.1.2-6 simultaneously. The "100%" curves show that the outermost particles still have safe enough distances to the bore apertures throughout the DTL accelerator, while from the "99%" and "95%" ones it is easy to see that the main beam has a smooth development in beam size and it is confined in the range of ±10mm only.

Third, compared to the original emittance growths for the three planes, 226%, 145% and 25%, the new ones are 60%, 66% and 32%, respectively.

To sum up, all analyses have confirmed the success of the employed optimization concepts again.
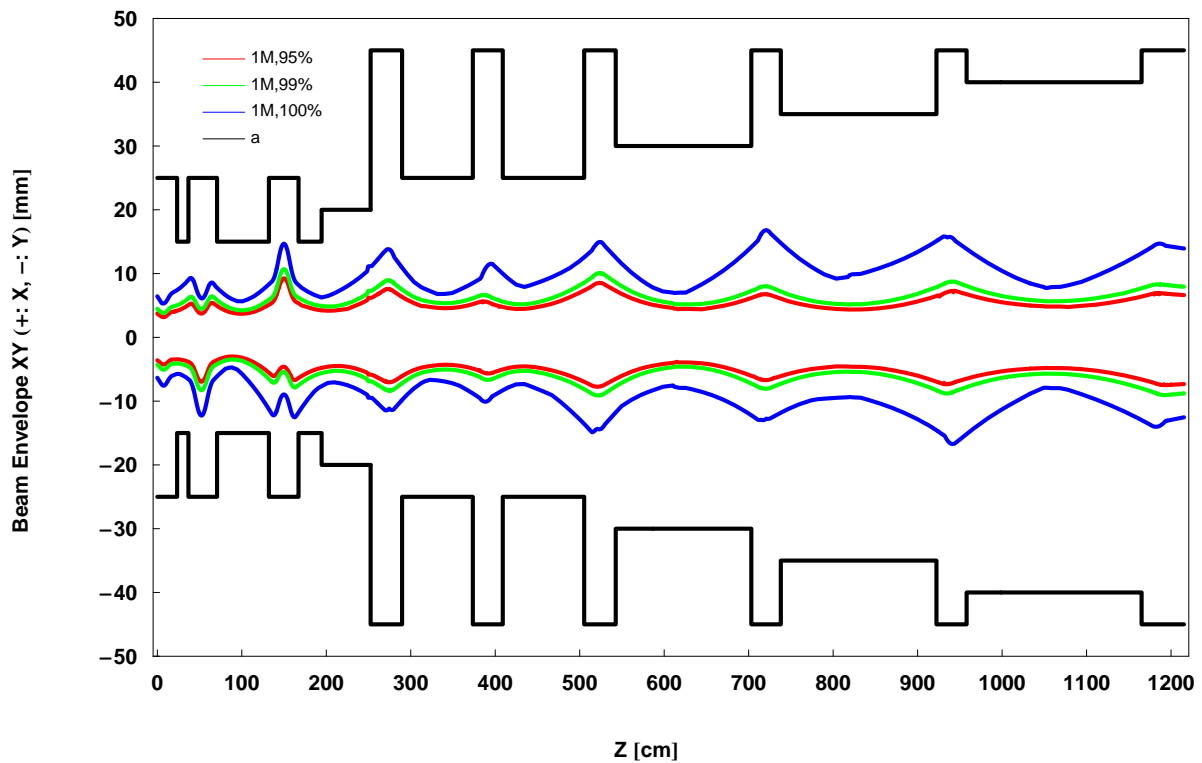
Fig. 5.1.2-6: Transverse envelopes including 95%, 99% and 100% of the beam.

5.2 Error-Tolerance Studies

For the design stage, only perfect accelerator components and ideal operating conditions have been taken into account. In reality, however, more or less perturbations to the design case are inevitable. Therefore, the error studies are particularly important for the IFMIF DTL which can tolerate almost no beam losses.

The errors influencing the beam dynamics can be roughly divided into three families:

- Beam-related errors, mainly from a non-ideal beam injection.

- Machine errors, which sources are manufacturing deviations, misalignments, inaccurate tuning, and so on.

- External errors, such as RF vibrations from the power sources and mechanical vibrations from the environment.

As shown in Fig. 5.2-1, so far four kinds of machine and external errors can be simulated by the recently integrated LORASR error-study subroutines [TIE07a, TIE07b], namely:

Fig. 5.2-1: Schematic plots of the errors can be used in the LORASR code [TIE07a,b].

- Transverse translations of magnetic lenses (QMIS): ΔX_{lens}, ΔY_{lens} (each singlet separately) with typical values ≤0.1mm.
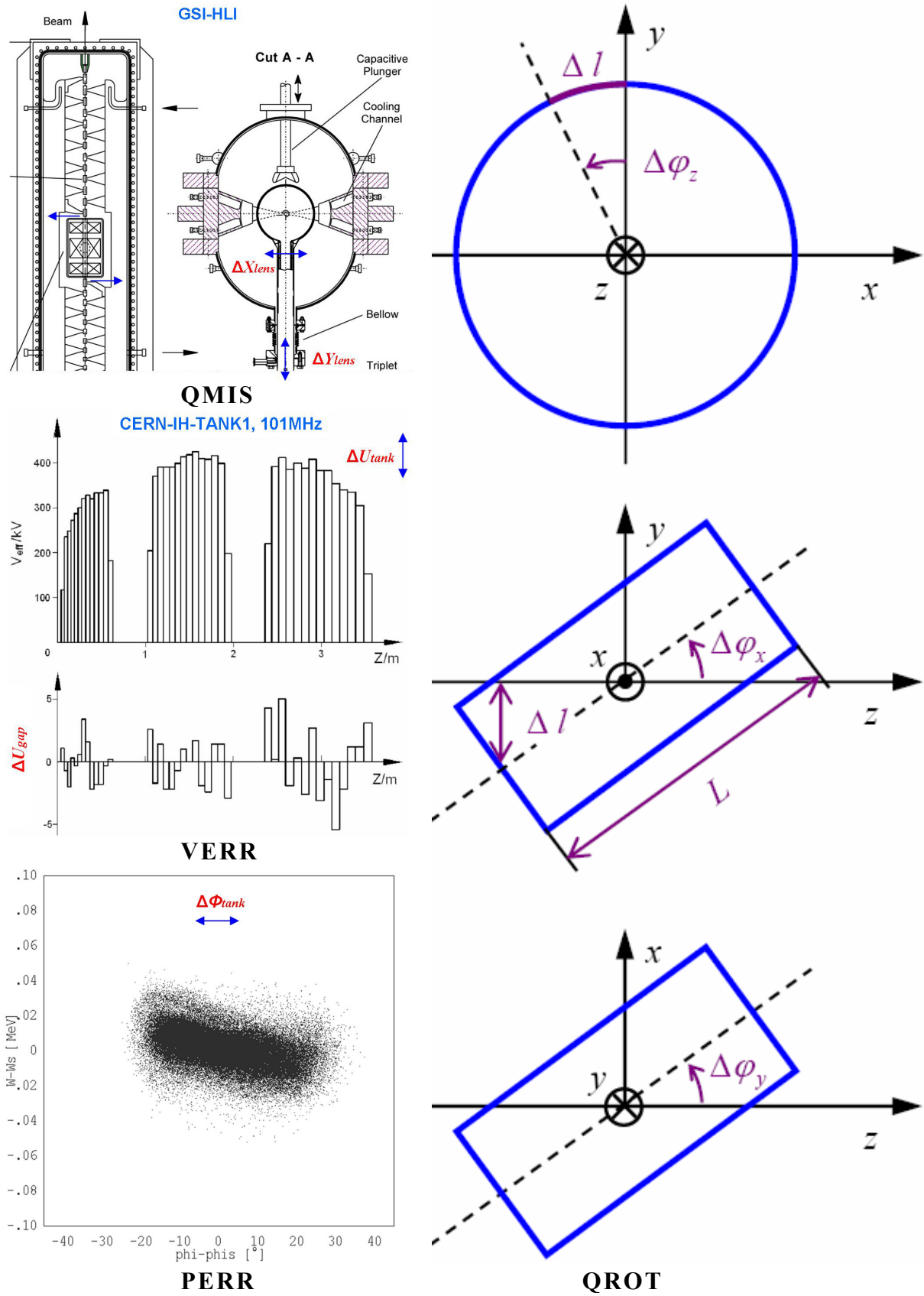
- Rotations of magnetic lenses (QROT): $\Delta\varphi_{x,y,z}$ (each singlet separately or the whole multiplet array together), which typical ranges are referring to the QMIS error (the typical length displacements caused by the rotations are ≤0.1mm).

- Gap and tank voltage amplitude errors (VERR): ΔU_{gap} (each gap separately) and ΔU_{tank} (equal for all gaps belonging to a same tank) with typical values $\Delta U_{gap}/U_{gap}$≤5% and $\Delta U_{tank}/U_{tank}$ ≤1%.

- Tank phase errors (PERR): $\Delta\Phi_{tank}$ (applied to the first gap of a tank) with typical values $\Delta\Phi_{tank}$ ≤1°.

Limited by the current version of the LORASR code, only 10^5 of input macro-particles, 1/10 of those adopted in the design studies, can be properly processed by error studies. Therefore, the DTL input distribution for the error studies was reproduced by the same RFQ design but with 10^5 of input macro-particles. To check the influences caused by the reduced particle quantity, a careful comparison of the simulation results between the two cases has been firstly performed.
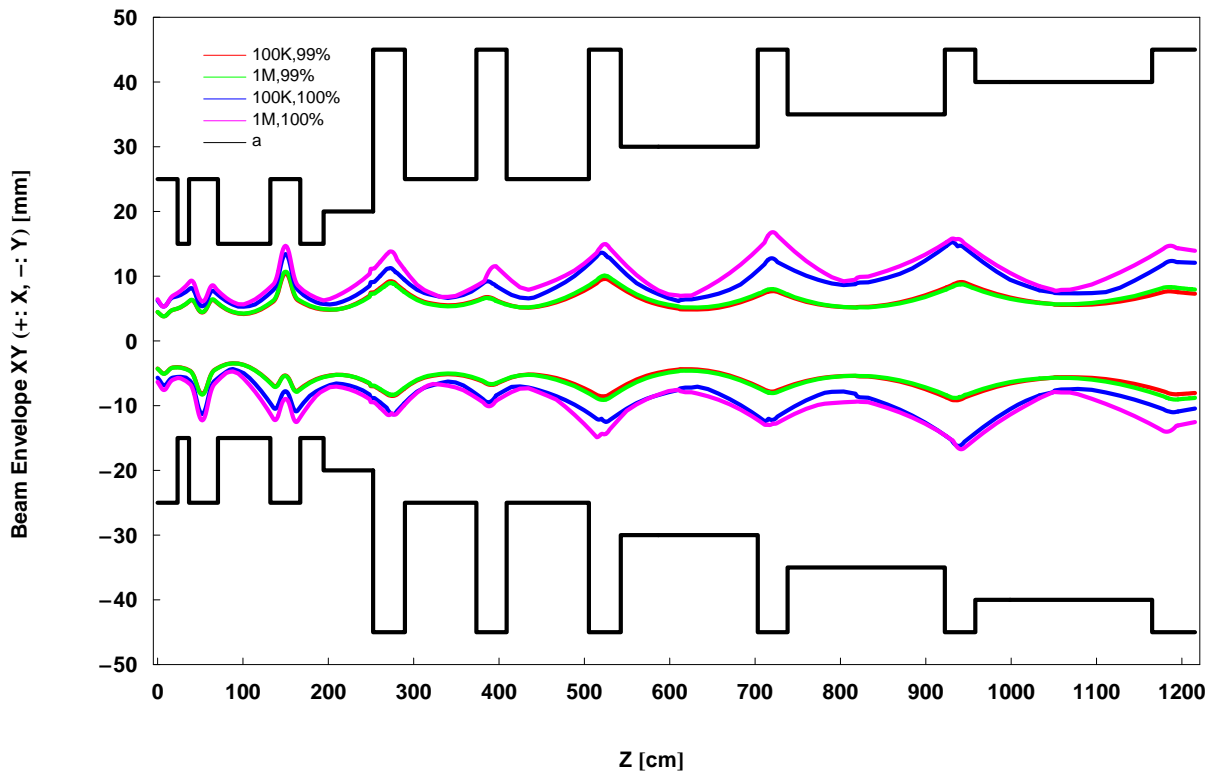
Fig. 5.2-2: Transverse beam envelopes for 10^6 and 10^5 of input macro-particles, respectively.

Firstly, the transverse beam envelopes are compared for the nominal case "1M" (1M=10^6 particles) and the less-particle case "100K" (100K=10^5 particles). In Fig. 5.2-2, clearly the transverse envelopes including the whole beam are already very similar for both cases and the ones for 99% of all particles are even identical to each other.
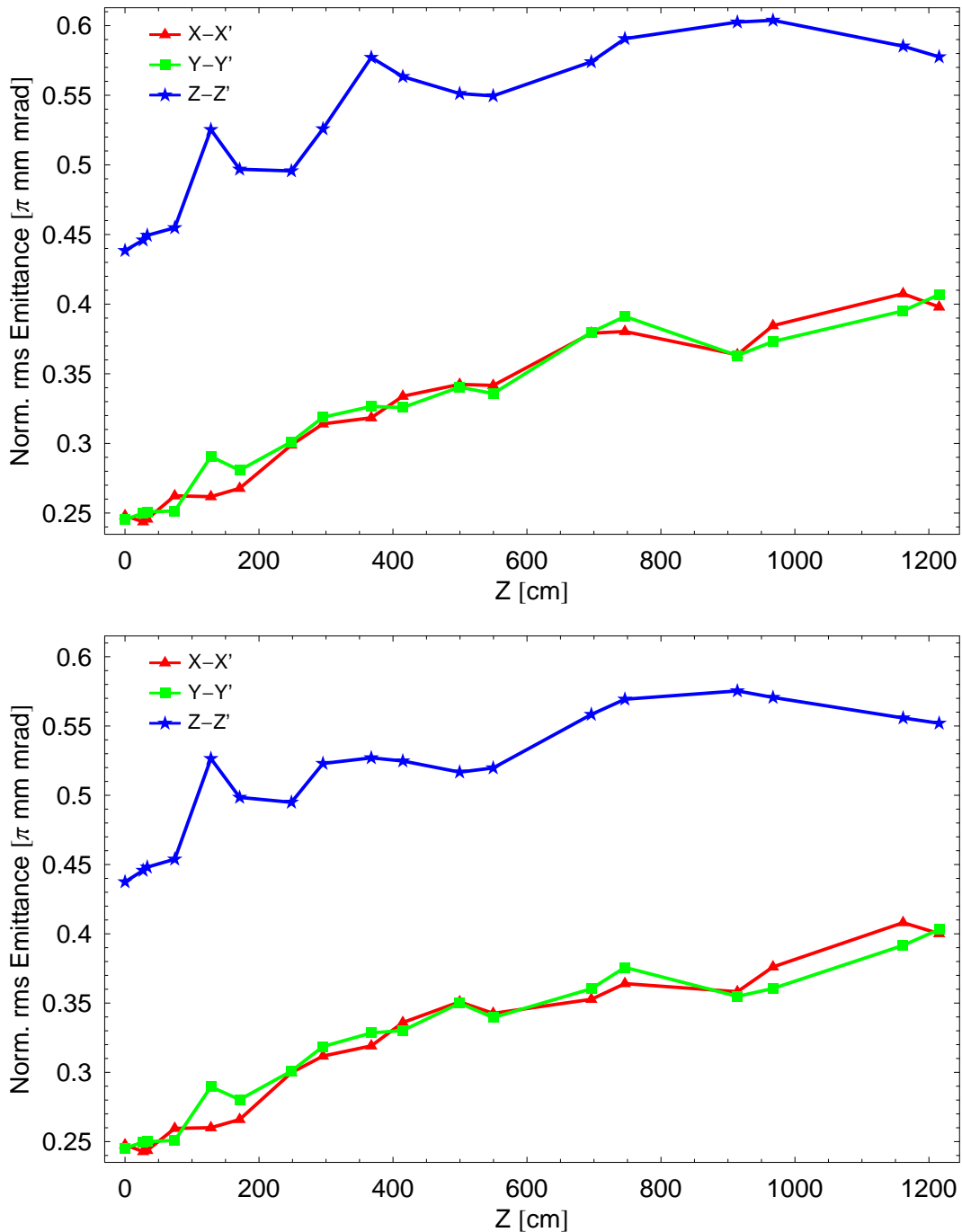
Fig. 5.2-3: Emittance growth evolutions for Case "1M" (top) and Case "100K" (bottom).

Secondly, the emittance growths along the DTL are compared between the "1M" case and the "100K" case in Fig. 5.2-3. It is easy to see that the differences between the two groups of development curves for the transverse and longitudinal emittances are also small, especially in the transverse planes (the "1M" longitudinal emittance growth is slightly larger after z=~3m).

As shown in Fig. 5.2-4, the last validation was made by comparing the input and output particle distributions of the two cases, where the red and green ellipses are including 98% and 90% of all particles, respectively. Generally speaking, they are still similar.
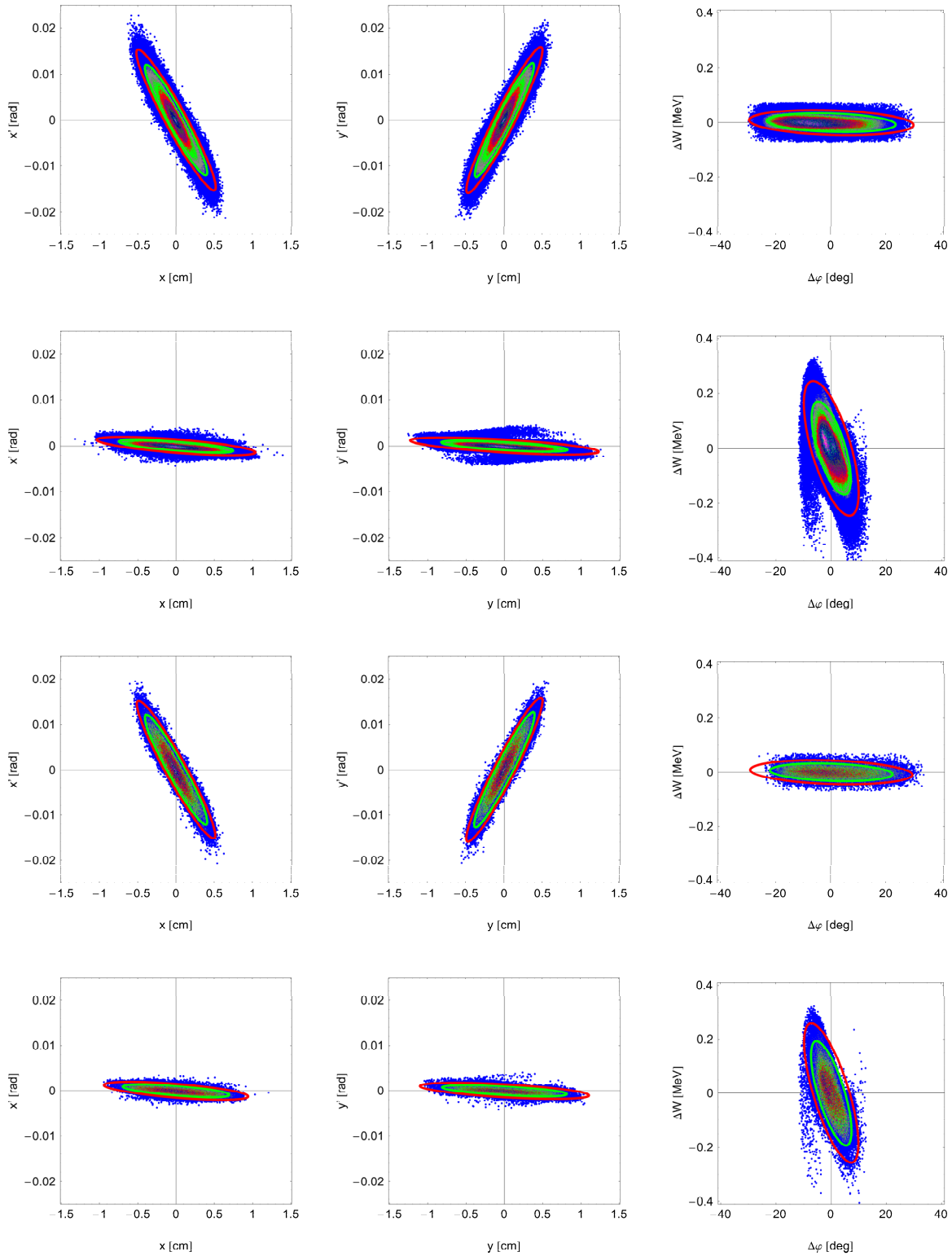
Fig. 5.2-4: Input and output distributions for Case "1M" (top) and Case "100K" (bottom).

In conclusion, one can use the "100K" input distribution for the error studies in the current optimization design stage. Of course, when the LORASR error-study subroutines are able to deal with 1 million particles, the error studies with the original "1M" input distribution had better be performed.

5.2.1 Single-Error Effects

To clearly investigate the effects from a specific error, the error studies have been firstly performed with one single error involved per time. Among the four kinds of errors, the QMIS and QROT errors are more important, so in the single-error studies, they were generated in the ranges two and three times the typical ones, respectively; while for the rest VERR and PERR errors, only the typical values were used.

As mentioned, the typical angle range of the lens-rotation error is determined by the rule that the corresponding length displacement caused by the rotation is ≤0.1mm. Because commercial doublet and triplet products, each of which is manufactured as a whole, will be used, the QROT error should also be applied to the whole lens. In case of the new design of the IFMIF H-type DTL, the shortest length from "pole-end" to "pole-end" in a lens is 11.5cm. Taking into account of the edges of the "lens house", the typical angle range of the lens rotation error for the IFMIF DTL is ≤1.5mrad (because the lenses used by the KONUS-based H-type DTLs are typically longer than 10cm, this ≤1.5mrad range can be generalized for all lenses in KONUS structures). In addition, the rotation about the z axis has no influence to the solenoids, so a relatively larger range, ≤2.5mrad, has been chosen for the $\Delta\varphi_z$ errors of the quadrupole lenses.

The following six settings of the limits for each error have been used to check the single-error effects:

- QMIS-A: ΔX_{lens}=±0.2mm & ΔY_{lens}=±0.2mm.
- QMIS-B: ΔX_{lens}=±0.3mm & ΔY_{lens}=±0.3mm.
- QROT-A: $\Delta\varphi_x$=±3.0mrad, $\Delta\varphi_y$=±3.0mrad & $\Delta\varphi_z$=±5.0mrad.
- QROT-B: $\Delta\varphi_x$=±4.5mrad, $\Delta\varphi_y$=±4.5mrad & $\Delta\varphi_z$=±7.5mrad.
- VERR-A: ΔU_{gap}=±5.0% & ΔU_{tank}=±1.0%.
- PERR-A: $\Delta\Phi_{\text{tank}}$=±1.0°.

For each case, 100 non-ideal DTLs have been generated randomly, and the errors are Gaussian-distributed and truncated at the maximum A=±2σ in the range of the corresponding setting.

Because the most important result for the IFMIF DTL is the beam-loss situation, only the maximum transverse beam sizes without and with a certain kind of error along the DTL are presented (see Fig. 5.2.1-1). In every picture, the blue curve plots the so-called common maximum transverse beam size which is defined as the perpendicular distance between the "common" outermost particle of the 100 non-ideal beams and the beam axis at every position along the DTL;

and the green curve is doing the same thing, except it firstly throws away 1% of particles from each non-ideal beam from outside and then to find the new "common" outermost particle.

QMIS-A

QMIS-B

QROT-A

QROT-B

VERR-A

PERR-A
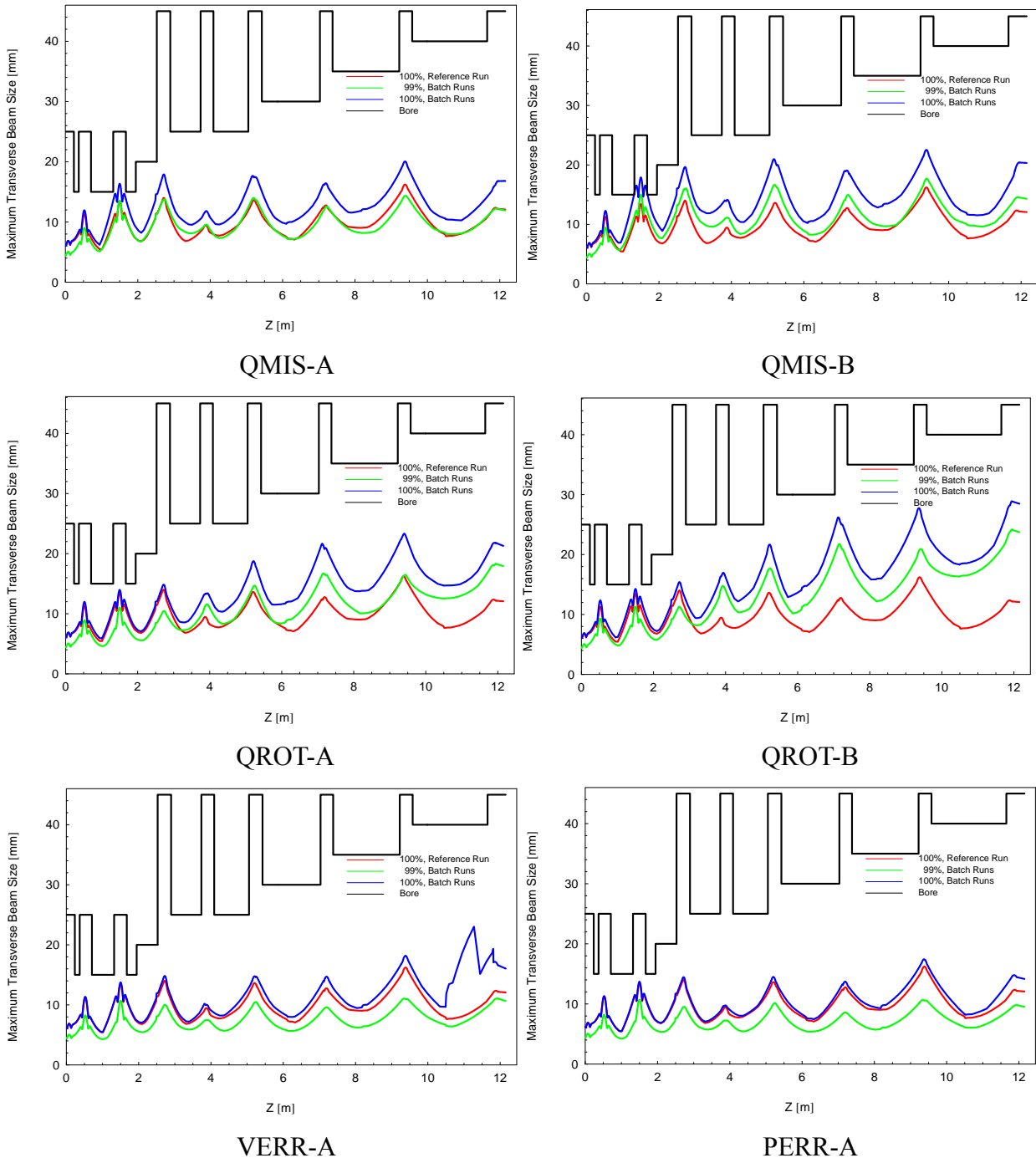
Fig. 5.2.1-1: Common maximum transverse beam sizes along the DTL with single-error effects.

From the pictures in Fig. 5.2.1-1, the following phenomena can be observed:

The quadrupole lenses are more sensitive to the QMIS errors but not the QROT errors, which is because: 1) Each singlet has been treated independently for the QMIS errors, so in a quadrupole lens the translations of the singlets might happen in two opposite directions. As a

result of the accumulated error effects, the particle trajectories could be obviously changed. 2) The QROT errors have been applied to a whole quadrupole lens. In case of a rotated triplet, the first singlet gives the beam a declination in one direction, the second one has almost no contribution to the error effects because its center is still on axis, but the third one will more or less push the beam back. As the non-ideal singlets compensate each other, the overall error effects could be small.

On the contrary, the QMIS errors have relatively more influences to the solenoid lenses, but the QROT errors do not.

The "100%" common maximum transverse beam sizes with the given VERR and PERR errors are almost same as those without errors, except at the end of the VERR-A curve (but the "99%" curve shows it's induced by small "noises").

The QMIS-B plot indicates the third lens could still be "the weakest link" for the whole machine in the presence of large errors.

5.2.2 Combined-Error Effects

In reality, various kinds of errors are mixed together, so it is more important to check the nominal design with combined errors.

Table 5.2.2-1 presents the two groups of combined-error settings used for the new H-type DTL design with the following considerations: 1) The Case1 setting defines the maximum errors as the typical values. 2) The QMIS and QROT ranges in Case2 are twice those of the Case1.

Table 5.2.2-1: Error ranges used for combined-error studies.

Error Type ╲ Case		1	2
QMIS [mm]	ΔX_{lens} ΔY_{lens}	±0.1 ±0.1	±0.2 ±0.2
QROT [mrad]	$\Delta\varphi_{\text{x, y}}$ $\Delta\varphi_{\text{z}}$	±1.5 ±2.5	±3.0 ±5.0
VERR [%]	ΔU_{gap} ΔU_{tank}	±5.0 ±1.0	±5.0 ±1.0
PERR [°]	$\Delta\Phi_{\text{tank}}$	±1.0	±1.0

Similar to the single-error studies, the batch simulation of each case includes 100 runs with randomly generated but mixed errors. The common maximum transverse beam sizes with the error settings of Case1 or Case2 are given in Fig. 5.2.2-1, where the nominal case is also shown for comparison. No beam losses have been observed even in the worst case. Especially for the SC cavities, the space between the beam and the accelerator elements are still fairly safe.
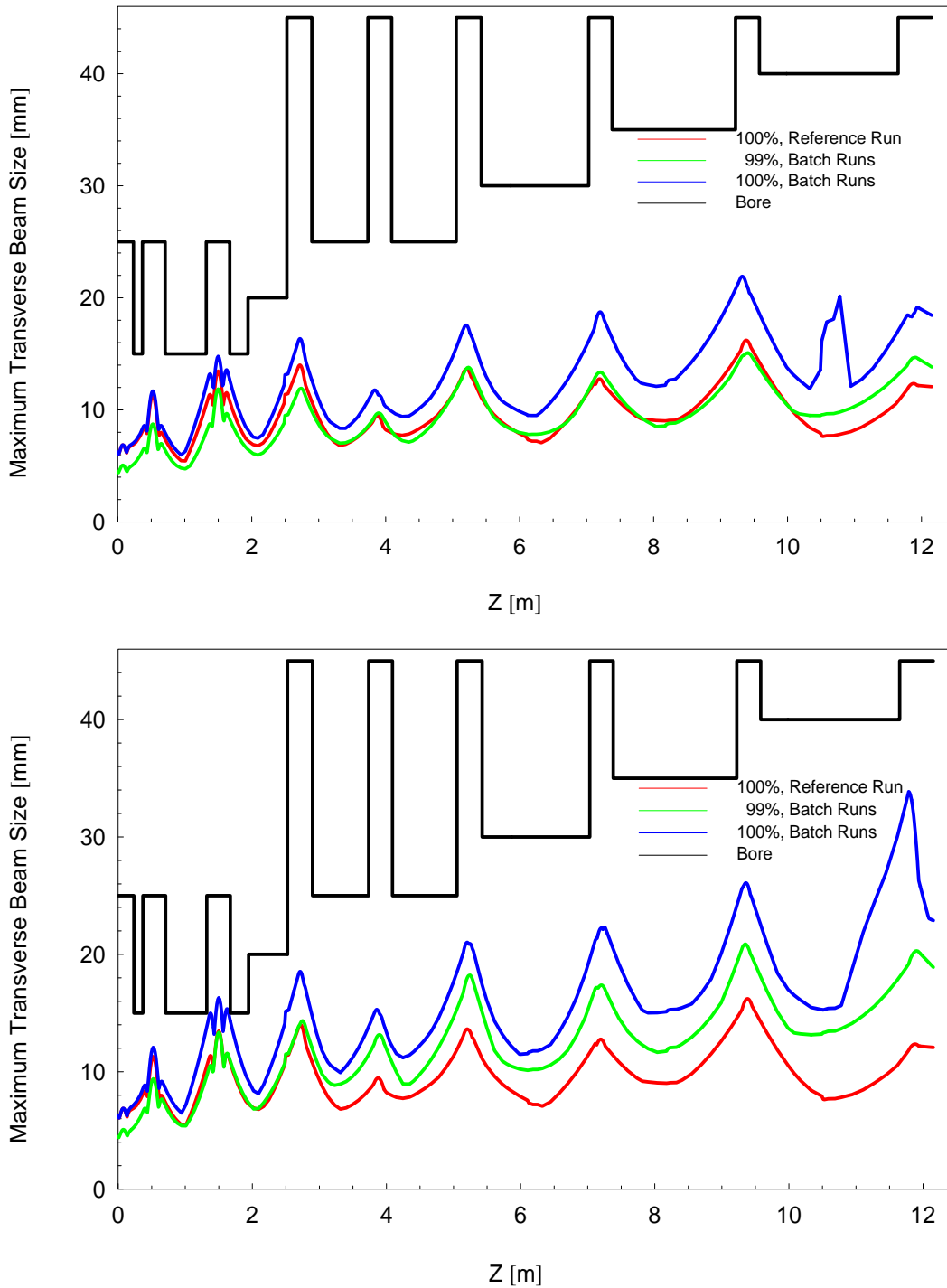
Fig. 5.2.2-1: Common maximum transverse beam sizes for Case1 (top) and Case2 (bottom) with and without errors.

Another analysis of the error effects on the beam quality is to take statistics of the additional emittance growths induced by errors. The definition for the additional emittance growth is given as below:

$$\Delta\varepsilon_{addi.} = \frac{\varepsilon_{DTL\,out}^{error} - \varepsilon_{DTL\,out}^{nominal}}{\varepsilon_{DTL\,in}^{nominal}} \tag{5.2.2-1}$$
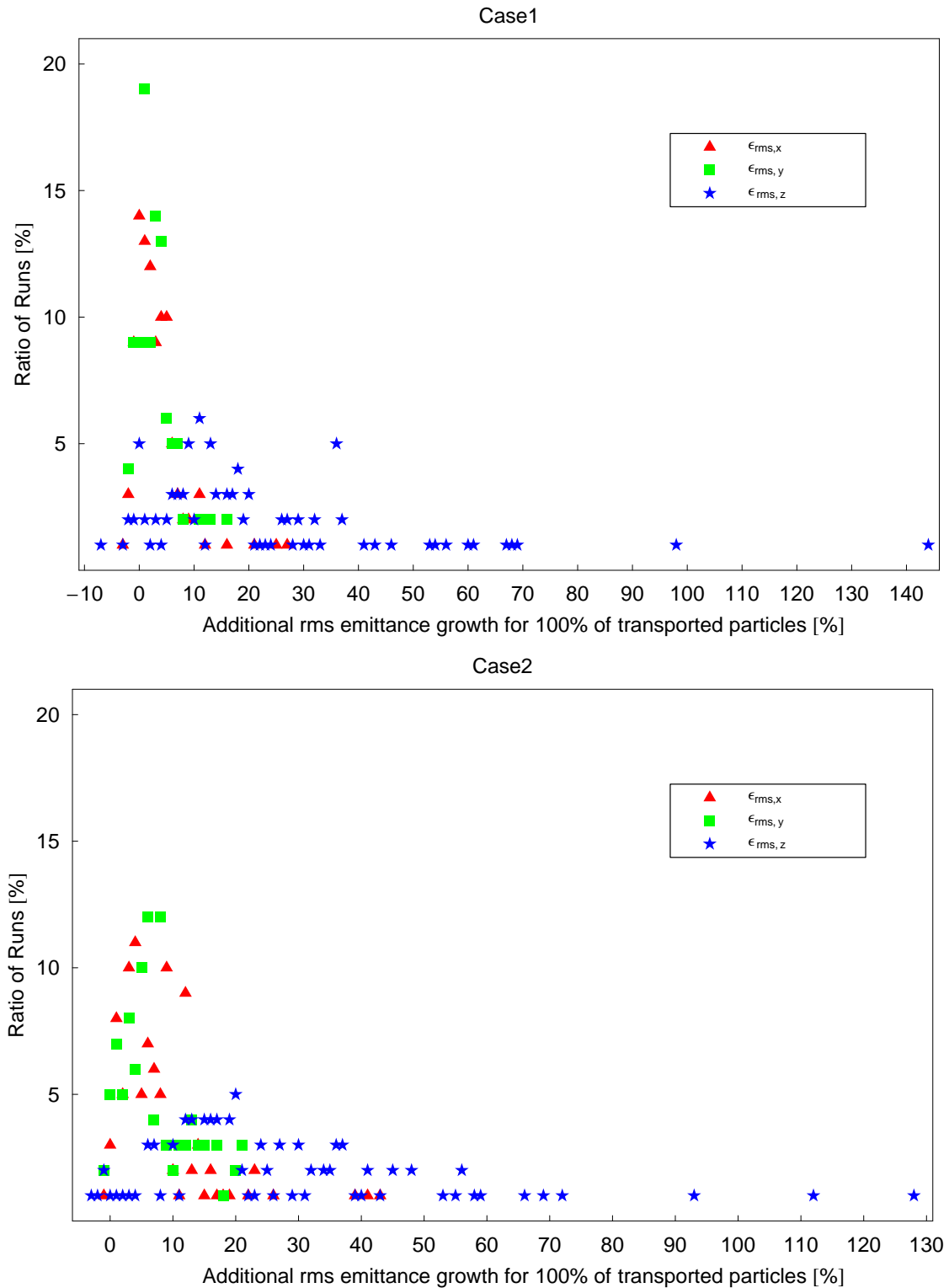
Fig. 5.2.2-2: Additional emittance growths induced by errors.

In Fig. 5.2.2-2, it is clear that: in the transverse planes, the maximum additional emittance growths are <30% and <45% for Case1 and Case2, respectively; while in the longitudinal plane, for both cases: 1) The maximum growths are <150%. 2) Most runs have growths smaller than 40%. 3) Only rare runs have growths ≥70%.

Therefore, the beam envelopes and the beam quality are still acceptable in case of combined errors.

5.3 A Comparison of Different Proposals

Besides the reference Alvarez-DTL design and the IAP H-type DTL design, there is another SC version of DTL design for IFMIF. Using the HWR (Half-Wave Resonator) structure, this SC design has been also proposed by CEA, France. To see the pros and cons of each design, it is worthwhile to do the following comparative analyses.
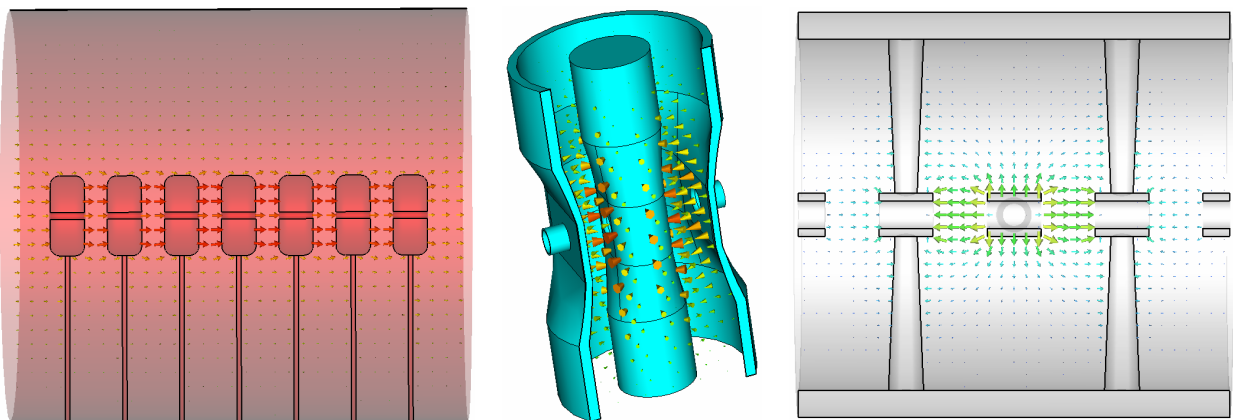
Fig. 5.3-1: Schematic plots of Alvarez (left), HWR (middle) and CH (right) structures with electric fields (Courtesy of M. Busch).

As schematically shown in Fig. 5.3-1, firstly the three candidate DTL structures have been compared, where the electric-field distributions are also demonstrated. The main characteristics of these DTL structures are listed in Table 5.3-1. Because the Alvarez-DTL and the HWR structure use the conventional negative-synchronous-phase dynamics strategy, so a higher lens-density is required to overcome the transverse RF defocusing effects. In an Alvarez-cavity, the lenses are usually housed in the drift tubes one after another, so it is only suitable for the room-temperature operation. As a kind of SC accelerating structure, HWR has to use a compact cavity – typically 2 accelerating cells per cavity – to keep the separation between two adjacent inde-

pendent lenses as short as possible for sufficient transverse focusing in the low- and medium-β regions. Based on significantly weakened RF defocusing effects by the special KONUS dynamics concept, a long lens-free accelerating section is possible for the CH-DTL, so it can be operated at either RT or SC with a multi-cell structure.

Table 5.3-1: Comparison of the three DTL structures for IFMIF.

Structure Feature	Alvarez	HWR	H-Type
Field mode	TM	TEM	TE
Period length	$\beta_s \lambda$	$\beta_s \lambda / 2$	$\beta_s \lambda / 2$
Synchronous phase	Negative	Negative	Mainly 0°
Transverse focusing method	Lenses integated in drift tubes	Independent lenses outside cavities	Independent lenses inside or outside (for SC) cavities
Accelerating cell number per cavity	Multi-cell	2	Multi-cell
Operation mode	RT	SC	RT and SC

As shown in Table 5.3-2, the IAP proposal using the H-Type DTL can realize the most compact structure for the lowest costs:

- Both numbers of the required tanks and transverse focusing elements are the least.

- The total length is only 12.2m (~1/2 or ~1/3 of that of the HWR or Alvarez DTL).

Table 5.3-2: Different proposals for the IFMIF DTL.

Design Parameter	Alvarez [SAU07]	HWR [CEA08]	H-Type
Number of tanks (RT/SC)	10 / 0	2 / 42	2 / 8
Number of cryo-modules	0	4	1
Number of magnets	~120 quadrupoles	3 quadrupoles 21 solenoids	8 quadrupoles 6 solenoids
Φ_{bore} **[mm]**	25	40-60	30-90
E_{acc} **[MV/m]**	0.5-1.7	4.5	2.7-5.3
E_{max} **[MV/m]**	18	30	25
B_{max} **[mT]**	N/A	50	55
L_{total} **[m]**	30.3	22.5	12.2

The beam dynamics performances for the three designs have been also compared. As shown in the left pictures of Fig. 5.3-2 (*Note: the scalings are different*), due to the denser transverse focusing, the Alvarez-DTL and the HWR-DTL mainly confine the transverse beam sizes to be ≤10mm and ≤14mm, respectively. Though the H-type DTL has a maximum beam size of ~19mm, the "99%" curve indicates the main beam is still within the range of ±10mm. From the emittance pictures and the emittance data in Table 5.3-3, one can learn that both SC designs have better controls on emittance growths than the pure RT design and the results are similar.
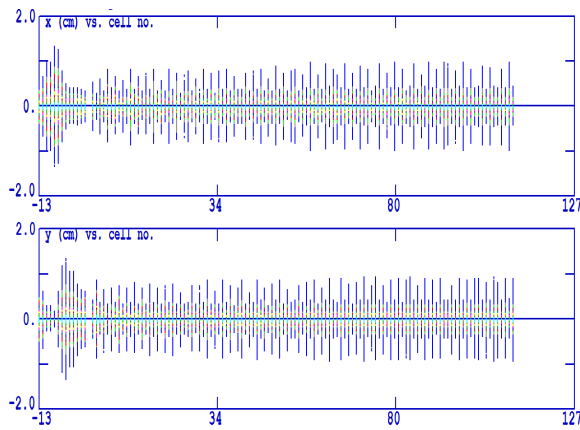
Alvarez: Transverse beam envelopes [SAU07]   **Emittance growths [SAU07]**
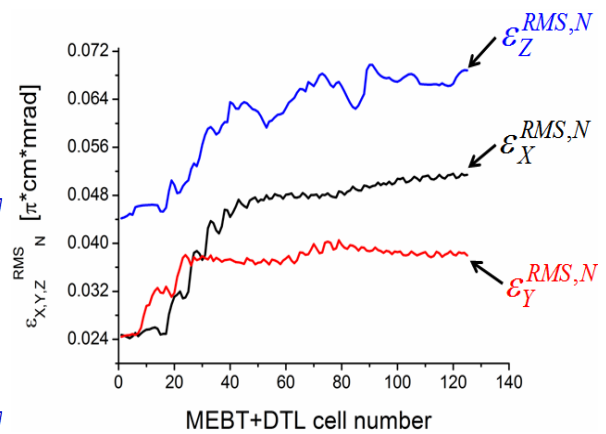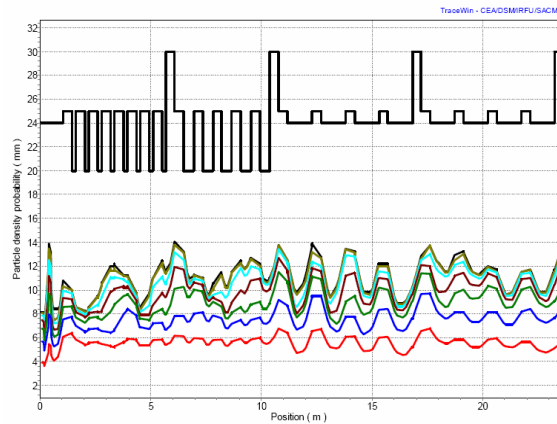
HWR: Maximum transverse beam sizes [CEA08]   **Emittance growths [CEA08]**
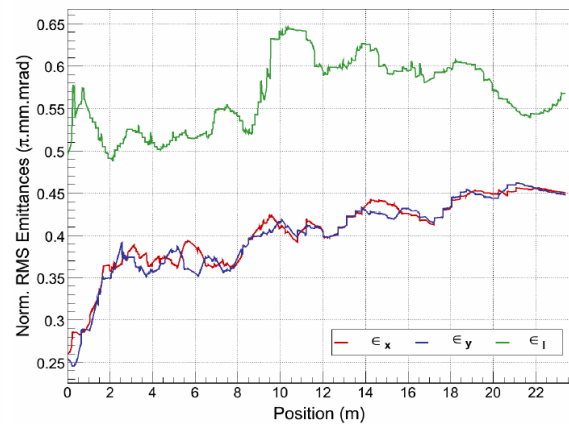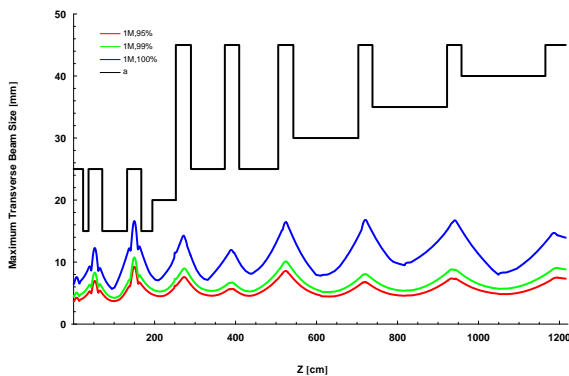
H-type: Maximum transverse beam sizes   **Emittance growths**
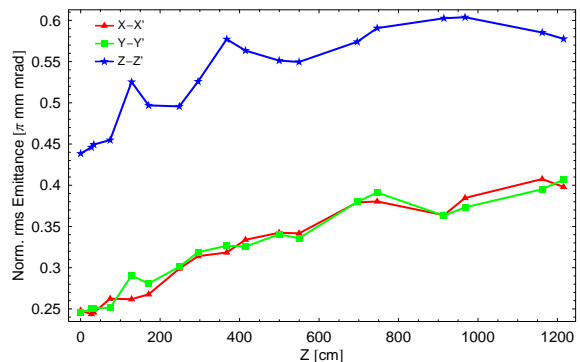
Fig. 5.3-2: Comparison of transverse beam sizes and emittance growths.

Table 5.3-3: Comparison of normalized rms input and output emittances.

Design ⟍ Emittance	Alvarez [SAU07]	HWR [CEA08]	H-Type
$\varepsilon_{out}^{x., norm., rms} / \varepsilon_{in}^{x., norm., rms}$	1.54	1.73	1.60
$\varepsilon_{out}^{x., norm., rms}$ [π mm mrad]	0.37	0.45	0.40
$\varepsilon_{in}^{x., norm., rms}$ [π mm mrad]	0.24	0.26	0.25
$\varepsilon_{out}^{y., norm., rms} / \varepsilon_{in}^{y., norm., rms}$	2.17	1.77	1.66
$\varepsilon_{out}^{y., norm., rms}$ [π mm mrad]	0.52	0.45	0.41
$\varepsilon_{in}^{y., norm., rms}$ [π mm mrad]	0.24	0.25	0.25
$\varepsilon_{out}^{z., norm., rms} / \varepsilon_{in}^{z., norm., rms}$	1.45	1.14	1.32
$\varepsilon_{out}^{z., norm., rms}$ [π mm mrad]	0.64	0.57	0.58
$\varepsilon_{in}^{z., norm., rms}$ [π mm mrad]	0.44	0.50	0.44
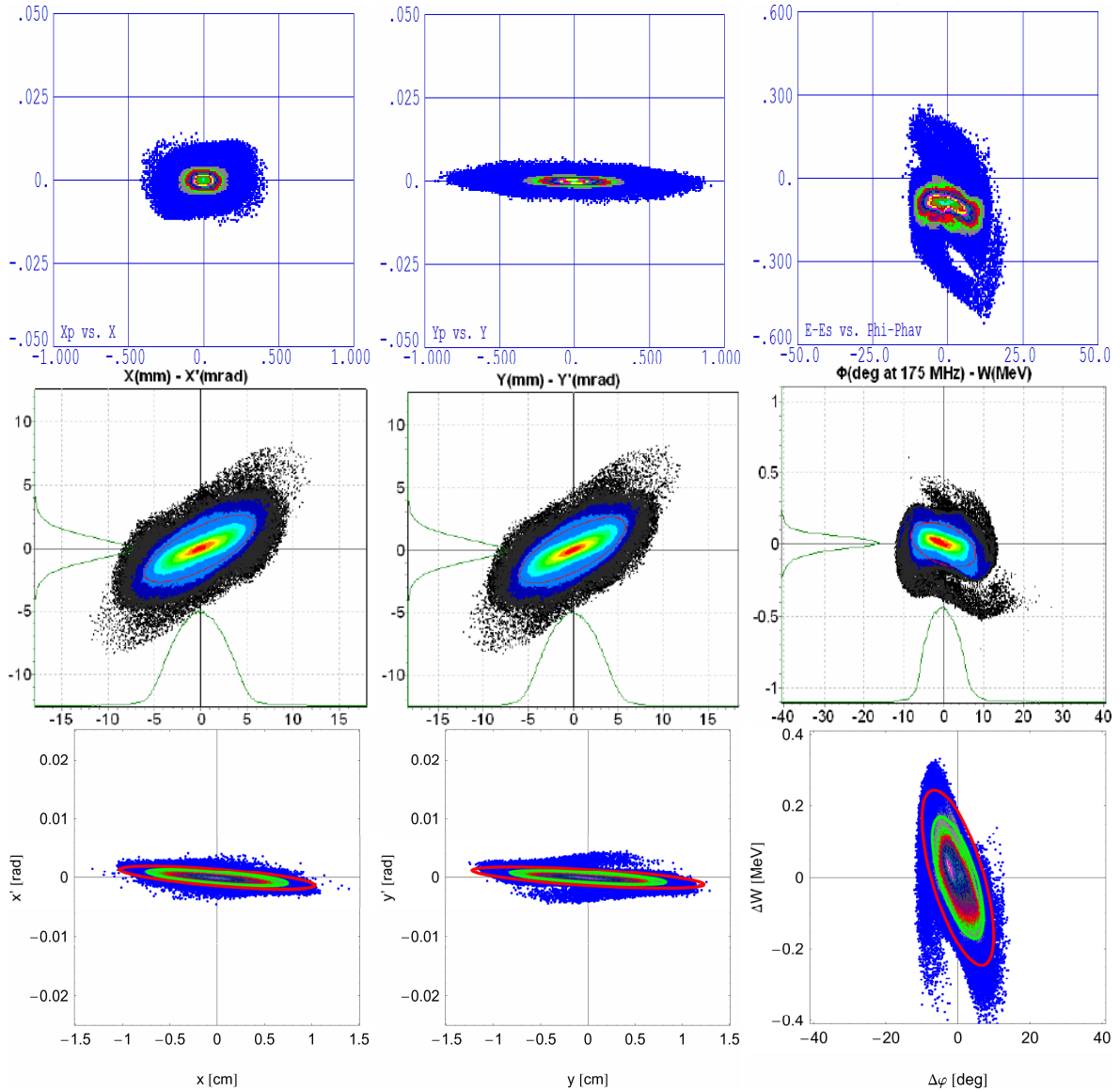
Fig. 5.3-3: Output phase spaces (top: Alvarez [SAU07] *using the same units as used by the H-type DTL plots*, middle: HWR [CEA08], bottom: H-type).

In Fig. 5.3-3, the output particle distributions of the three DTL accelerators are demonstrated (*Note: the scalings are different*). All three cases are similar, but the H-type DTL one has the smallest divergence angles in the transverse planes and also the narrowest phase spread in the longitudinal direction, so it is more favourable to result in a uniform beam footprint on the Li target.

Table 5.3-4: Error ranges used by the three designs.

Error type \ Design	Alvarez [SAU07]	HWR [CEA08]	H-Type
Lens misalignment [mm]	0.1	1.0	0.2
Lens rotation [mrad]	2.6	10	3.0 ($\Delta\varphi_{x,y}$) 5.0 ($\Delta\varphi_z$)
Lens field amplitude [%]	0.5	1.0	–
Tank misalignment [mm]	–	1.0	–
Tank field amplitude[%]	1.0	1.0 (static)	1.0
Tank field phase [°]	1.0	1.0 (static)	1.0
Gap field amplitude[%]	–	–	5.0
Measurement accuracy of beam position monitor [mm]	–	0.25	–

Finally, based on the error settings shown in Table 5.3-4, the error studies of the three DTLs should be mentioned. Though the reference case had used the least and smallest errors, beam losses already happened in ~10% of runs.

Within the given error ranges, no beam losses have been observed in the error studies of the two SC versions of DTL accelerators. Compared with the H-type DTL case, much larger misalignment and rotation errors were applied to the lenses of the HWR-DTL. However, actually the error-tolerance capabilities of these two designs can not be directly compared, because in the error studies of the HWR-DTL, beam-orbit corrections, which rely on beam position monitors and steering coils located at the solenoid package, have been implemented in the simulations. Therefore, after each HWR tank, the simulation code tried to "steer" the beam back to the design orbit according to the "observation" results from the "virtual" beam position monitors [CEA08]. However, so far this orbit-correction concept is not adopted by the LORASR code for the error studies of the H-type DTL design.

5.4 Conclusions

Characterized by remarkable reductions in both structure length and project costs, the preliminary IAP design had shown that the H-type DTL structure together with the KONUS dynamics strategy and RF superconducting technology could be a promising alternative of the reference Alvarez-type DTL for IFMIF.

To meet all project goals, further design studies were recommended to improve the linac system as well as the beam dynamics. Based on a series of optimization procedures, a new H-type DTL design with a more realistic layout and satisfying beam qualities has been made.

The compactness of the preliminary layout is kept: the new one is only ~80cm longer with one more SC cavity. However, actually the total project costs are even reduced, because:

- The extra SC cavity will only cost negligible RF power.

- The RT part was shortened.

- The 1MW units of RF amplifiers have been replaced by cheaper 300kW ones.

Though more and larger errors were checked, the beam losses which had appeared in the error studies of the preliminary design have been totally avoided in the error studies of the new design. Therefore, the robustness of the H-type DTL design has been enhanced.

Among the three competitive proposals for the IFMIF DTL, the latest H-type DTL design can achieve similar or better beam performances with the most compact layout which is only 1/2 and 1/3 as long as the other two layouts, respectively.

In conclusion, the design results, error studies and comparative analyses have all confirmed the feasibility and efficiency of the new H-type DTL design.

For the final version of the IFMIF DTL design, the following tasks can be added to the to-do list: 1) To further improve the RT part, especially the location of the third lens. 2) To perform the error studies with the original input distribution of ~1 million macro-particles which have been used for the design. 3) To take into account more error types and the orbit-correction method for the error studies. Of course, the last two jobs will need to be supported by the further development of the LORASR simulation code.

6. Front-End Design for EUROTRANS

EUROTRANS, an EUROpean Research Programme for the TRANSmutation of High Level Nuclear Waste in an Accelerator Driven System (ADS), has been started by European Union with the short-term and long-term objectives to develop a proto-type-scale demonstration plant and an industrial-scale one, respectively. For the prototype phase, a 2.5–4mA, 600MeV proton beam is required to be delivered to the spallation target by a CW driver linac. For the industrial one, the beam specifications will be increased to 20mA and 800MeV. Leaving safety margins, 5mA and 30mA have been decided as the design intensities for the two corresponding cases. Dominated by the requirements of extremely high reliability and easy upgradeability, the design of the 17MeV linac front end is one of the most demanding parts in the whole accelerator design, because the low-energy region is particularly important for both space-charge effects and beam trips. This chapter is mainly composed of two parts: the first part will focus on the design of an efficient layout for the linac front end which could show satisfying performances at both design intensities; and the second one will present the performed error studies to evaluate the robustness of the design scheme and to confirm the satisfaction of the project requirements.

At present, ~35% of electric power in Europe is provided by 145 nuclear fission reactors [ADS01]. However, a problem always companying the development of fission-based electricity generation is how to minimize the influence of the high-radioactive and long-lived spent fuel on the environment to an acceptable level for the public. One attractive solution to reduce the half-life and radio-toxicity of the nuclear waste efficiently is the transmutation technology based on an Accelerator-Driven System, which consists of a sub-critical nuclear reactor ($k<1$) and an intense spallation neutron source driven by a CW high-power proton accelerator to feed the fission reactions.

Determining the transmutation efficiency, the properties of the neutrons produced by the ADS method are strongly depending on the intensity and energy of the proton beam hitting on the n-production target. The typical specifications of the required proton beam are several hundred MeV to 1GeV in energy and a few mA to several ten mA in intensity. For EUROTRANS, a 2.5–4mA, 600MeV proton beam has been chosen for the prototype-scale phase (XT-ADS), and it will be upgraded to 20mA and 800MeV later in the industrial-scale phase (EFIT).

For an ADS application, the design of the driver linac is dominated by a stringent requirement to ensure an extremely high reliability. Because beam trips (i.e. beam interruptions on the target) with duration periods >1 second will cause serious thermal stress and fatal damages to the n-production target and the sub-critical core system, the number of long beam trips exceeding 1s has been restricted to <20 per year for XT-ADS and <3 per year for EFIT, respectively. In terms of the operation experience of existing accelerators, a particularly conservative and careful design should be made for the driver linac so that the risk of failures of accelerator components could be reduced to an utmost degree.

To reach the goal of high reliability, the most difficult step is to realize a reliable injector, because beam dynamics e.g. the space-charge effects is most complicated at the low-energy end of an accelerator. To follow the project guidelines i.e. over-design, redundancy and fault-tolerance, a linac front end including two identical injectors – one will be held on hot standby while another one is responsible for delivering the proton beam – has been foreseen. Nevertheless, the injector itself should be well designed firstly. For the 17MeV EUROTRANS injector, the prime design concern is not the activation problem (as the IFMIF case) but the quenching of SC cavities. The RF losses in an SC cavity are typically several ten W/m, so a few W/m of beam losses should be tolerable for the EUROTRANS injector.

Another exceptive constraint for the EUROTRANS injector design is that the designed accelerating structure should be suitable for the design intensities of both XT-ADS (5mA) and EFIT (30mA). This unusual "two-intensity injector" design concept will not only allow an easy upgrade from XT-ADS to EFIT but also bring uncommon challenges to the design studies.

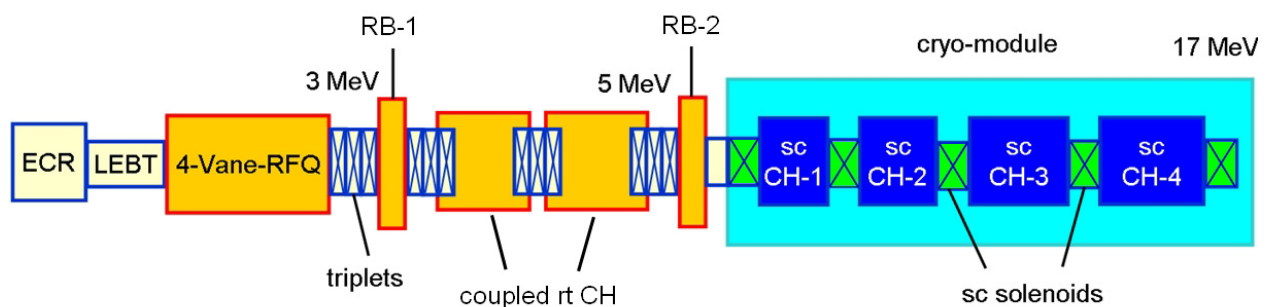Fig. 6-1: The proposed layout for the EUROTRANS injector [POD09].

Following an ECR ion source, the proposed 352MHz injector of the EUROTRANS driver linac (see Fig. 6-1) is mainly composed of a four-vane RFQ accelerator (0.05–3MeV), a room-temperature coupled CH-DTL cavity (3–5MeV) and four superconducting CH-DTL cavities (5–17MeV). The three major considerations for this injector configuration are:

- Characterized by the unique velocity-independent electric focusing, the RFQ is the standard structure for capturing, shaping, bunching and pre-accelerating the low-energy, high-intensity beam at injection.

- Due to the excellent features e.g. high accelerating gradients, negligible RF power dissipation and large bore apertures, superconducting structures are the ideal candidates for the main acceleration.

- An RT CH-DTL is well suited as a transition between the above-mentioned two parts, because it can not only provide higher acceleration efficiency than the RFQ but also "filter out" the potential unstable particles from the RFQ to avoid dangerous losses in the SC cavities.

6.1 RFQ Beam Dynamics: 0.05 – 3.0MeV

Standing at the beginning of the driver linac, the RFQ accelerator has a decisive influence on the performance of the whole machine, so its initial parameters have been carefully chosen as following:

- The 0.05MeV input energy is a trade-off of the RFQ length, ion source technology and space-charge effects for both beam currents, while the 3MeV output energy is a suitable transition value according to the acceleration efficiencies of the RFQ and DTL accelerators.

- The input normalized rms transverse emittance is 0.2π mm mrad, which is a typical value for 30mA and ~2 times the one for 5mA.

- To achieve high reliability and provide a reasonable accelerating gradient as well as sufficient transverse focusing forces for an up to 30mA beam, an inter-electrode voltage of 65kV and a maximum electrode modulation of 1.8 have been adopted so that the highest surface electric field can be kept under 1.7 times the Kilpatrick limit E_k without the risk of sparking.

Obviously, these choices are all conservative and compromising for both currents rather than optimum for one particular case. Based on the given conditions, an RFQ design has been achieved with a compact size and high beam qualities simultaneously also by the application of the unconventional dynamics strategy "BABBLE" which was successfully adopted by the design of a 200mA proton RFQ for FRANZ (see Chap. IV). Again, the evolutions of the transverse focusing strength B, the synchronous phase φ_s and the electrode modulation m along the RFQ are the trade-off results between the two intensities.
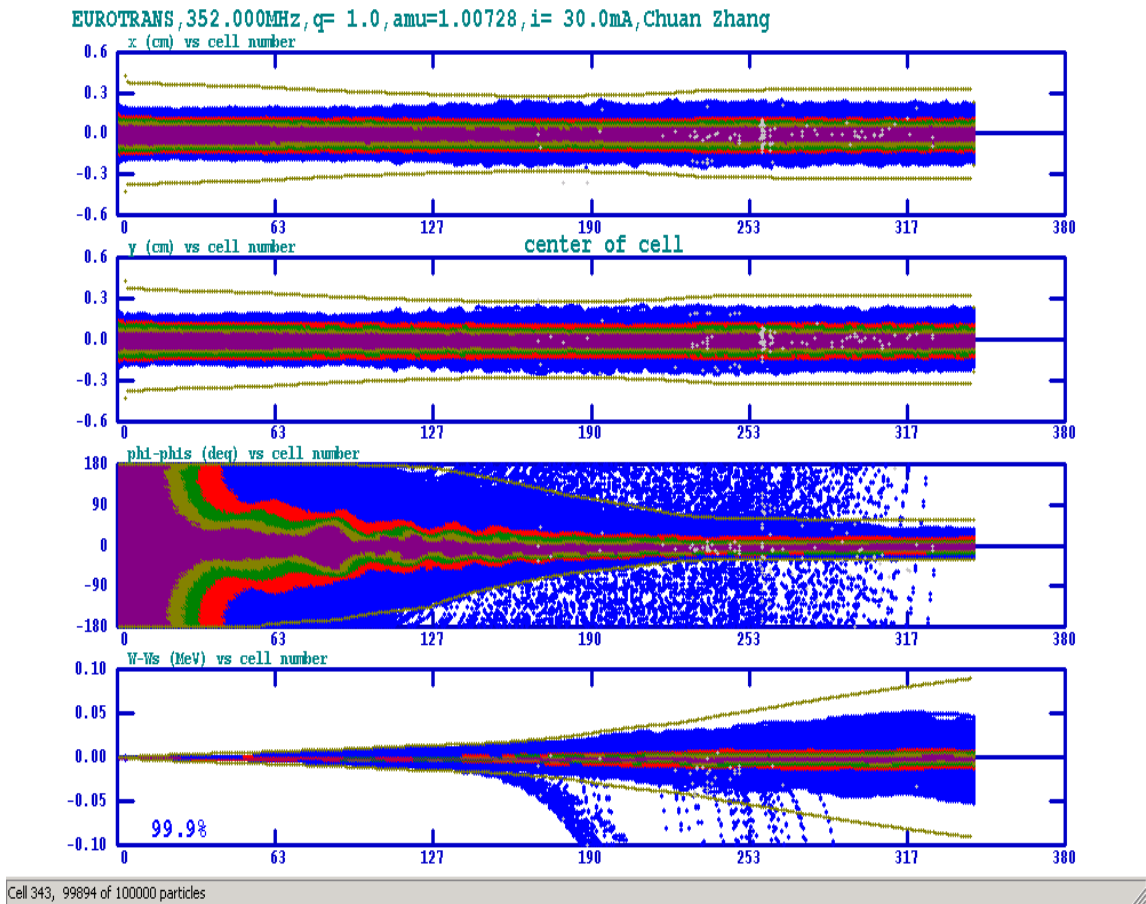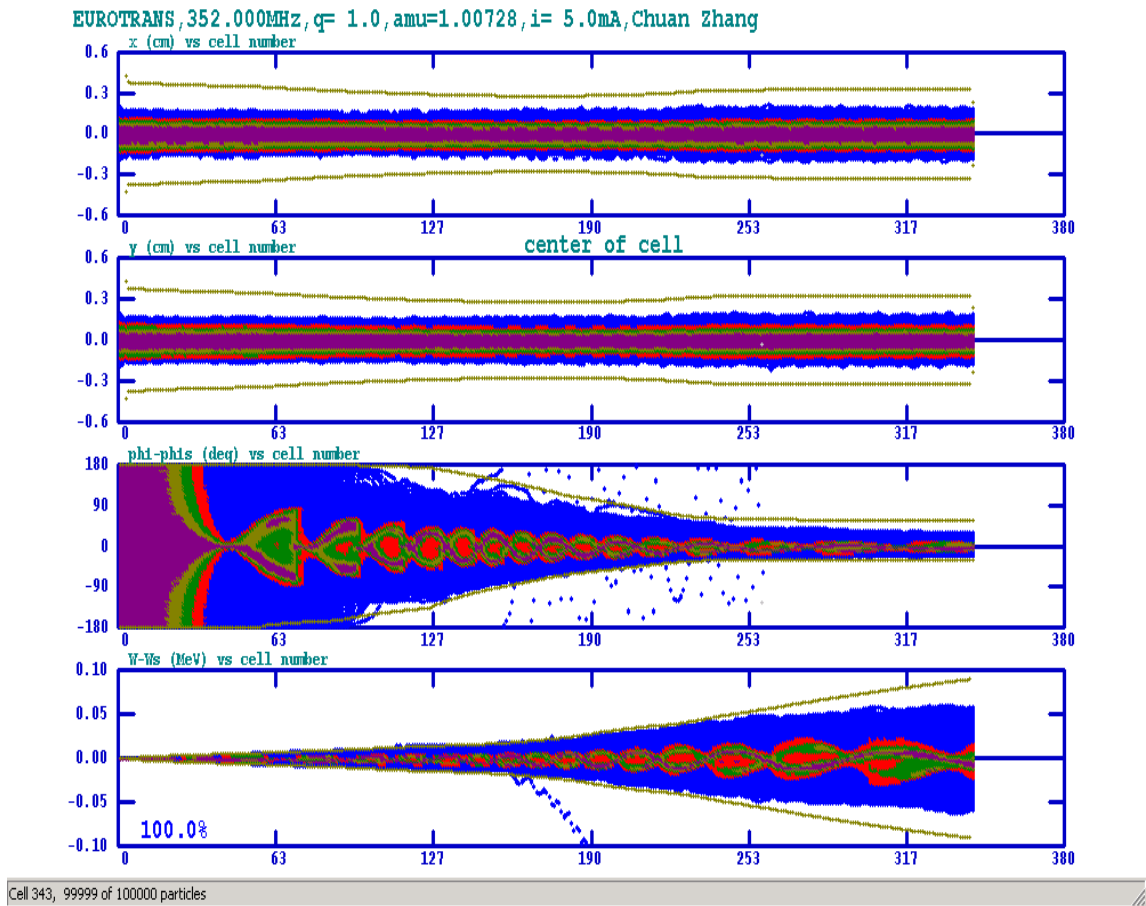
Fig. 6.1-1: Beam transport simulation plots for 5mA (top) and 30mA (bottom).

The beam transport simulations of the designed 343-cell, 4.23m-long RFQ accelerator are demonstrated in Fig. 6.1-1. For both 5mA and 30mA, an identical RFQ geometry and an equal-area input particle distribution have been used. The only difference is that the shapes and the orientations of the input emittance ellipses were slightly modified for each case due to the matching issue. At 5mA, almost all 10^5 of input particles passed through the accelerating channel successfully except only one particle was lost at Cell259 longitudinally; while at the high intensity, though the space-charge effects were much stronger, only ~0.1% of particles were lost and most of them had the energies lower than 1.5MeV (see Fig. 6.1-2). In both cases, therefore, these ignorable beam losses have totally no threat to the accelerator reliability.
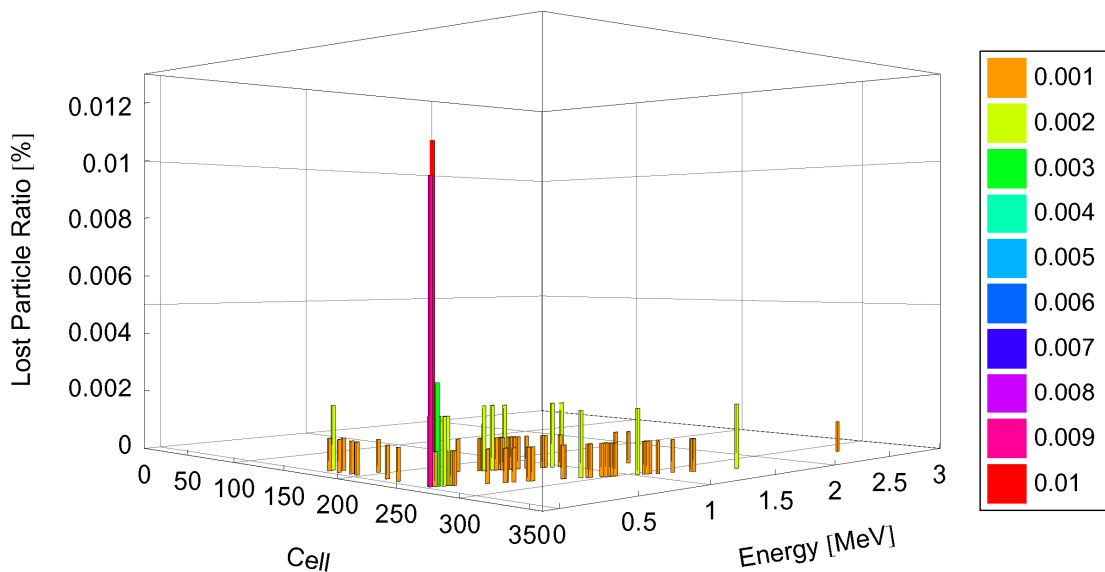
Fig. 6.1-2: The lost-particle distribution at 30mA.

Another strategy applied in the RFQ design is to perform the RFQ-DTL matching inside the RFQ, but not in the MEBT region, because the continuous, velocity-independent electric focusing is more efficient for a slow beam. At the RFQ exit, normally the major axes of the two transverse phase-space ellipses are not parallel to but crossed to each other. The difference between the orientations, which will cause uneven evolutions of the beam envelopes in the DTL part, can be eliminated by introducing two additional transition cells [PAR05] before the RFQ exit fringe-field cell. The first transition cell, also known as the Crandall cell [CRA94], makes a smooth transition from a full modulation (m>1) to no modulation (m=1) over a distance slightly shorter than a standard cell in order to end the RFQ vane tips with quadrupole symmetry for getting a relatively round output beam. The second transition cell, which has a modulation m=1, can be used as a "super-lens" to rotate the output transverse phase-space ellipses. The length of the 2nd transition cell can be calculated with $L= (\varphi_{out}-\varphi_{\Delta m})(\beta_s\lambda/2\pi)$, where $\varphi_{\Delta m}$ and φ_{out} are the synchronous phases of the 1st and 2nd transition cells, respectively.
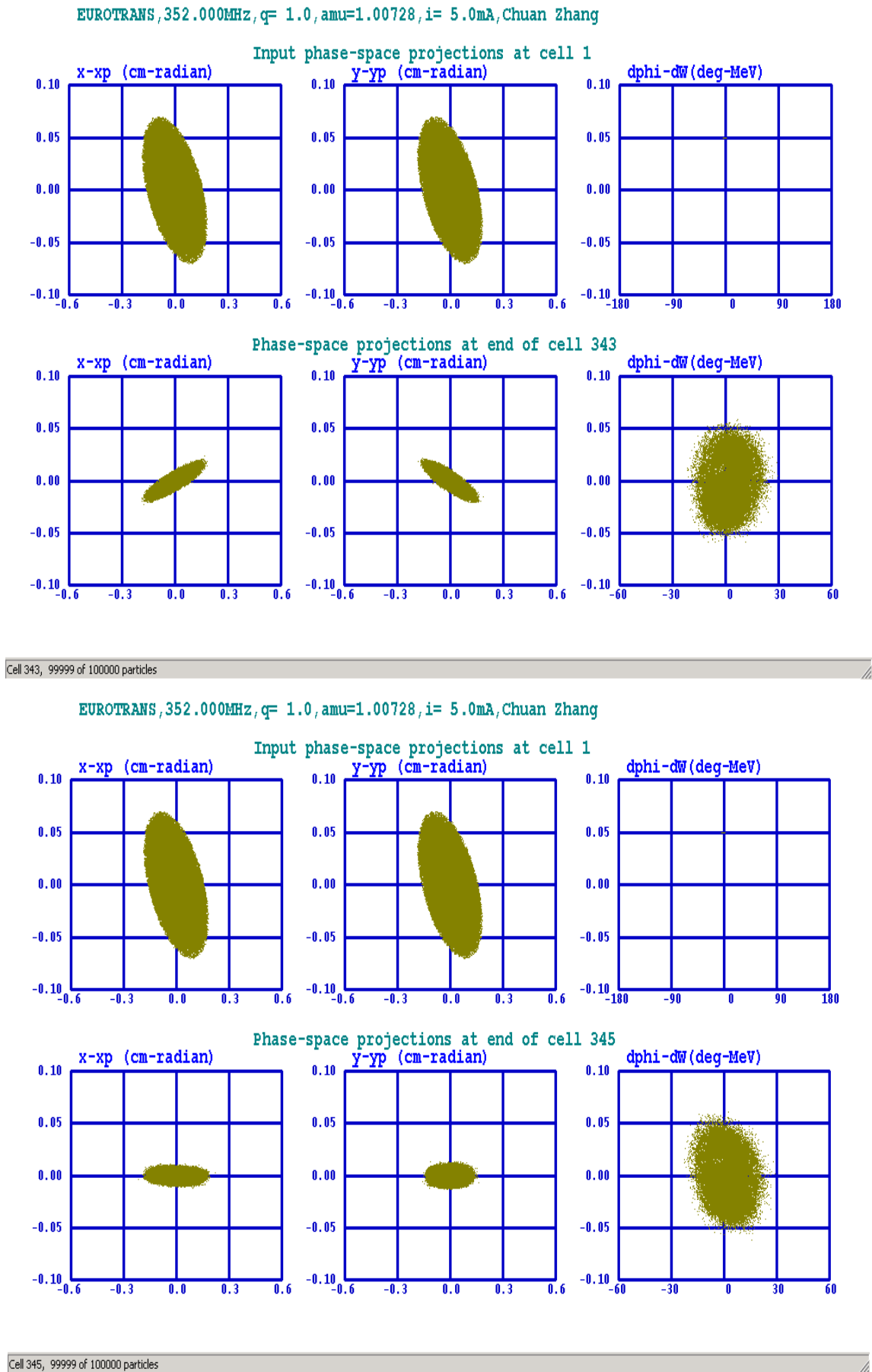
Fig. 6.1-3: Input/output distributions at 5mA without (top) or with (bottom) transition cells.
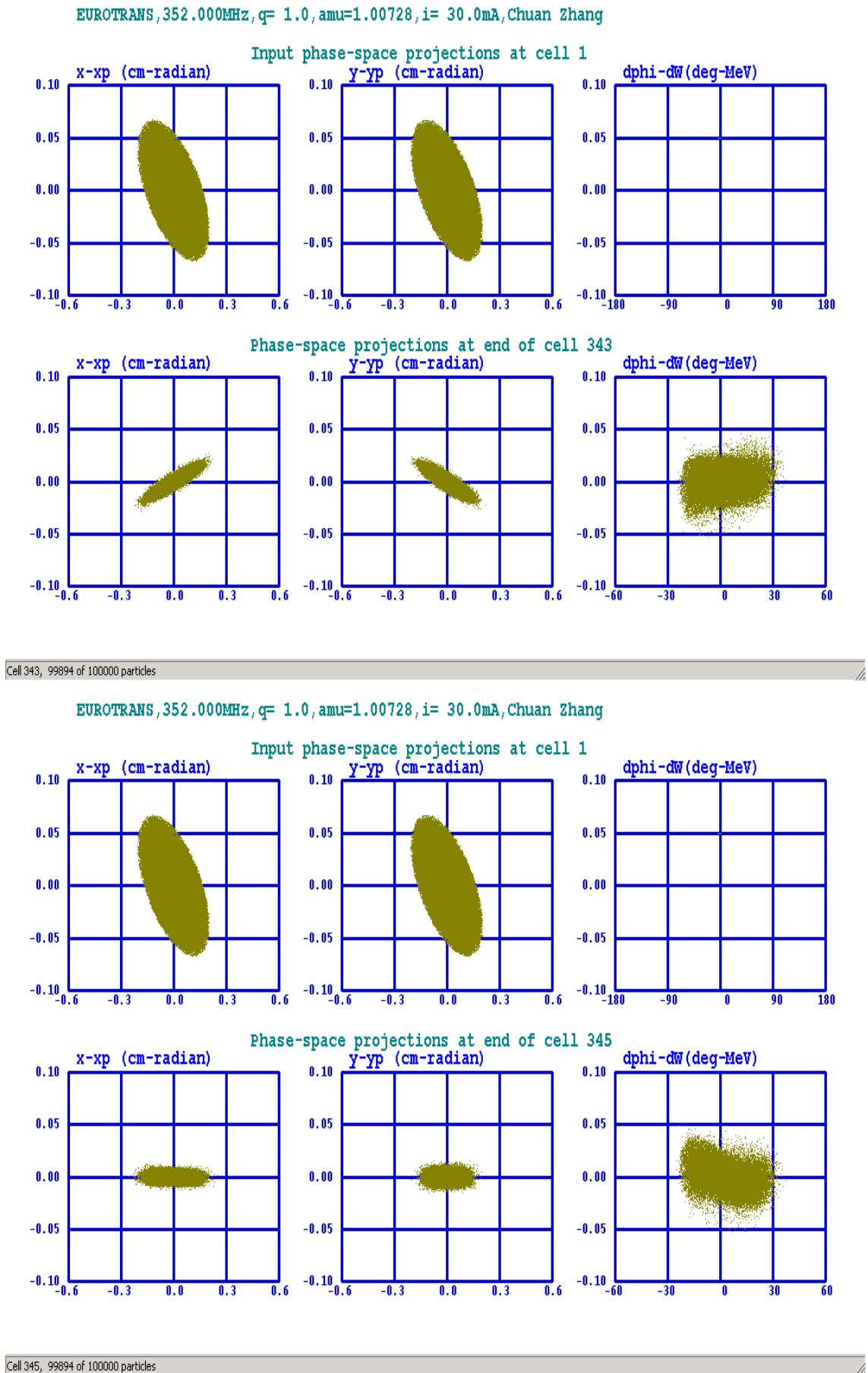
Fig. 6.1-4: Input/output distributions at 30mA without (top) or with (bottom) transition cells.

For the EUROTRANS RFQ, $\varphi_{\Delta m}$= -54° and φ_{out}=250° when the transverse particle distributions are axial-symmetric and similar at the RFQ exit for either 5mA or 30mA (see Fig. 6.1-3 and Fig. 6.1-4, respectively). With the two additional transition cells, the total RFQ length is only ~8cm longer.

As a result of the above-mentioned optimization strategies, the final design of the 3MeV RFQ is illustrated in Fig. 6.1-5, where a is the electrode aperture, m the electrode modulation, V the inter-electrode voltage, W_s the synchronous energy and φ_s the synchronous phase. Clearly, all these dynamics parameters are varying conservatively and smoothly throughout the RFQ.
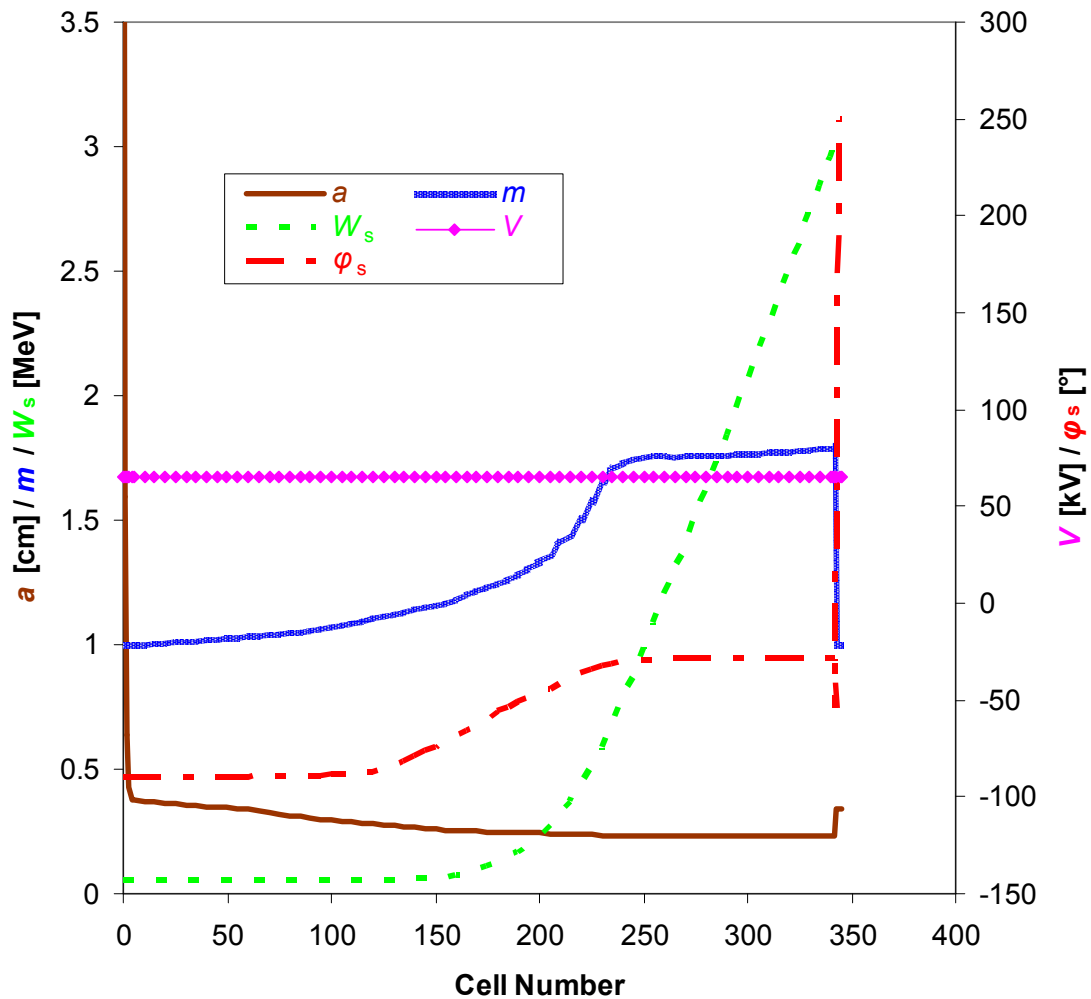
Fig. 6.1-5: Main dynamics parameters along the RFQ.

The simulation results of the final design are concluded in Table 6.1-1, where the Kilpatrick factor is 1.69, well below the safe value 1.8 proved by the successful CW operation of the worldwide most powerful LEDA-RFQ [YOU97]. In the design, therefore, the sparking risk has been avoided to ensure the high reliability.

Table 6.1-1: Main design parameters and simulation results of the RFQ.

Beam current [mA] / Parameter	5mA	30mA
Frequency [MHz]	352	
Input / output energy [MeV]	0.050 / 3.000	
Inter-electrode voltage [kV]	65	
Kilpatrick factor	1.69	
$\varepsilon_{in}^{trans., norm., rms}$ [π mm mrad]	0.20	
Maximum synchronous phase [°]	-28.76	
Minimum aperture [cm]	0.23	
Maximum electrode modulation	1.79	
$\varepsilon_{out}^{x., norm., rms}$ [π mm mrad]	0.2056 (100%) 0.1702 (90%)	0.2078 (100%) 0.1702 (90%)
$\varepsilon_{out}^{y., norm., rms}$ [π mm mrad]	0.2019 (100%) 0.1680 (90%)	0.2032 (100%) 0.1664 (90%)
$\varepsilon_{out}^{z, rms}$ [π MeV deg]	0.1086 (100%) 0.0753 (90%)	0.0889 (100%) 0.0609 (90%)
Cavity length [cm]	431.77	
Total number of cells	345	
Beam transmission efficiency [%]	~100	99.9
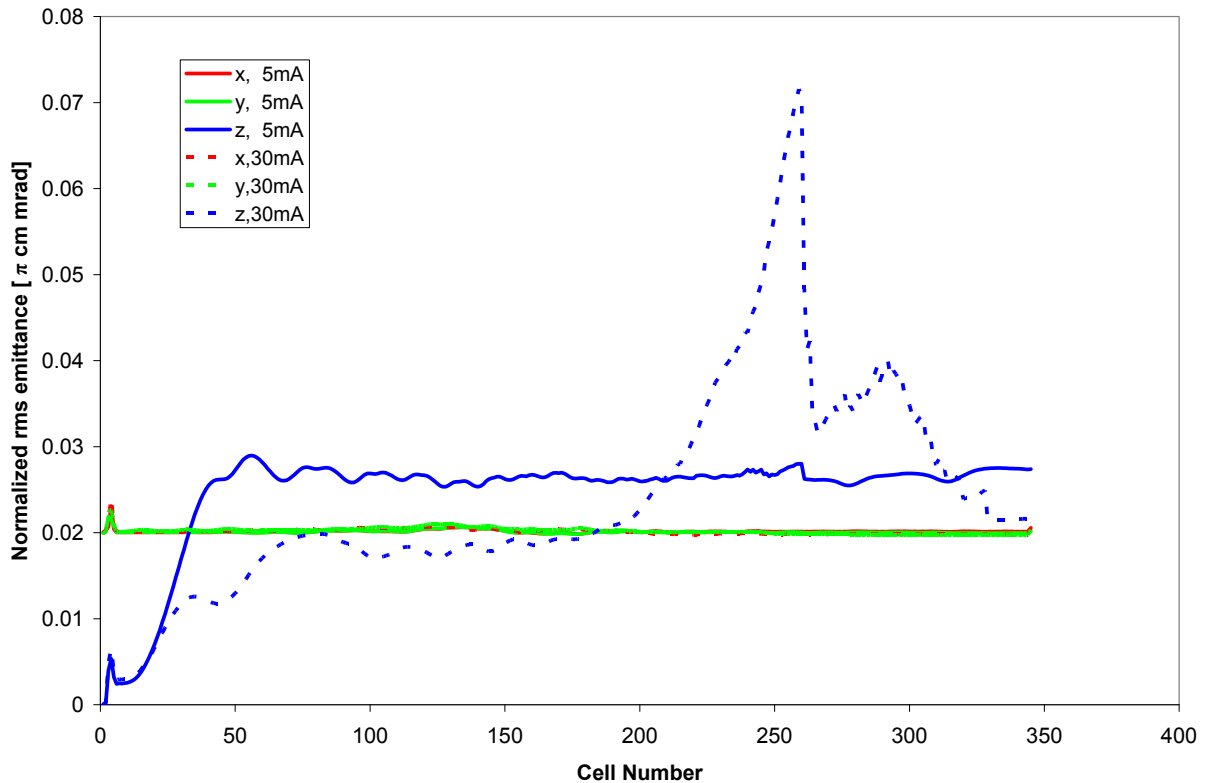
Fig. 6.1-6: Emittance growths along the RFQ for 5mA and 30mA.

A comparison of the emittance evolutions for all transported particles between the 5mA and 30mA cases is made in Fig. 6.1-6, from which the following points can be concluded: 1) Except the 30mA longitudinal emittance, all emittances have been held almost constant along the RFQ, especially in the transverse planes. 2) The 30mA longitudinal emittance curve has two growth "peaks" in the downstream part of the RFQ, but a trace of the particle trajectories showed that the "peaks" had been just contributed by a few not-well-accelerated particles, which total amount is less than 0.1%. After these "bad" particles had been lost, the 30mA longitudinal emittance fell down back to the level of the beginning of the first "peak" (20% smaller than the 5mA one). Actually, if the "noise" is not taken into account, this curve should be also similar to the other curves. 3) The flat and parallel evolutions of transverse and longitudinal emittances show that the particle motions at the two beam intensities have been both well balanced.

To learn why a larger output longitudinal emittance $\varepsilon_{l,out}$ happened even at the low intensity, the emittance development has been checked. For the beam transport simulation of an RFQ, usually a 4D-Waterbag input distribution, which has a uniform phase spread over the full 360° and no energy spread, is used, so did the EUROTRANS RFQ. Therefore, the longitudinal emittance is zero at the beginning and will grow quickly to a relatively stable value (which can be called as the "real" input longitudinal emittance $\varepsilon_{l,in}$) when the bunch begins to take shape. In Fig. 6.1-6, the following phenomena are of interest:

- $\varepsilon_{l,in}$ comes into being at Cell45 and Cell78 for the 5mA case and the 30mA case, respectively.

- $\varepsilon_{l,in}^{5mA} \approx \varepsilon_{l,out}^{5mA}$ and $\varepsilon_{l,in}^{30mA} \approx \varepsilon_{l,out}^{30mA}$.

- $\varepsilon_{l,in}^{5mA} > \varepsilon_{l,in}^{30mA}$ and $\varepsilon_{l,out}^{5mA} > \varepsilon_{l,out}^{30mA}$.

These hints indicate that the larger $\varepsilon_{l,out}^{5mA}$ should be caused by the formation of the "real" input longitudinal emittance. To look inside this formation period, therefore, the longitudinal phase spaces at Cell15, Cell30 and Cell45 (from top to bottom) are compared for both cases in Fig. 6.1-7, where the three pictures on the left or right side are related to the 5mA beam or the 30mA beam.

Obviously, under same external forces, the bunching is developing more quickly and the amplitudes of the particle-energy changes are larger at 5mA. The reason is that the space-charge effects in a 30mA beam are much stronger so that they can make a larger cancellation of the external bunching forces, which leads to a slower and gentler bunching process and consequently a smaller energy spread also very likely a smaller longitudinal emittance.
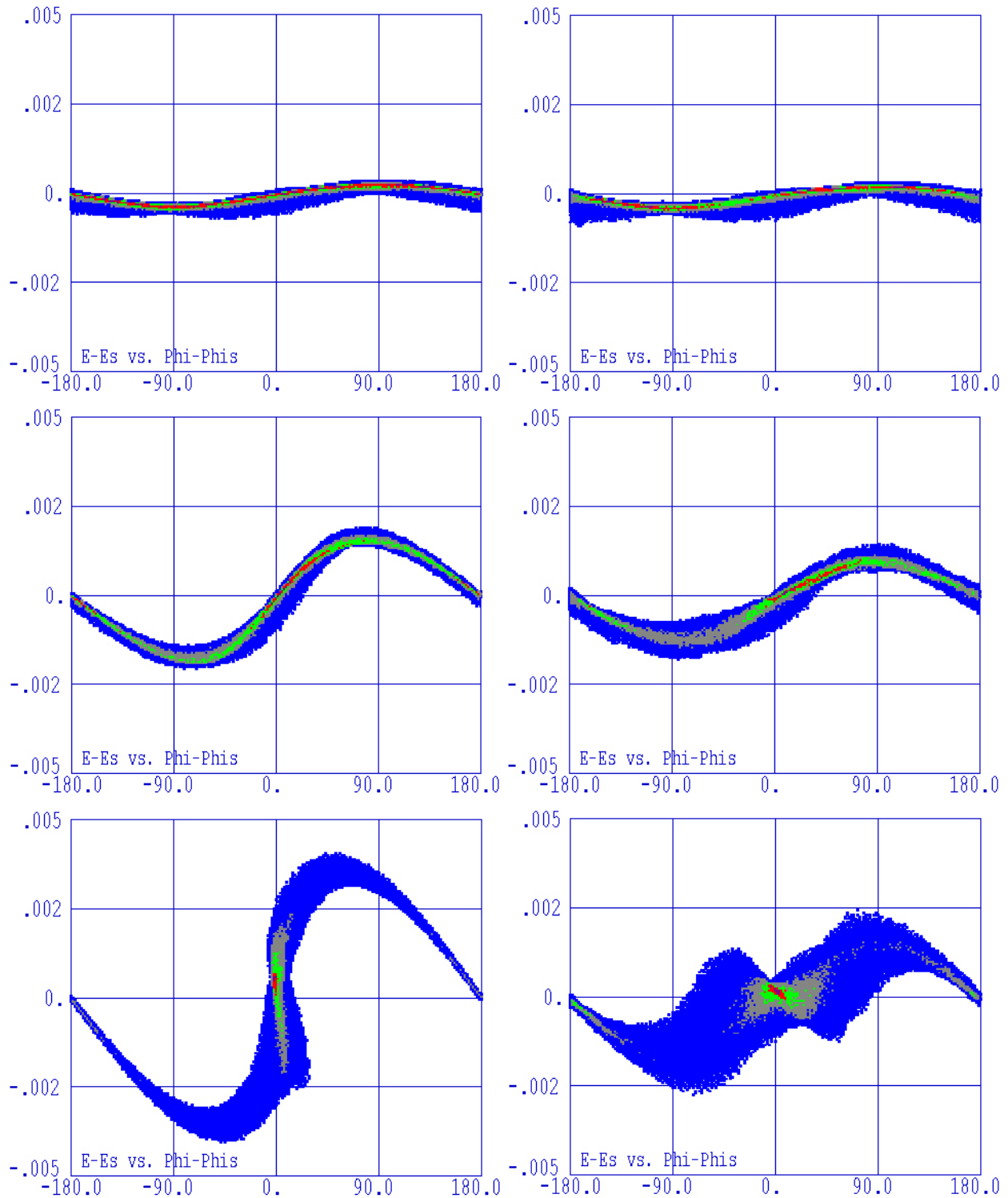
Fig. 6.1-7: Formation of the longitudinal emittance

(left: 5mA, right: 30mA, from top to bottom: Cell15, 30, 45).

All in all, it is a natural result for an identical RFQ structure to work with two different beam intensities. In principle, it is impossible to be overcome by the RFQ itself, so this situation will be improved in the DTL part. Another piece of important information from Fig. 6.1-7 is that the bunching is symmetrical at $\varphi_s = -90°$, so it proves the importance of the maximum-

separatrix section used by the "BABBLE" design strategy for the beginning of an RFQ (see Chap. IV).

Finally, to check the beam qualities as well as the matching issues at the exit of the RFQ for both beam intensities, the output particle cluster plots (in which the particle densities are distinguished by 10 colours) are zoomed in and shown in Fig. 6.1-8, where the red and green ellipses are containing 99% and 95% of transported particles, respectively. As analyzed above, the 5mA beam has a larger size in energy spread, but both beams are concentrated and similar to each other, especially in the transverse planes.
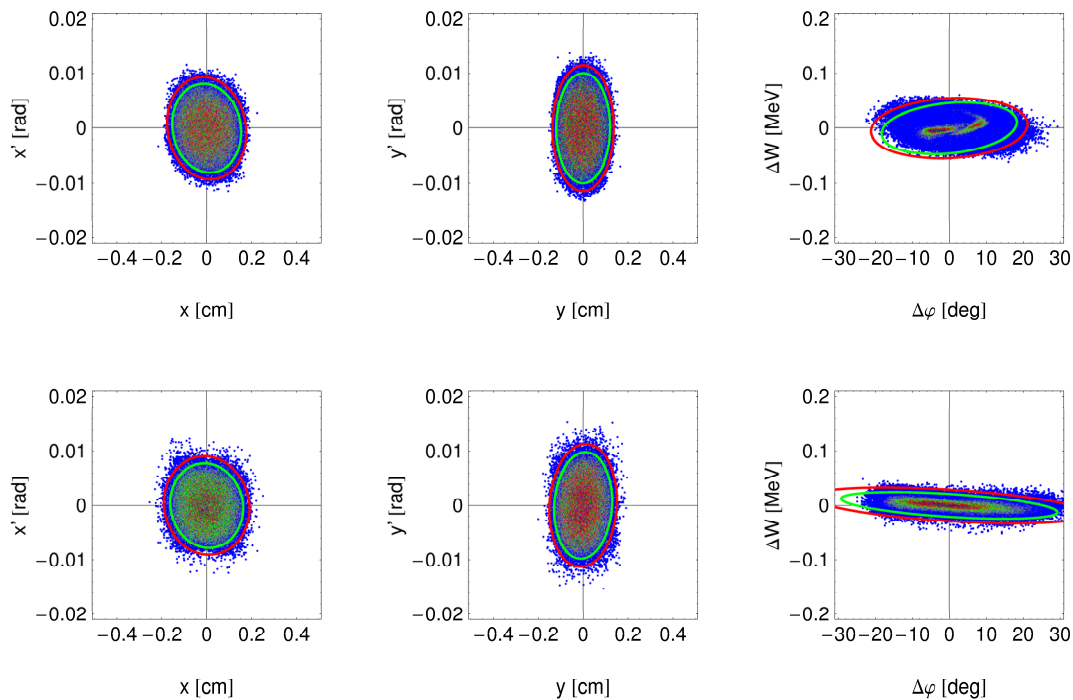
Fig. 6.1-8: RFQ output distributions with the red and green ellipses for 99% and 95% of transported particles, respectively (top: 5mA, bottom: 30mA).

Because of the applied RFQ-DTL matching, the first triplet (before RB-1) in the originally proposed layout (see Fig. 6-1) is not necessary any more.

So far, all performed studies have shown that the designed RFQ can reach good beam qualities at an intensity up to 30mA. To some degree, it also indicates that the design will be non-sensitive to the beam-related errors. Therefore, the RFQ design has provided a good starting point for the design of the following DTL part.

6.2 DTL Beam Dynamics: 3.0 – 17.0MeV

Covering the energy range from 3 to 17MeV, the CH-DTL structure based on the KONUS beam dynamics strategy and the superconducting technology has been adopted for the rest part of the injector to optimize the beam quality, the geometry length and the project costs.

In case of a fixed total gap number for one accelerating cavity, the smaller the ratio of the number of the conventional rebunching gaps with negative synchronous phases to the number of the 0° gaps which mainly used by the KONUS dynamics, $N_{gap, neg.} / N_{gap, 0°}$, is, the higher the acceleration efficiency will be. Typically, this ratio is between 0.25 and 0.5 for a KONUS structure. For the EUROTRANS DTL cavities, a modest value of around 0.4 has been adopted. Concerning the transverse focusing elements, conventional room-temperature quadrupole lenses (up to 1.3T) and powerful superconducting solenoid lenses (4–12T) can be used [TIE08]. Also conservatively, the field strengths of the RT and SC transverse focusing elements for EUROTRANS have been chosen as 1.2T and 5T, respectively.
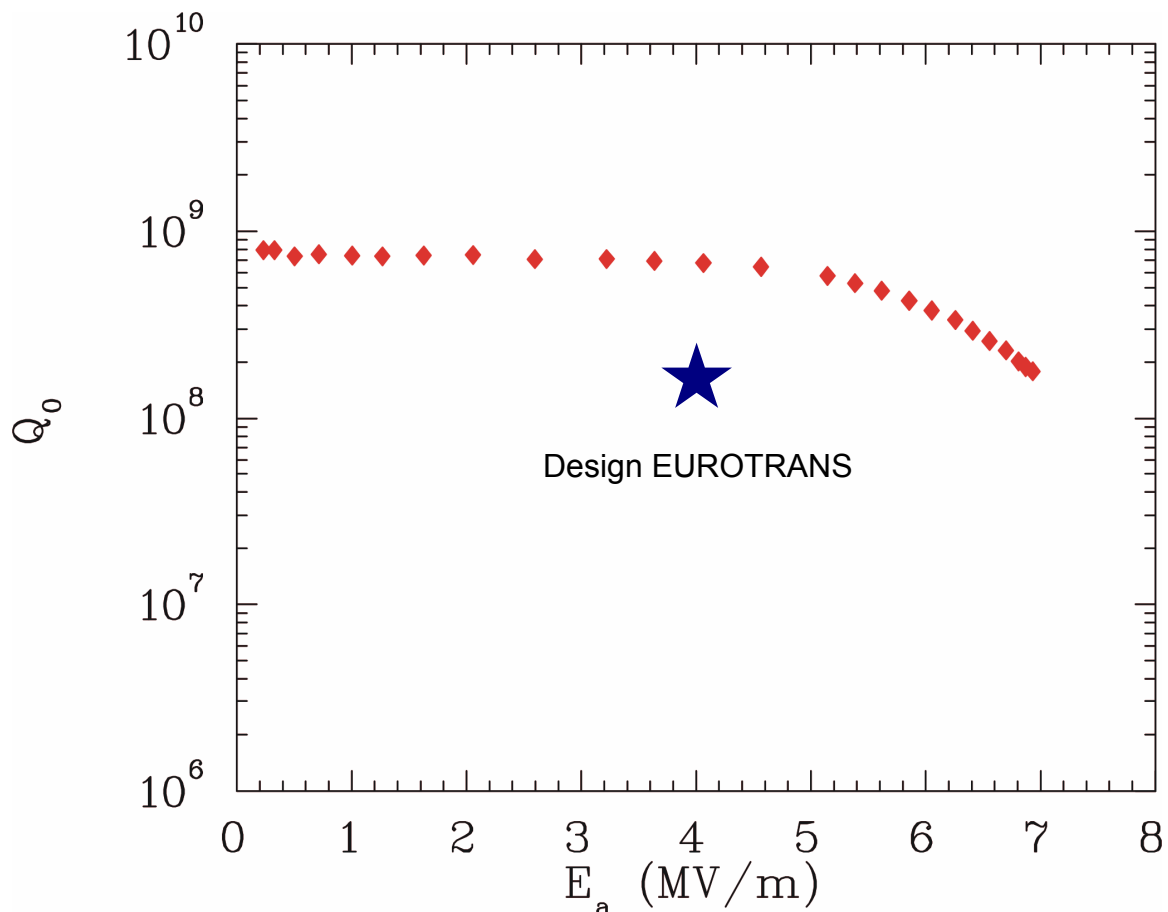
Fig. 6.2-1: The accelerating gradient choice for the SC CH-DTL cavities [POD08a].

The choice of the accelerating gradient for the EUROTRANS SC CH-DTL cavities is presented in Fig. 6.2-1, where the red-dot curve shows the measured unloaded Q_0-value of the SC CH prototype cavity as a function of the effective accelerating gradient E_a [POD08a] (the definition of the accelerating gradient has been given in Section 5.1.1 of Chap. V).

So far, the maximum achievable E_a is 7MV/m, which corresponds to an effective voltage of 5.6MV and to a peak electric field of 36MV/m. Because of the extremely high reliability requirement, an effective accelerating gradient of ~4MV/m has been conservatively adopted for the EUROTRANS SC CH-DTL cavities. Accordingly, four SC cavities can cover ~12MeV of energy gain, while the rest 2MeV will be completed by the RT CH-DTL at the front.

In the DTL design, there are two most difficult areas:

- Between the RFQ exit and the beginning of the DTL part, which requires a ~0.5m long drift distance for placing steerer, diagnostic devices and quadrupoles.

- The transition from the RT CH-DTL to the first SC CH-DTL, which needs more reserved space, ~1m, for housing the cryomodule, tuner, helium vessel and transverse focusing elements.

As a dual-use optimization procedure, two additional 2-gap rebunching cavities, so-called RB-1 and RB-2, in which the synchronous phases of all gaps are designed as $-90°$, have been introduced into the above-mentioned two areas, respectively.

At $\varphi_s = -90°$, both RB-1 and RB-2 can make the most of the gap voltages for beam bunching but contribute nothing to energy gain. This means, while the longitudinal beam dynamics is being improved, flexible operations of these rebunching cavities are feasible for the adjustments of the gap voltages (the bunching strengths) to fit different beam currents, but independently to the structure.

As mentioned in the last section, the 5mA beam has a relatively larger longitudinal emittance at the end of the RFQ, so higher gap voltages are needed for the two rebunching cavities to give it stronger longitudinal focusing forces as compensation.

Finally, a 7.1m-long, 82-cell DTL accelerator has been designed for the EUROTRANS injector, with the configurations of the effective gap voltages V_{eff} and the synchronous phases along the DTL for both intensities as shown in Fig. 6.2-2, where:

- The V_{eff} values of the SC CH-DTL cavities are ≥2 times higher than those of the RT-CH.

- Between the two intensity cases, the only difference is that in the RB cavities, the V_{eff} values are higher for the 5mA beam.

- $\varphi_s = -90°$ for the independent rebunching cavities, $\varphi_s = -40°$ for the rebunching sections inside the DTL cavities and $\varphi_s = 0°$ for most accelerating cells.
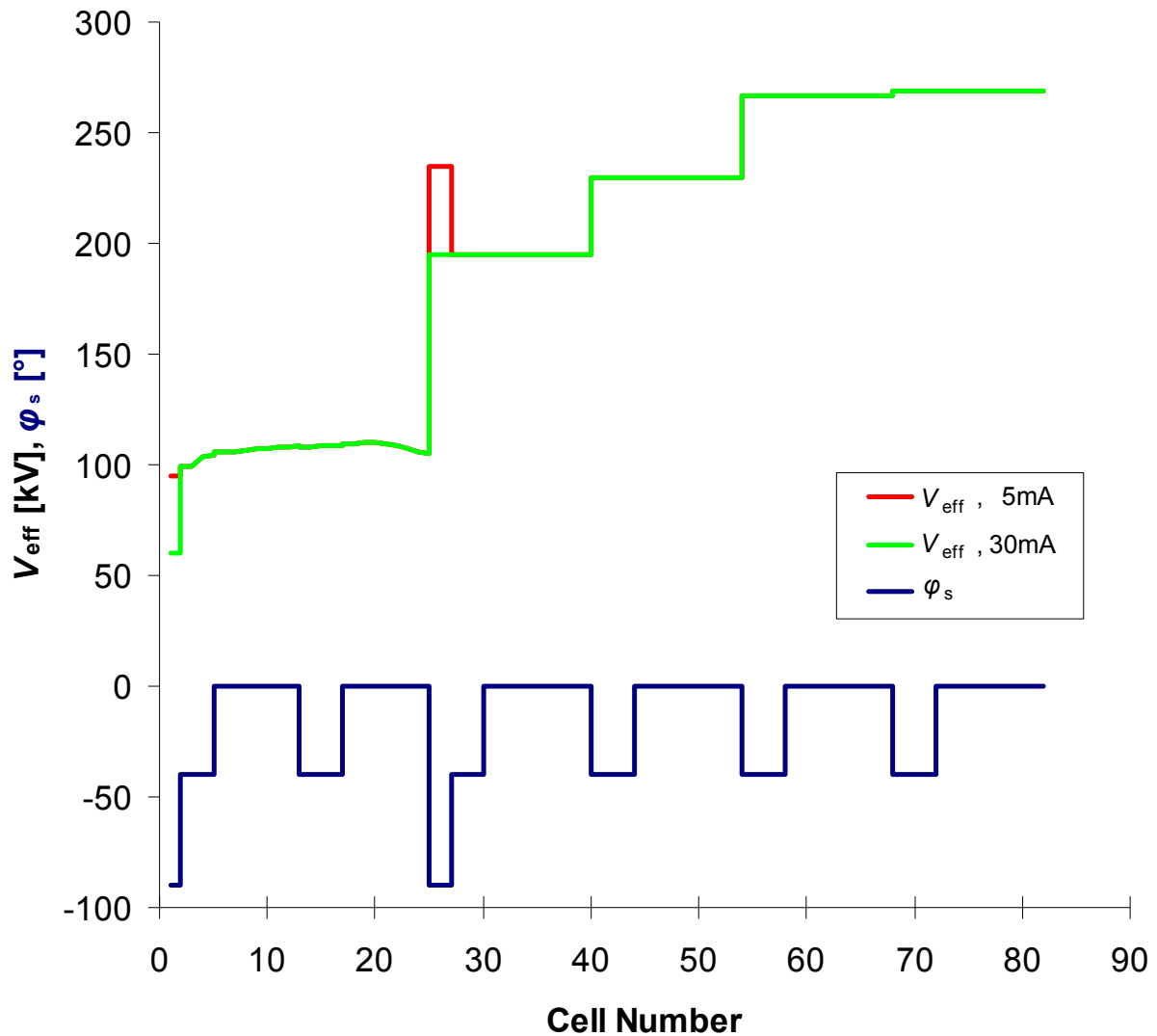
Fig. 6.2-2: Main dynamics parameters along the DTL.

Using the RFQ output particle distributions as the input distributions, the beam transport simulations of the designed DTL have been performed with the LORASR code for the two intensities, respectively. For both cases, no beam loss has been observed. At 5mA, the transverse and longitudinal emittance growths are all less than 10%; while at 30mA, they are 30%, 34% and 36%, respectively. The detailed design parameters and simulation results of the DTL are summarized in Table 6.2-1.

Table 6.2-1: Main design parameters and simulation results of the DTL.

Beam Current [mA] / Parameter	5	30
Frequency [MHz]	352	
Accelerating gaps	RB-1 : 2 (-90°) RT-CH : 3 (-40°) 8 (0°) 4 (-40°) 8 (0°) 2 (-90°) RB-2 : 3 (-40°) SC-CH-1: 10(0°) 4 (-40°) SC-CH-2: 10(0°) 4 (-40°) SC-CH-3: 10(0°) 4 (-40°) SC-CH-4: 10(0°) Total: 82	
Accelerating gradient E_a [MV/m]	RB-1 : 2.79 RT-CH : 2.73 RB-2 : 5.22 SC-CH-1: 3.99 SC-CH-2: 3.97 SC-CH-3: 3.97 SC-CH-4: 3.55	RB-1 : 1.76 RT-CH : 2.73 RB-2 : 4.33 SC-CH-1: 3.99 SC-CH-2: 3.97 SC-CH-3: 3.97 SC-CH-4: 3.55
$W_{out}^{bunch\ center}$ **[MeV]**	RB-1 : 3.01 RT-CH : 5.46 RB-2 : 5.25 SC-CH-1: 7.79 SC-CH-2: 10.71 SC-CH-3: 14.09 SC-CH-4: 17.05	RB-1 : 3.01 RT-CH : 5.46 RB-2 : 5.25 SC-CH-1: 7.78 SC-CH-2: 10.72 SC-CH-3: 14.09 SC-CH-4: 17.05
Maximum on-axis field [MV/cm]	0.12 (Gap26)	0.11 (Gap55)
$\varepsilon_{out}^{x.,\ norm.,\ rms}$ **[π mm mrad]**	0.22	0.27
$\varepsilon_{out}^{y.,\ norm.,\ rms}$ **[π mm mrad]**	0.22	0.27
$\varepsilon_{out}^{z.,\ rms}$ **[π keV ns]**	0.93	0.95
Total length [cm]	708.4	
Beam transmission efficiency [%]	100	

For each design intensity, the transverse and longitudinal beam envelopes including all particles are shown in the top or bottom plots of Fig. 6.2-3 and Fig. 6.2-4, respectively.
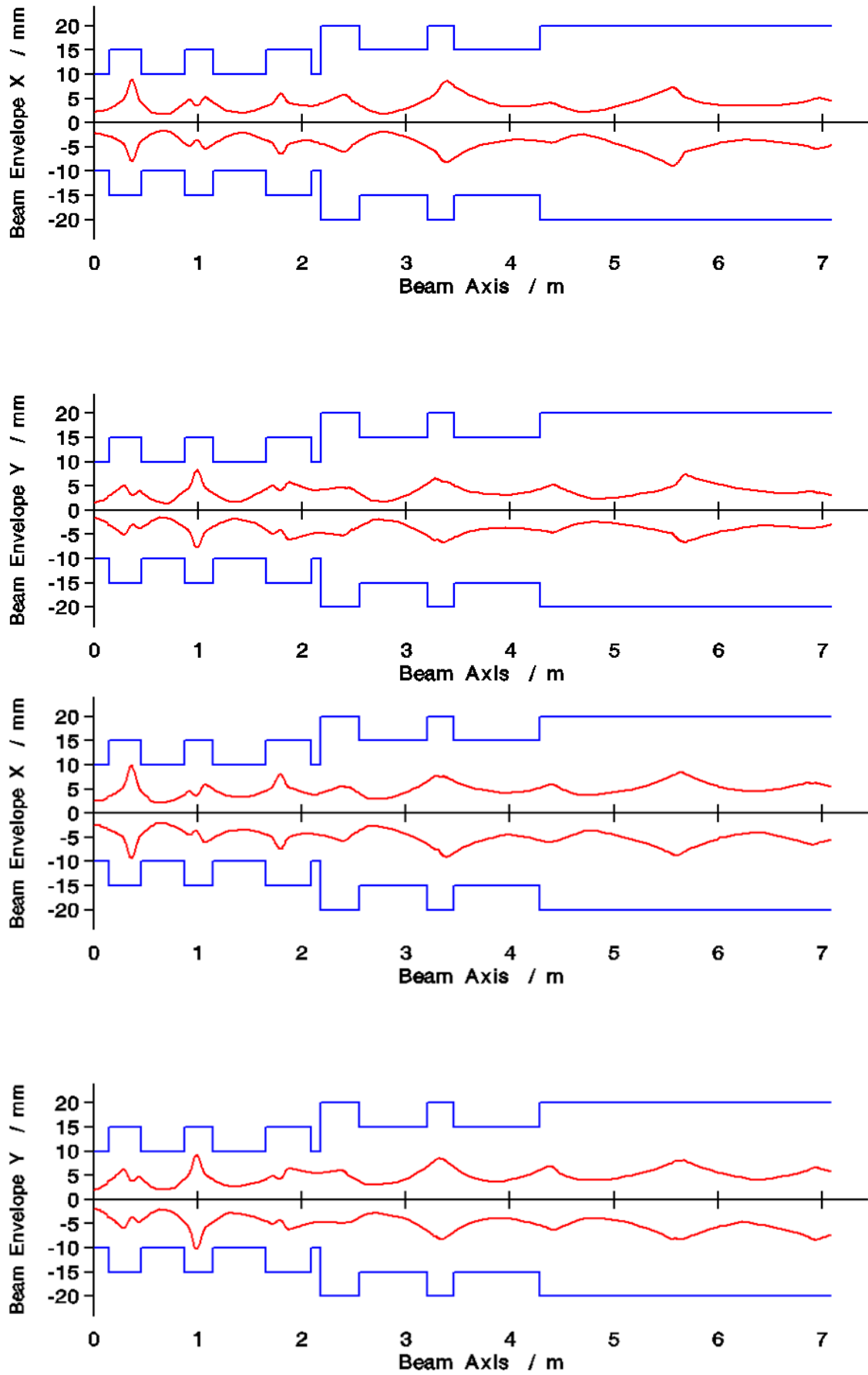
Fig. 6.2-3: Transverse beam envelopes along the DTL (top: 5mA, bottom: 30mA).
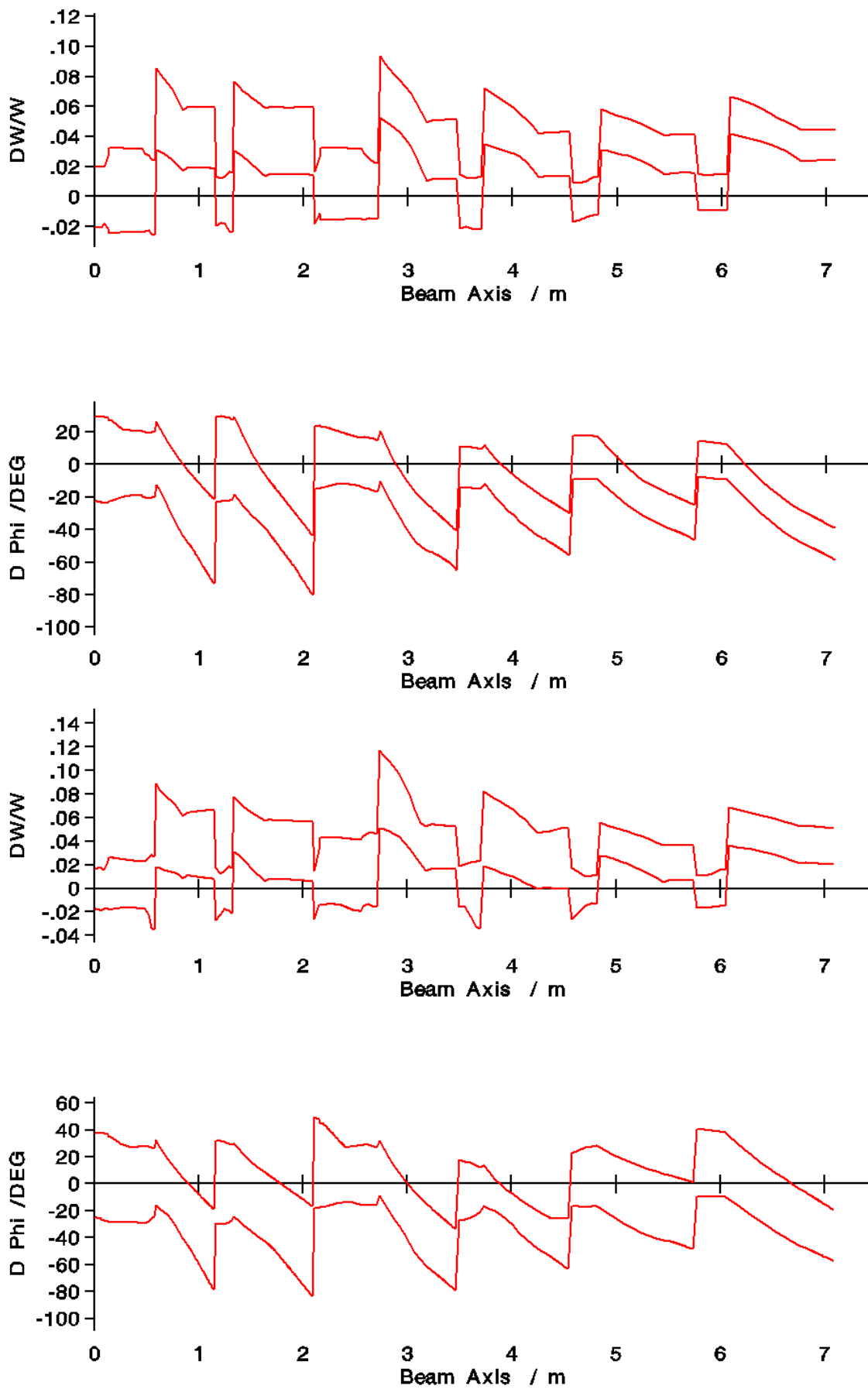
Fig. 6.2-4: Longitudinal beam envelopes along the DTL (top: 5mA, bottom: 30mA).

From the beam envelope plots, one can learn that:

- The beam envelopes for the 30mA beam are similar to the corresponding ones of the 5mA beam, just slightly larger in size.

- Transversely all the envelopes have been confined within the range of ±10mm so that a sufficient safety margin is available for no matter the 5mA beam or the 30mA beam.

- For every longitudinal plot, the top and bottom curves, which are corresponding to the maximum and minimum energy- or phase-spreads, respectively, are parallel at most positions along the DTL, especially in the last cavity.

Together with the still similar and concentrated output particle distributions of the DTL for both beam currents (see Fig. 6.2-5), all analysis results indicate both beams can be easily matched into the next accelerating structure.
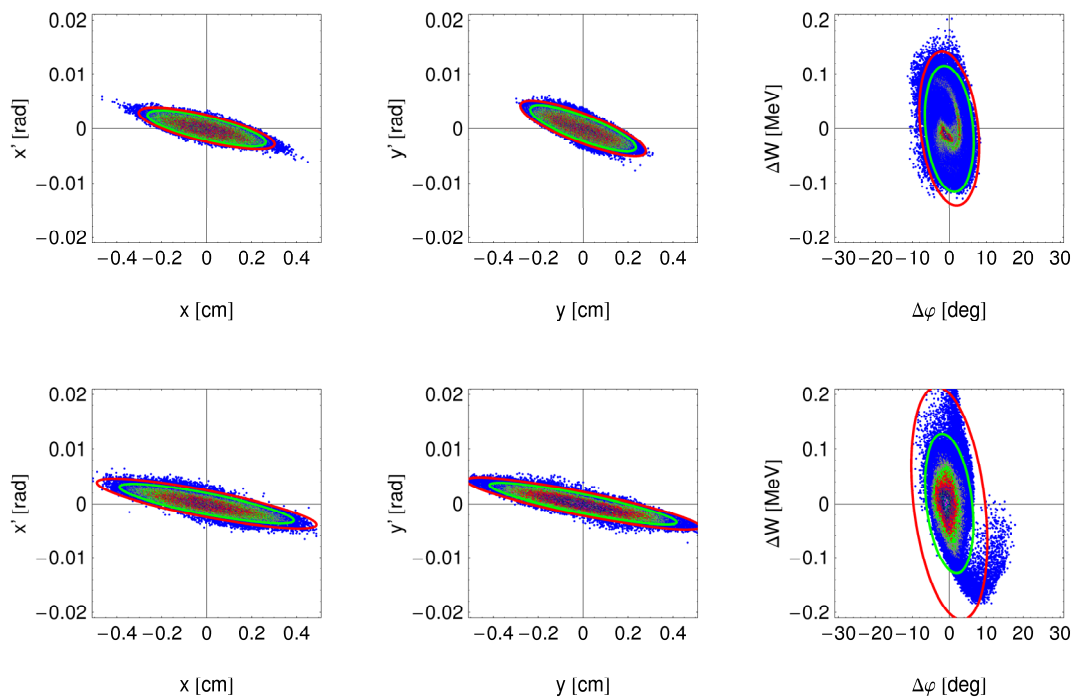
Fig. 6.2-5: DTL output distributions with the red and green ellipses for 99% and 95% of transported particles, respectively (top: 5mA, bottom: 30mA).

6.3 Start-to-End Design Results

On the basis of the RFQ and DTL designs, a layout scaled in length of the EUROTRANS injector is drawn in Fig. 6.3-1, where four RT cavities (from left to right: RFQ, RB-1, coupled RT-CH and RB-2) are marked in red, four SC CH-DTL cavities (SC-CH-1 to -4) sharing a same cryo-module in blue, three warm triplets in yellow and five cold solenoids in green.
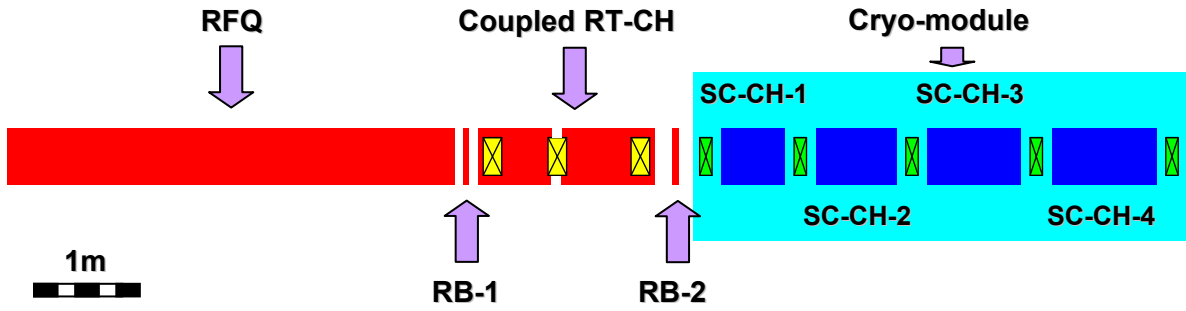
Fig. 6.3-1: The designed layout of the EUROTRANS injector.

As shown in Table 6.3-1, from the start to the end, the overall length of the EUROTRANS injector is ~11.4m, and the total beam transmission efficiencies for both currents are ≥99.9%.

Table 6.3-1: Start-to-end design results of the injector.

Beam current [mA] / Parameter	5mA	30mA
Frequency [MHz]	352	
Input energy [MeV]	0.05	
Output energy [MeV]	3.0 (RFQ), 17.0 (DTL)	
$\varepsilon_{in}^{trans., norm., rms}$ [π mm mrad]	0.20	
Total structure length [m]	11.4 (RFQ: 4.3, DTL: 7.1)	
$\varepsilon_{out}^{x., norm., rms}$ [π mm mrad]	0.21 (RFQ) 0.22 (DTL)	0.21 (RFQ) 0.27 (DTL)
$\varepsilon_{out}^{y., norm., rms}$ [π mm mrad]	0.20 (RFQ) 0.22 (DTL)	0.20 (RFQ) 0.27 (DTL)
$\varepsilon_{out}^{z., norm., rms}$ [π mm mrad]	0.27 (RFQ) 0.30 (DTL)	0.22 (RFQ) 0.31 (DTL)
Beam transmission efficiency [%]	~100	99.9

For the whole injector, the transverse beam envelopes for all transported particles are plotted in Fig. 6.3-2, where the innermost pair of green curves is showing the envelopes for the 5mA beam, the next red pair for the 30mA beam, and the outermost black one represents the mid-cell electrode aperture of each cell for the RFQ or the inner apertures of the drift tubes and the transverse focusing elements for the DTL. In the picture, both beams have quite similar envelope evolutions throughout the accelerating channel, which is meanwhile a strong proof of the success of the applied optimizations for current-adaptability. In the RFQ part, the transverse beam envelopes are small and almost constant everywhere; though after entering the DTL part obvi-

ous growths in beam size appear, the minimum distance between the beam surfaces to the accelerator components is still safe enough.
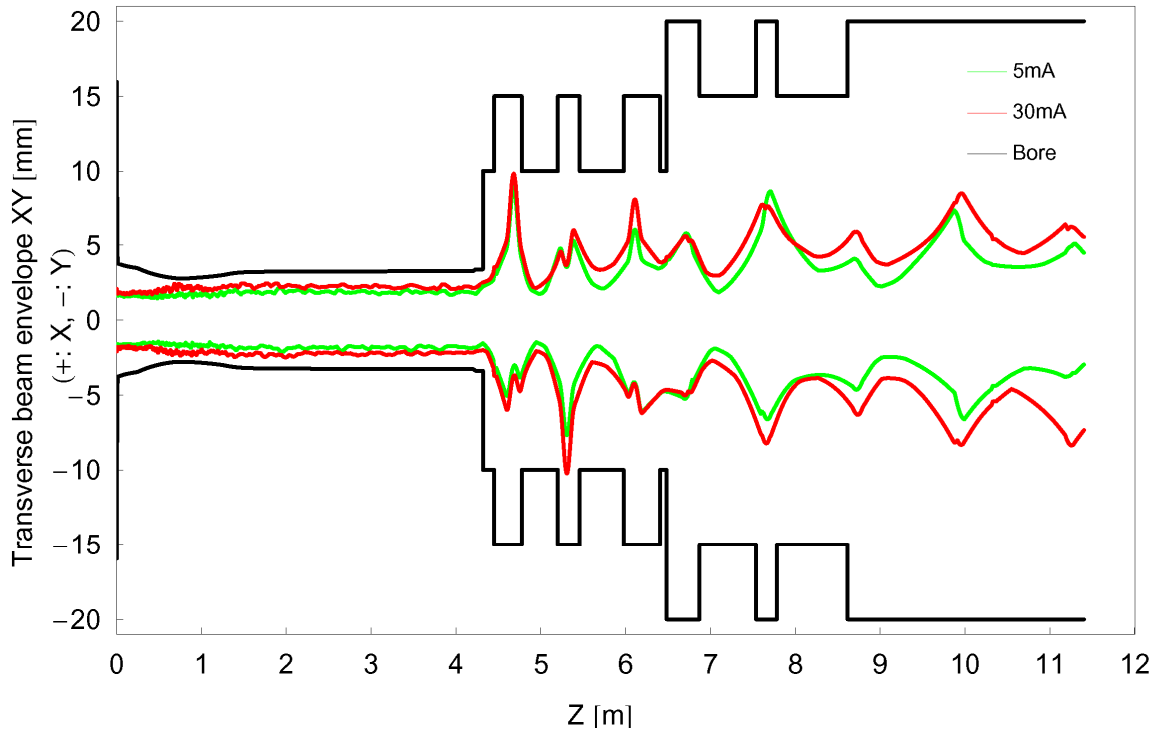
Fig. 6.3-2: Start-to-end transverse envelopes (positive: x-plane, negative: y-plane).
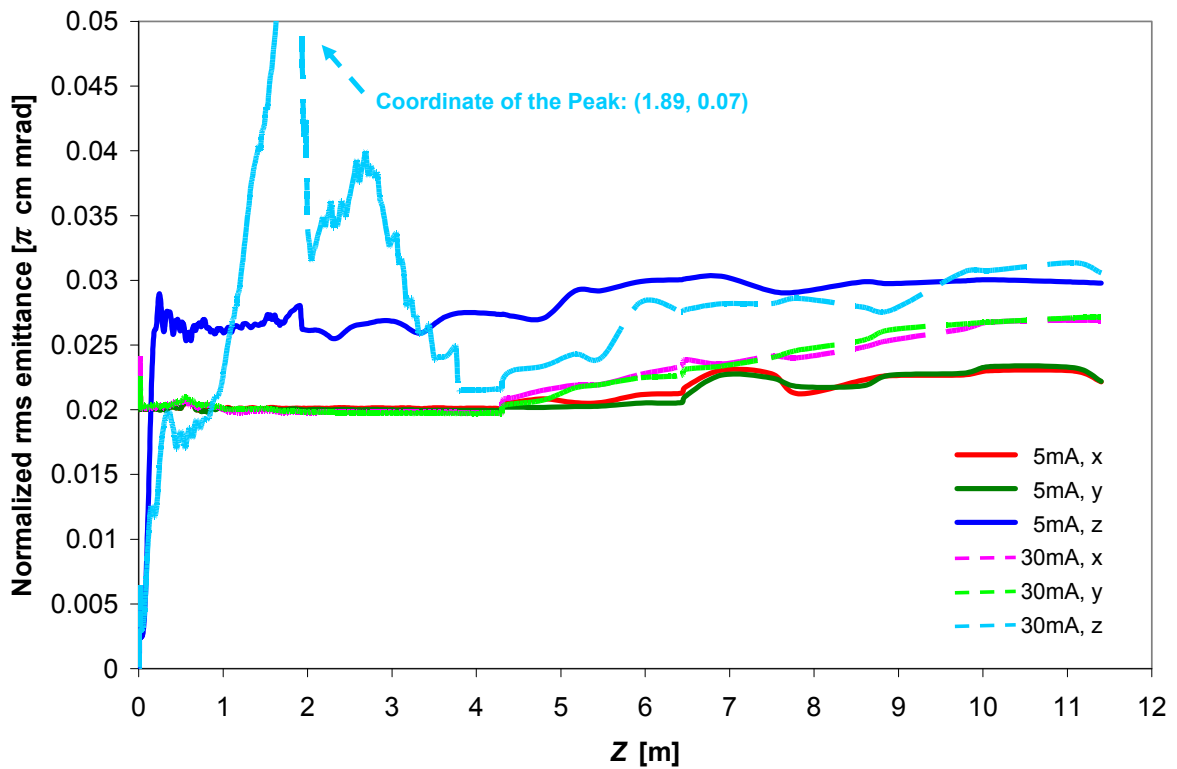
Fig. 6.3-3: Start-to-end emittance growths.

In Fig. 6.3-3, the emittance evolutions along the injector are presented for both cases, where the normalized rms emittances for 100% of transported particles with the unit of π cm mrad are used. Clearly, in the DTL part, the development curves of the transverse and longitudinal emittances are still fairly flat and parallel, which means that balanced beam acceleration as well as a controlled beam quality have been achieved throughout the EUROTRANS injector.

6.4 Start-to-End Error Studies

Since construction and operation errors are inevitable in reality and they play very important roles in the contribution to beam quality deterioration and particle losses, it is necessary to evaluate their influences and the robustness of the obtained design, in particular for EURO-TRANS such a project which requires extremely high reliability.

Based on a comprehensive consideration of the capability of the simulation codes, the degrees of influence of errors and the already known behavior of the design scheme, totally 5 kinds of non-ideal construction and operation situations have been chosen and studied for the EUROTRANS injector:

- BDIS: beam injection displacement with respect to the cavity axis.
- VERR: tank (gap) voltage amplitude errors from vibrations of RF source or inaccurate tuning.
- PERR: tank phase errors.
- QMIS: transverse translations of quadrupole and solenoidal lenses.
- QROT: rotations of quadrupole and solenoidal lenses.

For the RFQ part, the BDIS and VERR errors, which are schematically shown in Fig. 6.4-1, are examined as the representatives of the beam-related errors and the external errors, respectively; while for the DTL part, all above-mentioned errors except the BDIS error (because a non-ideal RFQ will naturally cause a beam injection displacement at the beginning of the DTL) are included.
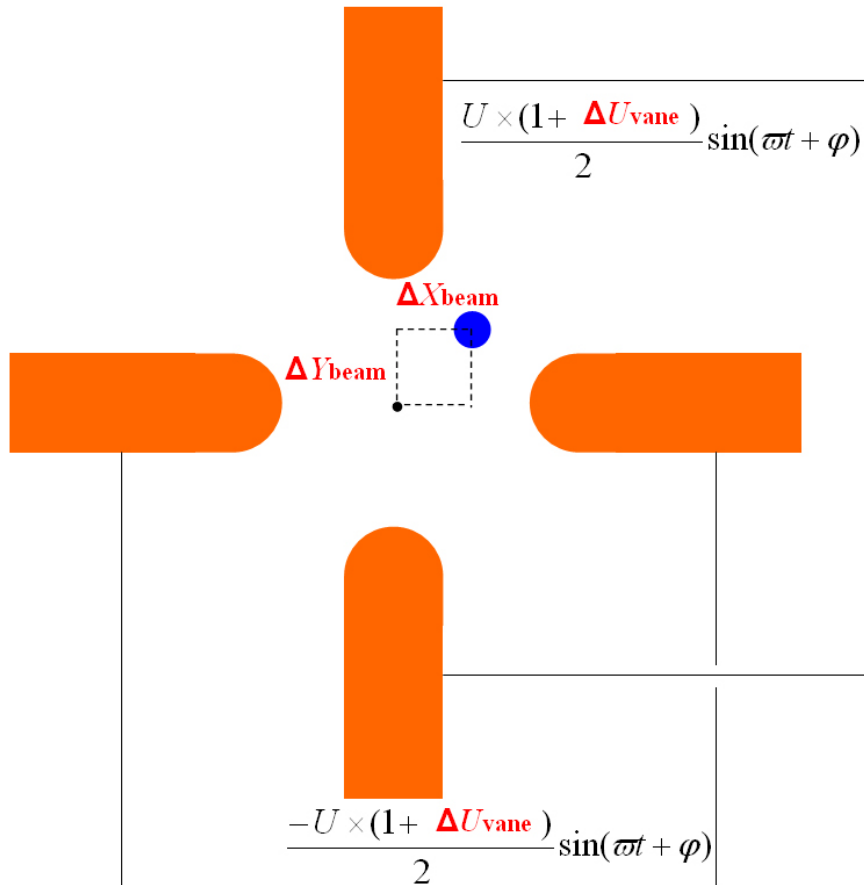
Fig. 6.4-1: The two kinds of errors used for the RFQ part.

By mixing the error types mentioned above, various quasi-realistic situations can be modeled. In order to avoid making the combinations of the errors excessively complicated, fixed and relatively large error values (ΔX_{beam}=ΔY_{beam}=0.2mm and ΔU_{vane} =±5.0%) are used for the RFQ. Using the output particle distributions from the two non-ideal RFQs as the input ones, the DTL part has been tested with two groups of errors randomly generated by the LORASR code within the same given limits which were used for the IFMIF DTL (see Chap. V). In addition, for a better understanding of the influence from the inter-vane voltage error of the RFQ, two extra cases with ΔU_{vane}=0 have been also checked and compared.

Therefore, for each intensity case, totally six batches of runs have been performed using the error settings as summed up in Table 6.4-1, where the differences between the settings are:

- The first two, the second two and the last two have an inter-vane voltage of the RFQ lower than, higher than and equal to the nominal value, respectively.
- The odd batches have the QMIS and QROT errors in the typical ranges, which are twice smaller than those for the even ones.

Every batch simulation consists of totally 101 runs, in which one is the so-called background run (this run has errors in the RFQ but no errors in the DTL). As in the error studies per-

formed for the IFMIF DTL, no orbit correction has been implemented, though in the design the space for steerer was already reserved.

Table 6.4-1: Error settings for the injector.

Batch / Error type			1	2	3	4	5	6	Note
RFQ	BDIS [mm]	ΔX_{beam} ΔY_{beam}	0.2	0.2	0.2	0.2	0.2	0.2	fixed
	VERR [%]	ΔU_{vane}	-5.0	-5.0	5.0	5.0	0.0	0.0	fixed
DTL	QMIS [mm]	ΔX_{lens} ΔY_{lens}	±0.1	±0.2	±0.1	±0.2	±0.1	±0.2	random
	QROT [mrad]	$\Delta\varphi_{x,y}$ $\Delta\varphi_{z}$	±1.5 ±2.5	±3.0 ±5.0	±1.5 ±2.5	±3.0 ±5.0	±1.5 ±2.5	±3.0 ±5.0	random
	VERR [%]	ΔU_{gap} ΔU_{tank}	±5.0 ±1.0	±5.0 ±1.0	±5.0 ±1.0	±5.0 ±1.0	±5.0 ±1.0	±5.0 ±1.0	random
	PERR [°]	$\Delta\Phi_{tank}$	±1.0	±1.0	±1.0	±1.0	±1.0	±1.0	random

Table 6.4-2: Error study results for 5mA (before the parenthesis) and 30mA (in the parenthesis).

Batch / Parameter	1	2	3	4	5	6
T_{RFQ} [%] with errors	99.7 (94.9)		100 (99.9)		99.9 (99.7)	
$T_{injector}$ [%] with RFQ & no DTL errors	99.7 (94.6)		100 (99.9)		99.9 (99.7)	
$T_{injector, min}$ [%] with RFQ & DTL errors	99.7 (94.6)	99.5 (93.8)	~100 (99.9)	~100 (98.8)	99.9 (99.7)	99.8 (99.0)

Table 6.4-2 lists the main simulation results of the error studies, from which the following remarks can be made:

- Even in cases of much larger errors than the typical values, the lowest transmission of the all non-ideal RFQ accelerators is still ~95%.

- The VERR errors of the RFQ have relatively larger influences than the BDIS errors, but obvious negative effects only appear when the available voltage is lower than the design voltage.

- Except the background run for Batch1 and Batch2 at 30mA has a decrease of ~0.28% in beam transmission efficiency throughout the DTL part, almost no DTL losses happen in the other background runs (especially the transmission efficiency of the background run for Batch3 and Batch4 in case of 5mA is even better than that of the reference run, because there is totally no particle loss throughout the injector).

- For all runs, the maximum beam losses in the DTL part are ~1%.
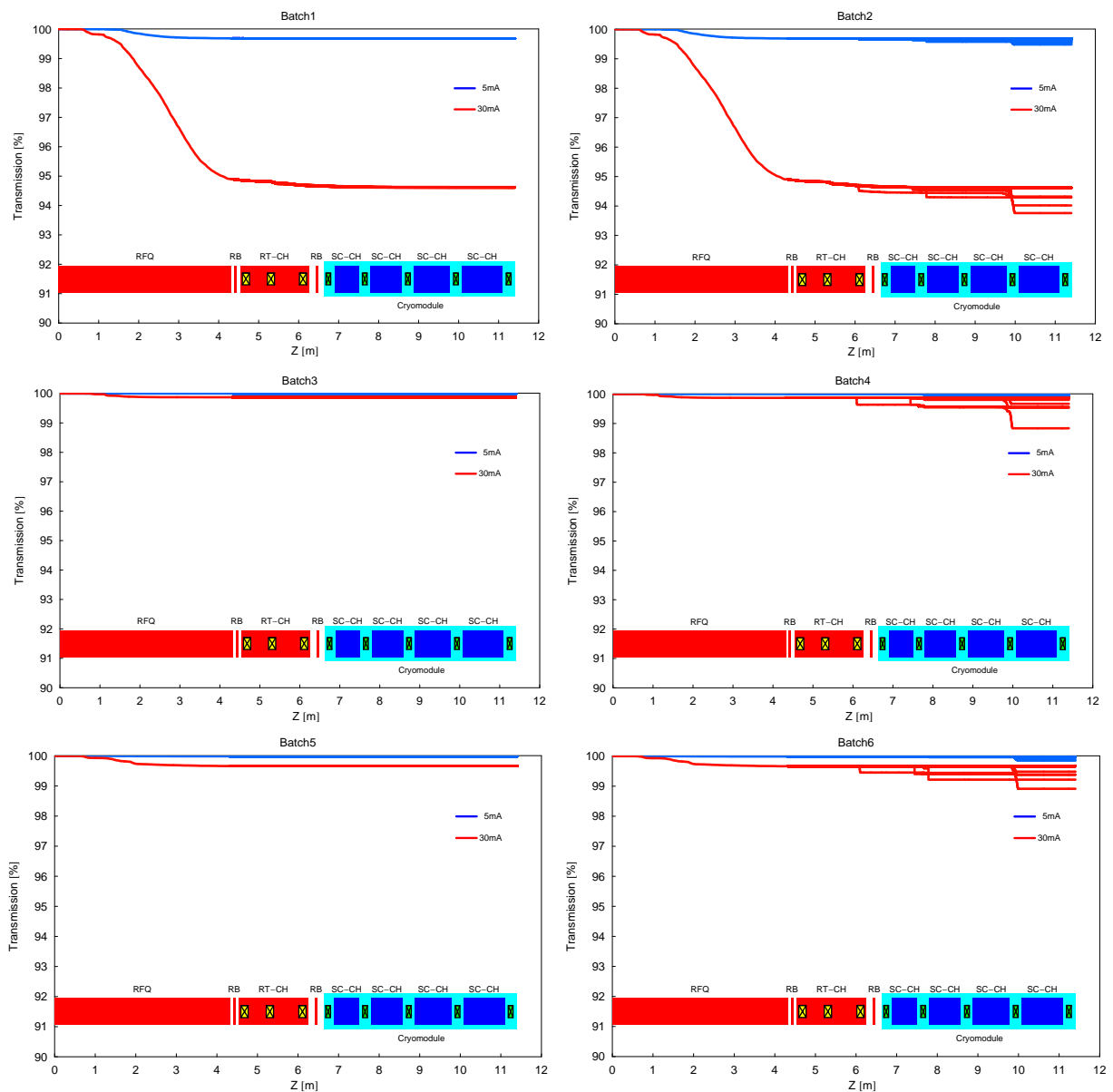
Fig. 6.4-2: Beam transmission evolutions of 101 non-ideal injectors.

The variations of the start-to-end beam transmission efficiencies along the whole injector for all runs of every batch simulation are plotted in Fig. 6.4-2, where the layout of the injector is shown together for a better observation on the corresponding beam-loss positions.

After the deduction of the related background run from each batch of calculations, the situations of the maximum additional beam losses in the DTL part are as below, respectively:

- Batch1: 0.001% (5mA) and 0.011% (30mA).

- Batch2: 0.202% (5mA) and 0.861% (30mA; the ratio of the "bad" runs, which have obvious differences in transmission efficiency than the most runs, is 5%).

- Batch3: 0.004% (5mA) and 0.010% (30mA).

- Batch4: 0.116% (5mA) and 1.035% (30mA; the ratio of the "bad" runs, which have obvious differences in transmission efficiency than the most runs, is 4%).

- Batch5: 0.000% (5mA) and 0.000% (30mA).

- Batch6: 0.137% (5mA) and 0.754% (30mA).

In the pictures of Fig. 6.4-2, these beam losses, which are all less than 1%, can be mainly observed in the following three places: 1) The first one is at the end of the last triplet. 2) The second one is between the SC-CH-1 cavity and the SC-CH-2 cavity. 3) The last one is between the SC-CH-3 cavity and the SC-CH-4 cavity.

Obviously, most of lost particles have not happened in the superconducting cavities, so they are not critical to the SC state and the operation of the injector will be reliable.

Embodying the summation of all worst cases, the common maximum transverse beam sizes along the beam axis of the injector for all runs of each batch simulation are plotted in Fig. 6.4-3, where:

- The pictures on the left side are for the small errors, and the right pictures are for the large errors.

- The top, middle and bottom pictures are for ΔU_{vane}= -5%, 5% and 0%, respectively.

- The red curves are the reference transverse beam envelopes without any errors.

- The blue and green curves are representing the collective effects of each batch runs in the presence of errors for 100% and 95% of transported particles, respectively.

- The black curves stand for the bore apertures (to plot continuous curves, the apertures of the neighboring tubes are simply adopted for the drift spaces between the tubes).

- The curves in the positive range are for the 5mA beam, while the curves with negative values are for the 30mA beam.
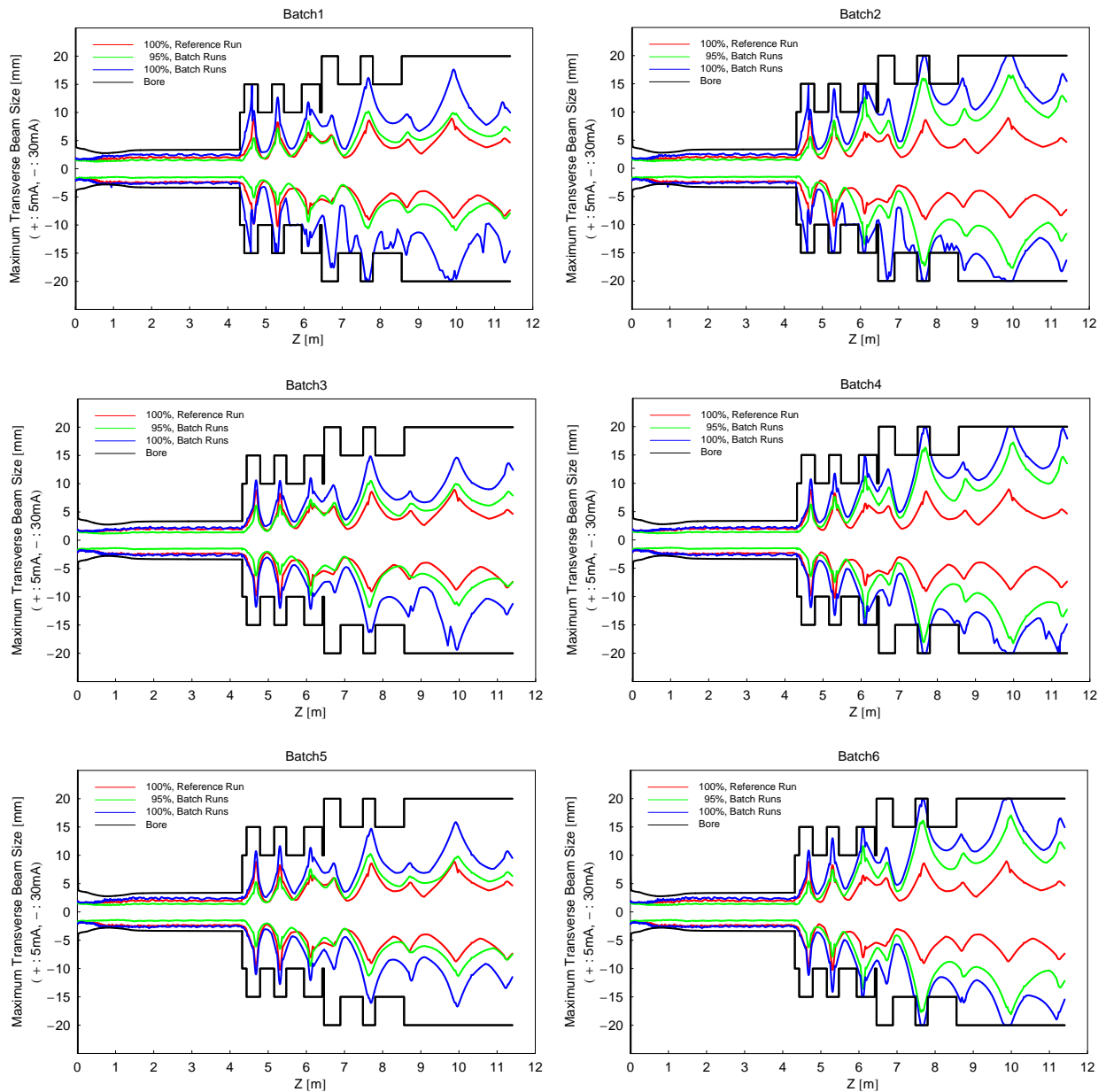
Fig. 6.4-3: Common maximum transverse beam sizes of 101 non-ideal injectors.

Obviously, the larger the errors are (or the higher the beam intensity is), the worse the situations are. In all cases with errors, the common maximum beam sizes for 95% of transported particles still have adequate distances to the hard boundaries at most positions along the accelerating channel.

In the pictures, the situations are best at the nominal RFQ voltage but worst at a lower one. The top pictures show that a decreased ΔU_{vane} will produce more unstable particles in the RFQ (some can be filtered out by the RT-CH, but some not). Therefore, except Batch5 and Batch6

used for comparison only, Batch3 and Batch4 are of practical significance, especially Batch3, which has totally no transverse losses in the presence of errors, is the safest case.
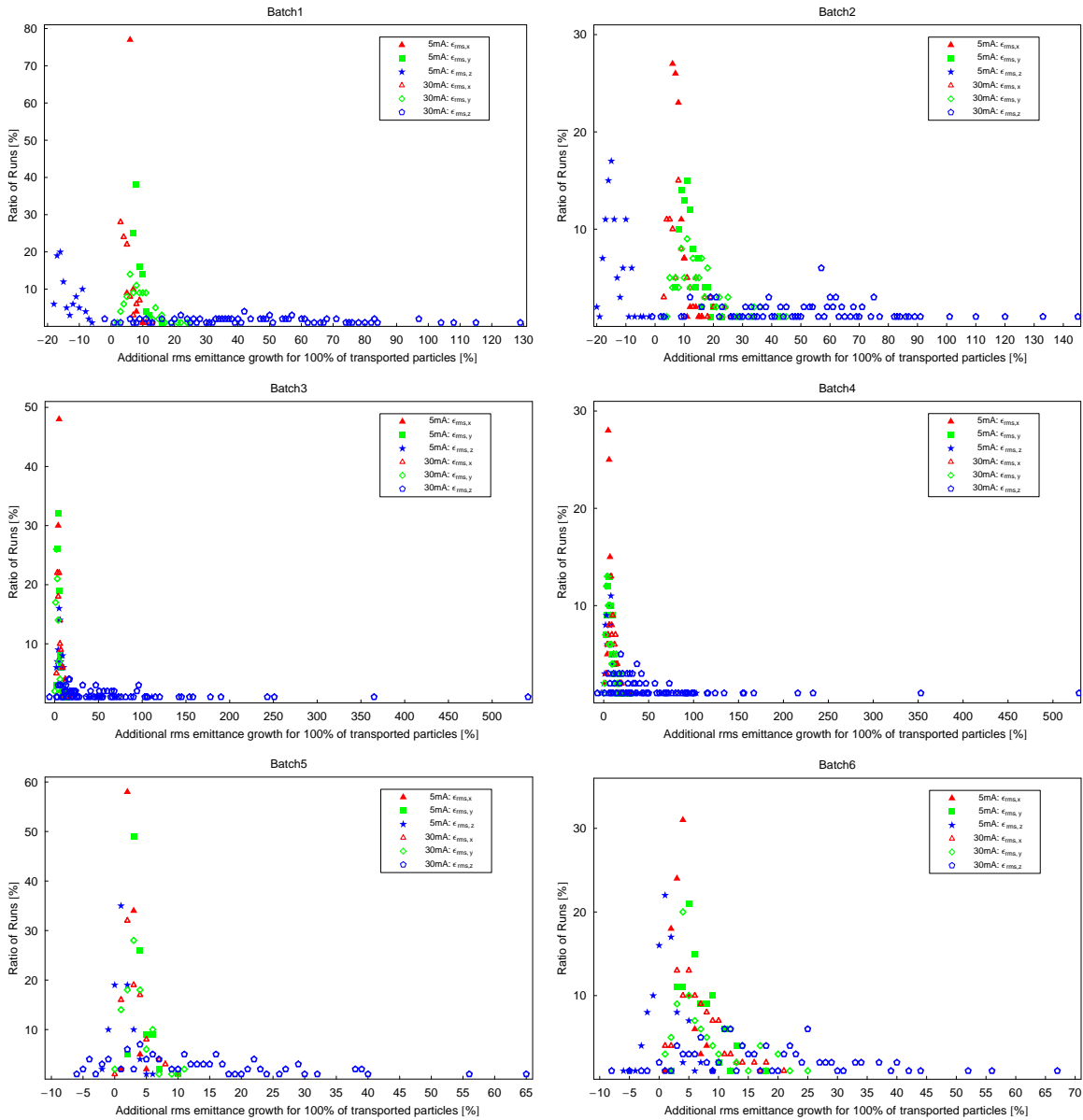
Fig. 6.4-4: Additional emittance growths for all transported particles of 101 non-ideal injectors.

Finally, based on the same definition made for the IFMIF case, the additional rms emittance growths $\Delta\varepsilon_{addi.}$ for each batch simulation are compared in Fig. 6.4-4, where the red, green and blue symbols are representing the results for the transverse and longitudinal planes, respectively. It's clear that most runs have the additional emittance growths in the range 0–20%; and the plots are similar for a same RFQ inter-electrode voltage, only the probabilities are decreased in case of larger errors (see the scalings of the y-axes):

- ΔU_{vane}=-5%: the range of $\Delta\varepsilon_{addi.}$ is -20–150% (the negative values are due to beam losses).

- ΔU_{vane}=5%: the $\Delta\varepsilon_{\text{addi.}}$ range is similar to the above case; just for rare runs, $\Delta\varepsilon_{\text{addi.}}$>200% in the longitudinal direction at 30mA.

- ΔU_{vane}=0%: all $\Delta\varepsilon_{\text{addi}}$<70%.

To remove the "noises" from a few not-well-accelerated particles at the output, the so-called "99%" additional rms emittance growths, $\Delta\varepsilon_{\text{addi.}}^{99\%}$, have been checked (see Fig. 6.4-5). It's difficult to know which input particle will turn bad finally, so the following definition is used:

$$\Delta\varepsilon_{\text{addi.}}^{99\%} \equiv \frac{\varepsilon_{\text{DTL out}}^{\text{error},99\%} - \varepsilon_{\text{DTL out}}^{\text{nominal},100\%}}{\varepsilon_{\text{DTL in}}^{\text{nominal},100\%}} \tag{6.4-1}$$

With all $\Delta\varepsilon_{\text{addi.}}^{99\%}$≤80%, the new additional-emittance-growth plots are similar, which indicates that the injector design is insensitive to various errors in a sense.
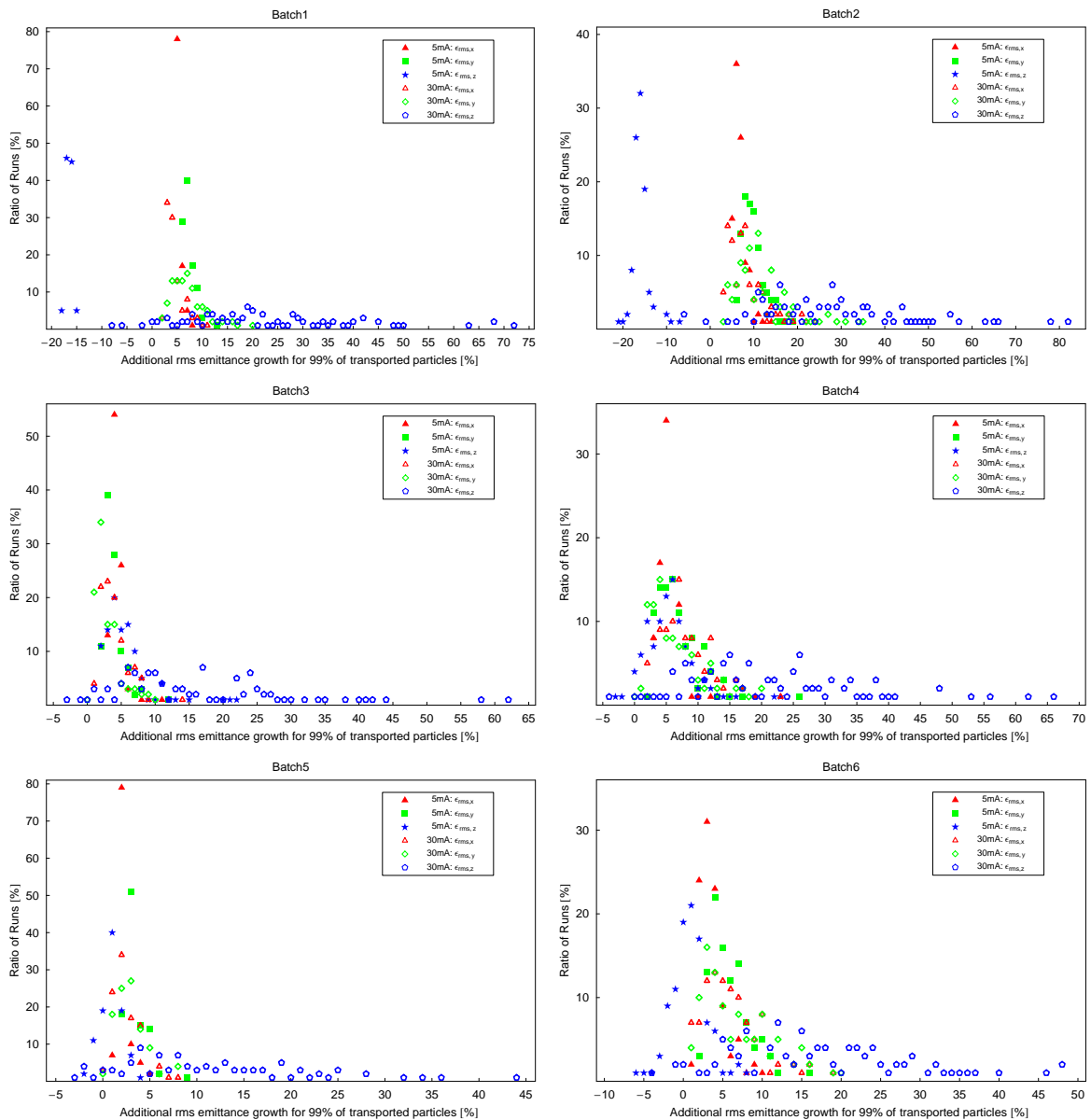
Fig. 6.4-5: The "99%" additional emittance growths of 101 non-ideal injectors.

6.5 Conclusions

Based on the conservative and compromising conditions, an efficient, robust and flexible injector design has been realized for the EUROTRANS driver linac as a result of a series of optimization methods, such as the "BABBLE" RFQ design strategy, the transverse matching technique between the RFQ and the DTL and the application of short adjustable rebunching cavities working at $\varphi_s = -90°$.

The results of the systematic start-to-end conceptual studies prove that the EUROTRANS injector design has fulfilled the design goals with respect to:

- High reliability:
    - ~100% of high beam transmission efficiency.
    - Concentrated particle distributions and low emittance growths throughout the injector.
    - Sufficient safety margins.
    - Robustness to various errors in wide ranges.
    - The drift spaces have been reserved for housing steerer which could further relax the tolerance limits to the errors by means of orbit corrections.
    - The duplication of the injector will also enforce the reliability.
- Current-adaptability: at both 5mA and 30mA, the designed injector always behaves well in either the design studies or the error studies, so the upgrade from the XT-ADS phase to the EFIT phase will be easy.
- Economical efficiency: a ~11.4m-long compact structure together with the SC operation can save the project costs significantly.

From the point of view of reliability, one suggestion to the future real operation could be that it is important to keep the inter-vane voltage of the RFQ same as or slightly higher than the nominal value.

7. Summary

Energy and environment are two major concerns in the 21st century. At present, the energy required for the daily life still mainly relies on the traditional fossil fuel resources, but the caused air pollution problem and greenhouse effect have seriously threatened the sustainable development of mankind. Another adopted energy source which can provide a large fraction of electricity for the world is the nuclear fission reaction. However, the increasing high-radioactive spent nuclear fuels, which half-lives are usually >1 million years, are becoming the hidden perils to the earth.

A great advance in accelerator physics and technology opens an opportunity to solve this dilemma between man and nature, because powerful accelerator-based neutron sources can play important roles for clean nuclear power production, for example:

- The Accelerator-Driven System (ADS) can serve as an easy control of a sub-critical fission reactor so that the nuclear fuels will be burnt more completely and safely.

- The EUROTRANS project launched by EU is investigating another application of the ADS technology to reduce the radiotoxicity and the volume of the existing nuclear waste greatly and quickly in a transmutation way.

- The developing international IFMIF plant will be used to test and qualify reactor materials for future fusion power stations, which can produce much cleaner nuclear electricity more efficiently than the fission ones.

Therefore, the R&D of high-power driver linacs (HPDL) is of a worldwide importance. As the proverb said, "everything is hard at the beginning", the front end is the most difficult part for realizing an HPDL machine. Based on the RFQ and H-type DTL structures, this dissertation is dedicated to study the beam dynamics in the presence of significantly strong space-charge effects while accelerating intense hardon beams in the low- and medium-β region. Besides the 5mA/30mA, 17MeV proton injector (RFQ+DTL) and the 125mA, 40MeV deuteron DTL of the above-mentioned EUROTRANS and IFMIF facilities, a 200mA, 700keV proton RFQ has been also intensively studied for a small-scale but ultra-intense neutron source FRANZ planned at Frankfurt University.

The most remarkable properties of the FRANZ RFQ and the IFMIF DTL are the design beam intensities, 200mA and 125mA, which are the record values for the proton and deuteron linacs, respectively. Though the design intensities for the two development stages, XT-ADS (5mA) and EFIT (30mA), of the EUROTRANS injector are well within the capability of the

modern RF linac technology, the special design concept for an easy upgrade from XT-ADS to EFIT brings unusual challenges to realize a linac layout which allows flexible operation with different beam intensities.

To design the 200mA FRANZ RFQ and the two-intensity EUROTRANS RFQ, the classic LANL (Los Alamos National Laboratory) Four-Section Procedure, which was developed by neglecting the space-charge forces, is not sufficient anymore. Abandoning the unreasonable constant-B (constant-transverse-focusing-strength) law and the resulting inefficient evolution manners of dynamics parameters adopted by the LANL method, a new design approach so-called "BABBLE", which can provide a "Balanced and Accelerated Beam Bunching at Low Energy", has been developed for intense beams.

Being consistent with the beam-development process including space-charge effects, the main features of the "BABBLE" strategy (see Pages 55–58) are: 1) At the entrance, the synchronous phase is kept at $\varphi_s = -90°$ while a gradual increase in the electrode modulation is started so that the input beam can firstly get a symmetrical and soft bunching within a full-360° phase acceptance. 2) In the following main bunching section, B is increasing to balance the stronger and stronger transverse defocusing effects induced by the decreasing bunch size so that the bunching speed can be fast and safely increased. 3) When the real acceleration starts, the quickly increased beam velocity will naturally weaken the transverse defocusing effects, so B is accordingly falling down to avoid longitudinal emittance growths and to allow larger bore apertures.

Taking advantage of the gentle initial bunching and the accelerated main bunching under balanced forces enabled by the "BABBLE" strategy, a 2m-long RFQ with beam transmission in excess of 98% and low emittance growths has been designed for FRANZ, and a 4.3m-long RFQ with almost no beam losses and flat emittance evolutions at both 5mA and 30mA has been designed for EUROTRANS. All design results have proven that the "BABBLE" strategy is a general design approach leading to an efficient and robust RFQ with good beam quality in a wide intensity-range from 0mA to 200mA (even higher).

To design the IFMIF DTL and the injector DTL part of the EUROTRANS driver linac, which have been foreseen as the first real applications of the novel superconducting CH-DTL structure, intensive attempts have been made to fulfill the design goals under the new conditions, e.g. long drift spaces, SC transverse focusing elements and high accelerating gradients. For the IFMIF DTL, the preliminary IAP design has been considerably improved with respect to the linac layout as well as the beam dynamics. By reserving sufficient drift spaces for the cryosystem, diagnostic devices, tuner and steerer, introducing SC solenoid lenses and adjusting the

accelerating gradients and accordingly other configurations of the cavities (see Pages 78–80), a more realistic, reliable and efficient linac system has been designed. On the other hand, the specifications and positions of the transverse focusing elements (see Pages 81–82) as well as the phase- and energy-differences between the bunch-center particle and the synchronous particle at the beginning of the φ_s=0° sections have been totally redesigned (see Pages 83–84) resulting in good beam performances in both radial and longitudinal planes. For the EUROTRANS injector DTL, in addition to the above-mentioned procedures, extra optimization concepts to coordinate the beam dynamics between two intensities, such as employing short adjustable rebunching cavities with $\varphi_s = -90°$ (see Page 116), have been applied.

In the beam transport simulations for both DTL designs, no beam losses were observed and all emittance growths were well under control. The performed design studies have been also useful for the realization of other high-reliable and upgradeable superconducting H-type DTL accelerators with intense beams of up to 125mA.

To solve the well-known transition problems between two kinds of different accelerating structures, some matching techniques have been developed and applied for the RFQ accelerator and the KONUS-based H-type DTL with the following idea: to perform the RFQ-DTL matching inside the RFQ, and not in the MEBT, because the continuous, velocity-independent electric focusing is very efficient for a low-β beam.

For the FRANZ project, the output longitudinal particle distribution has been rotated by the so-called Longitudinal-Rotation Technique (see Pages 62–63), which can narrow the phase spread of the beam to fit into the acceptance of a KONUS structure. For the EUROTRANS injector, the matching has been done in the transverse planes (see Pages 107–110): two additional transition cells at the end of the RFQ were introduced to turn both output transverse emittance ellipses axial-symmetric and into the same orientation, which helped leading to similar transverse beam developments in the DTL part. The design practices of the two accelerators showed that both longitudinal and transverse RFQ-DTL matching techniques had efficiently contributed to the beam dynamics resulting in a good beam quality.

In addition, the error study is another important topic of this dissertation. In the design study, usually only ideal operation conditions and perfect accelerator components have been taken into account. However, various mechanical, beam-related and field-related errors are inevitable during construction and operation. Therefore, error studies are essential especially for these three high-intensity machines in order to reduce risks of cavity activation and to ensure high reliability.

According to the capabilities of the simulation codes, seven kinds of RFQ errors and four kinds of DTL errors have been applied to the designed FRANZ RFQ and IFMIF DTL machines, respectively. For the EUROTRANS injector, combined RFQ and DTL errors were used. For a better check of the error effects, new tools have been developed to create some analysis functions and indexes which are so far still not available from the used simulation codes, e.g. the common maximum transverse beam size for 99% (instead of 100% only) of the beam along the accelerating channel (see Pages 128–129), the additional emittance growths for 99% of the beam (see Page 131), and so on. By these the few "bad" particles outside the beam core can be eliminated and the further analyses are very helpful to present the design behavior against errors more clearly. Including errors, all linac designs have shown large tolerances and sufficient safety margins.

Due to the good performances in the systematic design- and error-studies exhibited in this thesis, the FRANZ RFQ design will be taken as the base for the final design, the IFMIF DTL design has shown as the most competitive one among the three candidate proposals, and the EUROTRANS injector design has been officially adopted as the reference design of the project.

A. References

ADS01   The European Technical Working Group on ADS
§2, §6   "A European Roadmap for Developing Accelerator Driven Systems (ADS) for Nuclear Waste Incineration"
         ENEA, ISBN 88-8286-008-6 (April 2001)

BIA05   J-L. Biarrotte
§2   "General specifications for all the tasks of DM1/WP1.3"
         IP-EUROTRANS / Deliverable 1.18 (September 27, 2005)

BIA07   J-L. Biarrotte
§2   "Accelerator Design for ADS"
         Proceedings of the 18th Meeting of the International Collaboration on Advanced Neutron Sources in Dongguan, Guangdong, China, pp. 336-343 (April 25-29, 2007)

BIS84   C. Biscari, M. Weiss
§4   "Choice of Parameters for the CERN High Intensity RFQ (RFQ2 Project)"
         Proceedings of the 1984 Linear Accelerator Conference in Seeheim, Germany, pp. 106-108 (May 7-11, 1984)

BLE56   J.P. Blewett
§3   "Linear Accelerator Injector for Proton Synchrotrons"
         CERN Symposium 1956, pp. 162 (1956)

BRO98   J. Broere, H. Kugler, M. Vretenar, U. Ratzinger, B. Krietenstein
§3   "High Power Conditioning of the 202 MHz IH Tank 2 at the CERN Linac3"
         Proceedings of the XIX International Linear Accelerator Conference in Chicago, Illinois, USA, pp. 771-773 (August 23 - 28, 1998)

CAR93   F. Carminati, R. Klapisch, J.P. Revol, Ch. Roche, J.A. Rubio, C. Rubbia
§2   "An Energy Amplifier for Cleaner and Inexhaustible Nuclear Energy Production Driven by a Particle Beam Accelerator"
         European Organisation for Nuclear Research Report No. CERN/AT/93-47 (ET) (November 1, 1993)

CEA08   CEA-Saclay & CIEMAT

§5   "The Superconducting HWR Option for the IFMIF DTL - Revised Version"
           (February 12, 2008)

CHO99   W. Chou

§1   "Proton Driver" (in "Beam Halo and Scraping")
           Proceedings of the 7th ICFA Mini-Workshop on High Intensity High Brightness
           Hadron Beams in Interlaken Resort on Lake Como, Wisconsin, USA, pp. 7-12
           (September 13-15, 1999)

CRA79   K.R. Crandall, R.H. Stokes, T.P. Wangler

§4   "RF Quadrupole Beam Dynamics Design Studies"
           Proceedings of the 1979 Linac Accelerator Conference in Montauk, USA, pp. 205-
           216 (1979)

CRA94   K.R. Crandall

§6   "Ending RFQ Vane Tips with Quadrupole Symmetry"
           Proceedings of the 1994 International Linac Conference in Tsukuba, Japan, pp.
           227-229 (1994)

DEL93   J.R. Delayen, C.L. Bohn, B.J. Micklich, C.T. Roche, L. Sagalovsky

§2   "Design Considerations for High-Current Superconducting Ion Linacs"
           Proceedings of the 1993 Particle Accelerator Conference in Washington, D.C.,
           USA, pp. 1715-1717 (May 17-20, 1993)

ENG96   O. Engels, A. Schempp, H. Homeyer, W. Pelzer

§3   "RF Properties of the VE-RFQ Injector for the ISL Cyclotron"
           Proceedings of the 1996 European Particle Accelerator Conference in Sitges, Bar-
           celona, Spain, pp. 771-773 (June 10-14, 1996)

FLÜ59   S. Flügge (Editor)

§2   "Neutrons and Related Gamma Ray Problems" ("Encyclopedia of Physics")
           Springer-Verlag Berlin·Göttingen·Heidelberg, Volume XXXVIII/2 (1959)

GLU70   R.L. Gluckstern

§3   "Linear Accelerators"

North Holland Publishing Co., Amsterdam, Chapter 1.3d, pp. 827-836 (1970)

GOL75
§3

N.I. Golosai, G.N. Dernovoi, S.A. Il'evskii, V.V. Klokov, N.N. Kutorga, I.G. Mal'tsev, A.P. Mal'tsev, V.S. Sevost'yanov, V.B. Stepanov, V.A. Teplyakov, I.M. Shalashov

"Tests on the Initial Section of an Accelerator with Quadrupole HF Focusing" (in Russian)

Atomnaya Énergiya, Vol. 39, No. 2, pp. 123-126 (1975)

HAM80
§3

R.W. Hamm, K.R. Crandall, C.W. Fuller, L.D. Hansborough, R.A. Jameson, E.A. Knapp, M.D. Machalek, J.M. Potter, G.W. Rodenz, R.H. Stokes, J.E. Stovall, D.A. Swenson, T.P. Wangler, S.W. Williams

"The RF Quadrupole Linac: a New Low-Energy Accelerator"

Proceedings of International Conference on Low Energy Ion Beams 2 in Bath, United Kingdom, pp. 54-59 (1980)

HIL98
§4

C.E. Hill, A.M. Lombardi, E. Tanke, M. Vretenar

"Present Performance of the CERN Proton Linac"

Proceedings of the 1998 Linac Conference in Chicago, Illinois, USA, pp. 427-429

IFM96
§2

IFMIF CDA Team (Editor: M. Martone)

IFMIF International Fusion Materials Irradiation Facility Conceptual Design Activity Final Report, ENEA RT/ERG/FUS/96/11 (December 1996)

IFM04
§2, §5

IFMIF International Team

"An Activity of the International Energy Agency (IEA) Implementing Agreement for a Program of Research and Development on Fusion Materials"

IFMIF Comprehensive Design Report (January 2004)

JAM84
§3

R.A. Jameson

"Introduction to RFQ Session"

Proceedings of the 1984 Linear Accelerator Conference in Seeheim, Germany, pp. 49-52 (May 7-11, 1984)

JAM97
§4

R.A. Jameson

"A Discussion of RFQ Linac Simulation"

LANL Report No. LA-CP-97-54, pp. 85 (September 1997)

JAM07   R.A. Jameson
§5   "RFQ Designs and Beam-Loss Distributions for IFMIF"
           Oak Ridge National Laboratory Report No. ORNL/TM-2007/001 (January 2007)

KAP70   I.M. Kapchinskij, V.A. Tepljakov
§3, §4   "The Ion Linear Accelerator with Space-Uniform Strong Focusing" (in Russian)
           Pribory i Tekhnika Eksperimenta, No. 2, pp. 19-22 (1970)

KLE83   H. Klein
§3   "Development of the Different RFQ Accelerating Structures and Operation Experience"
           Proceedings of the 1983 Particle Accelerator Conference in Santa Fe, New Mexico, USA, pp. 3313-3322 (1983)

LAP00   P. Lapostolle, M. Weiss
§3   "Formulae and Procedures Useful for the Design of Linear Accelerators"
           CERN Report No. CERN-PS-2000-001 (DR) (2000)

LOM05   A.M. Lombardi
§3   "The Radio Frequency Quadrupole (RFQ)"
           CAS - CERN Accelerator School and KVI: Specialised CAS Course on Small Accelerators in Zeegse, The Netherlands, pp. 201-207 (May 24-June 2, 2005)

MEU08   O. Meusel, A. Bechtold, L.P. Chau, M. Heilmann, H. Podlech, U. Ratzinger, K.
§2   Volk, C. Wiesner
           "Injector Development for High Intensity Proton Beams at Stern-Gerlach-Zentrum"
           Proceedings of the XXIV Linear Accelerator Conference in Victoria, BC, Canada, pp. 49-51 (September 29-October 3, 2008)

MOB51   R.C. Mobley
§2   "Proposed Method for Producing Short Intense Monoenergetic Ion Pulses"
           Phys. Rev. 88 (2), pp. 360-361 (1951)

MÜL81   R.W. Müller, H. Deitinghoff, K. Halfmann, P. Junior, H. Klein, K. Langbein, J.
§3   Müller, W. Neumann, A. Schempp

"Proton Model of a Heavy-Ion RFQ Linac"

Proceedings of the 1981 Particle Accelerator Conference in Washington, D.C., USA, pp. 2862-2864 (1981)

PAD08   H. Padamsee

"RF Superconductivity: Science, Technology, and Applications"

Wiley-VCH Verlag GmbH & Co. KGaA, Weinheim, ISBN: 978-3-527-40572-5 (2009)

PAR05   J.H. Billen (Editor)

§2, §3, §4   Manual of LANL RFQ Design Codes

§6   LANL Report No. LA-UR-96-1836 (Revised December 7, 2005)

PIC00   N. Pichoff, H. Safa

§2   "Reliability of Superconducting Cavities in a High Power Proton Linac"

Proceedings of the 7th European Particle Accelerator Conference, Vienna, Austria, pp. 2049-2051 (June 26-30, 2000)

POD07   H. Podlech, U. Ratzinger, H. Klein, C. Commenda, H. Liebermann, A. Sauer

§3   "Superconducting CH structure"

Physical Review Special Topics - Accelerators and Beams, 10, 080101, pp.1-19 (2007)

POD08a   H. Podlech

§2, §3, §6   "Entwicklung von normal- und supraleitenden CH-Strukturen zur effizienten Beschleunigung von Protonen und Ionen"

Habilitationsschrift, Fachbereich Physik der Johann Wolfgang Goethe-Universität Frankfurt am Main, Germany (2008)

POD08b   H. Podlech, M. Amberg, A. Bechtold, M. Busch, F.D. Dziuba, U. Ratzinger, C.

§3   Zhang

"Recent Developments on Superconducting CH-Structures and Future Perspectives"

Proceedings of the XXIV Linear Accelerator Conference in Victoria, BC, Canada, pp. 797-799 (September 29-October 3, 2008)

POD09   H. Podlech, S. Barbanotti, A. Bechtold, J.-L. Biarrotte, M. Busch, S. Bousson, F.

§6   Dziuba, T. Junquera, H. Klein, M. Luong, A.C. Mueller, G. Olry, N. Panzeri, P. Pierini, U. Ratzinger, R. Tiede, C. Zhang

      "The 600 MeV EUROTRANS Proton Driver Linac"

      Proceedings of the International Topical Meeting on Nuclear Research Applications and Utilization of Accelerators in Vienna, Austria (May 4-8, 2009)

RAT91   U. Ratzinger

§3   "The IH-Structure and Its Capability to Accelerate High Current Beams"

      Proceedings of the 1991 IEEE Particle Accelerator Conference in San Francisco, USA, pp. 567-571 (1991)

RAT98   U. Ratzinger

§3   "Effiziente HF-Linearbeschleuniger für leichte und schwere Ionen"

      Habilitationsschrift, Fachbereich Physik der Johann Wolfgang Goethe-Universität Frankfurt am Main, Germany (1998)

RAT00   U. Ratzinger

§3   "H-type Linac Structures"

      CERN Accelerator School: Radio Frequency Engineering, in Seeheim, Germany, pp. 351 (May 8-16, 2000)

RAT07a   U. Ratzinger, L.P. Chau, O. Meusel, A. Schempp, K. Volk, M. Heil, F. Käppeler, R. Stieglitz

§2   "Intense Pulsed Neutron Source FRANZ in the 1 – 500 keV Range"

      Proceedings of the 18th Meeting of the International Collaboration on Advanced Neutron Sources in Dongguan, Guangdong, China, pp. 210-217 (April 25-29, 2007)

RAT07b   U. Ratzinger, C. Zhang, R.Tiede, H. Klein, H. Podlech

§5   "Improved Layout of the CH–DTL for IFMIF"

      IAP Internal Note No. IAP-ACCC-051007 (October 5, 2007)

SAU07   A. Sauer, H. Klein, H. Podlech, U. Ratzinger, R. Tiede

§5   "Assessment of Beam Losses along the Accelerator Line for Dose Calculations"

      Final Report on the EFDA Task TW5-TTMI-001, Deliverable 3 (July 23, 2007)

SCH83   A. Schempp, P. Junior, H. Klein, M., Daehne, M. Ferch, K. Langbein, N. Zoubek

§3   "Status of the Frankfurt Zero-Mode Proton RFQ"

Proceedings of the 1983 Particle Accelerator Conference in Santa Fe, New Mexico, USA, pp. 3536-3538 (1983)

SCH96   A. Schempp

§3, §4   "Design of Compact RFQs"

Proceedings of the XVIII International Linac Conference in Geneva, Switzerland, pp. 53-55 (1996)

STO79   R.H. Stokes, K.R. Crandall, J.E. Stovall, D.A. Swenson

§3   "RF Quadrupole Beam Dynamics"

Proceedings of the 1979 Particle Accelerator Conference in San Francisco, USA, pp. 3469-3471 (1979)

TEP68   V.A. Teplyakov, V.B. Stepanov

§3   "Investigation of an H-Cavity"

Radio Engineering and Electronic Physics, Vol. 13, No. 11, pp. 1724-1733 (1968)

TIE06   R. Tiede, G. Clemente, H. Podlech, U. Ratzinger, A. Sauer, S. Minaev

§5   "LORASR Code Development"

Proceedings of the 10th European Particle Accelerator Conference in Edinburgh, Scotland, United Kingdom, pp. 2194-2196 (June 26-30, 2006)

TIE07a   R. Tiede

§5   "Description of the New Machine Error Setting and Analysis Tools Available for the LORASR Beam Dynamics Code"

IAP Internal Note No. IAP-DYNA-070807 (2007)

TIE07b   R. Tiede

§5   "Description of the Lens Rotation Error Settings Implemented to the LORASR Beam Dynamics Code"

IAP Internal Note No. IAP-DYNA-211107 (2007)

TIE08   R. Tiede, U. Ratzinger, H. Podlech, C. Zhang, G. Clemente

§3, §6   "KONUS Beam Dynamics Using H-Mode Cavities"

Proceedings of the 42nd ICFA Advanced Beam Dynamics Workshop on High-Intensity, High-Brightness Hadron Beams in Nashville, Tennessee, USA (August 2008)

VLA70   V.V. Vladimirskiy, I.M. Kapchinskiy, V.A. Teplyakov

§3   USSR Patent No. 265312, Bulletin of Inventions, No. 10, pp. 75 (1970)

WAN80   T.P. Wangler

§3   "Space-Charge Limits in Linear Accelerators"

         Los Alamos Scientific Laboratory Report No. LA-8388 (1980)

WAN08   T.P. Wangler

§3, §4   "RF Linear Accelerators"

         Wiley-VCH Verlag GmbH & Co. KGaA, Weinheim, ISBN: 978-3-527-40680-7

         (2008)

YOU94   L.M. Young

§3   "An 8-Meter-Long Coupled Cavity RFQ Linac"

         Proceedings of the 1994 International Linear Accelerator Conference in Tsukuba,

         Japan, pp. 178 (August 21-26, 1994)

YOU97   L.M. Young

§6   "Simulations of the LEDA RFQ 6.7MeV Accelerator"

         Proceedings of the 1997 Particle Accelerator Conference in Vancouver, B.C., Can-

         ada, pp. 2752-2754 (May 12-16, 1997)

ZHA08   Chuan Zhang, Alwin Schempp

§4   "Beam Dynamics Studies on a 200mA Proton Radio Frequency Quadrupole Ac-

         celerator"

         Nuclear Instruments and Methods in Physics Research, A, Volume 586, Issue 2, pp.

         153-159 (2008)

B. Glossary of Acronyms and Abbreviations

ACC   Accelerator (*used for LANL Four-Section Procedure*)

ADS   Accelerator-Driven System

AG   Alternating-Gradient (Focusing)

APF   Alternating Phase Focusing

BABBLE   Balanced and Accelerated Beam Bunching at Low Energy

BCS   Bardeen-Cooper-Schrieffer

BDIS   Beam injection displacement (*used for error studies*)

CDR   Comprehensive Design Report

CEA   Commissariat à l'Energie Atomique (*Atomic Energy Commission*)

CERN   Européen pour la Recherche Nucléaire

                       (*European Organization for Nuclear Research*)

CH (-DTL)   Crossbar H-type (Drift-Tube Linac)

CW   Continuous Wave

DTL   Drift-Tube Linac

dpa   displacement per atom

ECR   Electron Cyclotron Resonance Source

EFIT   European Facility for Industrial Transmutation

EP   Equipartitioning Procedure

EU   European Union

EUROTRANS   EUROpean Research Programme for the TRANSmutation of High Level

                       Nuclear Waste in an Accelerator Driven System

FSP   Four-Section Procedure

FRANZ   Frankfurt Neutron Source at the Stern-Gerlach-Zentrum

FZ(K)   Forschungszentrum (Karlsruhe)

GB   Gentle Buncher (*used for LANL Four-Section Procedure*)

GSI   Gesellschaft für Schwerionenforschung (*Institute for Heavy Ion Research*)

HEBT   High Energy Beam Transport

HLI   Hochladungsinjektor (*High Charge State Injector*)

HPDL   High-Power Driver Linac

HWR   Half-Wave Resonator

IAP   Institut für Angewandte Physik (*Institute for Applied Physics*)

IFMIF   International Fusion Materials Irradiation Facility

IH (-DTL)	Interdigital H-type (Drift-Tube Linac)
K-T	Kapchinskiy-Teplyakov
KONUS	Kombinierte Null Grad Struktur (*Combined 0° Structure*)
LANL	Los Alamos National Laboratory
LEBT	Low Energy Beam Transport
LEDA	Low-Energy Demonstration Accelerator
Linac	Linear Accelerator
LORASR	Longitudinale und radiale Strahldynamikrechnungen mit Raumladung (*Longitudinal and Radial Beam Dynamics Calculations Including Space Charge*)
MEBT	Medium Energy Beam Transport
NC	Normal Conducting
PARMTEQM	Phase And Radial Motion in Transverse Electric Quadrupoles with Multipoles
PERR	Tank phase errors (*used for error studies*)
QMIS	Transverse translations of magnetic lenses (*used for error studies*)
QROT	Rotations of magnetic lenses (*used for error studies*)
QWR	Quarter-Wave Resonator
RB	Rebuncher
RF	Radio Frequency
RFQ	Radio Frequency Quadrupole
RIB	Radioactive Ion Beam
RM	Radial Matcher (*used for LANL Four-Section Procedure*)
rms	Root Mean Square
RT	Room-Temperature
SC	Superconducting
SCR	Split-Coaxial Resonator
SH	Shaper (*used for LANL Four-Section Procedure*)
SNS	Spallation Neutron Source
TE	Transverse Electric (Modes) (*also called as H-Modes*)
TEM	Transverse Electromagnetic (Modes)
TM	Transverse Magnetic (Modes)
VERR	Gap and tank voltage amplitude errors (*used for error studies*)
XT-ADS	eXperimental facility demonstrating the technical feasibility of Transmutation in an Accelerator Driven System

C. Lebenslauf, Akademische Lehrer und Veröffentlichungen

Name:	Zhang
Vorname:	Chuan
Geschlecht:	männlich
Geburtsdatum:	18.10.1974
Geburtsort:	Zhejiang, China
Familienstand:	verheiratet 1 Kind
Staatsangehörigkeit:	Chinesisch

1981 – 1985:	Besuch der Xiashi-Zentral-Grundschule, Haining, Zhejiang
1985 – 1986:	Besuch der Grundschule der Stadt Jiangshan, Jiangshan, Zhejiang
1986 – 1986:	Besuch der Nr.1 Grundschule von Xiashi, Haining, Zhejiang
1986 – 1990:	Besuch der Xiashi-Mittelschule, Haining, Zhejiang
1990 – 1993:	Besuch der Nr.1 Oberschule von Haining, Haining, Zhejiang, Abschluss: Gaozhong Biye
1993 – 1997:	Studium der Physik an der Zhejiang-Universität, Hangzhou, Zhejiang, Abschluss: Lixue Xueshi

| **1997 – 1999:** | Anstellung bei der Firma Zhejiang Medical Equipments & Instruments Company Hangzhou, Zhejiang, Vertriebsingenieur |

1997 – 1999: Anstellung bei der Firma Zhejiang Medical Equipments & Instruments Company
Hangzhou, Zhejiang, Vertriebsingenieur

1999 – 2004: Studium der Nukleare Techniken und Anwendungen an der Peking-Universität, Beijing, Abschluss: Gongxue Boshi

2005 – Jetzt: Anstellung am Institut für Angewandte Physik der Goethe-Universität in Frankfurt am Main wissenschaftlicher Mitarbeiter

Akademische Lehrer (Universität Frankfurt/Main):

R. Becker, I. Hofmann, J. Jacoby, R.A. Jameson, H. Klein, H. Podlech, U. Ratzinger, A. Schempp, J. Struckmeier.

Veröffentlichungen (2006 – 2009)

(2009)

Design of an Upgradeable 45-100mA RFQ Accelerator for FAIR
Chuan Zhang, Alwin Schempp
Nuclear Instruments and Methods in Physics Research, A, Volume 609, Issues 2-3, pp. 95-101

An Efficient 125mA, 40MeV Deuteron DTL for Fusion Material Tests
Chuan Zhang, Marco Busch, Horst Klein, Holger Podlech, Ulrich Ratzinger
Proceedings of the 23rd Particle Accelerator Conference in Vancouver, Canada (May 4-8, 2009)

The 600MeV EUROTRANS Proton Driver Linac
H. Podlech, S. Barbanotti, A. Bechtold, J.-L. Biarrotte, M. Busch, S. Bousson, F. Dziuba, T. Junquera, H. Klein, M. Luong, A.C. Mueller, G. Olry, N. Panzeri, P. Pierini, U. Ratzinger, R.

Tiede, <u>C. Zhang</u>

Proceedings of the International Topical Meeting on Nuclear Research Applications and Utilization of Accelerators in Vienna, Austria (May 4-8, 2009)

(2008)

Beam Dynamics Studies on a 200mA Proton Radio Frequency Quadrupole Accelerator

<u>Chuan Zhang</u>, Alwin Schempp

Nuclear Instruments and Methods in Physics Research, A, Volume 586, Issue 2, pp. 153-159

Recent Developments on Superconducting CH-Structures and Future Perspectives

Holger Podlech, Alexander Bechtold, Marco Busch, Florian Dziuba, Horst Klein, Holger Liebermann, Ulrich Ratzinger, Rudolf Tiede, <u>Chuan Zhang</u>, Gianluigi Clemente

Proceedings of the XXIV International Linear Accelerator Conference in Victoria, British Columbia, Canada, pp. 784-786 (September 29 - October 3, 2008)

A Coupled RFQ-Drift Tube Combination for FRANZ

Alexander Bechtold, Ulrich Bartz, Philipp Kolb, Holger Liebermann, Oliver Meusel, Holger Podlech, Ulrich Ratzinger, Alwin Schempp, <u>Chuan Zhang</u>, Gianluigi Clemente

Proceedings of the XXIV International Linear Accelerator Conference in Victoria, British Columbia, Canada, pp. 46-48 (September 29 - October 3, 2008)

RF-Tuning of the EBIS-RFQ

Markus Vossberg, Benjamin Hofmann, Alwin Schempp, <u>Chuan Zhang</u>, J.G. Alessi, D. Raparia, L. Snydstrup

Proceedings of the XXIV International Linear Accelerator Conference in Victoria, British Columbia, Canada, pp. 139-141 (September 29 - October 3, 2008)

KONUS Beam Dynamics Designs Using H-Mode Cavities

R. Tiede, U. Ratzinger, H. Podlech, <u>C. Zhang</u>, G. Clemente

Proceedings of the 42nd ICFA Advanced Beam Dynamics Workshop on High-Intensity, High-Brightness Hadron Beams, Nashville, Tennessee, USA, pp. 223-230 (August 25-29, 2008)

KONUS Dynamics and H-Mode DTL Structures for EUROTRANS and IFMIF

Chuan Zhang, Marco Busch, Horst Klein, Holger Podlech, Ulrich Ratzinger, Rudolf Tiede

Proceedings of the 11th European Particle Accelerator Conference in Genoa, Italy, pp. 3239-3241 (June 23-27, 2008)

A Superconducting CH-Linac for IFMIF

H. Podlech, A. Bechtold, M. Busch, H. Klein, U. Ratzinger, R. Tiede, C. Zhang

Proceedings of the 11th European Particle Accelerator Conference in Genoa, Italy, pp. 3548-3550 (June 23-27, 2008)

(2007)

Conceptual Studies of the EUROTRANS Front-End

Chuan Zhang, Marco Busch, Horst Klein, Holger Podlech, Ulrich Ratzinger

Proceedings of the 22nd Particle Accelerator Conference in Albuquerque, New Mexico, USA, pp. 3274-3276 (June 25-29, 2007)

RFQ and IH Accelerators for the New EBIS Injector at BNL

A. Schempp, U. Ratzinger, R. Tiede, C. Zhang, J. Alessi, D. Raparia, L. Snydstrup

Proceedings of the 22nd Particle Accelerator Conference in Albuquerque, New Mexico, USA, pp. 1439-1441 (June 25-29, 2007)

(2006)

Development of an Intense Neutron Source "FRANZ" in Frankfurt

O. Meusel, L. P. Chau, I. Mueller, U. Ratzinger, A. Schempp, K. Volk, C. Zhang, S. Minaev

Proceedings of the XXIII International Linear Accelerator Conference in Knoxville, Tennessee, USA, pp. 159-161 (August 21-25, 2006)

Development of a High Current Proton Linac for FRANZ

C. Zhang, A. Schempp

Proceedings of the 10th European Particle Accelerator Conference in Edinburgh, Scotland, United Kingdom, pp. 2799-2801 (June 26-30, 2006)

Danksagung

Mein herzlicher Dank gilt meinem Doktorvater Herrn Prof. Dr. Horst Klein. Er hat mir die ersten Impulse gegeben, am Institut für Angewandte Physik, Goethe-Universität über Beschleuniger zu studieren und zu forschen. Mit seiner sachkundigen Unterstützung habe ich an zwei attraktiven Projekten, EUROTRANS und IFMIF, gearbeitet. Ohne sein Vertrauen und seine langfristige Unterstützung wäre die Anfertigung dieser Doktorarbeit nicht möglich gewesen.

Ich danke ebenfalls Herrn Prof. Dr. Alwin Schempp, meinem zweiter Gutachter, der mir nicht nur bei meiner wissenschaftlichen Arbeit, sondern auch bei meinen privaten Angelegenheiten immer freundlich geholfen hat. Seine Hilfe ermöglichte mir, am FRANZ RFQ der Universität Frankfurt, am FAIR-Protonen-RFQ und HLI-RFQ der GSI und am EBIS-RFQ des BNL in USA zu mitarbeiten. Dadurch habe ich sehr nützliche Erfahrung über RFQs gesammelt.

Danken möchte ich auch Herrn Prof. Dr. Ulrich Ratzinger für seine wichtige Hinweise zur KONUS-Dynamik, Herrn PD Dr. Holger Podlech für seine freundliche Hilfe bei der supraleitenden CH-Struktur und Herrn Dr. Rudolf Tiede für seine geduldige Beratung in programmiertechnischen Fragen über den LORASR-Code.

Mein Dank gilt ebenfalls den Herren Dr. Robert A. Jameson und Dr. James Billen vom Los Alamos National Labortory. Die Diskussion mit ihnen erweiterte meine Kenntnisse über RFQ-Theorie und -Simulation.

Frau Tanja Harji und Herrn Dr. Horst Deitinghoff möchte ich danken. Ohne ihre Hilfe bei privaten Angelegenheiten hätte ich mich nicht auf meine Doktorarbeit konzentrieren können.

Ein großes Dankeschön geht an meine Zimmergenossen: Dr. Alexander Bechtold, Marco Busch, Dipl. Phys. Johannes Maus, Dipl. Phys. Markus Vossberg, und auch andere Kollegen: Dipl. Phys. Ulrich Bartz, Dr. Martin Droba, Florian Dziuba, Dr. Philipp Fischer, Dr. Benjamin Hofmann, Philipp Kolb, Dr. Holger Liebermann, Dr. Oliver Meusel, Dipl. Phys. Nobert Müller, Patrick Nonn, Dipl. Ing. Junchao Sun, Dr. Andreas Sauer, Dr. Jan Thibus, Dr. Hartmut Vormann, Dr. Holger Zimmermann, usw.

Den Herren Dr. Norbert Angert und Prof. Dr. Ingo Hofmann von der GSI Darmstadt und Dr. Anton Möslang vom Forschungszentrum Karlsruhe danke ich für ihre großzügige Hilfe.

Bei der Übersetzung der Zusammenfassung helfen mir Dr. R. Tiede, Frau T. Harji und M. Busch. Das Englisch für Teile dieser Arbeit wurde verbessert durch Prof. Dr. H. Klein, Prof. Dr. A. Schempp, PD Dr. H. Podlech und Dr. R.A. Jameson. Vielen Dank!

Ein ganz besonderes herzliches Dankeschön geht an meine Familie. Ich schulde euch viel. Ihr seid so wichtig für mich wie eine HF-Leistungsquelle für einen Beschleuniger.